Practical Aspects of Integrated 1D2D Flood Modelling of Urban Floodplains using LiDAR Topography Data

By

Deepak Bhimrao Kharat

Submitted for the degree of Doctor of Philosophy

Heriot-Watt University

School of the Built Environment

August 2009

ABSTRACT

Flood risk, a major risk facing mankind today, is projected to aggravate in view of the future predictions pertaining to the assessment of climate change scenarios.

Traditionally, flood risk assessment exercises of urban floodplains have been carried out using 1D model as well as 1D model with storage cells. In view of the recent availability of high quality Light Detection and Ranging (LiDAR) topography data, availability of higher computing capacities, developments in the numerical computing techniques and the merits of an integrated 1D2D computing modelling method, integrated 1D2D modelling has gained a momentum for strategic flood risk management (SFRM) and detailed urban flood risk analysis.

The research discussed in this thesis evaluates this modelling method using high quality LiDAR data in light of the results from the traditionally used 1D model with storage cells modelling method.

The research study was carried out using laboratory experimental observation data, hypothetical urban floodplain data and data for a section of the River Clyde and adjoining urban floodplain in Glasgow, a major city in Scotland, UK.

It concludes that, while integrated 1D2D models are of much benefit for a detailed flood risk analysis, specific attention needs to be paid towards the lateral extents of 1D model and the source of the river bank elevations while integrating it with a 2D model, particularly so when such a study is carried out for urban floodplains; and that the high quality LiDAR data significantly facilitates Strategic Flood Risk Modelling (SRFM) of urban floodplains.

To Rani

ACKNOWLEDGEMENTS

With my wife, Sanghmitra's belief that I can do better and the encouragement by my friend Simon Matthews helped me to look for research opportunities in the field I am passionate about. I take this opportunity to thank them and to thank Dr. G. N. Paudyal, Prof. D. Nagesh Kumar and Prof. S. K. Kar for recommending me to the University.

I am very much thankful to Prof. Gareth Pender and Dr. Adebayo Johnson Adeloye for accepting to supervise my research and their constant guidance and support during the research.

Without the James Watt scholarship by The Heriot-Watt University, it would not have been possible to undertake this research.

I am thankful to Jim Fleming of Glasgow City Council, David Reid of South Lanarkshire City Council and Dr. Pascal Lardet of Halcrow Group Limited for providing hydrodynamic model of the River Clyde and LiDAR data.

Thanks to DHI Water, Environment and Health's Simon Matthews, Morten Rungø, Henrik Kofoed-Hansen and Jørgen Bo Nielsen for providing me with the MIKE FLOOD (MIKE11+MIKE21) software without any limitations, and their technical help.

Thanks are due to Sandra Soares-Frazão of Université Catholique de Louvain for providing laboratory experimental observation data set even while being on holidays.

I wish to thank the IT and administration staff in the School of the Built Environment for their help.

I could not realise that it is been three years in the company of my friends Yahaya Ibrahim Makarfi, David A Kelly and Dr. Christopher Lang. Thanks for their wonderful company. Also thanks to my friend Martin Krupka for sharing thoughts.

The excellent support of my family, particularly my wife and daughter has inspired me to finish my studies faster, I can't thank them less! I owe them a lot!

ACADEMIC REGISTRY
Research Thesis Submission

Name*:*	DEEPAK BHIMRAO KHARAT		
School/PGI:	SCHOOL OF THE BUILT ENVIRONMENT		
Version: *(i.e. First, Resubmission, Final)*	Final	Degree Sought: (Award **and** Subject area)	Ph.D.

Declaration

In accordance with the appropriate regulations I hereby submit my thesis and I declare that:

1) the thesis embodies the results of my own work and has been composed by myself
2) where appropriate, I have made acknowledgement of the work of others and have made reference to work carried out in collaboration with other persons
3) the thesis is the correct version of the thesis for submission*.
4) my thesis for the award referred to, deposited in the Heriot-Watt University Library, should be made available for loan or photocopying, subject to such conditions as the Librarian may require
5) I understand that as a student of the University I am required to abide by the Regulations of the University and to conform to its discipline.

* *Please note that it is the responsibility of the candidate to ensure that the correct version of the thesis is submitted.*

Signature of Candidate*:*		Date:	

Submission

Submitted By *(name in capitals):*	
Signature of Individual Submitting:	
Date Submitted:	

For Completion in Academic Registry

Received in the Academic Registry by *(name in capitals):*

1. 1 Method of Submission

(Handed in to Academic Registry; posted through internal/external mail):

Signature: **Date:**

Table of Contents

List of Tables

List of Figures

Chapter 1
Introduction

1.1 Introduction

This thesis presents a methodology for the prediction of flood inundation extents, depths, duration and velocities in densely populated urban floodplains.

Among other definitions, a flood can be defined as "a temporary covering of land by water outside its normal confines" (Gouldby & Samuels 2005). Flooding is one of the most frequent natural disasters affecting human life worldwide. In addition to floods, other significant natural disasters are: drought, earthquake, epidemic, extreme temperature, famine, insect infestation, landslide, volcano, tsunami, wild fire and windstorm.

This chapter introduces flooding as a phenomenon, its causes and effects, various approaches to dealing with the mitigation of the impacts of flooding as well as the need for predicting the characteristics of a flood wave. The layout of the thesis is detailed at the end of the chapter.

1.2 Types and causes of floods

Based on the source of the floodwater, floods can be categorised as:

- Fluvial floods,
- Pluvial floods,
- Coastal floods and
- Groundwater floods.

Fluvial floods arise from incapacity of water courses, such as, rivers and streams to convey catchment runoff whereas, pluvial floods are due to overland flow, blocked or overloaded drains & sewers and broken water mains. Coastal flooding is caused by breach or overtopping of coastal defences due to extreme tides, storm induced waves and sea surges. Groundwater flooding is caused due to the rise of the groundwater table resulting in flooding of basements and filling up of the sewers and drains.

Flood events affecting urban areas in Europe stem from six main causes; these are (Douglas et al. 2007):

1. In mountain areas, the effects of heavy, warm spring rains on winter snow causing sudden melting.

2. Regional weather systems that are blocked by high pressure systems and produce widespread heavy rain over large sections of major river catchments.

3. Flash floods in hilly and mountainous regions.

4. Short duration, high intensity thunderstorm driven local flooding on small streams entirely within the urban areas.

5. Sewer flooding associated with blocked sewer overflows to larger rivers or surcharging through manhole covers.

6. Groundwater flooding as a result of prolonged heavy rainfall in certain geological conditions.

In addition to the above, dam failures also lead to rapid flooding of floodplains downstream of the dam structure.

1.3 Effects of floods

A study to understand the global perspectives on loss of human life caused by freshwater floods alone i.e. fluvial and pluvial floods, in the period 1975 to 2001 indicates that a total of 1816 worldwide freshwater flood events killed over 175,000 persons and affected more than 2.2 billion persons and of the 30 natural disasters, which affected most people in the period 1975 – 2001, 21 were floods. Further, no significant differences in average mortality (number of killed / number of affected) per flood event could be observed between different continents (Jonkman 2005). While these figures indicate the enormous impacts of flood disasters on a worldwide scale, they also indicate that the floods affect the developed, the developing and the underdeveloped civilisations alike. Flooding causes over one-third of the total estimated cost of damage and is responsible for two-thirds of people affected by natural disasters worldwide (United Nations 2004).

However, flooding is not disastrous in all the cases. It becomes a matter of concern and attention only when it results into loss of lives and / or damage to property. Flooding is a natural phenomenon and is essential and helpful for natural irrigation, improving soil fertility, maintenance of wetland ecosystem, survival of some species of trees and shrubs which depend on floods for spreading of seeds, etc.

1.4 Climate change and floods

The Intergovernmental Panel on Climate Change (IPCC) set up by the World Meteorological Organization (WMO) and by the United Nations Environment Programme (UNEP) in its Fourth Assessment Report (Intergovernmental Panel on Climate Change 2007) concludes that it is "unequivocal" that the Earth's climate is warming. As a result, increasingly severe weather leading to extreme and frequent droughts, precipitation events and increased sea level rise together with higher and more frequent storm surges is projected in many areas although some areas will become drier. This will invariably increase the risks of flooding.

The IPCC findings indicate increased flooding in Europe's South and North coasts affecting several million people and estimate that some 70 million people in Africa, 17 million people in Vietnam, 15 million people in Bangladesh and 7 million people in

India to be at risk of flooding due to climate change. Further, risk of flooding is estimated to be increasing in other parts of the world like the Gulf and Florida in North America. For Oceania, the population living in flood risk areas is estimated to be increased by 200 times as a result of climate change.

Thus, in view of the predicted change of climate, the number of people worldwide vulnerable to a devastating flood is expected to grow to 2 billion by 2050 from the current 520+ million due to climate change, deforestation, rising sea levels and population growth in flood-prone lands (UNU-EHS 2004).

The UK Climate Impacts Programme (UKCIP), established in 1997 to help co-ordinate scientific research into the impacts of climate change and to help organisations adapt to those unavoidable impacts, has outlined the risks that the current climate already poses to individuals, landscapes, organisations and the economy in the UK (Hulme et al. 2002).

Similarly academicians, too, are concerned and are carrying out assessment and research in this direction (Hunt 2002; Dale 2005; Dankers et al. 2007; Lehner et al. 2006).

1.5 Flood management

Eliminating flood risk altogether is neither technically possible nor environmentally and economically feasible and it is now generally accepted that the future will require careful management of flood risk. Despite the accepted risk of flooding, many settlements remain located near potential flood sources like rivers and seas due to the social and economic benefits offered by such locations. Therefore, it has been recommended that such communities must learn to live with rivers by adopting a holistic approach to flood risk management (Fleming 2002).

To encourage this approach, several regional, national and international legislative frameworks, planning policies and guidelines have been formulated by various governments, non government bodies, agencies and organisations; some of which are discussed below.

The European Union's Water Framework Directive (WFD) issued several guidelines and legislations to maintaining the rivers as healthy aquatic habitats while maintaining an integrated approach towards managing whole landscape. This is desirable as what happens in one part of a catchment will affect another.

The Foresight Future Flooding Report, released in 2004 by the Department of Trade and Industry (DTI), UK attempted to answer questions like: How will climate change affect us in 30 to 100 years time? How much will flooding increase in that time? How should we deal with any changes?

On similar lines, the "Go with the Flow: Lowland Catchment Research Programme" (LOCAR) by Natural Environment Research Council, UK stressed the need to manage water resources sustainably so that the needs of people, industry and agriculture are balanced with the needs of the environment.

The 'Turning the Tide on Flooding in Scotland' document produced during the 'UK Flood Risk 2030 to 2100: Responding to the Challenge' project work by WWF (Scotland) in 2003 presented similar holistic views for dealing with the sustainable flood management.

In addition, several local Councils in the UK have prepared their own flood prevention reports. Guidelines for improving the flood resilience by individuals and businesses are outlined in several public communications by various government and non – government agencies (CIRIA 2003; Association of British Insurers 2003; Department for Environment, Food and Rural Affairs 2008b; Scottish Executive 2004; Department for Environment, Food and Rural Affairs 2008a; World Health Organization 2002).

1.6 Need for flood modelling

Using flow and topography data, computer based flood modelling studies or physical model studies can be undertaken. The knowledge and information gained from a flood modelling exercise can be used in a variety of ways for building resilience to the hazard due to flooding i.e. capacity building to recover from flooding related damages e.g. generate flood maps, carry out local and catchment scale development planning, prepare

emergency plans, undertake risk assessment based on vulnerability data for various socio-economic factors, carry out diagnostic exercise for the sources and causes of flooding, flood warning, etc.

Thus, risk assessment is rapidly becoming the basis for decision making in all these areas for more integrated flood management (Environment Agency, UK 2006; Sayers et al. 2002) and methodologies for national scale (Hall et al. 2005; Hall et al. 2003), regional scale (Black & Burns 2002; Gouldby et al. 2008) and local scale (Haynes et al. 2007) flood risk assessment are being proposed, assessed and evaluated. The level of detail needed for a particular flood modelling exercise depends on the end use of the results or the purpose of the modelling exercise.

As mentioned earlier, to help in reducing the potential losses of lives and damage to property and possessions, computer based studies or physical model studies can be undertaken. Physical model studies play an important role in understanding the processes governing the physical movement of water and verifying computer models. However, physical model studies are complicated given the time, cost and effort required to carry out these types of studies and hence computer model studies are preferred. In addition to flood risk assessment purposes, these can be an effective tool for the communication of flood risk with the stakeholders like the public, planners and policymakers (Pender & Néelz 2007).

Various zero-dimensional (0D), one-dimensional (1D), two-dimensional (2D), three-dimensional (3D) mathematical computer modelling methods and combinations thereof have been developed so far and are being used by the academic and professional community for the purposes of flood modelling in urban floodplains. Depending on additional considerations in the 1D and 2D models, these models can be further categorised as $1D^{+}$, $2D^{-}$ and $2D^{+}$ (Pender 2006).

Although computer based flood risk assessment exercises have been carried out in the past, the need for taking on a national overview of all flood risk in UK including surface water and groundwater flood risk, to further develop tools and techniques for predicting and modelling river flooding taking into account the extreme and multiple events and depths and velocities of water, and to improve the technical capability to forecast,

model and warn against all sources of flooding has been stressed again in recent times (Pitt 2008b).

1.7 Research aims and objectives

This research evaluates the practical and comparative aspects as well as feasibility of using two of the available computer modelling methods – 1D model with storage cells and integrated 1D2D model to support flood risk assessment studies of an urban floodplain. A detailed discussion and justification of the research aims and objectives is presented in Chapter 3.

1.8 Research resources – data and software

The research utilises published reduced-scale model laboratory observation data, hypothetical urban floodplain data and recently available high spatial resolution Light Detection and Ranging (LiDAR) topography data of an urban floodplain.

Computer software, MIKE FLOOD, developed by DHI Water, Environment & Health, Denmark is used for carrying out computer model simulations. MIKE FLOOD has an interface that allows an integration of MIKE 11, a 1D model and MIKE 21, a 2D model by establishing a dynamic link between the 1D and 2D models. Thus, for this research, a 1D modelling software MIKE 11, a 2D modelling software MIKE 21 and the MIKE FLOOD software which facilitates linking of these models, are used.

1.9 Thesis layout

The thesis contains seven chapters. This chapter, Chapter 1 presents the background and introduces the research.

Chapter 2, "Flood Modelling Methods and Tools" presents details of the various flood modelling methods as well as the various topography data types currently available for flood modelling studies.

Chapter 3, "Research Aims, Objectives and Methodology" justifies and defines the research aims and objectives whilst presenting the research methodology.

As stated earlier, this research uses laboratory observations data, hypothetical urban floodplain data and a real catchment & floodplain data for floodplain modelling studies, see section 1.8. Chapter 4, "Simulation of Laboratory Experimental Observations" presents the study carried out using published reduced-scale model laboratory observation data whereas Chapter 5, "Hypothetical Urban Topography Study" details the studies using prototype scale hypothetical urban floodplain data with various urban settlement layouts.

The research findings and conclusions are extended to a real urban floodplain to evaluate issues surrounding an integrated 1D2D model. These are described in detail in Chapter 6, "Glasgow City Case Study".

The research findings, limitations and conclusions from the research study as well as suggestions for further research are presented in the last chapter, Chapter 7, "Conclusions and Recommendations".

Chapter 2
Flood Modelling Methods and Tools

2.1 Introduction

As outlined in brief in the earlier chapter (see section 1.6), to reduce the potential loss of life and damage to property and possessions, physical model studies or computer based studies can be undertaken. However, due to ease of use and cost-effectiveness, computer based studies are preferred. Various computer modelling methods viz. zero-dimensional (0D), one-dimensional (1D), two-dimensional (2D), three-dimensional (3D) and combinations thereof are available for carrying out flood modelling studies for urban floodplains. The choice of modelling method will depend on the purpose, the spatial scale of the problem, the level of detail required, data availability and the time and cost constraints for the flooding problem being investigated. A particular modelling method will have an advantage in terms of performance, data requirement and accuracy (Apel et al. 2007) for a particular case. This chapter details the currently available computer modelling methods and the topographical data available to support modelling studies.

Traditionally fluvial and pluvial modelling exercises are carried out using computer models employing the 1D modelling method. In view of the recent advances in numerical methods, easy availability of high spatial resolution topographical data and the availability of low cost computing power, flood modelling in urban floodplains is being carried out using 2D models.

Flood studies using 3D models have so far been limited to simulation of laboratory experimental data and 3D model validation studies. This is due to the high computational cost associated with this particular modelling approach. However, recently 3D models are finding their way into the mainstream flood modelling with promising results (Li et al. 2006; Gems et al. 2007). The computational cost, however, still remains a significant issue. Therefore, only 1D and 2D models are discussed further and considered for this research.

It is also important to note that computing resources required increase from 0D models to 3D models.

2.2 Flood modelling methods and tools

A summary of the various flood modelling methods and the names of some of the computer software tools currently available is presented in Table 2.1 (Pender 2006).

Table 2.1: Summary of modelling methods (Pender 2006)

Method reference	Distinguishing features	Some available software tools	Potential application
0D	No physical laws included in simulation	ArcGIS, DeltaMapper, etc.	Broad-scale assessment of flood extents and flood depths.
1D	Solution of the one-dimensional St Venant equations	Infoworks RS, ISIS, MIKE 11, HEC-RAS	Design scale modelling which can be of the order of 10s to 100s of km depending on catchment size.
$1D^{+}$	1D plus a flood storage cell approach to the simulation of floodplain flow	Infoworks RS, ISIS, MIKE 11, HEC-RAS	Design scale modelling which can be of the order of 10s to 100s of km depending on catchment size, also has the potential for broad-scale application if used with sparse cross-sectional data.
$2D^{-}$	2D minus the law of conservation of momentum for the floodplain flow	LISFLOOD-FP	Broad-scale modelling or urban inundation depending on cell dimensions.
2D	Solution of the two-dimensional shallow wave equations	TUFLOW, MIKE 21, TELEMAC, DIVAST	Design-scale modelling of the order of 10s km. May have the potential for use in broad-scale modelling if applied with very coarse grids.
$2D^{+}$	2D plus a solution for vertical velocities using continuity only	TELEMAC 3D	Predominantly coastal modelling applications where three-dimensional velocity profiles are important. Has also been applied to reach-scale river modelling problems in research

Method reference	Distinguishing features	Some available software tools	Potential application
			projects.
3D	Solution of the three-dimensional Reynolds averaged Navier-Stokes equations	CFX, FLUENT, PHEONICS	Local predictions of three-dimensional velocity fields in main channels and floodplains

2.2.1 0D flood modelling method

This method of flood risk assessment is the most simplistic among the various flood risk assessment methods discussed earlier and involves predicted water level in a river being projected onto the adjoining floodplain. The area having elevations below the water surface is then considered to be prone to flooding should the river water level reach that level. No estimate is made of the route floodwater takes to arrive on the floodplain nor is the volume of water transferred onto the floodplain calculated. Traditional geographical information system (GIS) software like ArcGIS®, MapInfo®, DeltaMapper®, etc. can be used for this type of study. Flood inundation maps can easily be prepared using this method for high level planning.

2.2.2 1D flood modelling method

Flows in rivers and channels are predominantly one-dimensional. Therefore, 1D modelling is the most widely used method for flood modelling of river networks. The 1D modelling method is useful in relatively long river systems as it requires little computational effort and cost. It is also best suited to areas where there has been little development on the floodplain.

A 1D model consists of linked river and floodplain cross-sections perpendicular to the river centreline, thus representing the flow path. To account for the variation in depth and velocity across a floodplain section, the channel cross-section is often subdivided into number of panels and the conveyance computed separately for each of them. Conveyance, K is a quantitative measure of the discharge capacity, Q of a watercourse (Samuels et al. 2002) normally calculated from (Cruise et al. 2007):

$$K = \frac{1}{n} AR^{\frac{2}{3}}$$

where, n is the Manning's roughness coefficient, A = cross-sectional area and R = hydraulic radius given by A/P where, P is the wetted perimeter.

K is related to Q as:

$$Q = KS^{\frac{1}{2}}$$

where, S = channel slope

With inflow and outflow boundary conditions for a model domain specified, water levels and discharges can then be predicted along a river reach using the Saint Venant equations of conservation of volume (or continuity equation) and conservation of momentum. The equations are based on the following assumptions (Chanson 2004):

1. The flow is one dimensional: i.e. the velocity is uniform in a cross-section and the transverse free-surface profile is horizontal,

2. the streamline curvature is very small and the vertical fluid accelerations are negligible; as a result, the pressure distributions are hydrostatic,

3. the flow resistance and turbulent losses are the same as for a steady uniform flow for the same depth and velocity, regardless of the trends of the depth i.e. the flow is subcritical,

4. the bed slope is small enough to satisfy the approximations: $\cos \theta \approx 1$ and $\sin \theta \approx \tan \theta$; where θ is the angle between the channel invert and the horizontal, and

5. the water density is constant i.e. the water is incompressible and homogeneous.

The definition sketch of the Saint Venant equations is shown in Figure 2.1 (Chanson 2004).

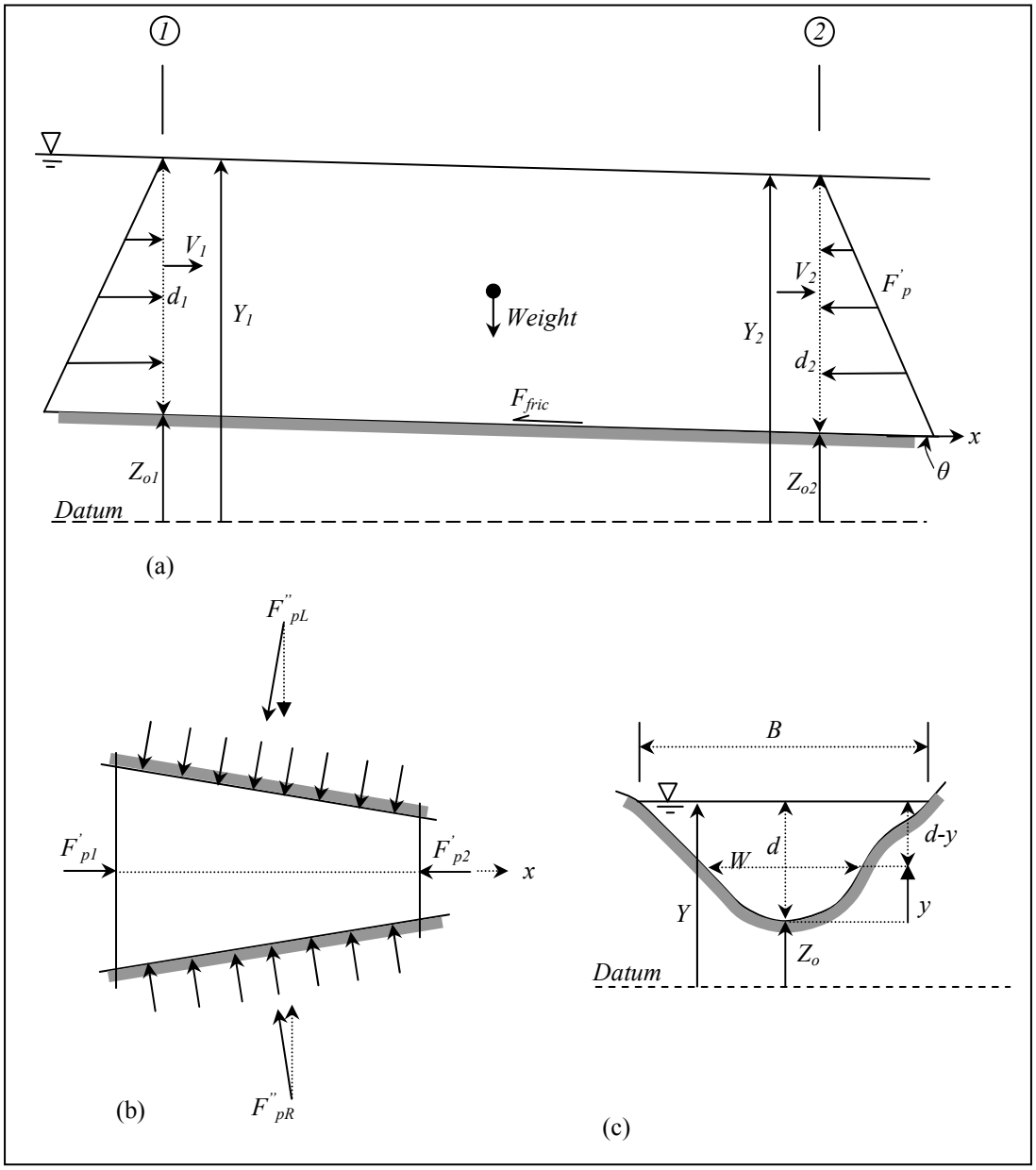

Figure 2.1: Definition sketch of Saint Venant equations – (a) side view, (b) top view and (c) cross-section (Chanson 2004)

With the above basic assumptions, the continuity equation can be derived as

$$\left(\frac{\partial A}{\partial t} + \frac{\partial Q}{\partial x} \right) = 0 \qquad \textbf{Equation 2.1}$$

where, A = cross-sectional area and Q = discharge

and the momentum equation can be derived as

$$\frac{\partial Q}{\partial t} + \frac{\partial}{\partial x}(V^2 A) + gA\frac{\partial d}{\partial x} = gA(S_o - S_f) \qquad \textbf{Equation 2.2}$$

where, V = average flow velocity, g = gravitational acceleration, S_o = channel slope and S_f = friction slope.

Friction slope, S_f is defined as:

$$S_f = \frac{4\tau_o}{\rho g D_H}$$

where τ_o is the average boundary shear stress and D_H is the hydraulic diameter.

The continuity and momentum equations can take various forms, e.g. in terms of free surface elevation, Y and average flow velocity, V the equations become:

$$\frac{\partial Y}{\partial t} + \frac{A}{B}\frac{\partial V}{\partial x} + V\left(\frac{\partial Y}{\partial x} + S_o \right) + \frac{V}{B}\left(\frac{\partial A}{\partial x} \right)_{\text{d = constant}} = 0 \qquad \textbf{Equation 2.3}$$

$$\frac{\partial V}{\partial t} + V\frac{\partial V}{\partial x} + g\frac{\partial Y}{\partial x} + gS_f = 0 \qquad \textbf{Equation 2.4}$$

where, B = Channel width.

Equation 2.3 and Equation 2.4 are the basic Saint Venant equations and are also known as dynamic wave equations (Chanson 2004).

Including the hydraulic resistance using the Chezy's description and the lateral inflow, q into the equations Equation 2.1 and Equation 2.2 form the basic equations used in the

MIKE 11 model used for the research as below (DHI Water, Environment & Health 2005a):

$$\left(\frac{\partial A}{\partial t} + \frac{\partial Q}{\partial x} \right) = q \qquad \textbf{Equation 2.5}$$

$$\frac{\partial Q}{\partial t} + \frac{\partial \left(\alpha \frac{Q^2}{A} \right)}{\partial x} + gA \frac{\partial d}{\partial x} + \frac{gQ|Q|}{C^2 AR} = 0 \qquad \textbf{Equation 2.6}$$

where α = momentum distribution coefficient and C = Chezy's resistance coefficient.

Chezy's resistance coefficient is related to Manning's roughness coefficient, n as below:

$$C = \frac{R^{\frac{1}{6}}}{n}$$

For flood inundation modelling, these equations are solved by using a numerical method such as method of characteristics or explicit / implicit finite difference methods. In the method of characteristics, the approximations of the derivatives in the above mentioned governing equations in the characteristic form are approximated on the characteristic grid along the characteristics themselves whereas, in the explicit and implicit finite difference methods, the approximations of the derivatives in the above mentioned governing equations are approximated on a fixed rectangular *x*-*t* grid. Explicit finite difference methods advance the solution to the end of the time step at a single grid node whereas implicit finite difference methods approximate the derivatives using values of the dependent variables both at the beginning of the time step and at the end of the time step. The method of characteristics is utilised only in special cases, often as a check on some other method whereas the explicit finite difference method is used in problems of rapid transients and ordinarily are not applied to flood routing problems in large rivers, which often are treated by implicit methods (Sturm 2002). The implicit finite difference method is implemented by employing the most popular Preismann scheme or Abbott - Ionescu scheme among others such as Vasiliev implicit scheme. A detailed description

of these schemes with further references is presented by Liggett and Cunge (Liggett & Cunge 1975) as well as Wood (Wood 1993).

MIKE 11 solves Equation 2.5 and Equation 2.6 by transforming them into implicit finite difference equations and solving them by employing Six-point Abbott numerical scheme (DHI Water, Environment & Health 2005a). The Six-point Abbott numerical scheme consists of a computational grid and alternating *Q*- and *h*-points at which the discharge, *Q* and water level, h are computed at each time step. The numerical scheme is centred at a *h* point (see Figure 2.2) for the solution of the continuity equation and at a *Q*-point for the solution of the momentum equation.

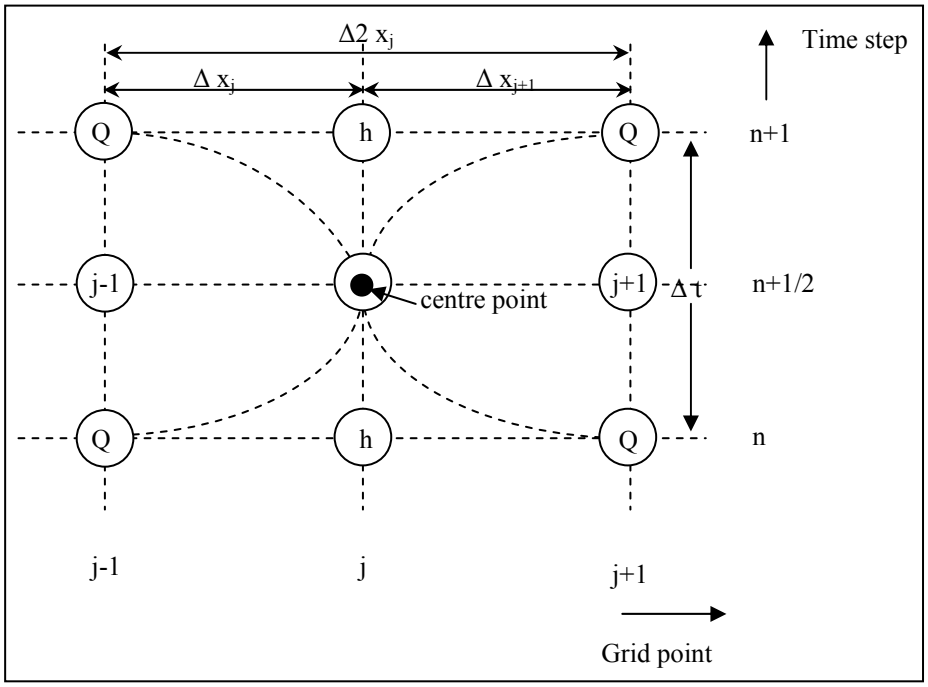

Figure 2.2: Six-point Abbott numerical scheme for solution of continuity equation (DHI Water, Environment & Health 2005a)

In the continuity equation the storage width, b_s is introduced as:

$$\frac{\partial A}{\partial t} = b_s \frac{\partial h}{\partial t}$$ giving

$$\frac{\partial Q}{\partial x} + b_s \frac{\partial h}{\partial t} = q$$ **Equation 2.7**

As only Q has a derivative with respect to x, the equation can easily be centred at an h-point, see Figure 2.2.

Derivatives in Equation 2.7 are expressed at the time level, $n+½$, as follows:

$$\frac{\partial Q}{\partial x} \approx \frac{\left(Q_{j+1}^{n+1} + Q_{j+1}^{n}\right)/2 - \left(Q_{j-1}^{n+1} + Q_{j-1}^{n}\right)/2}{\Delta 2 x_j}$$

$$\frac{\partial Q}{\partial t} \approx \frac{\left(h_j^{n+1} - h_j^{n}\right)}{\Delta t}$$

b_s in Equation 2.7 is approximated by:

$$b_s = \frac{A_{0,j} + A_{0,j+1}}{\Delta 2 x_j}$$

where, $A_{0,j}$ = surface area between grid point *j-1* and *j*, $A_{0,j+1}$ = surface area between grid point *j* and *j+1* and $\Delta 2x_j$ = distance between point *j-1* and *j+1*.

Substituting for the derivatives in Equation 2.7 gives a formulation of the following form:

$$\alpha_j Q_{j-1}^{n+1} + \beta_j h_j^{n+1} + \gamma_j Q_{j+1}^{n+1} = \delta_j$$

where, α, β and γ are functions of b and δ, moreover, depend on Q and h at time level n and Q on time level $n+½$.

The momentum equation is centred at Q-points as shown in Figure 2.3.

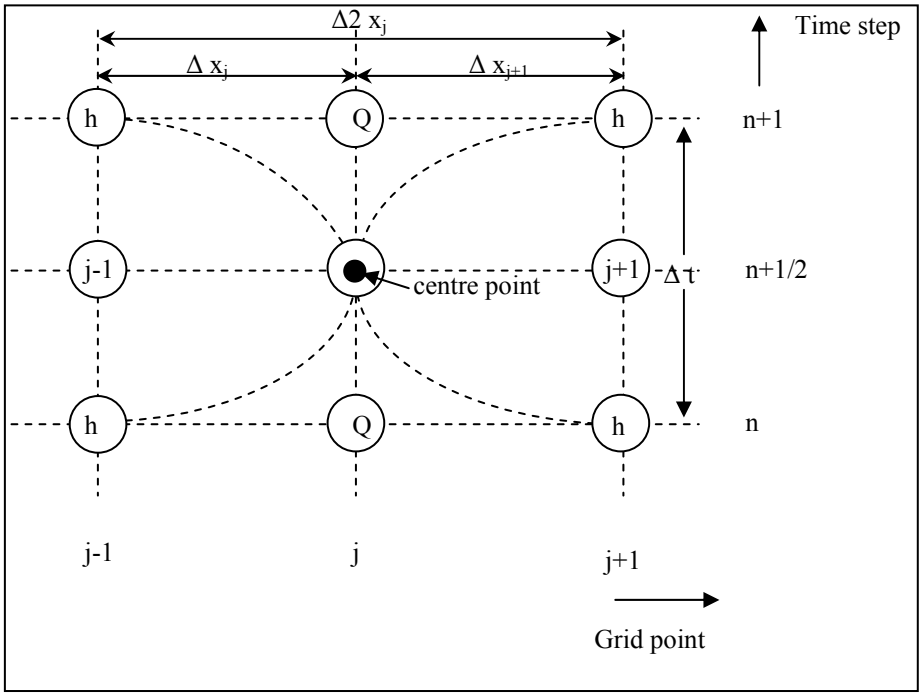

Figure 2.3: Six-point Abbott numerical scheme for solution of momentum equation (DHI Water, Environment & Health 2005a)

The derivatives of the Saint Venant equation, Equation 2.6 are expressed in the following way:

$$\frac{\partial Q}{\partial t} \approx \frac{Q_j^{n+1} - Q_j^n}{\Delta t}$$ **Equation 2.8**

$$\frac{\partial\left(\alpha \frac{Q^2}{A}\right)}{\partial x} \approx \frac{\left[\alpha \frac{Q^2}{A}\right]_{j+1}^{n+½} - \left[\alpha \frac{Q^2}{A}\right]_{j-1}^{n+½}}{\Delta 2 x_j}$$ **Equation 2.9**

$$\frac{\partial h}{\partial x} \approx \frac{\frac{\left(h_{j+1}^{n+1} + h_{j+1}^n\right)}{2} - \frac{\left(h_{j-1}^{n+1} + h_{j-1}^n\right)}{2}}{\Delta 2 x_j}$$ **Equation 2.10**

The momentum equation then can be written in the following form:

$$\alpha_j h_{j-1}^{n+1} + \beta_j Q_j^{n+1} + \gamma_j h_{j+1}^{n+1} = \delta_j$$ **Equation 2.11**

where,

$\alpha_j = f(A)$

$\beta_j = f(Q_j^n, \Delta t, \Delta x, C, A, R)$

$\gamma_j = f(A)$

$\delta_j = f(A, \Delta x, \Delta t, \alpha, q, v, \theta, h_{j-1}^n, Q_{j-1}^{n+½}, Q_j^n, h_{j+1}^n, Q_{j+1}^{n+½})$

To obtain a fully centred description of A_{j+1}, these terms should be valid at time level $n+½$ which can only be fulfilled by using iterative calculation approach, viz. two (but can be user defined) iterations , the first starting from the result from the previous time step and the second using the centred values from this calculation.

Since the Saint Venant equations are applicable for subcritical flows only, additional consideration is given in the MIKE11 solution scheme while applying these equations for supercritical and subcritical to supercritical transitional flow conditions. This is achieved by applying a reduced momentum equation (see Equation 2.7) which neglects the convective momentum term for supercritical flows (DHI Water, Environment & Health 2005a).

$$\frac{\partial Q}{\partial t} + gA\frac{\partial h}{\partial x} + \frac{gQ|Q|}{C^2 AR} = 0$$ **Equation 2.12**

For subcritical to supercritical flow transition, a gradual reduction of the convective momentum term based on the Froude number is made as described below (DHI Water, Environment & Health 2005a):

The characteristics of the St. Venant equations are given by:

$$C_{1,2} = \frac{Q}{A} \pm \sqrt{gA / w} = \frac{Q}{A}\left(1 \pm \frac{1}{F}\right)$$

Equation 2.13

where, Q = discharge, A = cross-sectional area, w = surface width of cross-section, g = acceleration due to gravity and F = Froude number.

For $F > 1$ the characteristics are both positive, implying that the St. Venant Equations take two upstream boundary conditions, and for $F = 1$ the solution becomes singular. The numerical algorithm adopted in MIKE 11 is based on a staggered computational grid and cannot accommodate two boundary conditions at the same boundary or a singular solution. To avoid these situations a modified momentum equation is implemented in MIKE 11(DHI Water, Environment & Health 2005a), viz.

$$\frac{\partial Q}{\partial t} + \beta \frac{\partial\left(\alpha \frac{Q^2}{A}\right)}{\partial x} + gA \frac{\partial h}{\partial x} + friction = 0$$

where, h = water surface elevation, α = momentum distribution coefficient and β = factor for suppression of convective momentum term.

The default formulation in MIKE 11 is:

$$\beta = \begin{cases} 1 - F^2 \; for \;\; F \le 1 \\ 0 \;\; for \;\; F > 1 \end{cases}$$

This ensures excellent stability properties of the numerical solution and is sufficiently accurate for most flood routing studies where generally the Froude number is relatively small and the resolution used is coarse i.e. the space step is much larger than the water depth. For water surface profiling with high Froude number and small space steps an alternative formulation, as below, has been implemented(DHI Water, Environment & Health 2005a).

$$\beta = \begin{cases} 1 & for \;\; F \le a \\ 1/(F + 1 - a)^b & for \;\; F > a \end{cases}$$

For the default value of a and b (a=1 and b=2) the two characteristics, never have the same sign. The solution is considerably more accurate for high Froude numbers. Various tests showed that the new formulation performs well for transition from sub- to supercritical flow.

The suppression factor β varies from 1 (full convective term) to 0 (no convective term) according to the Froude number. The β factor also modifies the energy calculation, thus energy head at any location in a model is affected. This means that when velocities are high (when the convective term is significant), energy head is significantly affected i.e. energy is not conserved.

Although the use of 1D models for flood inundation studies is very common, research to solve these equations more efficiently and to suit every situation (like highly transient flows, vegetated floodplains, etc.) are still being investigated (Macchione & Viggiani 2004; Sole & Zuccaro 2005; Graf & Qu 2004; Bleninger et al. 2006; Singh 2004; Tchamen et al. 2006; Yasuda 2006; Mark et al. 2004; Helmiö 2005; Martin-Vide et al. 2008; Ying & Wang 2008).

2.2.3 1D$^+$ flood modelling method

Saint Venant equations are not suitable for flood propagation problems over inundated floodplains as flows over floodplains are two-dimensional in nature. Accordingly, in an alternative application of the 1D modelling method, a main river is modelled using the method described earlier but the floodplains are modelled as flood storage reservoirs with a horizontal water level, thus forming a quasi-2D model. This type of model is commonly known as '1D model with storage cells' and falls in the 1D$^+$ category. This modelling approach is commonly applied in practice. The definition sketch of 1D model with storage cells is shown in Figure 2.4.

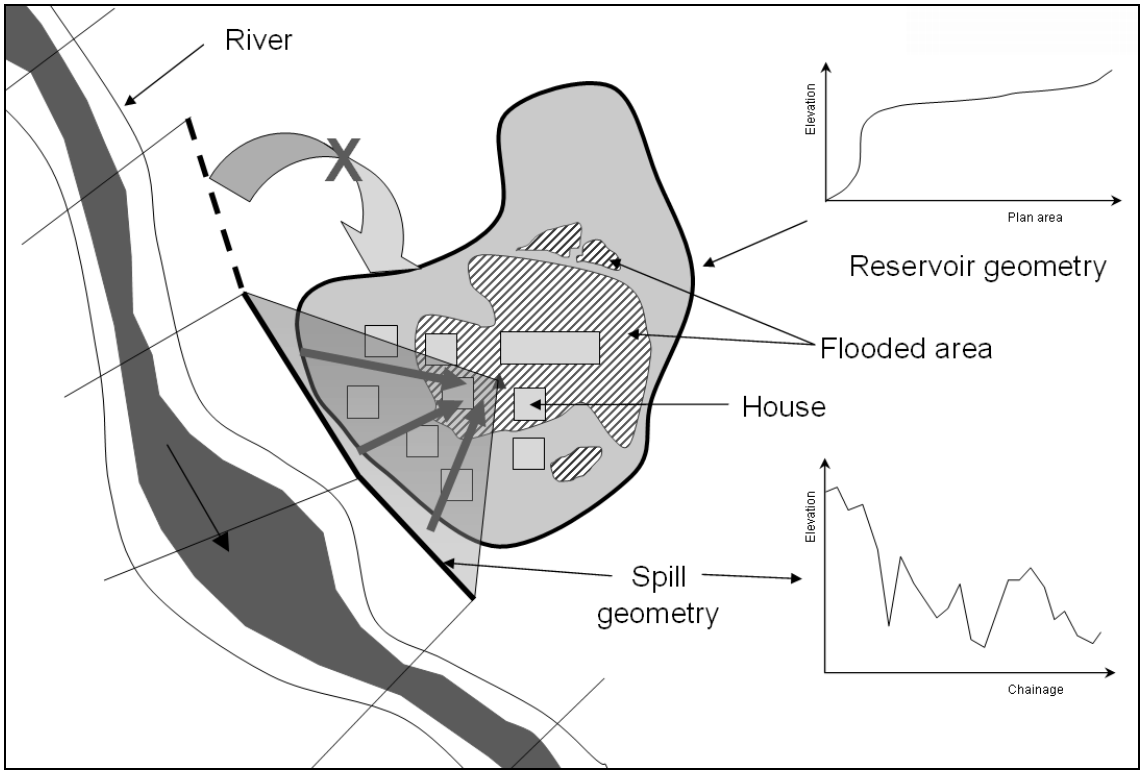

Figure 2.4: Definition sketch of 1D model with storage cells (reservoirs)

Almost all currently available academic and commercial computer codes for 1D modelling support this modelling approach and thus a large number of flood risk assessment studies have been carried out worldwide using this modelling method. There can be multiple reservoirs or storage cells on either bank. The reservoirs or storage cells can also exchange water between themselves and with the river through the spill units as shown in Figure 2.5.

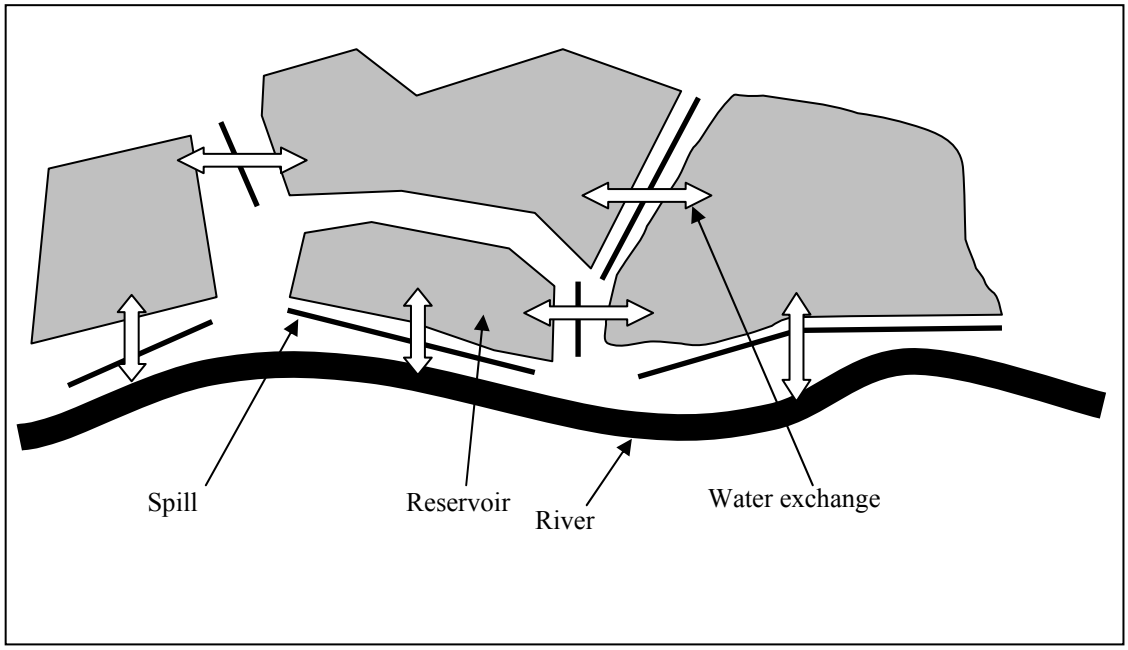

Figure 2.5: Typical model layout - 1D model with storage cells (reservoirs)

During an overbank flow, the exchange of water between the river and the flood storage reservoirs, which is driven by the difference in the water levels in the river and the reservoir, is computed using weir flow based discharge relationships over the spills. The definition sketch for the flow over a spill is shown in Figure 2.6.

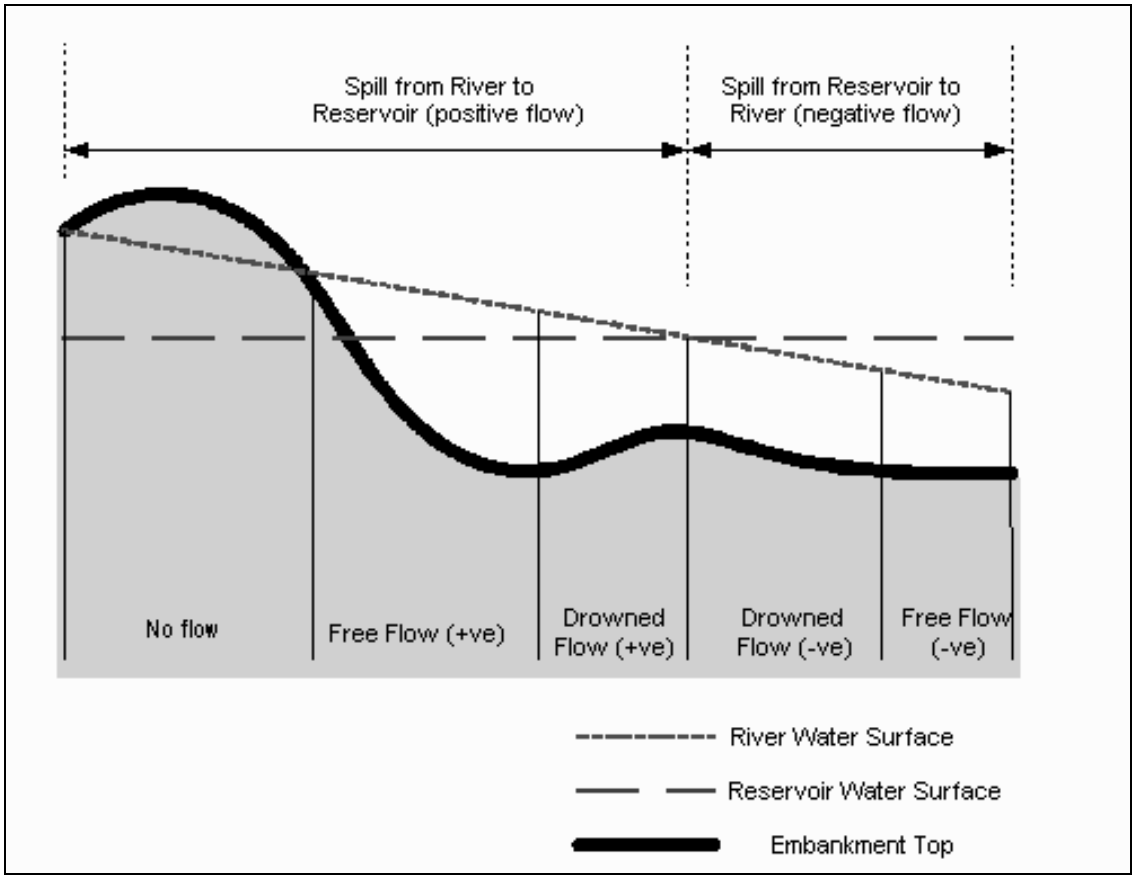

Figure 2.6: Definition sketch for flow over a spill (Wallingford Software Ltd and Halcrow Group Ltd 2005)

The basic weir equation for flow over a weir is:

$$Q = C_d b h^{\frac{3}{2}}$$ **Equation 2.14**

where, C_d is the coefficient of discharge for the weir, b is the crest width and h is the head of water above the crest of the weir.

From Figure 2.6, it can be observed that there are four possible modes of flow over the weir depending on the water levels on either side of the weir. Equation 2.14 is modified further to compute the discharges under these flow conditions. The negative or positive free and drowned discharge over the segment, using appropriate weir equations depending on the flow conditions, when summed up, yield the net discharge over the spill.

Thus, the amount of water that is transferred to a reservoir or storage cell is the function of the water level difference (in the reservoir / storage cell and the river or the storage cells / reservoirs when they are connected through a spill) and the time duration of the overbank flow. The amount of water transferred to a reservoir or storage cell and the storage - area curve for the reservoir or storage cell are used to map the flood extents. The transfer of the water across the reservoir or storage cell is instantaneous with no velocity information associated with the progress of the flood wave across the floodplain. The flood extent mapping process is carried out by starting from the lowest point in the reservoir or storage cell (shown as ▲ in Figure 2.4). A horizontal spread of the water surface over the area represented by the reservoir or storage cell is considered. Therefore, the final flood extent map may show flooding in isolated areas.

This method is similar to the 0D method described earlier in section 2.2.1. However, the use of this method of flood risk assessment over the 0D method can be justified as the amount of water transferred to the floodplain is accounted for and, therefore, results in more reliable flood extent map for a flood event of specified magnitude.

Caution needs to be exercised, however, in identifying the potential spills. A potential spill not identified as contributing to a reservoir (shown as ✘ in Figure 2.4) may lead to a reduced flood extent (or no flooding for lower flow magnitudes). On the contrary, a misidentified connection may lead to 'forced flooding' of the area covered by the reservoir.

2.2.4 2D⁻ flood modelling method

Recent availability of high resolution topographical data (see section 2.3), advances in computing codes used for simulating overland flow and the phenomenal growth in available computing power in recent times has triggered a trend of using 2D modelling tools for predicting inundation to support flood risk assessment.

The simplest approach extends the concept of the 1D model with storage cells to a much finer level – the raster size of the topography data. These types of models have been developed since 1962 (Hunter 2005) although it is only relatively recently that computing power and data availability have permitted their application at a large scale.

This approach leads to an enhanced flood inundation extent calculation. These models, however, do not carry out calculations for the momentum exchange and therefore are categorised as 2D$^-$ models. The definition sketch for this type of model is shown in Figure 2.7.

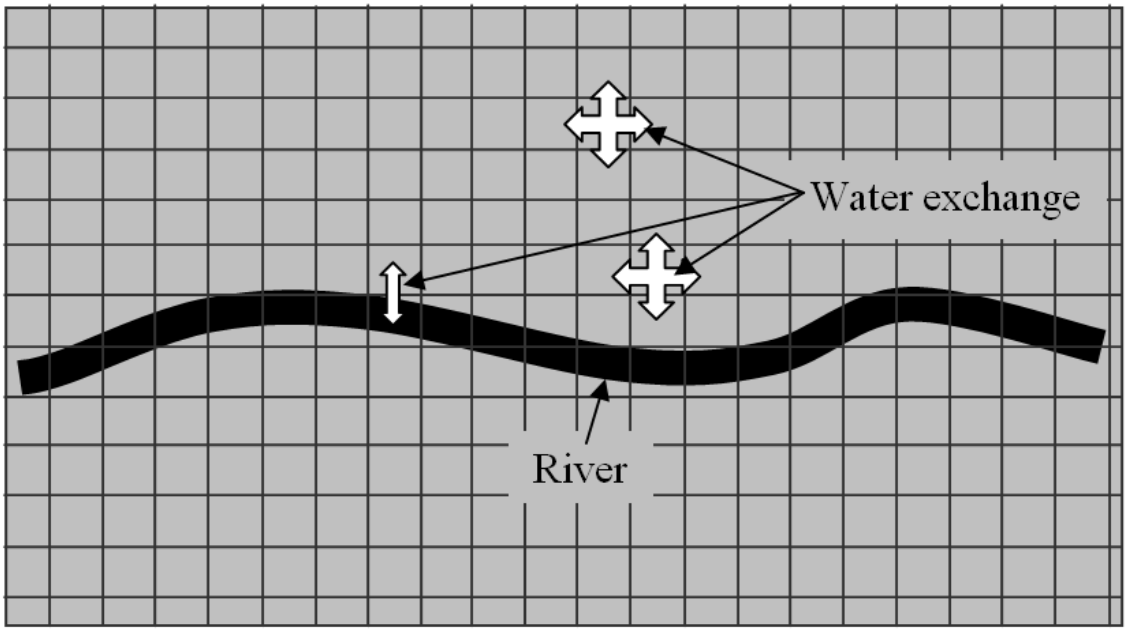

Figure 2.7: Definition sketch for a raster based storage cell model

In this approach, each of the cells of the topographic data is considered to be a storage reservoir. The cells then exchange water between themselves based on a uniform flow, a gradually varied flow, a diffusive wave or a weir equation approximation. The flow rate and direction are governed by the water surface gradient and the topography of the floodplain.

One such model, LISFLOOD-FP employs the kinematic wave form of the Saint Venant's equation obtained by neglecting the local acceleration, convective acceleration and pressure terms and assuming that the water surface elevation is parallel to the channel bottom. The resulting equations are (Bates & De Roo 2000):

Continuity: $$\frac{\partial Q}{\partial x} + \frac{\partial A}{\partial t} + q = 0$$ **Equation 2.15**

Momentum: $$S_o = S_f$$ **Equation 2.16**

During the computations, each cell contained in a channel is attributed with the channel width, the slope, the friction coefficient, the bankful depth and a marker indicating the direction of the next downstream cell. Similarly, every floodplain cell is attributed with the dimensions, the elevation and the friction coefficient.

During a flood, LISFLOOD-FP solves (Hunter et al. 2005) a continuity equation relating flow into a cell and its net change in volume as:

$$\frac{\partial h^{i,j}}{\partial t} = \frac{Q_x^{i-1,j} - Q_x^{i,j} + Q_y^{i,j-1} - Q_y^{i,j}}{\Delta x \Delta y} \qquad \textbf{Equation 2.17}$$

and a momentum equation for each direction where flow between cells is calculated according to Manning's law (only the x direction is given here, Q_y is defined analogously) as:

$$Q_x^{i,j} = \frac{h_{flow}^{5/3}}{n}\left(\frac{h^{i-1,j} - h^{i,j}}{\Delta x}\right)^{1/2} \Delta y \qquad \textbf{Equation 2.18}$$

where, $h^{i,j}$ is the water free surface height at the node (i, j), Δx and Δy are the cell dimensions, n is the Manning's friction coefficient, and Q_x *and* Q_y describe the volumetric flow rates between the floodplain cells. The flow depth, h_{flow} represents the depth through which water can flow between two cells, and is defined as the difference between the highest water free surface in the two cells and the highest bed elevation. These equations are solved explicitly using a finite difference discretisation of the time derivative term:

$$\frac{^{t+\Delta t}h^{i,j} - {}^{t}h^{i,j}}{\Delta t} = \frac{{}^{t}Q_x^{i-1,j} - {}^{t}Q_x^{i,j} + {}^{t}Q_y^{i,j-1} - {}^{t}Q_y^{i,j}}{\Delta x \Delta y} \qquad \textbf{Equation 2.19}$$

Where, ${}^{t}h$ and ${}^{t}Q$ represent depth and volumetric flow rate at time t, respectively, and Δt is the model time step.

Storage cell models developed earlier were marred with problems like an inability to develop solutions that are independent of time step or grid size, an unrealistic lack of

sensitivity to floodplain friction and underpredicted spatially distributed (i.e. inundation extent, flood depths) and bulk (i.e. wave volume, travel time) flood characteristics within the domain when compared with other modelling approaches (Hunter 2005). Those have recently undergone improvements such as the use of optimal adaptive time step determined using a flow-limiter equation and a condition for model stability analogous to the Courant-Freidrichs-Levy condition for advective flows termed as adaptive time step technique (ATS) (Hunter et al. 2005). The use of ATS has shown considerable improvement over a standard raster cell model by yielding results that are independent of grid size or initial time step and also showing an intuitively correct sensitivity to floodplain friction. These models are being successfully applied for floodplain modelling (Hunter et al. 2005; Hunter et al. 2006). However the ATS solution is applied most efficiently at larger grid resolutions such as 50 m which may not be able to represent small scale but significant topographical features explicitly (Hunter et al. 2005)

In a further improved approach using raster based storage cell models, pre-calculations are carried out for the flood volume over topography at cell level. The flood extents then are carried out without the time stepping unlike the raster cell based models. The model run times, once the pre-calculations are performed, are in the range of few seconds. Therefore, this approach is particularly suitable where a number of different scenarios are to be assessed for various risk management purposes (Krukpa et al. 2007; Lhomme et al. 2008) like high level assessment. Approaches to utilise the more accurate simulation results from any available fine grid high resolution simulations are currently also being explored (Néelz et al. 2008). An insight into which scenarios need to be analysed further for detailed flood risk assessment, then, can be gained by such a modelling exercise.

2.2.5 2D flood modelling method

The full 2D, or commonly referred to as 2D, models are based on hyperbolic partial differential vertically integrated Shallow Water Equations (SWE) solved by finite difference, finite elements or finite volume methods. The SWEs are developed with an assumption that the depth of the water over land is small compared to the wave length or free–surface curvature and the pressure distribution in the flow is hydrostatic.

The version of the MIKE 21 software used during this research is based on finite difference computational scheme (DHI Water, Environment & Health 2005b). Therefore, the governing equations viz. conservation of mass and momentum equations, integrated over the vertical (i.e. depth) and the solution scheme are described below from this perspective.

Conservation of mass:

$$\frac{\partial \zeta}{\partial t} + \frac{\partial p}{\partial x} + \frac{\partial q}{\partial y} = \frac{\partial d}{\partial t}$$

Equation 2.20

Conservation of momentum in x – direction:

$$\frac{\partial p}{\partial t} + \frac{\partial}{\partial x}\left(\frac{p^2}{h}\right) + \frac{\partial}{\partial y}\left(\frac{pq}{h}\right) + gh\frac{\partial \zeta}{\partial x} + \frac{gp\sqrt{p^2 + q^2}}{C^2 \cdot h^2} - \frac{1}{\rho_w}\left[\frac{\partial}{\partial x}\left(h\tau_{xx}\right) + \frac{\partial}{\partial y}\left(h\tau_{xy}\right)\right] - \Omega_q - fVV_x + \frac{h}{\rho_w}\frac{\partial}{\partial x}\left(p_a\right) = 0$$

Equation 2.21

Conservation of momentum in y – direction:

$$\frac{\partial q}{\partial t} + \frac{\partial}{\partial y}\left(\frac{q^2}{h}\right) + \frac{\partial}{\partial x}\left(\frac{pq}{h}\right) + gh\frac{\partial \zeta}{\partial y} + \frac{gq\sqrt{p^2 + q^2}}{C^2 \cdot h^2} - \frac{1}{\rho_w}\left[\frac{\partial}{\partial y}\left(h\tau_{yy}\right) + \frac{\partial}{\partial x}\left(h\tau_{xy}\right)\right] - \Omega_p - fVV_y + \frac{h}{\rho_w}\frac{\partial}{\partial y}\left(p_a\right) = 0$$

Equation 2.22

where,

t	time
x, y	space coordinates
$\zeta(x, y, t)$	surface elevation
$d(x, y, t)$	time varying depth
$h(x, y, t)$	water depth
$p, q(x, y, t)$	flux densities in x- and y- directions
$C(x, y)$	Chezy resistance
g	acceleration due to gravity

$V, V_x, V_y (x, y, t)$	wind velocity and components in x- and y- direction
$f(V)$	wind friction factor
Ω	Coriolis parameter, latitude dependent
p_a	atmospheric pressure
ρ_w	density of water
$\tau_{xx}, \tau_{xy}, \tau_{yy}$	components of effective shear stress

MIKE 21 uses the Alternating Direction Implicit (ADI) technique to integrate the equations for mass and momentum conservation in the space-time domain. The difference terms of the equations expressed on a staggered grid in (x, y) space are shown in Figure 2.8.

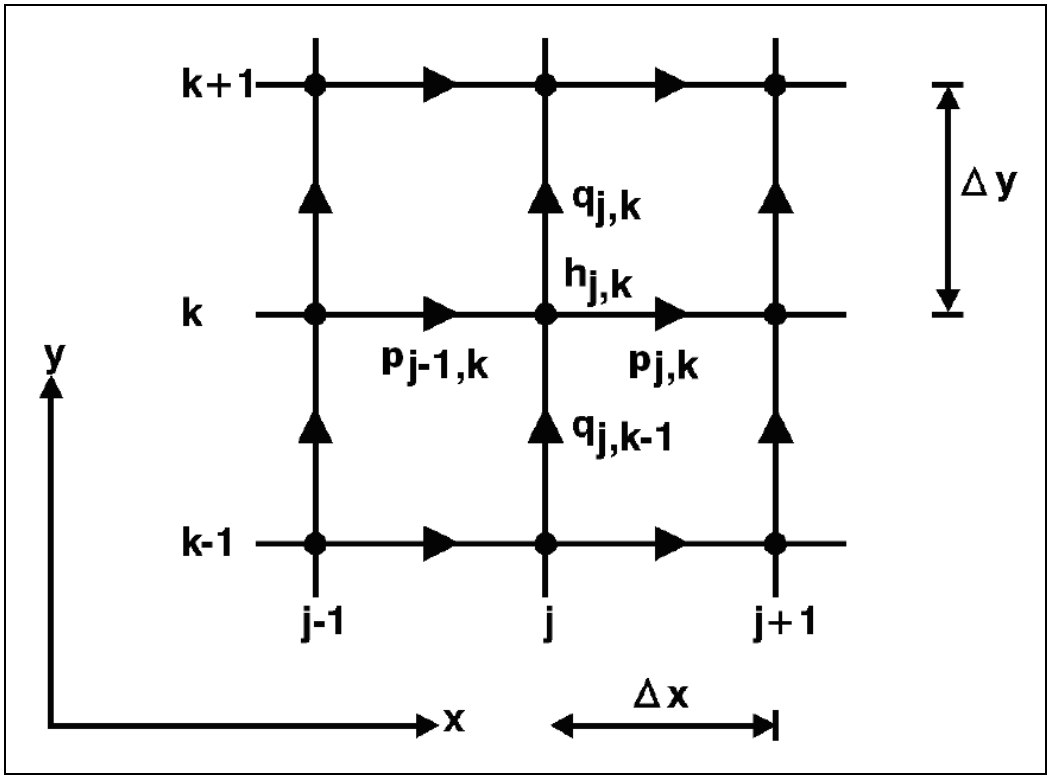

Figure 2.8: Finite difference grid in x, y space (DHI Water, Environment & Health 2005b)

The resulting equation matrices for each direction and each individual grid line are resolved by a Double Sweep (DS) algorithm (see Figure 2.9) which employs one-dimensional sweeps alternating between x- and y-directions. The two sweeps are added together for time centring as shown in Figure 2.9.

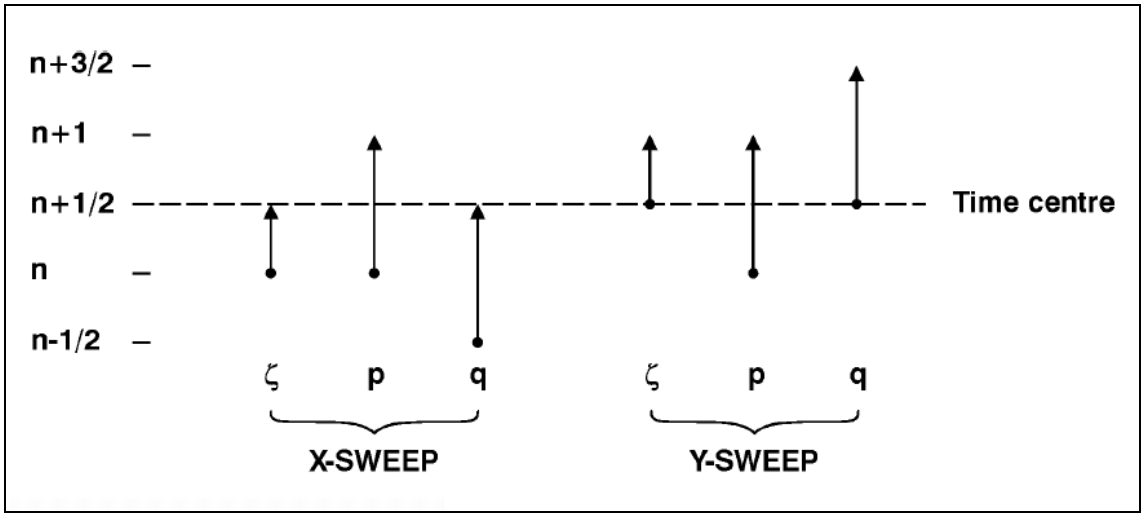

Figure 2.9: Time centring using Double Sweep algorithm (DHI Water, Environment & Health 2005b)

Figure 2.10 shows the computational cycle progressing through time.

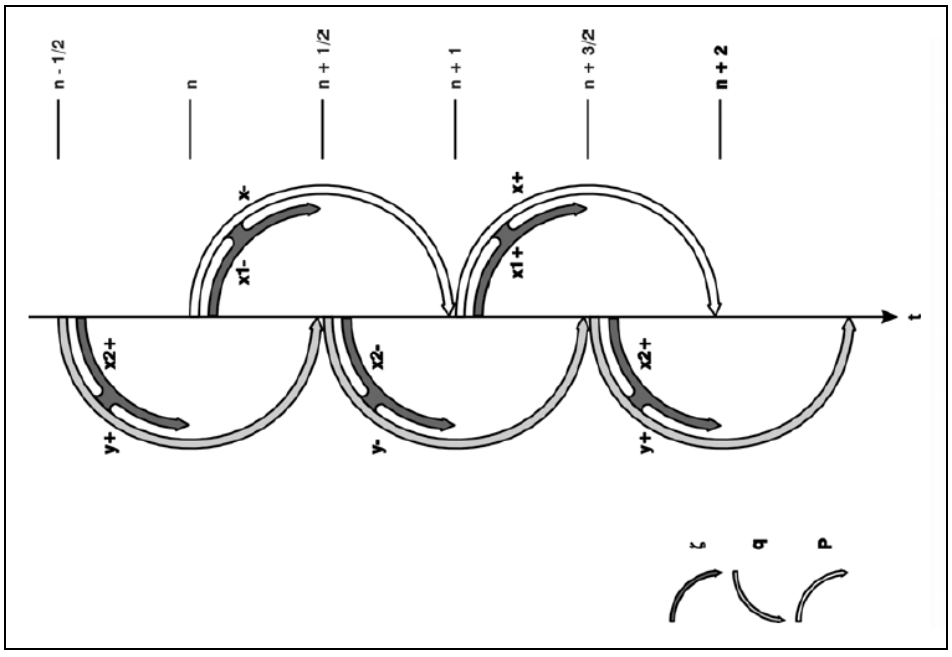

Figure 2.10: Computational cycle progress through time (DHI Water, Environment & Health 2005b)

The Alternating Direction Implicit (ADI) technique, although very successful in balancing numerical accuracy with computational efficiency, works well only when the flows are slow and smooth i.e. the Froude number is much less than unity but struggle to adequately describe the flow when the Froude number exceeds unity e.g. shocks,

jumps or bores found in mountainous rivers, storm surges, the sudden opening of sluice gates, dam-breaks, levee breaches, flash floods, etc. (Liang et al. 2007).

Shock-fitting and shock-capturing approaches aim at resolving these discontinuities. The shock-fitting approach isolates the shock from adjacent smooth regions and treats it separately as a moving internal boundary, it becomes unmanageable when detecting and tracking the shocks accurately in an unsteady flow problem. Therefore, the shock-capturing methods which utilize a universal solution strategy over the whole domain have become preferable to the shock-fitting methods. There have been two major families of shock-capturing schemes in use in computational fluid dynamics. Godunov method, which solves Riemann problems at the interfaces of grid cells and the arithmetical combination method of 1st - and 2nd order upwind schemes are two major families of shock-capturing schemes (Liang et al. 2007).

To simulate local supercritical flows, flows over levees (considered as broad crested weir flow) and hydraulic jumps, MIKE 21 applies selective up-winding of the convective momentum terms based on the Froude number. It damps out high frequency numerical instabilities while having little effect on the overall computation. Since it is selective, it does not affect accuracy of solutions in other areas (DHI Water, Environment & Health 2005b).

These models are preferred over 3D models where the depth of water is small compared to the spatial extents, such as flows over floodplains, coastal areas and dam-break flood modelling. Unlike the $1D^{+}$ and $2D^{-}$ models, the 2D models account for the momentum transfer during the flood wave propagation over the topography.

In addition to the finite difference solution method described above, solutions to the flooding problem can also be achieved by employing finite elements or finite volume methods.

Until recent times, the use of 2D models was limited to coastal studies mainly due to the associated high computational cost. The application of these models has extended to flood risk assessment due to the availability of high resolution digital elevation data of

floodplains and as the computing power has increased in recent times (Bates & Anderson 1993; Frazão & Zech 1999; Syme et al. 2004; Clyde Flood Strategy Team 2005; Tarrant et al. 2005; Mignot et al. 2006; Han et al. 2007; Andres et al. 2008; Frazão et al. 2008; Hartnack et al. 2008; Coulet et al. 2008; Rehman et al. 2008; Nardi et al. 2008; Paquier et al. 2008; Williams et al. 2008).

Being the most realistic flood prediction method as compared to the earlier techniques, the results from these models are often used as benchmarks for other model predictions (Villanueva & Wright 2006b). In addition to the inundation extents, this modelling approach gives additional information about the flood wave, like temporal information of the velocities and fluxes for the entire computational domain.

It should be noted that although 2D models are computationally demanding (Villanueva & Wright 2006b), they may be comparatively less demanding than storage cell models for some particular model configurations (Hunter et al. 2008). Further, even though a 2D model is more realistic than a 1D model, the results are not always better or more accurate than the results from a 1D model, if the flow in the model is predominantly 1D (Morris 1999; Wicks et al. 2004) – such as flow in a long but narrow river channel. Therefore, the choice of an appropriate modelling method needs to be made with due understanding of the flow behaviour in the model domain.

2.2.6 Nested grid 2D modelling method

For flood modelling of rural areas and areas where topography changes gradually, simulations using grids of relatively low resolution (coarser grids) such as 20 m × 20 m lead to satisfactory assessment of flooding situations although important topographic features and properties are not simulated explicitly.

Finer grid resolution results down to 1 m × 1 m enhance representation of topographical features and may lead to revelation of new flow paths and / or blockages to flow. In urban areas, features like roads, buildings, dykes and river banks can have a significant effect on the flow dynamics and flood propagation. While the bulk characteristics of the flood wave like the outflow hydrograph and percentage inundation extent may have little or no effect, the patterns of inundation, flow velocities and floodwater depths can

be directly affected (Marks & Bates 2000; Néelz & Pender 2008; Asselman, et al. 2008). In general, the results obtained using higher resolution grids provide a more realistic prediction of flow paths and characteristics of flood inundation.

However, use of high resolution grids results in a very large number of computational grid points and accordingly requires much more computing power, time and memory. Even with the Moore's law regarding the increase in computer power having been found to be true to date – and is thought to be valid for some years in the near future – resulting in substantial increase in computing power in the last decade or so (Verwey 2007), 2D and 3D flood model studies for large areas using commonly available desktop computers are currently not feasible. However, given the pace of development of computing facilities and data availability, the modelling community believes that the natural way to simulate urban flood flows – even for real-time flood forecasting – will soon be with 2D models (Fortune 2008).

Since, typically the area of main interest for a model is much smaller, many of the computational grid points are often wasted in areas of only limited interest for the model. Therefore, use of high resolution grids can be restricted to the areas of main interest and where the topographic feature representation is important. With such nested grids the high resolution grids are embedded within the low resolution grid. Thus, the use of high spatial resolution simulations can be optimised to save computer time (DHI Water, Environment & Health 2005c). The nested grid model geometry is as shown in Figure 2.11.

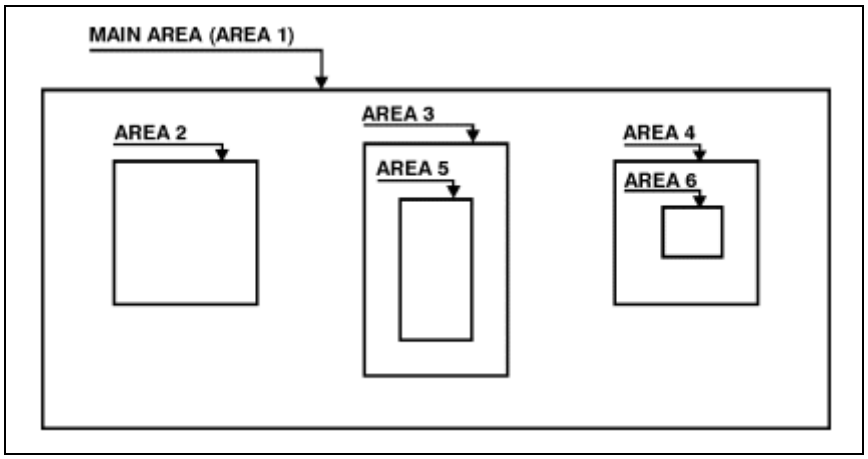

Figure 2.11: Nested grid model geometry (DHI Water, Environment & Health 2005c)

Depending on how the coarse grids and fine grids exchange boundary conditions, nested grid modelling can be undertaken using either of the two methodologies as described below:

In a simple approach, a coarse grid model is first run and the results are then subsequently used to run a fine grid model. Since in this case the grids are not coupled dynamically, no feedback from the fine resolution grid to the enclosing coarser grid can be achieved.

In an advanced approach, a fine grid is enclosed in a coarse grid ensuring dynamic coupling and, therefore, exchange of mass and momentum between the two different resolution grids at every computational time step.

As an alternative to the nested grids, various unstructured grid generating techniques exist to generate computational grids over a floodplain e. g. curvilinear grid, triangular grid. Flood modelling using these can be undertaken by solving the Shallow Water Equations, described in earlier section, over the computational domain by finite element and finite volume numerical methods. Such processes of grid generation are highly interactive and a modeller needs to spend much more time in refining the grid to be suitable for floodplain simulations.

However, automatic grid generating methods are available which rely on prescribed criteria and not on the perception of an individual. The grids can be altered or regenerated during the simulation based on prescribed criteria. This may result in further saving in computer time by reducing the number of computational grid points during certain phases of the simulation. The quadtree grid is an example of such a grid structuring technique.

Quadtree grids are created automatically by recursive subdivision of a rectangle (generally square) about discretised boundary, bathymetric or flow related seeding points. As the flow field develops, the grids may be adapted using a parameter based on

vorticity and grid cell size (Borthwick et al. 2001). Further refinements to the grids to adapt to the feature boundaries can be achieved by applying techniques like the Cartesian cut cell algorithm. This approach is found to be computationally promising as compared to the uniform grids (Krámer & Józsa 2007; Liang et al. 2007; Liang et al. 2004) but is still in development, testing and validation stage.

It should, however, be mentioned that a newer technique, Multi-cell Difference Solver, has now been developed which offers a reduction in model runtime by a factor of 5 to 10 when compared with a standard 2D finite difference solution to the Saint Venant equations. The Multi-cell Difference Solver uses a coarse scale topographical data to carry out time-varying water surface and flow velocity calculations while the fine scale topographical data is utilised when evaluating the governing equations for the 2D solver (Hartnack et al. 2008).

2.2.7 Integrated 1D2D models

The 1D and 2D modelling approaches discussed earlier have their own benefits and drawbacks.

While the 1D approach is particularly suited for relatively long river systems and areas where there has been little development on the floodplain, the use of this modelling approach for complex urban areas may result in a very complex network. This is a limitation in urban areas where manmade topographic features like roads, buildings, river banks and dykes make the floodplain flow paths extremely complex and difficult to define *a priori*. Considerable user skill is required to adequately conceptualise such models (DHI Water, Environment & Health 2005d). Two-dimensional models do not suffer from this limitation of defining flood paths *a priori*.

Flow paths in complex urban areas need not be defined beforehand for a 2D model set up. Therefore, a 2D model can be created with relative ease. However, a 2D model requires considerable computational time, although, this can be reduced by using the nested grid approach or using latest high – end computers.

The 2D modelling approach requires minimal pre– and post– processing of input and output data (Villanueva & Wright 2006b), compared to the 1D modelling approach; thus, offsetting some of the modellers time against the longer model run times. Flood inundation maps, ready to be used for various end uses can be easily extracted from the simulation results of 2D models. Further, high resolution topographical data such as that obtained from the LiDAR is now readily available in a form ready to be used with 2D models.

Therefore, to gain the fullest benefits offered by these modelling methods whilst overcoming their individual drawbacks, an integrated 1D2D modelling approach is the most obvious and logical choice. An integrated model that exchanges data between different computational engines during a simulation is the most effective way forward for flood inundation modelling (Andres et al. 2008).

There are numerous situations where flows are best described by integrated 1D2D schematisations (Verwey 2007). This can be explained better by taking a perspective view of a typical river system. In a typical river system, an urban floodplain is a relatively small part of the overall model domain. The hydraulics of the main river system is, therefore, better described by a 1D model. By coupling a small urban floodplain represented by a 2D model to the 1D model of a river, no major changes to the 1D model are required whilst the 2D model benefits by having boundary conditions that are derived from the 1D model.

The integrated 1D2D modelling approach provides a good compromise between data requirements, simulation effort, and an acceptable accuracy (Apel et al. 2007) and therefore, there is an obvious trend towards integrated 1D2D models (Tayefi et al. 2007).

However, linking of a 1D model with a 2D model is not straightforward as various linking options are possible. These linking options are detailed in the next section.

2.2.8 1D2D model linking options and significance for flood modelling

Depending on the connecting points in a river cross-section, the following four options are available for linking a 1D model with a 2D model. These linking options are shown in Figure 2.12. A 1D model can be linked with a 2D model:

1. at the river centreline or at thalweg, or
2. at the extents of the main river channel, or
3. at the extents of the floodplain, or
4. at modeller defined extents.

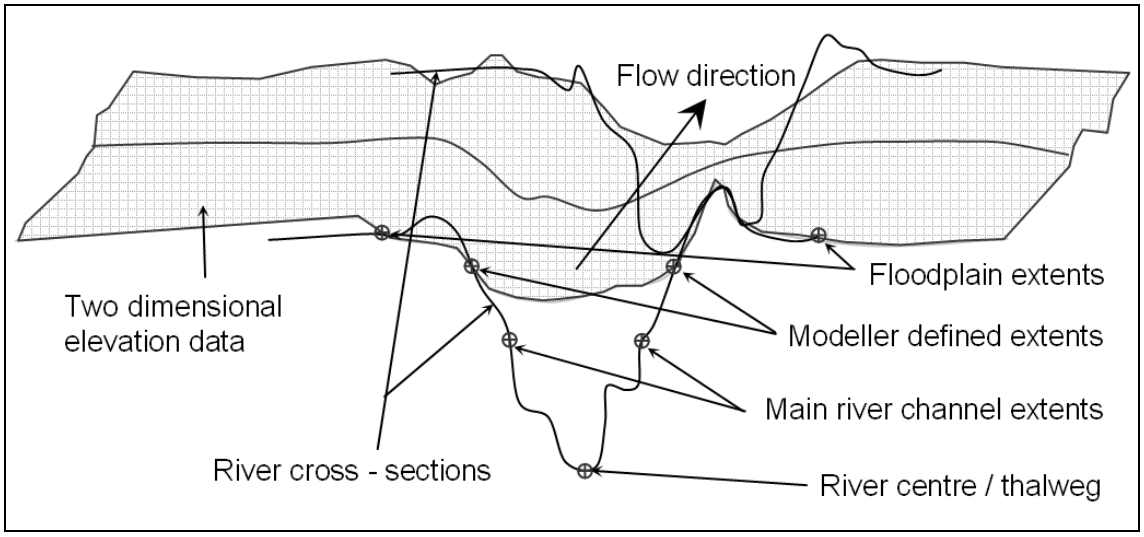

Figure 2.12: Linking options for an integrated 1D2D model configuration

A literature review for finding out which linking options out of the options listed above are commonly used in integrated 1D2D model studies did not reveal any mention of a particular linking option apart from an additional survey (Villanueva & Wright 2006a). The studies simply mention that a 1D model was linked with a 2D model or an integrated 1D2D model study was carried out.

The first option – where a 2D model is linked with a 1D model along the river centreline or along the thalweg – is not considered in the current research because when the water level in the river channel exceeds the ground elevations in the 2D model, an additional conveyance, as shown in Figure 2.13 becomes available in the 2D model.

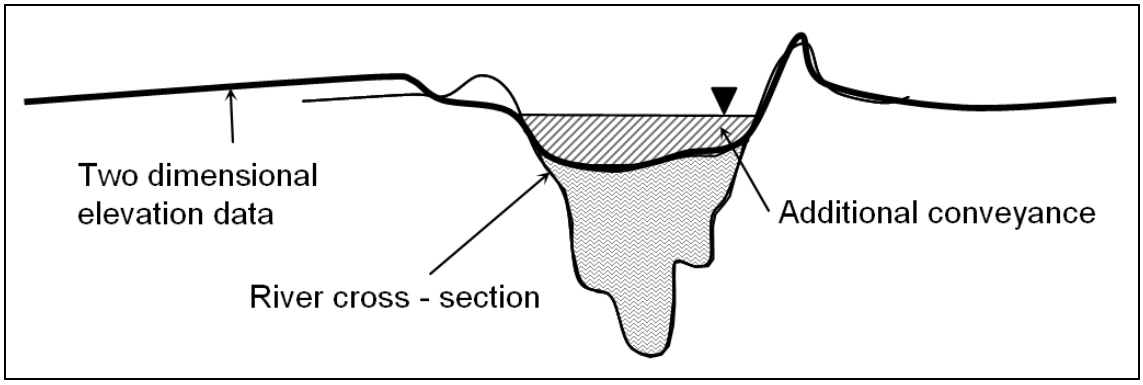

Figure 2.13: Additional conveyance availability when 2D model is linked with 1D model along the river centreline or along the thalweg

The above situation arises as, in a river corridor, the elevations in a 2D data obtained by a remotely sensed data acquisition techniques are generally higher than the elevations in a 1D data – which is acquired by ground survey and / or bathymetric survey. This leads to a 2D data profile being higher than a 1D cross-section profile (see section 2.3.1).

The conveyance is dynamic in time and depends on the water level in the main river channel and cannot be accounted for during the model runs. Thus, the predicted overbank flows on to the floodplain will be erroneous.

However, some flood modelling programs such as SOBEK-1D2D use this approach of linking a 1D model with a 2D model (Dhondia & Stelling 2002; Dhondia & Stelling 2004). In SOBEK-1D2D, the interaction between the 1D and the 2D model takes place via mutual volumes. This is achieved by combining the appropriate 1D and 2D volumes which includes the flows across banks so that they share the same water level, see Figure 2.14.

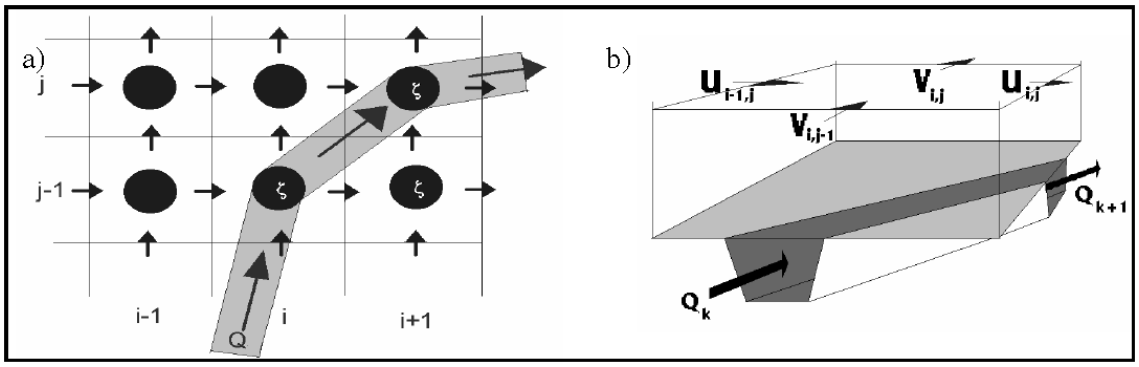

Figure 2.14: Schematisation of the SOBEK-1D2D model: a) combined 1D2D staggered grid; b) combined finite mass volume for 1D/2D computations. (Dhondia & Stelling 2002; Dhondia & Stelling 2004)

The connection between the 2D model cells and the 1D network is done as shown in Figure 2.15.

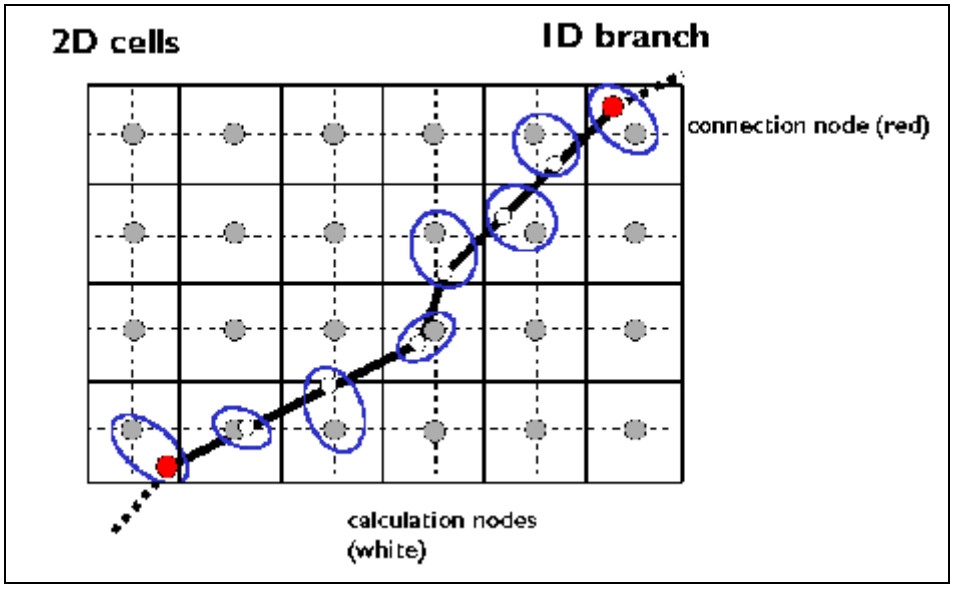

Figure 2.15: Connection between 1D and 2D models in SOBEK (Delft Hydraulic Software 2009)

For the other available model configurations described above, a 1D model is connected with a 2D model at the loci of two chosen extent points along the river channel. As shown in Figure 2.12, these points can be the extents of the main river channel, the extents of the floodplain or some modeller defined points. The extent points are fixed throughout the simulation and therefore the part of the 2D topography falling within the area defined by these extents can be excluded from the 2D calculations. This can be easily achieved by artificially raising the elevation of the area identified so that the

ground levels are well above the possible river water levels. A typical layout of such a configuration when a 1D model is connected with a 2D model at the main river channel extents is shown in Figure 2.16.

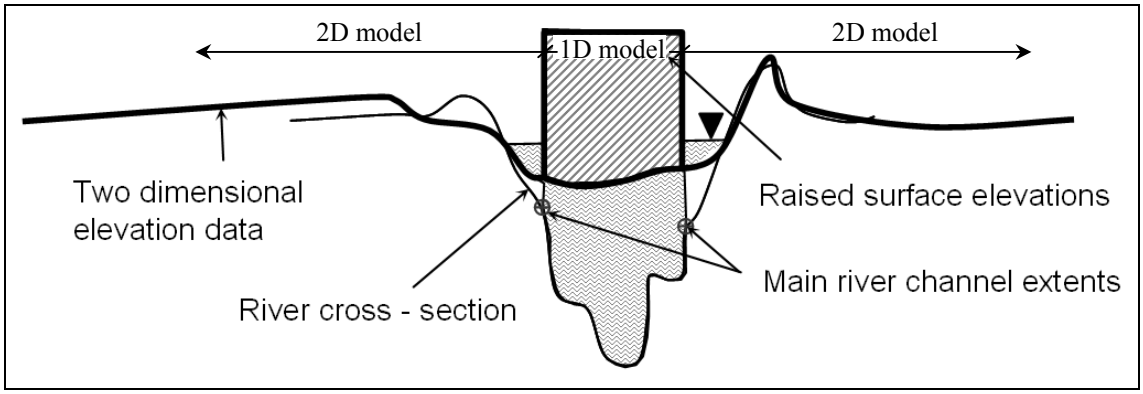

Figure 2.16: Exclusion of additional conveyance within river channel in an integrated 1D2D model

Thus, in terms of deciding on the lateral extent of the 1D model in an integrated 1D2D model setup, three options are available: first, up to the full extents of the floodplain in the 1D model survey, second to the main river channel extents determined by a walking survey and a third where the 1D model extends somewhere between the main river channel and the floodplain extents (see Figure 2.12).

However, the adjacent floodplain along a river bank between two river cross-sections is not flat but is undulating. As the 2D model will contain computational points between the cross-sections, consideration needs to be given to which elevation data is used at these points: interpolated elevations from the 1D cross-section data or elevations from the 2D topography data? This is analogous to the spill geometry in a 1D model with storage cells.

In the MIKE FLOOD software used for this research, the bank elevations or spill geometry for an integrated 1D2D model can be obtained from three different sources: from the 1D cross-section data, from the 2D topography data or the maximum of 1D cross-section data and 2D topography data. A fourth option is available where the banks are surveyed and the data used as boundaries for the 1D and 2D models. The alignment of the survey line for such a survey will need to be decided by a

reconnaissance survey. Such a methodology was employed for a test case at Upton-upon-Severn in the UK (Villanueva & Wright 2006a). This option is not considered in this research as this involves additional data collection activity and thus is not based on off-the-shelf available data. The three possibilities considered in this research are shown in Figure 2.17.

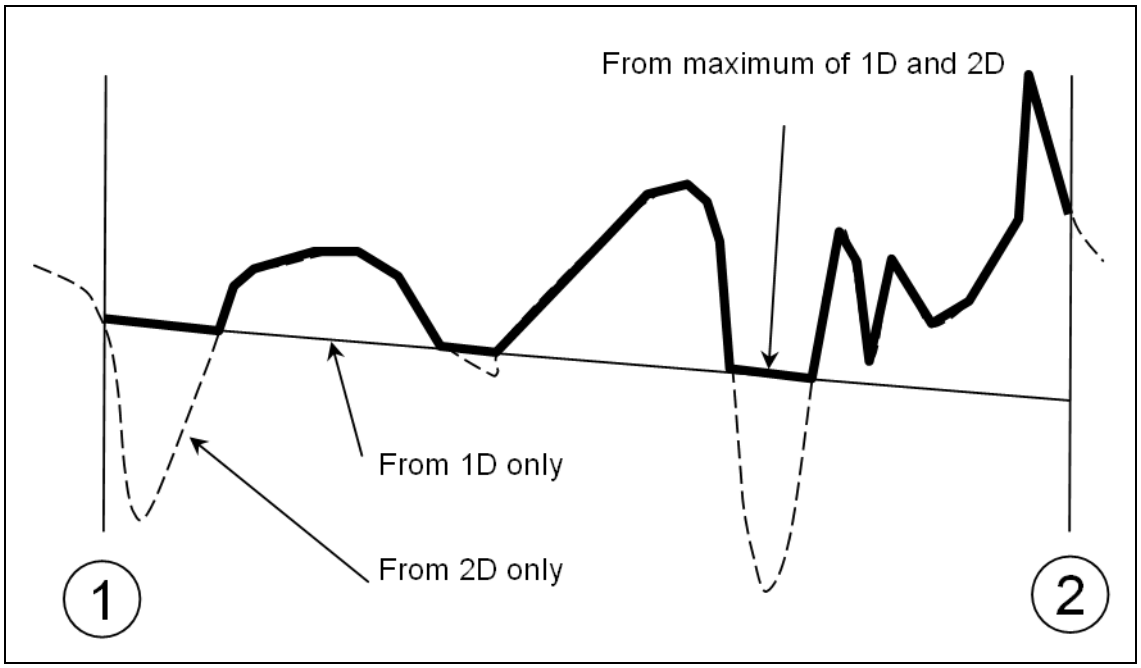

Figure 2.17: Sources for river bank elevations in an integrated 1D2D model

When the bank elevations from the 1D data only are used, the elevations along the bank are obtained from a straight line interpolation between the connecting cross-section endpoints. Thus, any information pertaining to the undulations of the bank in between the two cross-sections is not taken account of in determining the volume exchange between the two models.

If the second option of using ground level data from the 2D model is used to define the bank elevations, this can lead to significant errors in predicted exchange volumes. These arise due to errors contained in the LiDAR topographic data. Typically these can be of the order of ±150 mm on flat ground but are known to increase in locations where the underlying terrain is steep and / or heavily overgrown. Both these conditions arise close to riverbanks (see section 2.3.1).

Alternatively, in MIKE FLOOD, the bank elevations can be taken as the maximum of the interpolated bank elevation based on the 1D cross-section data and the corresponding elevation in the 2D topographic data. This option will limit the volume exchange between models and reduce the flood extent predicted on the 2D domain.

In light of the discussion above, nine possible integrated 1D2D model configurations, summarised and named as options 1 to 9 in Table 2.2, are available to a modeller.

Table 2.2: Options for linking a 1D model with a 2D model in an integrated 1D2D model setup

1D model extents	Source of lateral link elevations		
	1D data only	**2D data only**	**Maximum of the 1D and 2D data**
Floodplain extents from 1D data **Options 1 - 3**	Floodplain+1D **1**	Floodplain+2D **2**	Floodplain+1D2D **3**
Main river channel extents from inspection **Options 4 - 6**	Channel+1D **4**	Channel+2D **5**	Channel+1D2D **6**
Modeller defined extents **Options 7 - 9**	Custom+1D **7**	Custom+2D **8**	Custom+1D2D **9**

The linking options 1 – 3 in Table 2.2 pertain to the scenarios where the full widths of the surveyed cross-section data extending onto the adjoining floodplain in a 1D model is used. Part of the floodplain is, thus, simulated using a 1D model. This considerably reduces the computational burden but the detailed information regarding the flooding process of the floodplain cannot be obtained from the 2D model.

The bank levels along the floodplain are generally higher, sometimes with flood protection works. Therefore, a 1D model extending onto the floodplain-limits leads to the creation of a canal like river representation in the integrated 1D2D model. The river, thus, contains most of the flow and any spill over onto the floodplain through overbank flows is in reduced quantities as compared to the cases where the 1D model is limited only to the main river channel extents, see below.

The linking options 4 – 6 in Table 2.2 pertain to the scenarios where the 1D model extends only up to the main river channel width. Since, in these scenarios the floodplain is transferred to the 2D model, the computational burden is increased considerably. Further, it may not be a preferred option from the hydraulic point of view as the flow is predominantly 1D but a 2D model is employed for the computations. This however, leads to more realistic representation of the floodplain close to the river.

The use of above methodology may call for additional model checks to see if the integrated 1D2D model setup, particularly the 2D model, represents the river corridor adequately, e.g. representation of high river banks and any flood protection works, roughness coefficient for the floodplain, etc.

However, in practice, depending on the available data characteristics of the river corridor and adjoining floodplain data, a modeller may take a decision not to constrain the 1D model extents to the floodplain extents or to the main river channel extents and instead examine individual cross-sections and decide the extents of the 1D model at individual cross-sections along the river reach. The linking options 7 – 9 in Table 2.2 represent these scenarios.

These linking options affect representation of the left and right bank geometry in the integrated 1D2D model setup. Since the geometry of the linked bank, defined earlier as a lateral link, is used for the overbank flow computations, see section 2.2.9, the amount of overbank flow – and hence the inundation extents – obtained from the integrated 1D2D models utilising the various linking options may be different.

Discussed below is the hydrodynamics of the linking of a 1D model with a 2D model in an integrated 1D2D model setup.

2.2.9 Hydrodynamics of 1D2D linking

In an integrated 1D2D model the left and the right banks in the 1D model are linked with the 2D model. During overbank flow, the flow from the 1D model is passed into the 2D model domain through these lateral links. The river banks, thus, form the lateral boundaries of the 1D model and the inflow boundary of the 2D model.

As stated earlier, for this research MIKE 11, MIKE 21 and MIKE FLOOD software are used, see section 1.7. To calculate the flow between MIKE 11 and MIKE 21 through the lateral boundary, typically a weir structure formulation employing weir equation similar to Equation 2.14 is employed. The exercises presented in this thesis also use a weir structure formulation for the lateral links.

The MIKE FLOOD software interface allows for automated cell selection for the linking of the river bank in 1D model with the corresponding computational grid cells in the 2D model. At first, the lateral link geometry is defined based on the river centreline location and the cross-section data and then the intersected 2D cells are selected. Further, the geometry of the weir structure gets affected in view of the elevation data chosen (i.e. from 1D alone, from 2D alone or from the maximum of 1D and 2D) as described in relation with the linking options, see section 2.2.8.

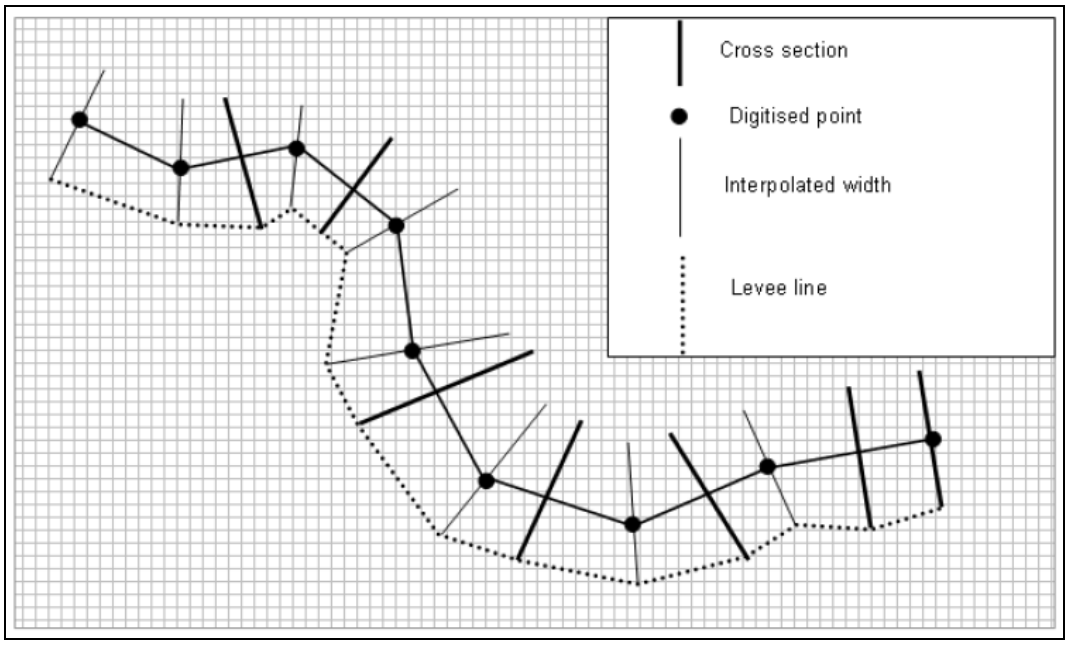

Figure 2.18: Automated lateral link definition (DHI Water, Environment & Health 2005d)

The flow thorough a lateral link represents the overtopping of the river bank or levee the magnitude of which depends on the weir equation and the water level difference between the river i.e. MIKE11 and the floodplain i.e. MIKE 21.

The flow through the lateral link is distributed into several MIKE 11 points where water level is computed (h-points) and several MIKE 21 cells. A lateral link is further subdivided into several weir substructures based on the information defining the link geometry. Interpolated water levels, based on the water levels at the MIKE 11 h-points and the corresponding MIKE 21 cells, as shown in Figure 2.19 are then assigned to these substructures.

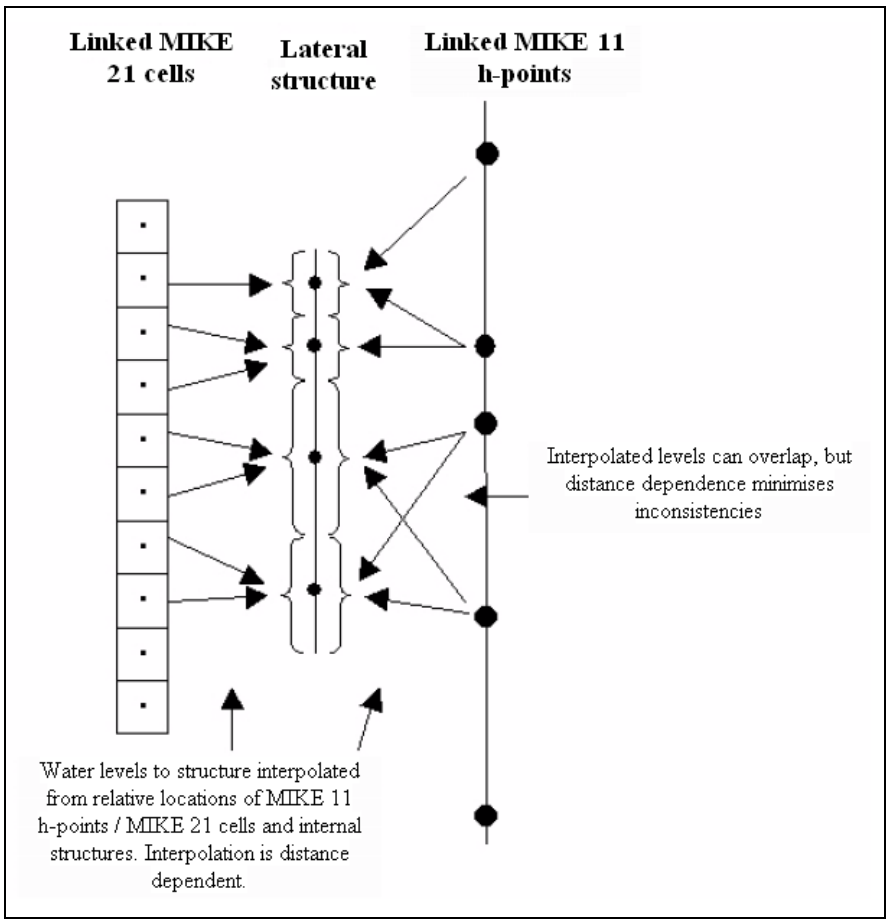

Figure 2.19: Lateral link - interpolation of water levels (DHI Water, Environment & Health 2005d)

The flow from each substructure is then distributed to / from the MIKE 11 h points and MIKE 21 cells based on its range of influence as shown in Figure 2.20. It should be noted that in this figure, the link geometry is not defined by automated linking and hence not all the linked MIKE 21 cells are intersected by the link alignment.

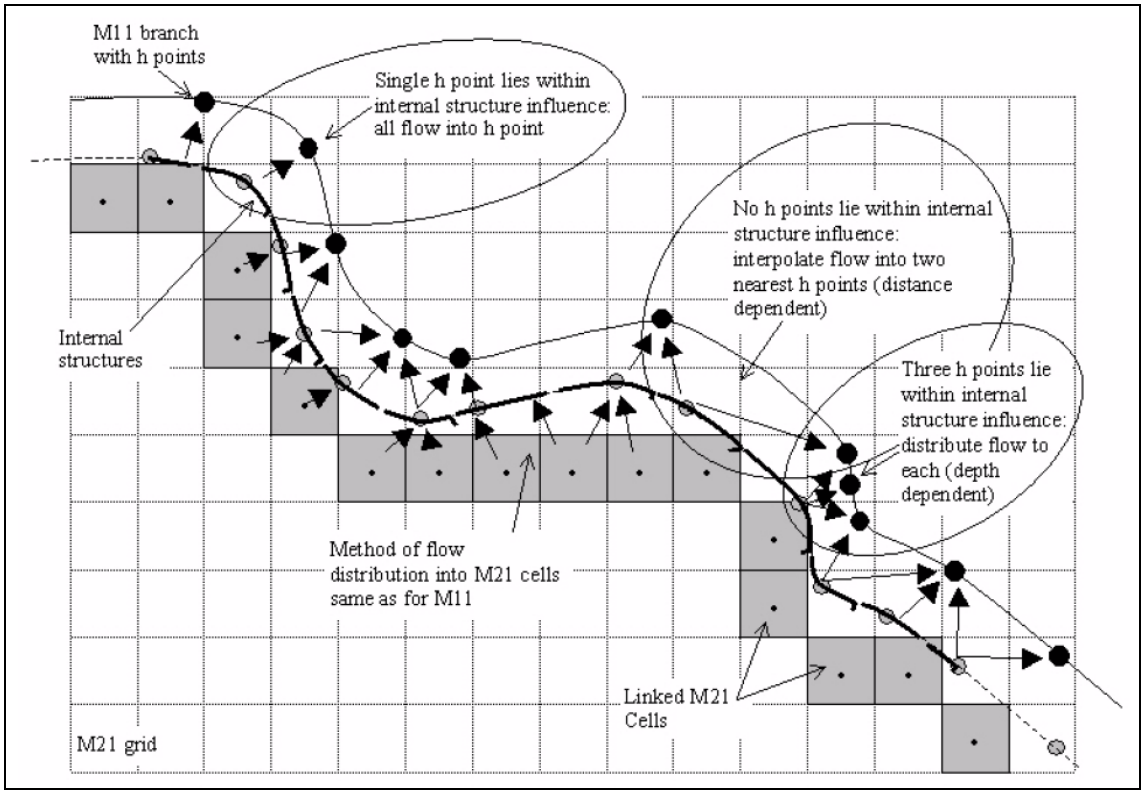

Figure 2.20: Lateral link - interpolation of flows (DHI Water, Environment & Health 2005d)

In addition to an accurate knowledge of flows, all the above modelling approaches require topographic data of the urban floodplain and the river channel. Various topographic data acquisition techniques are currently available. The quality of the data and the suitability of these for flood modelling purposes are discussed in the next section.

2.3 Topographic data for 2D flood modelling

Topographic data for flood modelling purposes can be acquired by various methods which range from ground survey to satellite imagery. Ground survey techniques are thought to be the most accurate but are uneconomical to carry out for large areas and are difficult for an inaccessible area whilst an aeroplane based data acquisition technique, LiDAR, has emerged as the preferred method of topographic data acquisition. A summary of the merits and limitations of various topographic data generating techniques is presented in Table 2.3 (Smith et al. 2006).

Table 2.3: Summary of merits and limitations of available DEM techniques (Smith et al. 2006)

Method	Merits	Limitations
Cartographic	Simple to generate if digital contours are available. Economic for large areas.	Highly dependent on the scale and quality of the base map. Does not accurately characterise low lying areas such as floodplains. Influenced by the skill of operator digitising the map.
Ground surveying	Extremely accurate. Total Stations can acquire elevations under canopy. Provides measurements for filling in voids in other datasets.	Expensive and time consuming to collect for large areas. GPS does not provide reliable heights under canopy. Access required to property for measurement of heights.
Digital Aerial Photogrammetry	It is a proven and well understood approach. Potential for high accuracies in plan and height. Provides an optical image for interpretation. Relatively economical for surveys of large areas.	Delay between acquisition of images and production of DEM. Dependant on scale and quality of imagery. Limitations in the automatic matching algorithm. Manual measurements require an experienced observer.
Interferometric SAR	Can “see” through clouds and operate day or night. Rapidly map very large areas.	Volume scattering in vegetated areas lead to poor coherence. Performance can degrade in urban areas due to bright targets and shadows. Artefacts in the DEM due to topography or atmospheric propagation.
LiDAR	Potential for high accuracy. Can generate DEM for surface with little or no texture. Could measure vegetation height when set to record first and last phase.	May require a lot of flying time for extremely large areas. Cannot operate in cloudy, rainy or windy conditions. May require complementary data, such as photo, if interpretation of points is necessary.

However, it was concluded that no one method provides the ideal solution when considering accuracy, completeness and optimum economy and therefore, fitness-for-purpose of a given data type needs to be evaluated on a project by project basis.

The LandMap DTM produced using the spaceborne repeat pass InSAR techniques, has a spatial resolution of 25 m with an accuracy ranging from a minimum of – 38 m to a maximum of + 162 m and standard deviation of approximately ± 11 m.

Shuttle Radar Topography Mission (SRTM) DTM has a vertical accuracy of approximately 16 m with a spatial resolution of 30 m within the USA and 90 m in all other areas.

Ordnance Survey LandForm Profile DTM has a vertical accuracy of ± 5 m whereas NextMap Britain InSAR has accuracies better than ± 1 m.

UK Perspectives DTM, available as 1 square kilometre tiles with 10 m grid spacing has a vertical accuracy of approximately ± 1 m.

Bluesky's Point-Z DTM, derived from a range of remote sensing methods such as aerial photography and LiDAR, is generated at 5 m spacing and has height accuracies varying from as little as 5 cm to 1 m.

A summary of the characteristics of available DEM data types generated using various data acquisition methods is provided in Table 2.4 (Smith et al. 2006)

Out of the various available DEMs, LiDAR DEM with height discrepancies better than ± 15 cm is the most suitable for floodplain modelling studies in the UK (Smith et al. 2006) although the Shuttle Radar Topography Mission (SRTM) data is also advocated to be a good source of terrain data for flood modelling globally (Sanders 2007).

Table 2.4: Summary of characteristics of generally available DEMs (Smith et al. 2006)

Available DEMs	Method of generation	Spatial resolution (m)	Vertical accuracy ± (m)	Formats	Coverage	Estimate of costs	Organisation responsible
LandMAp Elevation Data	Repeat-pass spaceborne InSAR	25	Varies (10-100)	DSM	Entire UK	Free for academics via EDINA	MIMAS www.landmap.ac.uk
SRTM	Single-pass spaceborne InSAR	90	-16	DSM	Entire UK	Free for research	JPL at NASA www.nasa.org www.edina.com
LandForm Profile	Cartographic (Digitised Contours)	10	-2.5 - 5.0	DTM	Entire UK	Free for academics via EDINA or £4.20 per 5 km×5 km	Ordnance Survey
LandForm Profile Plus	Photogrammetry LiDAR	2	0.5	DTM	Being rolled out on a needs basis	£61 - £575 per 5 km×5 km	Ordnance Survey
		5	1.0				
		10	2.5				
NextMap Britain	Airborne InSAR	5	0.5 - 1.0	DSM	England, Wales & Scotland	From £40 per sq km (or £1 per sq km via CHEST: minimum £500)	Intermap, Getmapping or BlueSky
		5 or 10	0.7 - 1.0	DTM			
LiDAR	Airborne LiDAR	0.25 - 3.0	0.05 - 0.25	DSM / DTM	Selected low lying and coastal areas	From £800 per 2 km×2 km	Environment Agency
UK Perspectives	Photogrammetry	10	1.0	DTM	England	£25 per sq km	Simmons Aerofilms Ltd. or UK Perspectives

2.3.1 LiDAR topography data types

The acquisition of Light Detection and Ranging (LiDAR) topography data is achieved by flying an aircraft equipped with a laser beam transmitter and a receiver to measure the reflections of the laser beam that is reflected off the ground surface.

The surface elevations of the area surveyed are then estimated by relating the measurements with the aircraft position data. The surface elevation data thus estimated in the first instance forms the raw data set. This raw data set is further processed to obtain the Digital Elevation Model (DEM) or Digital Terrain Model (DTM) data sets. The processes to obtain DEMs or DTMs include formatting, filtering, segmentation and object reconstruction (Smith et al. 2004).

The data produced after the processing using algorithms to filter out the presence of vegetation and man made structures like buildings from the acquired raw topography data is the Digital Terrain Model (DTM). Whereas, any buildings present in the raw data are retained while preparing the Digital Elevation Model (DEM) data.

Both of these LiDAR topography data types are now being made available for flood modelling purposes. For the flood modelling of urban areas, the flow paths of floodwaters may get significantly altered due to the presence of buildings, roads, bridges and other man made structures which are evident in the DEM data. The difference between the DEM and DTM topography data types is illustrated in Figure 2.21.

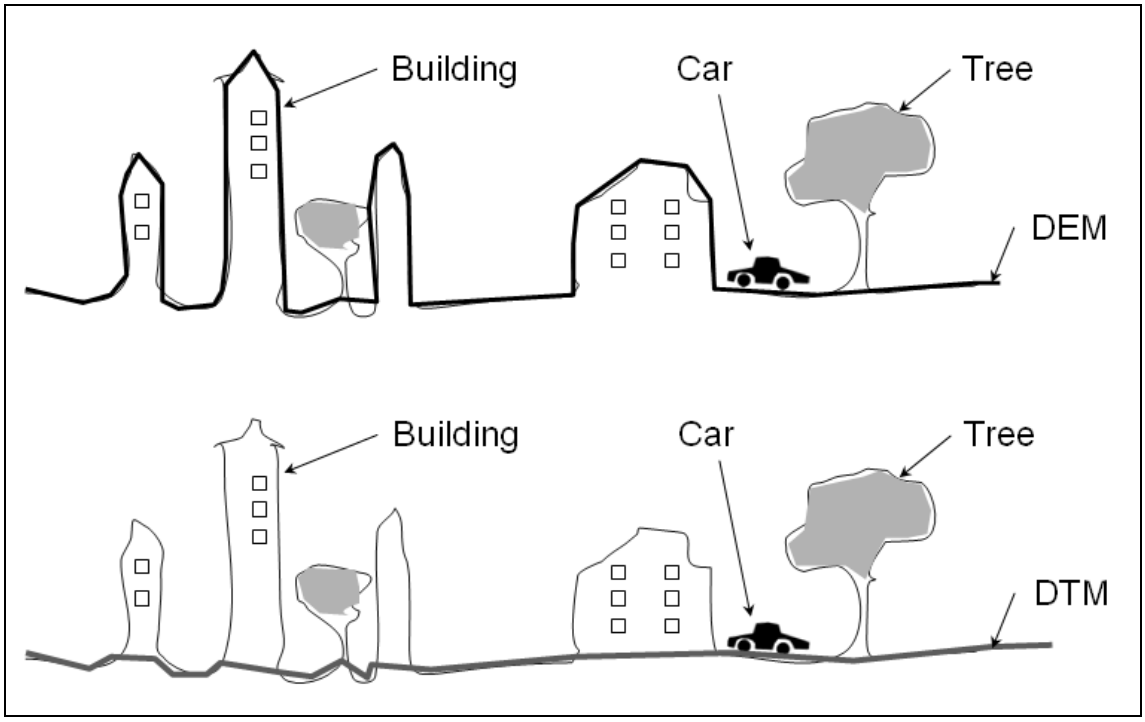

Figure 2.21: Topography data types - DEM and DTM

It should, however, be mentioned that the elevation data within riverbanks obtained by LiDAR survey represents the river water levels at the time of the survey as laser rays are reflected by water surface. Therefore, the elevations in 2D data are higher than the elevations in the 1D cross-section data (see Figure 2.13 above) along river corridors. The elevations near the banks are also erroneous due to the presence of vegetation and steep banks and the differences can range up to a meter (Néelz et al. 2006; Villanueva & Wright 2006a). A further discussion about the significance of the accurate representation of bank levels is presented by Villanueva and Wright (Villanueva & Wright 2006a).

2.4 Summary

To reduce the potential loss of life and damage to property and possessions, computer based studies or physical model studies can be undertaken. As physical model studies are complicated given the time, cost and effort required to carry out these types of studies, computer modelling studies using zero-dimensional (0D), one-dimensional

(1D), two-dimensional (2D), three-dimensional (3D) mathematical modelling methods and combinations thereof are preferred.

This chapter detailed the various computer modelling methods, tools and topography data types which can be used for detailed flood risk assessment of urban floodplains.

The research aims and objectives in view of the current state-of-the-art computer modelling and available topography data are justified and defined as well as the research methodology detailed in the next chapter, Chapter 3, "Research Aims, Objectives and Methodology".

Chapter 3
Research Aims, Objectives and Methodology

3.1 Introduction

The ability of computer models of rivers to predict future scenarios of flooding means that they are often used to support flood risk assessments, where temporal changes in risk are an important component of the analysis. For an organisation or agency commissioning such a study the cost of modelling, comprising software licences, modellers' time and data collection are important factors. The cost of modelling increases with the size and complexity of the area to be modelled as these directly influence the time required for pre– and post– processing of data, assembling and running the model and the computer processing power needed to undertake successful simulations.

In recent years there have been significant developments in remotely sensed data collection techniques to obtain detailed Digital Elevation Models (DEMs) of river floodplains. Methods in common use now include Light Detection and Ranging (LiDAR) and Synthetic Aperture Radar (SAR), see section 2.3 for a review of this technology. The availability of this data has driven a change from traditional 1D modelling, see sections 2.2.2 and 2.2.3, to more sophisticated 2D methods based on numerical solutions to the shallow water equations, see sections 2.2.4 and 2.2.5.

There is no doubt that such models provide significantly more information in terms of the timing and detail of floodplain inundation, however, the successful implementation of the method and interpretation of the resulting predictions raises significant practical issues.

The aim of the research is to investigate these practical aspects surrounding 2D modelling of floodplains, focusing on issues surrounding:

1. model validation,

2. model grid resolution and topography data types, and

3. comparison of 2D model predictions with 1D model predictions

The latter is significant as considerable savings in the costs of modelling can be achieved if new modelling studies are built on the previous models of the urban floodplain in the location of interest (Pitt 2008a). As until relatively recently most modelling studies were 1D, the effective integration of 2D methods with existing 1D models is an important issue.

3.2 Research objectives and methodology

3.2.1 Model validation

As mentioned previously (see sections 2.2.2 and 2.2.3), computer models using the 1D method have been used successfully for numerous modelling exercises for flood risk assessment worldwide. Therefore, a validation exercise of 1D model used for this research MIKE11 was not considered to be necessary. Since 2D modelling of flooding on urban floodplains is an important part of this research, and a limited number of simulations of floodplain inundation using 2D models have been carried out so far, a validation exercise for the 2D mathematical modelling software used for this research, MIKE 21, is carried out to assess the ability of the software to accurately model flooding of urban floodplains.

Ideally, validation of the 2D models would be undertaken by comparing model predictions with observed field data. However, such a dataset was not available for this research. Therefore, the validation was undertaken by comparing model predictions with experimental physical model observations. The physical model used was of the Toce River in Italy (Testa et al. 2007). One advantage of using physical model data rather than field data for validation is the data available is generally of a higher quality and collected at a greater number of locations than is typically the case for field data. Unfortunately, the data set available only contained measured variations of water level on the floodplain, meaning validation of model velocity predictions was not possible.

The software validation exercise is carried out by comparing the observed experimental data from the model studies of the Toce River with the computer model predictions. The details of this exercise and the results and the conclusions are described in the next chapter.

3.2.2 Model grid resolution and topography data types

The spatial resolution of LiDAR data that is available for flood modelling purposes ranges from 0.25 m to 3.0 m, see Table 2.4. However, since the grid size chosen affects the quality of the predictions and the computational resources required, see section 2.2.6, consideration needs to be given to the choice of the appropriate spatial resolution used while undertaking flood modelling. This may involve resampling of the originally available LiDAR topography data or the use of nested grid models instead of regular grid models. Thus, an evaluation of the effect of grid size on the model predictions is one of the objectives of the research.

For 2D flood modelling purposes it is necessary to have access to a suitable Digital Elevation Model (DEM) or a Digital Terrain Model (DTM). When a DEM is used, the buildings contained within the elevation model and through the inclusion of elevated areas in the grid act as obstacles to the flow. In such circumstances, water is not stored in the area covered by the buildings nor is any conveyance capacity provided through these grid cells. Whereas, when a DTM data is used, floodwaters find additional conveyance and storage capacity in the areas covered by the buildings. Thus, an evaluation of the effect of using DEM and DTM topography data on the model predictions is one of the objectives of the research.

During flooding of an urban area, when the water level rises above the threshold of the buildings, it will enter through openings like doors, windows, cracks in the outer walls, ventilation openings and other gaps. The floodwater that enters the building may exit from other similar flow routes. Thus, buildings allow storage of as well as reduction of velocity of floodwaters while it passes through them. Therefore, lower water depths and velocities are expected when buildings are considered as water storage areas as opposed to when considered as being obstacles to flow. Thus, an evaluation of the

effect of considering buildings as water storage areas on the flood modelling predictions is one of the objectives of the research.

The effect of considering buildings as storage areas can be simulated by introducing a porosity term in the computation code or by applying a higher resistance to the area representing the buildings (Guinot & Soares-Frazao 2006; Frazão et al. 2008; Sanders et al. 2008).

The porosity accounts for the restriction in (i) the area locally available to mass and momentum storage and (ii) the mass and momentum fluxes in both directions of space. Shallow water models with porosity allow the influence of urbanized areas on the flow to be represented using the statistical property of the urban network without the need for a detailed description of the urban geometry and the subsequent mesh refinement, particularly so when the urban area influences the flow characteristics but the flow details wherein are of no direct interest i.e. local variations in water levels, etc. in the porous domain and when preferential flow paths do not exist (Guinot & Soares-Frazao 2006).

Porosity can be defined as the fraction of the cross-section available to the flow i.e. conveyance porosity and fraction of the plan view available to the flow i.e. storage porosity (Frazão et al. 2008).

A modified shallow water equation solver using conveyance porosity was proposed and successfully validated by applying the formulation to Toce River model laboratory observations demonstrating an advantageousness of replacing refined models with coarser models with porosity implying lower computational costs (Guinot & Soares-Frazao 2006).

This solver subsequently was modified to account for the storage porosity and validated for the Toce River model case (Frazão et al. 2008). However, this particular application considered the values of the conveyance porosity and the storage porosity to be identical. The use of this approach in terms of accuracy and computational time were found to be comparable to the higher friction approach. However, as porosity

parameters are related to the geometrical properties of the urban area, these, thus, are not subject to calibration, contrary to the higher friction approach, which needs calibration (Frazão et al. 2008).

Storage porosity can also be termed as volumetric porosity. The conveyance porosity is also termed as areal porosity defined as fraction of plane slicing an urban area. The areal porosity is, thus, direction dependent or anisotropic which depends on the direction of the plane making it important in urban floodplains where identification of preferential flow paths is important (Sanders et al. 2008). The use of both volumetric porosity and the areal porosity using an anisotropic flow model yielded promising results in the Toce River model test case (Sanders et al. 2008).

Further research in this area includes investigation of applicability to real scales, validity of the porosity parameters at a larger scale (Frazão et al. 2008) and the possibility of estimating the porosity parameters directly from the remotely sensed data (Sanders et al. 2008).

Since the 2D modelling software MIKE 21 used in this research does not have porosity term implemented in the computational scheme (DHI Water, Environment & Health 2005b) and estimating a higher resistance value does not require any additional data or effort, the effect of considering buildings as porous media was simulated in this research by applying a very high resistance value at the building footprints to study any effect on the floodwater depths and velocities.

Studies in line with the above mentioned research objectives are carried out in the first instance by using prototype scale hypothetical urban topographies which represent complex geometries of typical urban district. The details of these exercises and the results and conclusions are described in Chapter 5, “Hypothetical Urban Topography Study”.

The research findings are further validated by using data for an urban floodplain case study area adjoining the River Clyde in Glasgow City, UK. These exercises and the results and conclusions are described in Chapter 6, “Glasgow City Case Study”.

3.2.3 Comparison of 2D model predictions with 1D model predictions

Further to the discussion in section 3.1 above, comparison of the predictions obtained from integrated 1D2D models with those obtained from $1D^+$ models is the most important issue surrounding the justification of using 2D models in general and integrated 1D2D models in particular for Strategic Flood Risk Management (SFRM).

While configuring an integrated 1D2D model, a modeller has various choices for locating the linking elements, see section 2.2.8 for the details of these options and Table 2.2 for a summary of these options.

Thus, investigating the practical aspects of linking an existing 1D model with a newly constructed 2D model that is based on the latest available LiDAR topography data is one of the objectives of this research.

To achieve this, integrated 1D2D models are constructed and simulations carried out using data for an urban floodplain adjoining the River Clyde in Glasgow City, UK.

The predictions from the 1D2D models are compared with the predictions obtained by using a $1D^+$ model. The details of this exercise and the results and conclusions are described in Chapter 6, "Glasgow City Case Study".

3.2.4 Computing resources

As discussed earlier, see sections 2.2 and 3.1, the cost of computing is a major concern when 2D flood modelling studies and particularly integrated 1D2D flood modelling studies are undertaken as it affects the project costs and timelines. Thus, to evaluate the viability of undertaking such a study using typical desktop computing facilities is one of the objectives of this research.

The research is carried out using a moderately costing desktop computer installed with Microsoft Windows XP Professional Version 2002 operating system and the following configuration:

Processor: Intel® Core2™ CPU 6400 - Clock Speed 2.13 GHz, L2 Cache 2 MB

Memory: 2.00 GB

Further, the default maximum size, 2 GB of the page file - which is a reserved portion of the computer hard disk and is used as an extension of random access memory - was set to a custom size of 3 GB. It should also be mentioned that although the computer is installed with a dual core processor, the version of the MIKE 21 software was not upgraded to utilise the two processors simultaneously. It has since been upgraded and therefore a lower model runtimes than the ones reported in this research are now achievable.

All the simulations were undertaken while no other programs were running.

3.2.5 Summary

The research study has the following objectives:

1. To investigate if 2D computer models of urban floodplains can accurately predict measured water levels obtained from physical model studies.

2. To investigate the effect of 2D grid size and topographic data type on flood inundation predictions.

3. To investigate the consequences of representing buildings as areas of high roughness in the computer grid.

4. Compare the benefits of using 1D2D models to predict urban floodplain inundation compared with predictions obtained from $1D^+$ models.

5. Investigate the significance on the selection of the location of 1D to 2D model links on flood volume transferred between models and the consequence of this to predicted inundation extents.

6. To investigate if integrated 1D2D model studies for a typical urban floodplain can be carried out using typical desktop computing facilities.

Chapter 4
Simulation of Laboratory Experimental Observations

4.1 Introduction

As mentioned in the research methodology, see section 3.2.1, since 2D modelling of flooding in urban floodplain is an important part of this research, a validation exercise for the 2D modelling software used for this research, MIKE 21, has been carried out. This attempts to assess the ability of the software to model flooding of urban floodplains accurately by comparing model predictions with measured reduced scale physical model data.

The physical model data used consist of observations of water levels for a flash flood flow experiment in a simplified urban district in a river valley (Testa et al. 2007). The data is detailed in sections 4.3 to 4.4. The purpose of carrying out the experiments and publishing the data was to provide a data set, which can be readily used for validation of mathematical models of flood propagation in urban areas (Testa et al. 2007). The data was published in an electronic format, ready for use in computer model validation exercises. This chapter details the data used, simulations carried out and the findings of the study.

4.2 Other validation exercises

The mentioned dataset was used for testing a modified Harten-Lax-van Leer (HLL) solver for the solution of modified two-dimensional shallow water equations with porosity on unstructured grids (Guinot & Soares-Frazao 2006; Frazão et al. 2008). Further, a Godunov-based scheme with an adaptive scheme of slope limiting and variable reconstruction further modified to solve porous shallow water equations was validated (Sanders et al. 2008) using the dataset being used in this study.

4.3 Experimental setup

The experimental set up is arranged and managed by Centro Elettrotecnico Sperimentale Italiano, (CESI) at its facilities in Milan, Italy. The *original topography* comprises a 50 m long reduced scale (1:100) concrete physical model of a 5 km reach of the Toce River valley located in the Northern Alps, Italy with topographical resolution of 5 cm. A feed tank is located at the upstream end of the model. The origin for the set up is arbitrarily located close to the right downstream corner of the feed tank and all spatial data references use this origin. Figure 4.1 shows a general view of the physical model looking upstream.

Figure 4.1: General view of Toce River Valley physical model looking upstream (Alcrudo et al. 2003)

Flooding of the model is achieved by raising the water level in the feed tank. The feed tank is fed by an electrically driven and electronically controlled variable-discharge pump. Figure 4.2 shows the upstream end of the physical model.

Figure 4.2: Upstream end of the model (Frazão & Zech 1999)

Experiments were carried out with two urban district layouts – *aligned* and *staggered*. In both the cases, buildings are represented by 15 cm concrete cubes. In the *aligned* case, buildings are placed in the channel in rows approximately parallel to the main axis of the valley and hence, approximately aligned with the flow direction. In the *staggered* layout, buildings are placed in the channel in a checker board configuration. Figure 4.3 shows the upstream part of the physical model with the *aligned* layout. In addition to the concrete blocks representing buildings, this figure also shows the pump discharge pipe feeding the upstream feed tank.

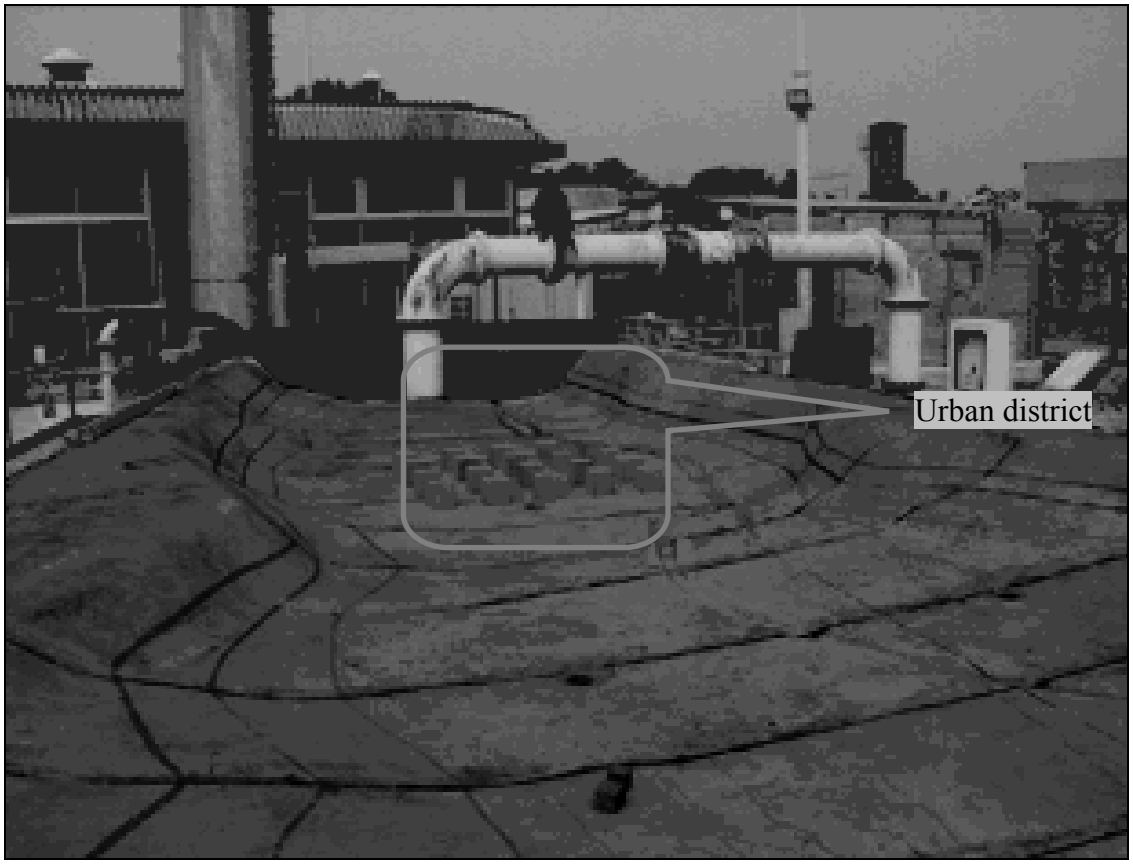

Figure 4.3: Upstream part of the original topography showing model buildings (aligned city layout) (Alcrudo et al. 2003)

In a modified test setup, in order to separate the effects due to the valley topography on the flood wave from those caused solely by the urban district, two masonry walls parallel to the main axis of the valley (thus providing a channelling effect on the flow) are placed in the *original topography* of the physical model as shown in Figure 4.4.

Figure 4.4: Modified topography by placement of two masonry walls (staggered city layout) (Alcrudo et al. 2003)

While placing the two masonry walls, the physical model was stretched upstream with a concrete slab that protrudes a few centimetres into the feed tank. The characteristics of the masonry walls are summarised in Table 4.1.

Table 4.1: Characteristics of the masonry walls

Left wall	Length = 4.788 m Height = 0.3 m X_1 = 0.941 Y_1 = 7.548	Angle with X axis = -6° X_2 = 5.701 Y_2 = 7.022
Right wall	Length = 5.287 m Height = 0.3 m X_1 = 0.208 Y_1 = 5.855	Angle with X axis = -8° X_2 = 5.445 Y_2 = 5.128

As stated earlier, buildings in the urban district are represented by 15 cm side cubic concrete blocks. The actual number and position of the buildings depends on the topography and layout used as detailed below:

4.3.1 Original-aligned layout

This setup comprises 20 buildings placed in the *original* topography as shown in Figure 4.5. Buildings are numbered consecutively starting at the bottom left and then proceeding first upwards and then rightwards. Hence first column in the figure comprises buildings 1 to 5, second column buildings 6 to 10 and so on. The building numbers are shown inside the buildings (dark black squares). The numbered crossed circles in the figure show the probe locations, details of which are discussed in section 4.3.5.

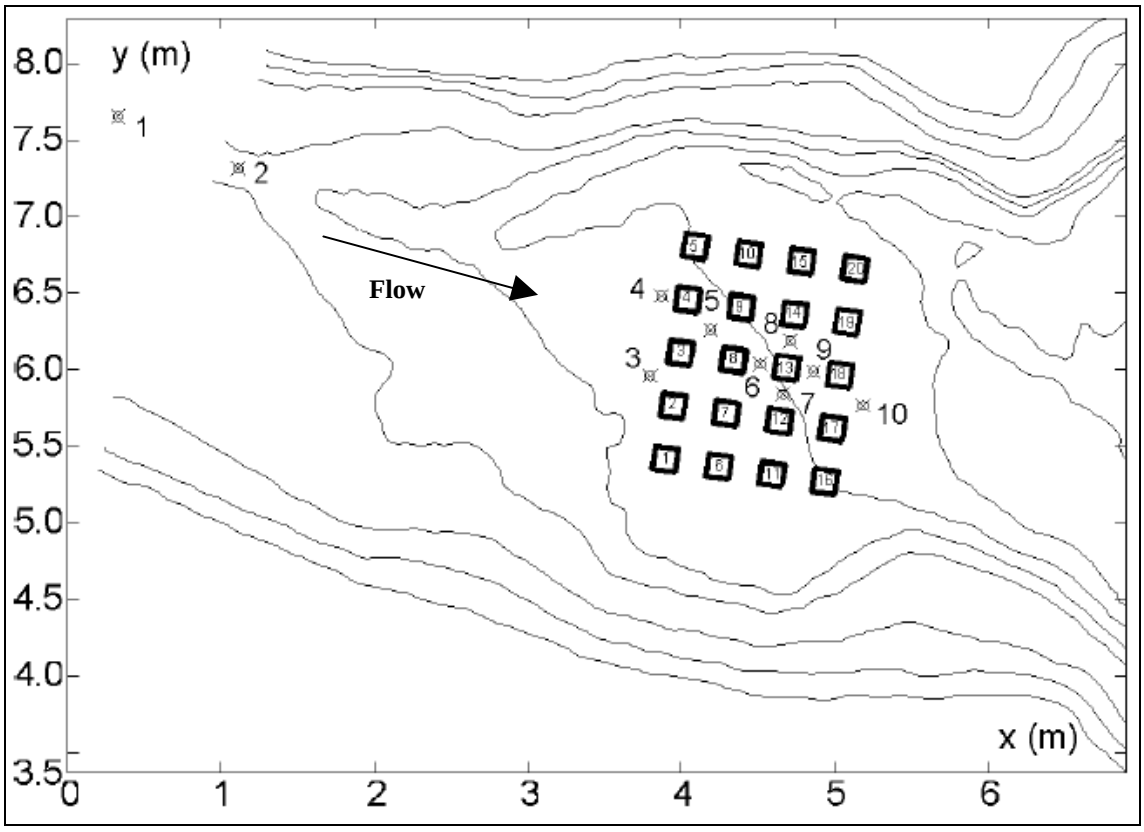

Figure 4.5: Urban district layout (original - aligned case) (Testa et al. 2007)

4.3.2 Original-staggered layout

Taking the above Figure 4.5 as reference, the *staggered* arrangement is obtained by displacing the second and fourth rows (buildings 6 - 10 and 16 - 20) parallel to

themselves in the (nearly) vertical direction by approximately one block. In order to keep a symmetrical pattern, buildings 10 and 20 are, therefore, eliminated in the *staggered* layout.

4.3.3 Modified-aligned layout

In the *modified topography*, the space available for the buildings is narrower due to the existence of the walls. Therefore, the buildings closer to the right wall are removed. Thus, the *modified-aligned* setup comprises 16 buildings with buildings 1, 6, 11 and 16 removed. The *modified-aligned* layout is shown in Figure 4.6.

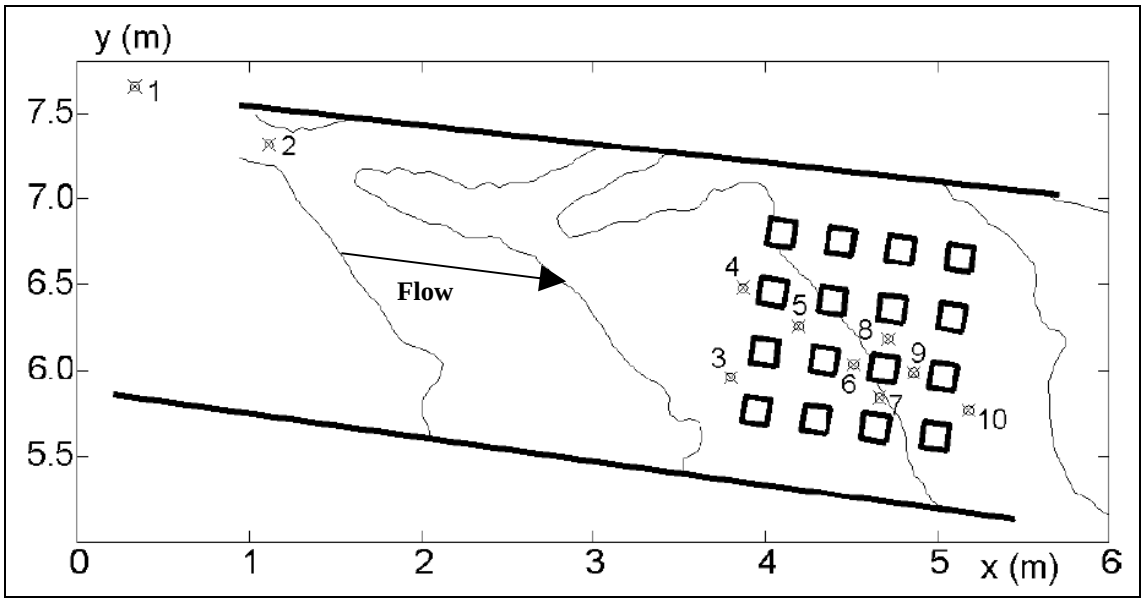

Figure 4.6: Urban district layout (modified- aligned case) (Testa et al. 2007)

The coordinates of the four corners of the buildings for *modified-aligned* layout are as given in Table 4.2.

Table 4.2: Coordinates of building corners (Modified - aligned geometry)

	Building No. 2		Building No. 3		Building No. 4		Building No. 5	
	X (m)	Y (m)	X (m)	Y (m)	X (m)	Y (m)	X (m)	Y (m)
1st corner	4.010	5.677	4.058	6.023	4.107	6.370	4.156	6.717
2nd corner	4.030	5.825	4.079	6.172	4.128	6.519	4.177	6.865
3rd corner	3.882	5.846	3.931	6.193	3.979	6.539	4.028	6.886

	Building No. 2		Building No. 3		Building No. 4		Building No. 5	
	X (m)	Y (m)	X (m)	Y (m)	X (m)	Y (m)	X (m)	Y (m)
4th corner	3.861	5.698	3.910	6.044	3.958	6.391	4.007	6.738
	Building No. 7		Building No. 8		Building No. 9		Building No. 10	
	X (m)	Y (m)	X (m)	Y (m)	X (m)	Y (m)	X (m)	Y (m)
1st corner	4.356	5.628	4.405	5.975	4.454	6.321	4.502	6.668
2nd corner	4.377	5.777	4.426	6.123	4.474	6.470	4.523	6.816
3rd corner	4.229	5.798	4.277	6.144	4.326	6.491	4.375	6.837
4th corner	4.208	5.649	4.256	5.996	4.305	6.342	4.354	6.689
	Building No. 12		Building No.13		Building No.14		Building No. 15	
	X (m)	Y (m)	X (m)	Y (m)	X (m)	Y (m)	X (m)	Y (m)
1st corner	4.703	5.579	4.751	5.926	4.800	6.273	4.849	6.619
2nd corner	4.724	5.728	4.772	6.075	4.821	6.421	4.870	6.768
3rd corner	4.575	5.749	4.624	6.095	4.673	6.442	4.721	6.789
4th corner	4.554	5.600	4.603	5.947	4.652	6.294	4.700	6.640
	Building No. 17		Building No.18		Building No.19		Building No. 20	
	X (m)	Y (m)	X (m)	Y (m)	X (m)	Y (m)	X (m)	Y (m)
1st corner	5.049	5.531	5.098	5.877	5.147	6.224	5.195	6.571
2nd corner	5.070	5.679	5.119	6.026	5.168	6.372	5.216	6.719
3rd corner	4.922	5.700	4.970	6.047	5.019	6.393	5.068	6.740
4th corner	4.901	5.552	4.950	5.898	4.998	6.245	5.047	6.591

4.3.4 Modified-staggered layout

As in the above case, the buildings closer to the right wall are removed as are buildings 10 and 20 in order to keep a symmetrical pattern. Thus, the *modified-staggered* setup comprises 14 buildings. The *modified-staggered* layout is shown in Figure 4.7.

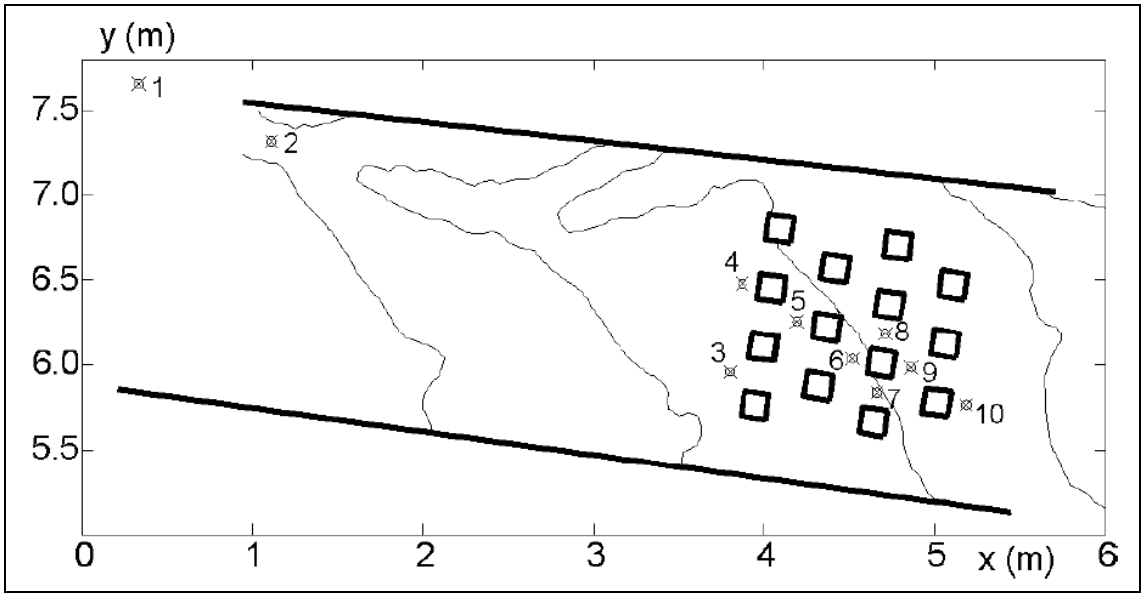

Figure 4.7: Urban district layout (modified- staggered case) (Testa et al. 2007)

The coordinates of the four corners of the buildings for *modified-staggered* layout remain the same as those in the *modified-aligned* layout except for buildings in the second and fourth row and are as given in below.

Table 4.3: Coordinates of building corners (Modified - staggered geometry)

	Building No. 7		Building No. 8		Building No. 9	
	X (m)	Y (m)	X (m)	Y (m)	X (m)	Y (m)
1st corner	4.381	5.801	4.429	6.148	4.478	6.495
2nd corner	4.401	5.950	4.450	6.297	4.499	6.643
3rd corner	4.253	5.971	4.302	6.317	4.350	6.664
4th corner	4.232	5.822	4.281	6.169	4.329	6.516
	Building No. 17		Building No. 18		Building No. 19	
	X (m)	Y (m)	X (m)	Y (m)	X (m)	Y (m)
1st corner	5.074	5.704	5.122	6.051	5.171	6.397
2nd corner	5.095	5.853	5.143	6.199	5.192	6.546
3rd corner	4.946	5.873	4.995	6.220	5.043	6.567
4th corner	4.925	5.725	4.974	6.072	5.023	6.418

4.3.5 Location of water depth probes

Electrical conductivity probes at selected locations in and around the urban district are placed to record the water depth history for each run. The location of the probes were conceived to observe the flow characteristics at the front arrival line (the first row of the houses), in the middle streets and at the wake of some buildings.

Probe 1 is located inside the feed tank whereas Probe 2 is at the entrance of the model and gives information about the flood hydrograph entering the valley. Probes 3 and 4 are placed just upstream of the first row of buildings and will first detect the arrival of the flood, while Probe 5 is amidst the main or central street. Probes 6, 7, 8 and 9 are located around building number 13. Finally Probe 10 lies at the downstream end of one of the streets parallel to the valley axis in the *aligned* layout, or in the wake of building 17 in the *staggered* one.

The locations of the probes are kept fixed irrespective of the topography type or urban district layout type.

The coordinates of the location of water depth probes are as given in Table 4.4 below.

Table 4.4: Coordinates of water depth probes

Probe	X (m)	Y (m)	Probe no.	X (m)	Y (m)	Probe no.	X (m)	Y (m)
1	0.331	7.655	2	1.111	7.317	3	3.797	5.959
4	3.870	6.479	5	4.192	6.257	6	4.514	6.035
7	4.663	5.837	8	4.712	6.184	9	4.861	5.986
10	5.183	5.764						

The electric conductivity probes along with the supporting spars are visible in Figure 4.4 and Figure 4.8. The probe locations are also shown in Figure 4.5 to Figure 4.7.

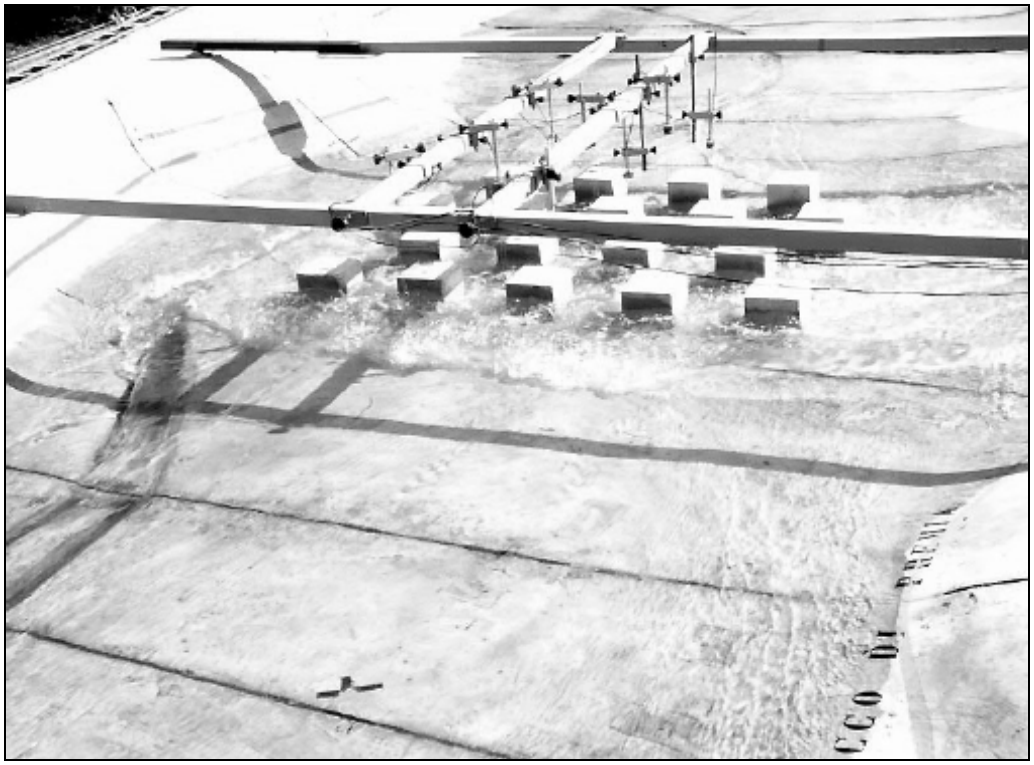

Figure 4.8: A typical run on the original topography with staggered city layout (Alcrudo et al. 2003)

The probes are used to record water depths for approximately 60 s at 0.2 s intervals for each of the physical model runs.

The boundary conditions for the model setup are described below:

4.3.6 Initial condition

The experimental team recommends that the initial condition of the models can be considered as dry, although in some cases the presence of a very thin film of water or moisture wetting the concrete bed was observed.

4.3.7 Upstream boundary condition

Pump discharge into the feed tank with time is known. The experimental team took care to ensure that the water level in the feed tank was equal to the level of the inlet section prior to the pump start up. The experimental team, therefore, suggests that the pump flow can be assumed to be a reasonable approximation to the total discharge entering the model valley through its upstream end; but also observes that this may not be exact at the beginning of the test as water level in the tank rises by a few cm while

water flows into the model. The water level in the feed tank represents an approximation to the total head of the flow down the channel. The flow distribution across the inlet section is unknown. The angle of inflow velocity relative to the X-axis (α_{inflow}) is equal to -23.5°.

The experimental team tested three different inflow hydrographs of *Low, Medium* and *High* relative peak discharge intensities for the four topographies viz. *original-aligned, original-staggered, modified-aligned* and *modified-staggered*. Figure 4.9 shows the three inflow hydrographs as measured by the flow through the pumps corresponding to the *original* topography with the *staggered* building layout.

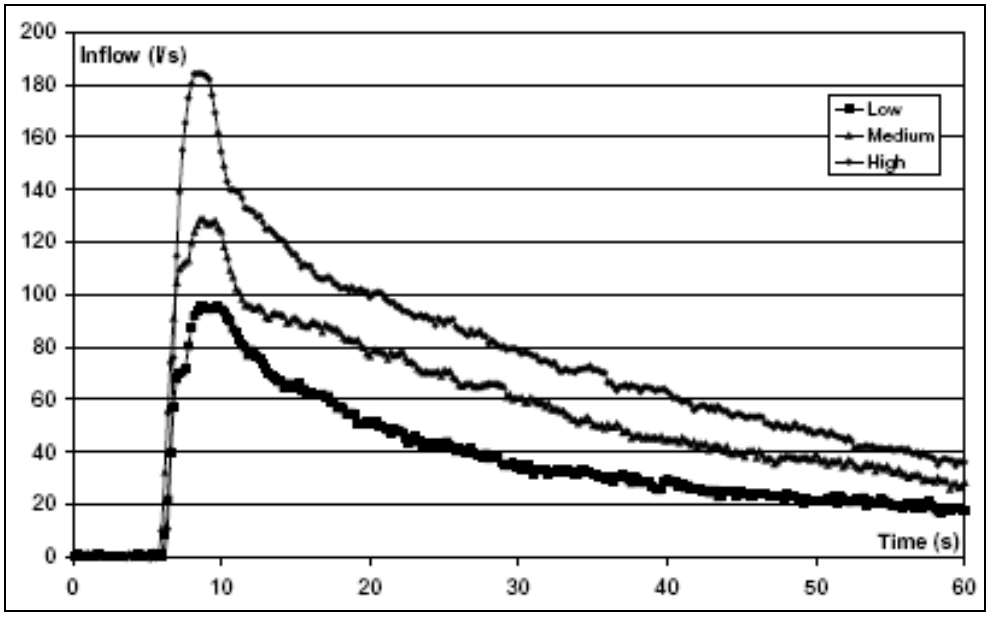

Figure 4.9: Inflow hydrographs corresponding to the original topography with staggered building layout (Testa et al. 2007).

4.3.8 Downstream boundary condition

For these runs, only 5 m out of the available 50 m long region close to the upstream end of the channel was used. Thus, the physical model extends some 45 m downstream of the urban district area. The flow leaves the urban area in mixed sub / supercritical conditions.

4.4 Details of laboratory runs, data recorded and observations

The experimental team carried out a total of 12 experimental runs – two topographies times two city layouts times three inflow hydrographs – using *original* as well as *modified* topographies for both *aligned* and *staggered* urban district layouts.

As stated earlier, pump discharge into the feed tank is known with time. The 10 probes recorded water levels for approximately 60 s at 0.2 s intervals for each of the runs.

The experimental team observed that, regardless of the topography and the city layout, the flow pattern showed an almost standing, strong hydraulic jump located at the upstream end of the city (the first row of houses). This jump propagated very slowly in the upstream direction until its intensity diminished with time according to the inflow discharge.

Though it can be said that the building density in the experiments is high enough to make the city appear as a compact obstacle to the main flow, the experimental team observed that the intensity of the almost standing hydraulic jump in front of the city did not depend on the structure of the city layout.

After the occurrence of the strong hydraulic jump, water entered the urban district through its streets. The intensity of flooding inside the urban district, due to the complex flow and wave pattern caused by the buildings, depended strongly on the location where water depth was measured. As expected, the *aligned* layout exhibited less resistance to the propagation of the flood wave than the *staggered* one.

The experimental team observed that these effects were weakened as the flood progressed into the city because friction and reflections damped out the wave pattern and the flow better aligned to gaps between the buildings. The differences between configurations also diminished with the inflow hydrograph intensity.

The differences between probe readings, both for a given city layout between probes and between layouts for the same probe, were more pronounced in the original model topography, which the experimental team attributed to the channelling effect of the two

masonry walls that constrained the flow and made it more one dimensional in the modified topography.

4.5 Details of simulation model setup

In the current study, out of the 12 experimental observations for the urban district layouts, only the observations for four cases of modified topography viz. *aligned-high, aligned-low, staggered-high* and *staggered-low* are simulated.

4.5.1 Model bathymetries

The topography data for the two *modified* urban district setups and details of walls as well as buildings were used to construct bathymetries for the simulation models. The original physical model topography is prepared using a 5 cm grid spacing. However, as the representation of buildings and walls in the bathymetry is better with finer resolution, the bathymetries used for the simulations are prepared with 1 cm spatial resolution. The *aligned* and *staggered* bathymetries constructed using the topographic data are as shown in Figure 4.10 and Figure 4.11.

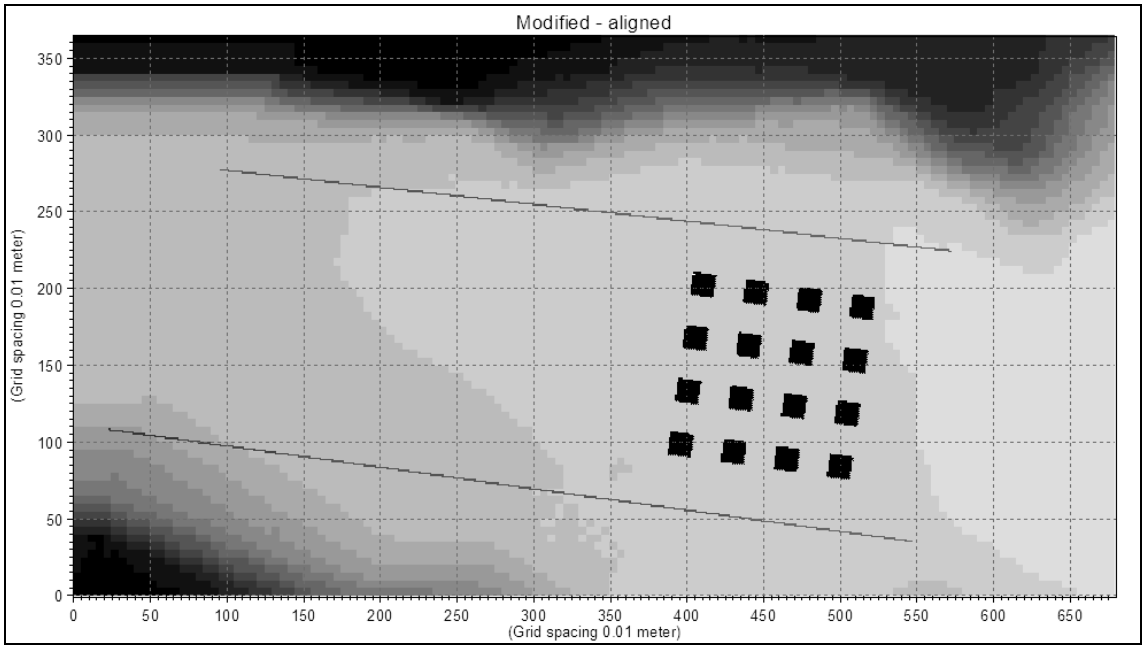

Figure 4.10: Modified - aligned bathymetry

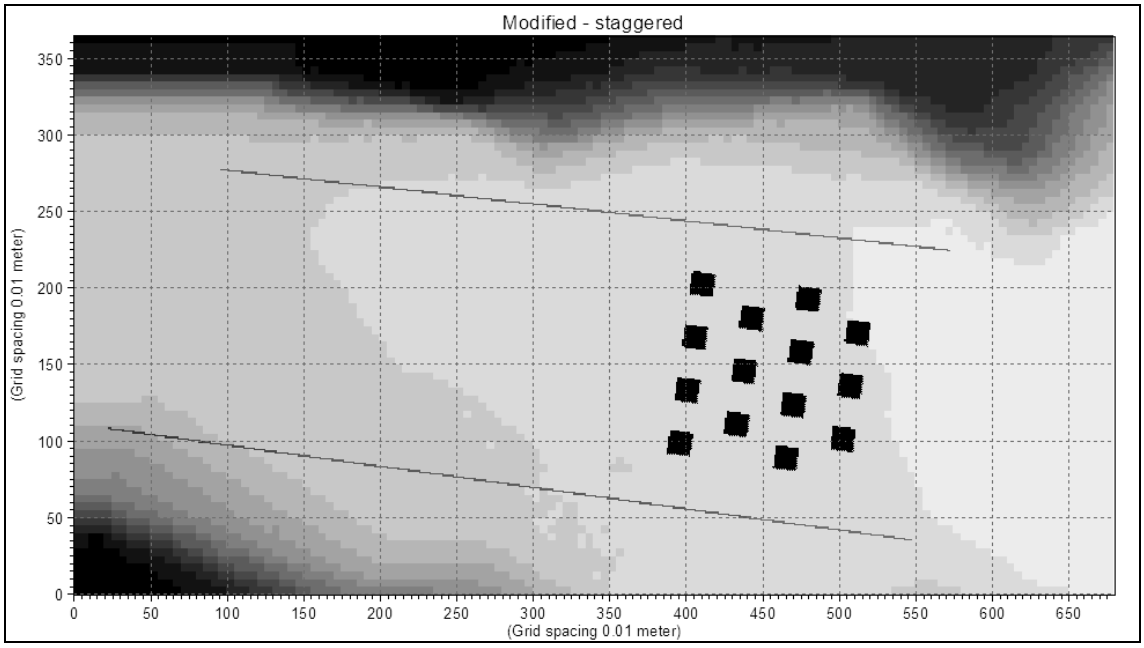

Figure 4.11: Modified - staggered bathymetry

The bathymetries are 6.80 m long and 3.65 m wide. These bathymetries were further modified for the simulations because of the boundary condition considerations as discussed in sections 4.5.2 and 4.5.3 below. The details of the bathymetries adopted for this research are detailed in section 4.5.4.

4.5.2 Upstream boundary condition

The elevations for all the outermost cells along the four sides of the bathymetry are raised to an elevation of 9.0 m to avoid any software detectable open boundaries. All the necessary open boundaries, therefore, are specified manually.

As stated earlier in section 4.3.7, pump discharge into the feed tank is known with time. However, due to other limitations as stated therein, pump flow can only be taken as an approximation to the total discharge entering the model valley. This discharge entering the model may not be equal to the corresponding pump discharge at the very beginning of the test as water level in the tank rises a few centimetres while water flows into the model. Further, as no details of the feed tank geometry are available and the flow distribution across the inlet section is unknown, the water level in the feed tank measured by Probe 1 – which represents an approximation to the total head of the flow as shown in Figure 4.15 – is taken as the upstream boundary condition. Therefore, in all the simulations carried out, the corresponding water level measurement by Probe 1 is

applied as the upstream boundary condition for that particular setup. The water level at all the points along the line passing through the Probe 1 location parallel to Y-axis for the setups as shown in Figure 4.10 and Figure 4.11 is thus the same.

To avoid any reflections from the upstream wall and reduce the computational burden by exclusion, the elevation of the area in between the upstream wall and upstream boundary is raised to an elevation of 9.0 m.

The 2D simulation software used for this research, MIKE 21, does not allow dry open boundaries. Therefore, two fake sources – Fake source-1 and Fake source-2 – as shown in Figure 4.12 are placed at two low points in the bathymetry along the upstream boundary. Figure 4.12 shows the channel bed profile through Probe 1 parallel to Y-Axis. Each of the two sources discharge a nominal amount of water at a constant rate of 0.001 m^3 / s at 0.001 m / s velocity into the model.

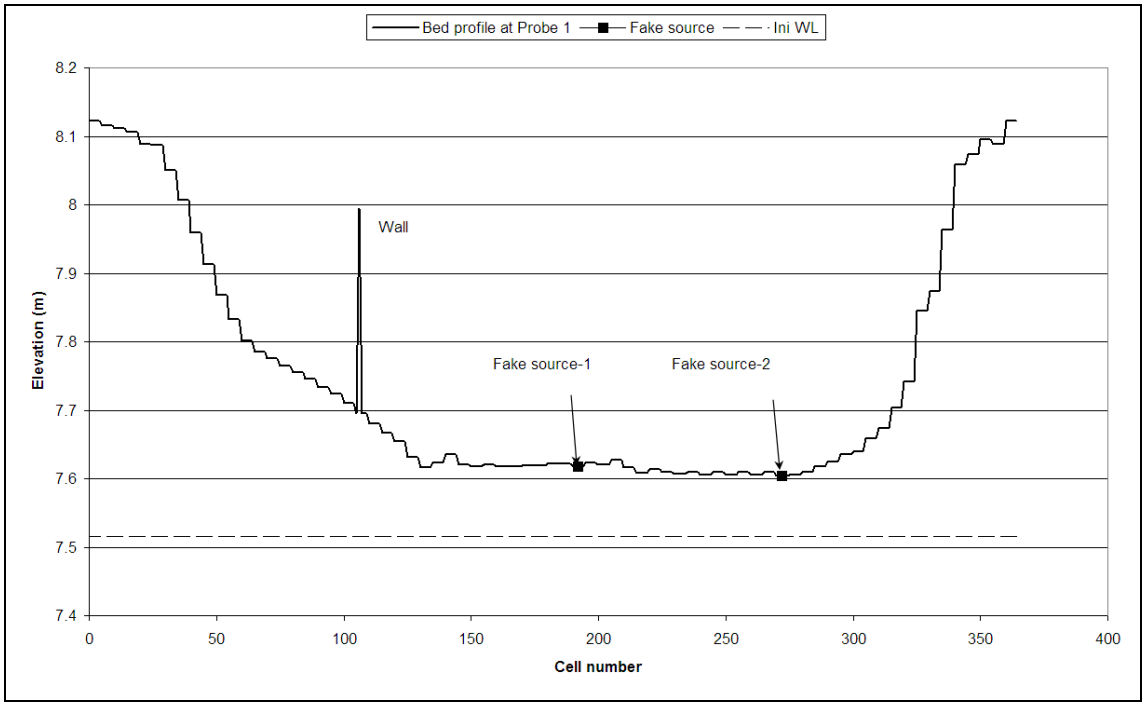

Figure 4.12: Channel bed profile through Probe 1 parallel to Y-axis

4.5.3 Downstream boundary condition

In the experimental setup, the physical model extends about 45 m downstream of the urban district and the flow leaves the urban area along the channel. The topography

details for this part of the channel are not available and, therefore, this part of the channel is not considered in the computer model. Therefore, in the computer model, boundary conditions need to be imposed at the end of the urban district zone.

Among various open boundary specifications possible, constant water level provided the best numerical stability. Therefore, constant water level type of downstream boundary specification was used for the simulations.

The downstream boundary is located along the innermost column of cells parallel to the downstream wall boundary. In addition, to eliminate the reflections from the right boundary wall, water level boundary with the same value as the downstream boundary was imposed along the innermost row of cells parallel to the right boundary wall. Either of the two different values of water level, 5.6 m and 5.8 m, were used as constant water level downstream boundary for the simulations.

4.5.4 Adopted bathymetries

The constructed bathymetries were further modified to comply with the requirements for boundary conditions as discussed earlier in sections 4.5.2 and 4.5.3. Figure 4.13 shows the adopted model bathymetry for *modified-aligned* setup whereas Figure 4.14 shows the adopted model bathymetry for *modified-staggered* setup with a different perspective view.

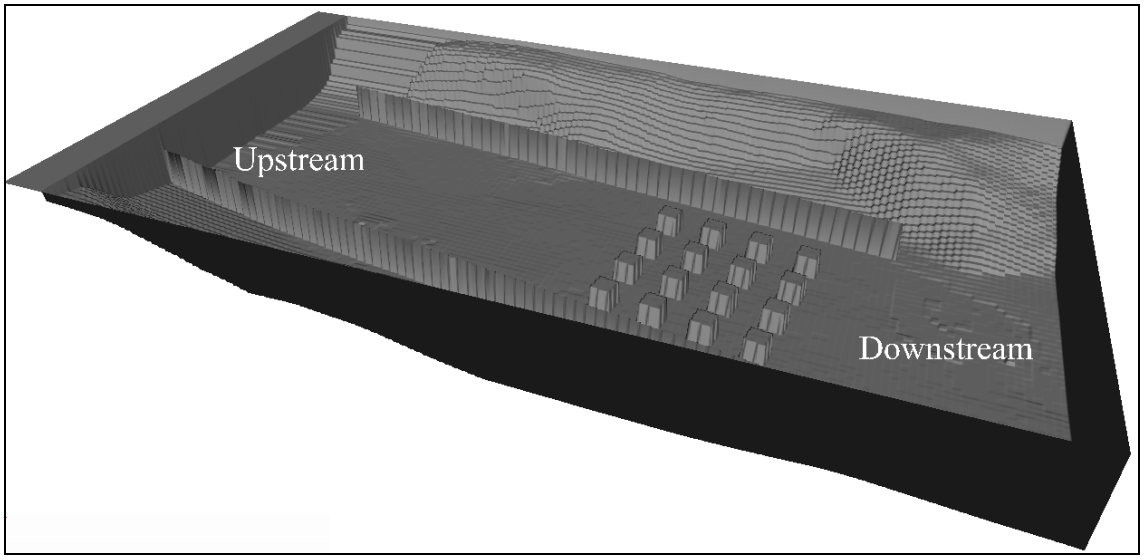

Figure 4.13: Adopted modified-aligned bathymetry

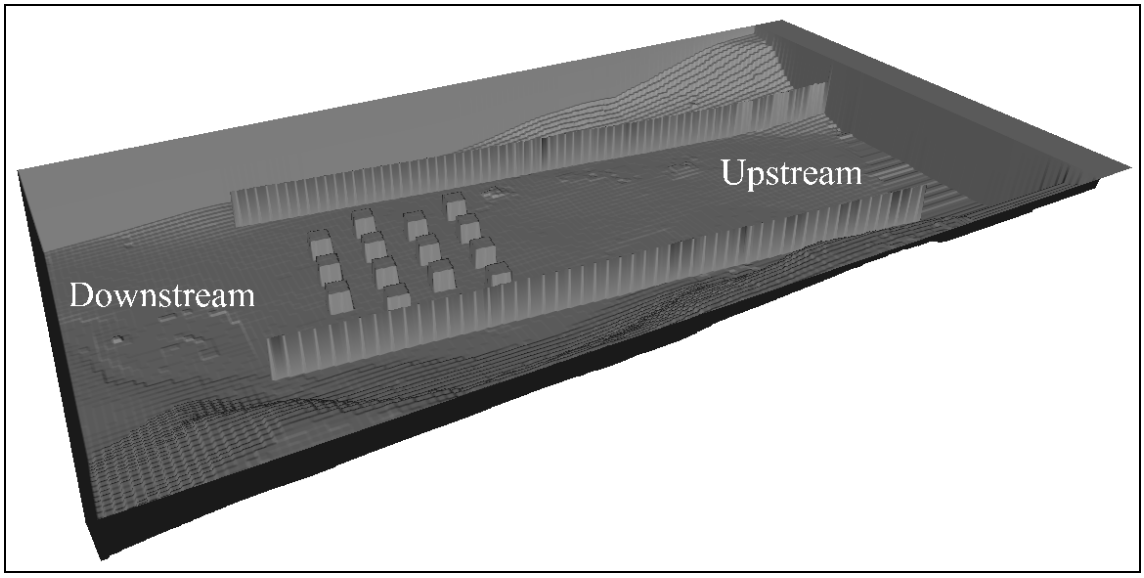

Figure 4.14: Adopted modified-staggered bathymetry

4.5.5 Initial water level

As stated earlier, MIKE 21 does not allow dry open boundaries. Therefore, to keep the downstream boundary wet at the start of the simulation, an initial water level just sufficient to keep the downstream boundary wet needs to be assigned. The minimum elevation in the bathymetry along the downstream boundary is 7.414 m. An initial water level equal to 7.515 m is assigned for the simulations. With this initial water level, the spread of the water is minimal and is far away from the urban district. Therefore, the simulation start condition can be considered as dry.

4.5.6 Bed resistance

The experimental team at CESI suggested a Manning's roughness coefficient for the concrete bed as well as the walls of n = 0.0162 (Testa et al. 2007). This same value was used in all the simulations.

4.5.7 Wetting and drying depth

The wetting and drying depth used for the simulations was 0.02 m and 0.01 m respectively. This means that a computational point is taken into calculations once the depth at that point reaches the wetting depth of 0.02 m and is taken out of the calculations when it falls below 0.01 m.

4.5.8 Simulation time step

The probes in the experimental setup recorded water level values at 0.02 s intervals. However, the computer simulations were not stable at time step equal to 0.02 s, and therefore, a lower time step of 0.01 s was used for all of the simulations.

4.6 Details of simulation runs

A total of four simulations – two city layouts (*aligned* & *staggered*) times two inflow hydrographs (*High* & *Low*) – with the *modified* topography and called hereafter as *Aligned – High*, *Aligned – Low*, *Staggered – High* and *Staggered – Low* were carried out.

As stated in section 4.5.2, the water level recorded at Probe 1 was used as upstream boundary condition. Therefore, for all Probe 1 graphs, the simulated water depths coincide with the observed water depths. The water depth hydrographs are as shown in Figure 4.15 below.

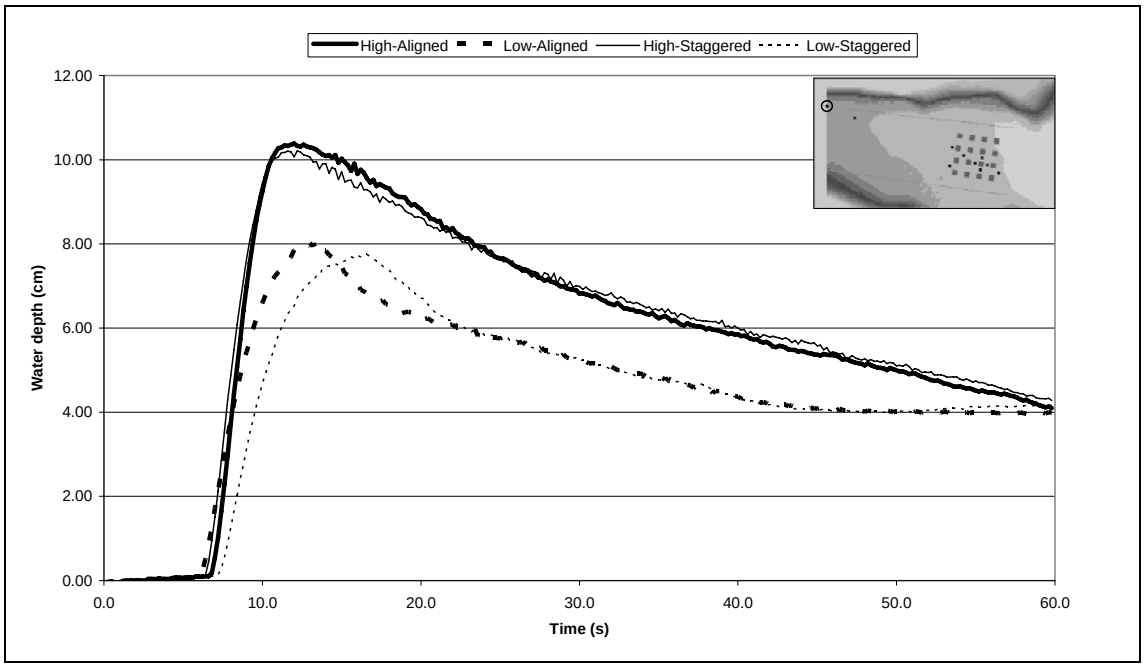

Figure 4.15: Inflow hydrographs used as upstream boundary condition for simulation

4.7 Analysis of results

The water depths extracted for cells at the probe locations were used to compare the simulation results with the experimental results. Figure 4.16 shows the locations of all the probes over the *modified* topography.

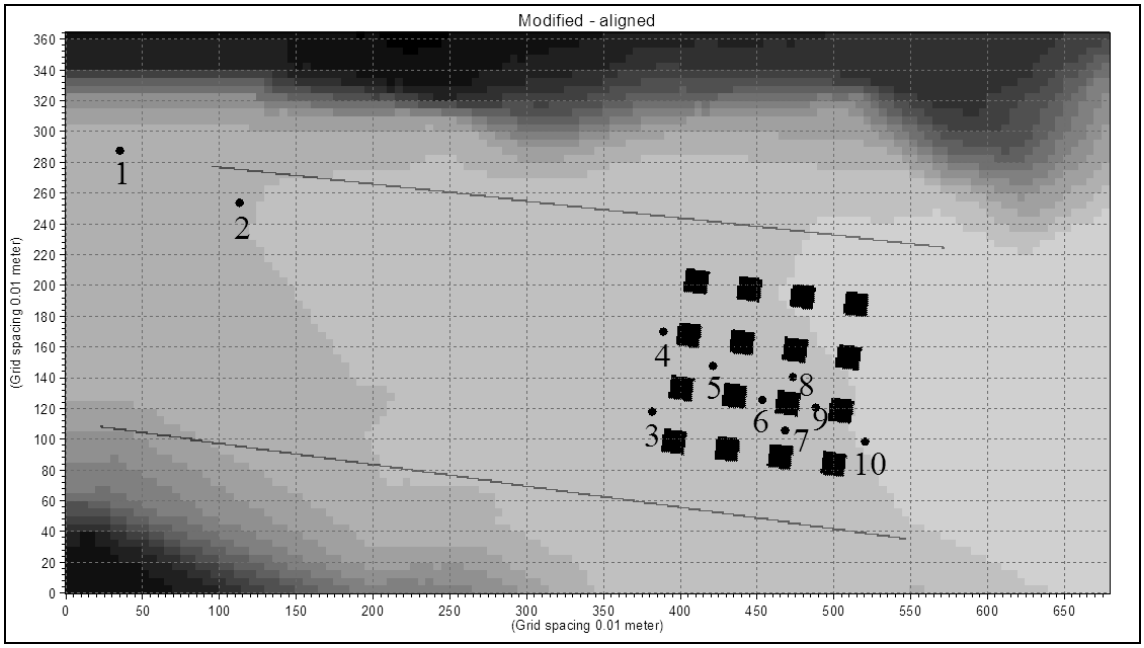

Figure 4.16: Probe locations

A more detailed view of the probe locations around the urban district for the *aligned* layout is shown in Figure 4.17 and that for the *staggered* layout is shown in Figure 4.18.

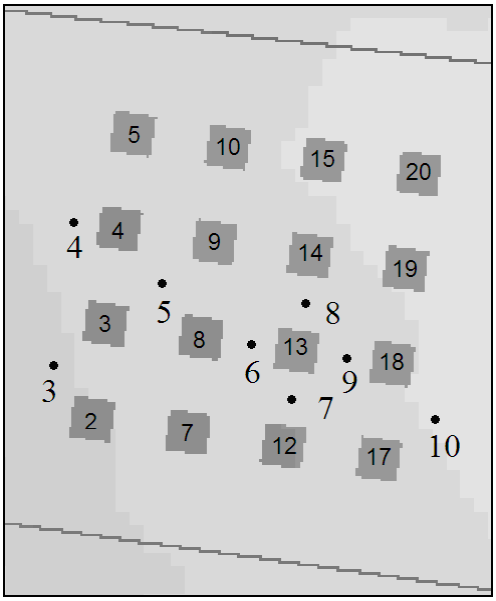

Figure 4.17: Probe locations – aligned layout

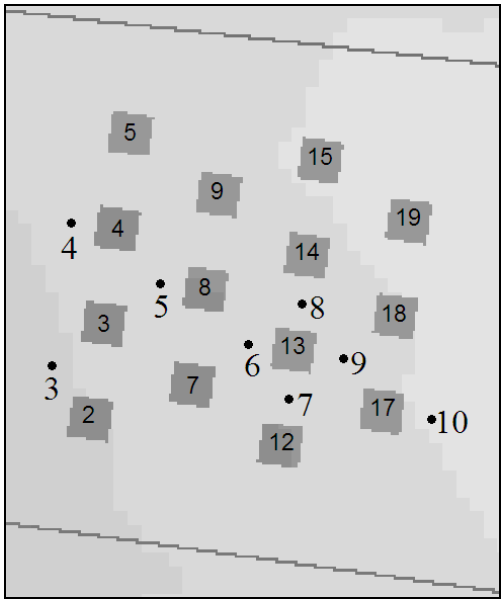

Figure 4.18: Probe locations – staggered layout

4.7.1 Aligned – High and Aligned – Low setups

Figure 4.19 to Figure 4.27 show the comparison of simulated water depths with those observed during the experimental runs for *Aligned – High* and *Aligned – Low* setups at the probe locations. The items containing label HW denote the simulated water depths whereas the items containing label IMPACT denote the observed water depths. Continuous lines represent *Aligned – High* setup and dotted lines represent *Aligned – Low* setup. Further, simulated water depths are represented by thick lines and the observed ones with thin lines.

As can be seen in Figure 4.17, Probes 3, 5, 7, 8 and 10 are located on flow paths between buildings. Probe 4 is located just in front of building number 4. Probes 6 and 9 are located in front of building numbers 13 and 18 but also in the wake of building numbers 8 and 13 respectively.

The simulated and observed water depths at Probe 1 should be the same and this can be seen to be the case in Figure 4.19.

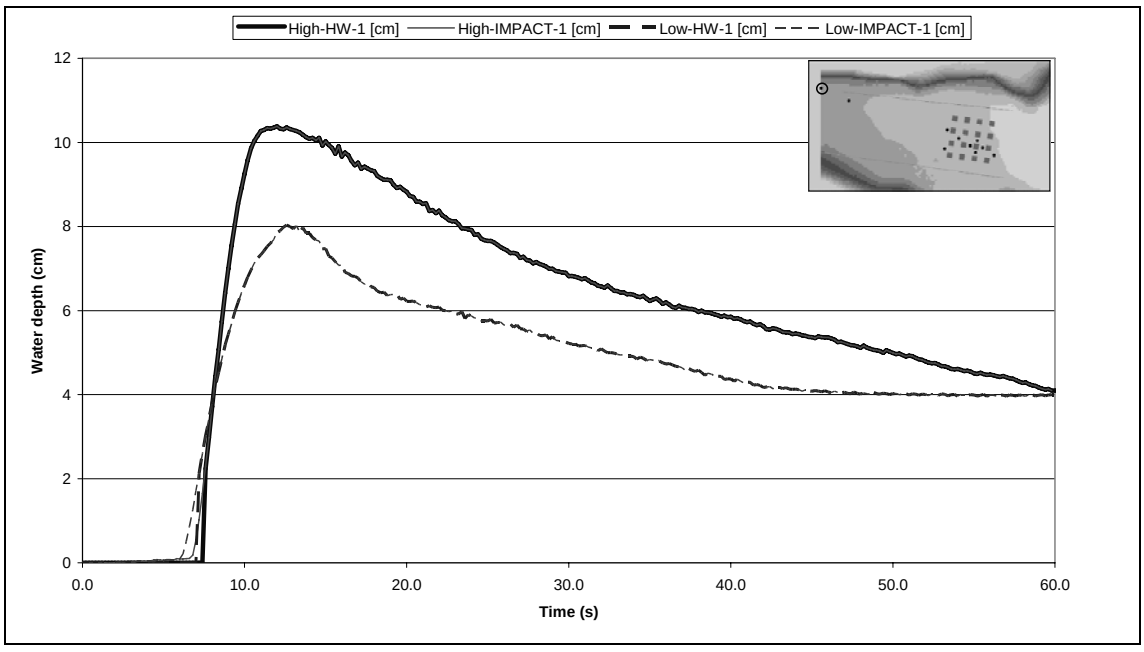

Figure 4.19: Simulated and observed water depths at Probe 1 (Aligned urban district)

From the plots of simulated water depths versus the observed water depths at Probes 3 – 10, it can be seen that at almost all the probes the predicted water depths are well or

slightly over predicted except at Probes 3 and 10 where there is slight under prediction in the early stages for high flow and low flow respectively. At Probes 5 and 6, the water levels are over predicted by up to 2 cm consistently.

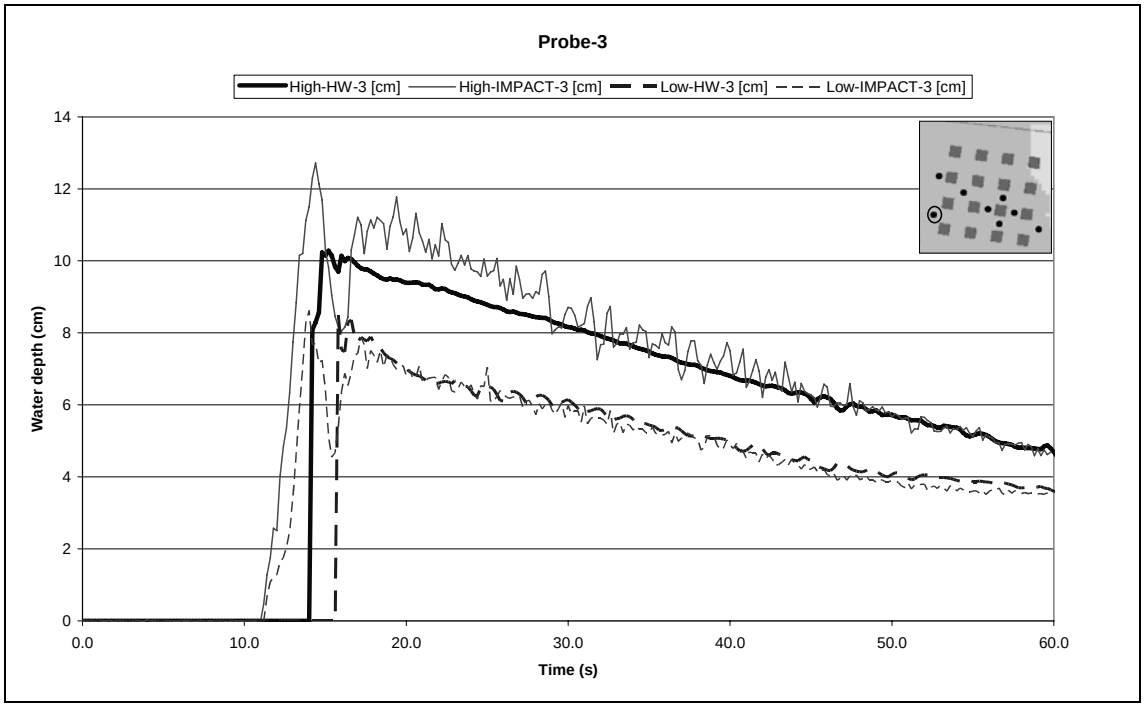

Figure 4.20: Simulated and observed water depths at Probe 3 (Aligned urban district)

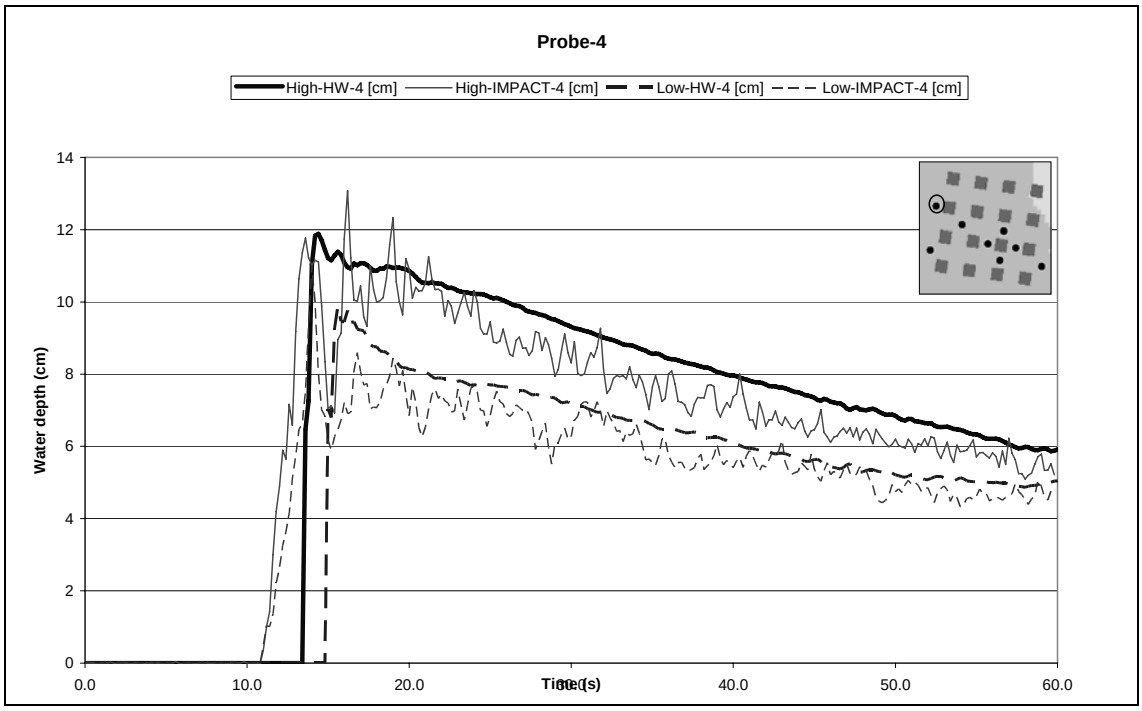

Figure 4.21: Simulated and observed water depths at Probe 4 (Aligned urban district)

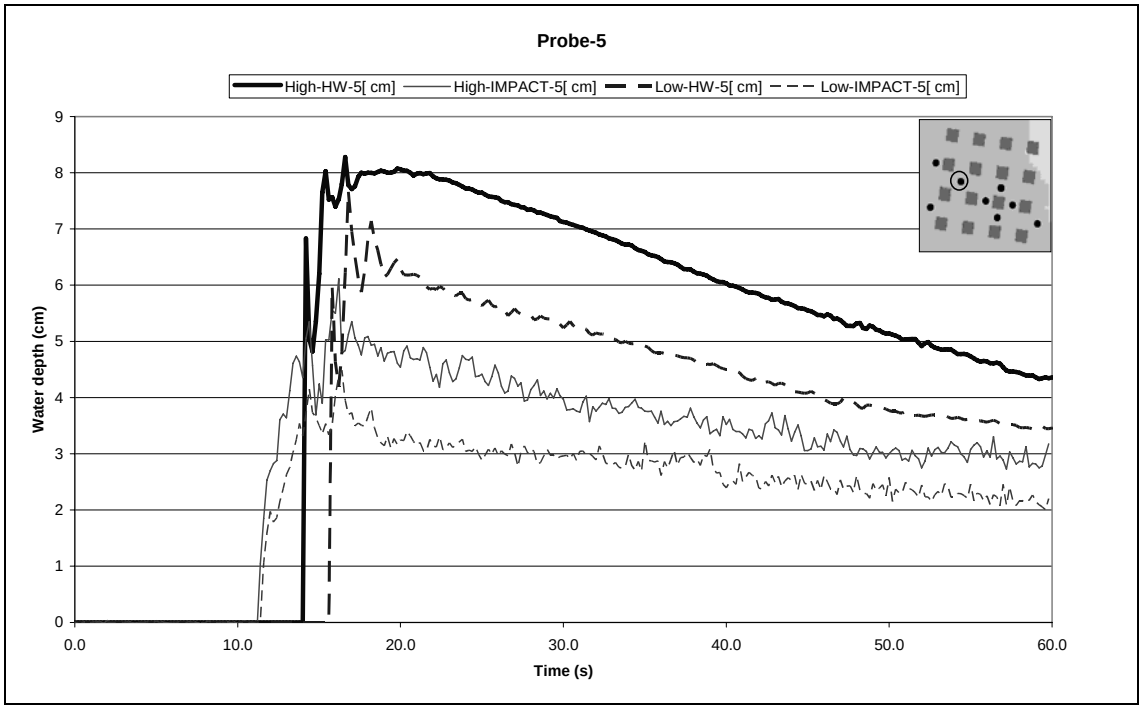

Figure 4.22: Simulated and observed water depths at Probe 5 (Aligned urban district)

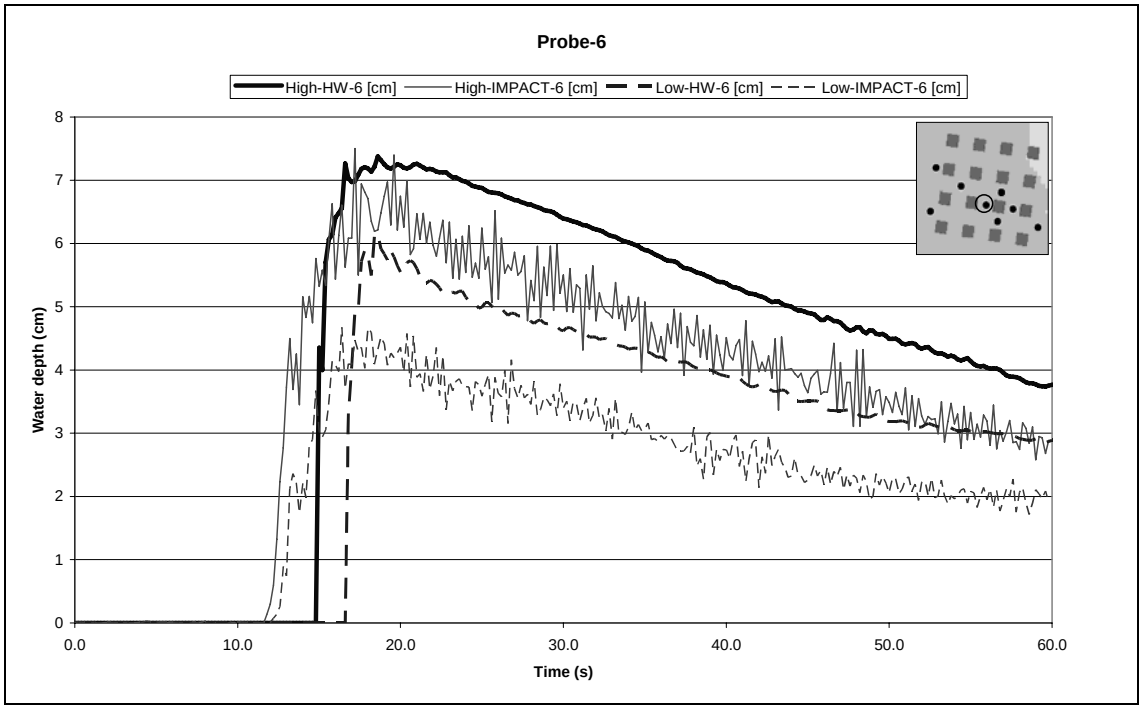

Figure 4.23: Simulated and observed water depths at Probe 6 (Aligned urban district)

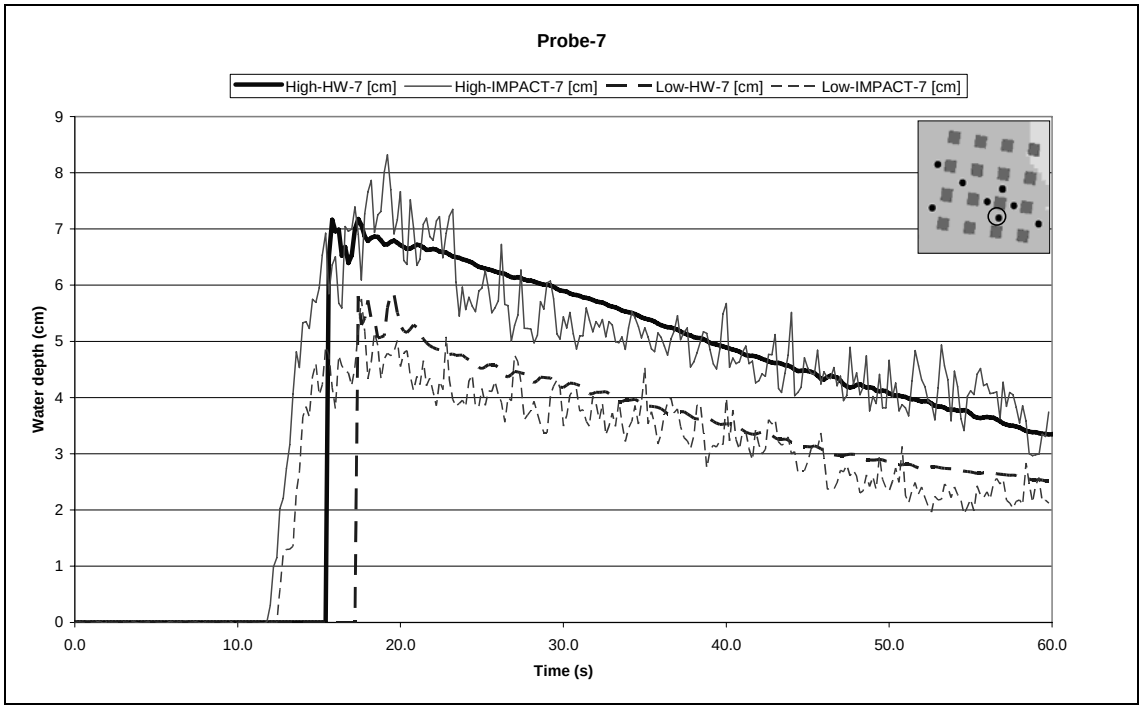

Figure 4.24: Simulated and observed water depths at Probe 7 (Aligned urban district)

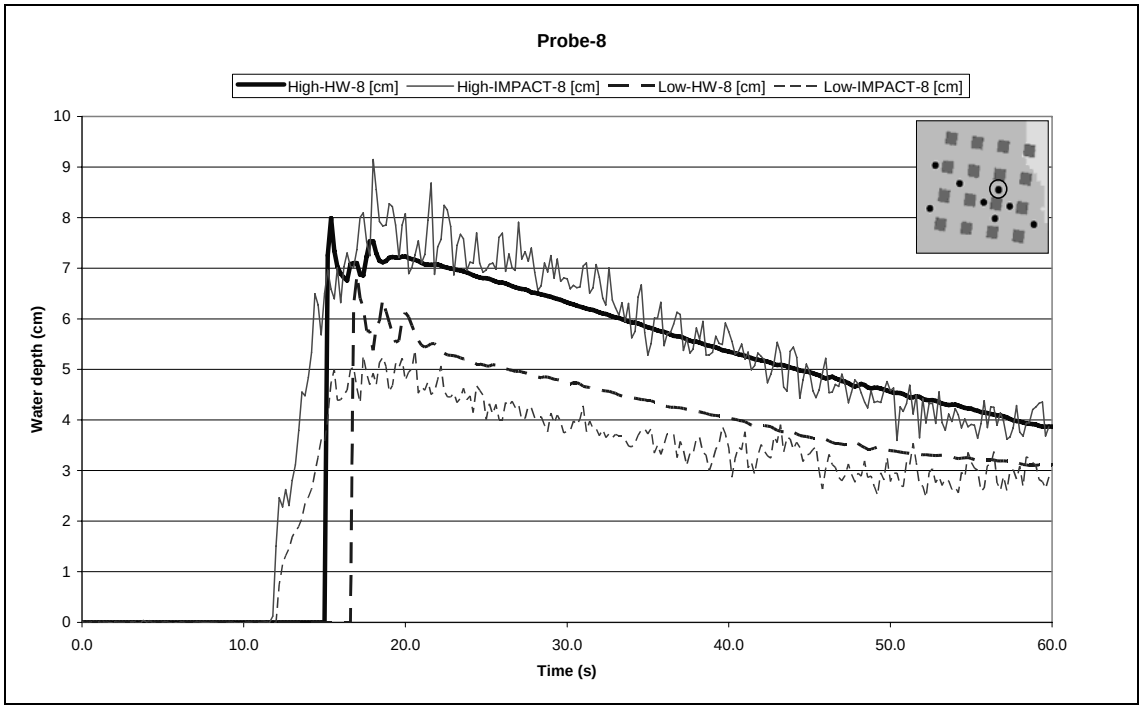

Figure 4.25: Simulated and observed water depths at Probe 8 (Aligned urban district)

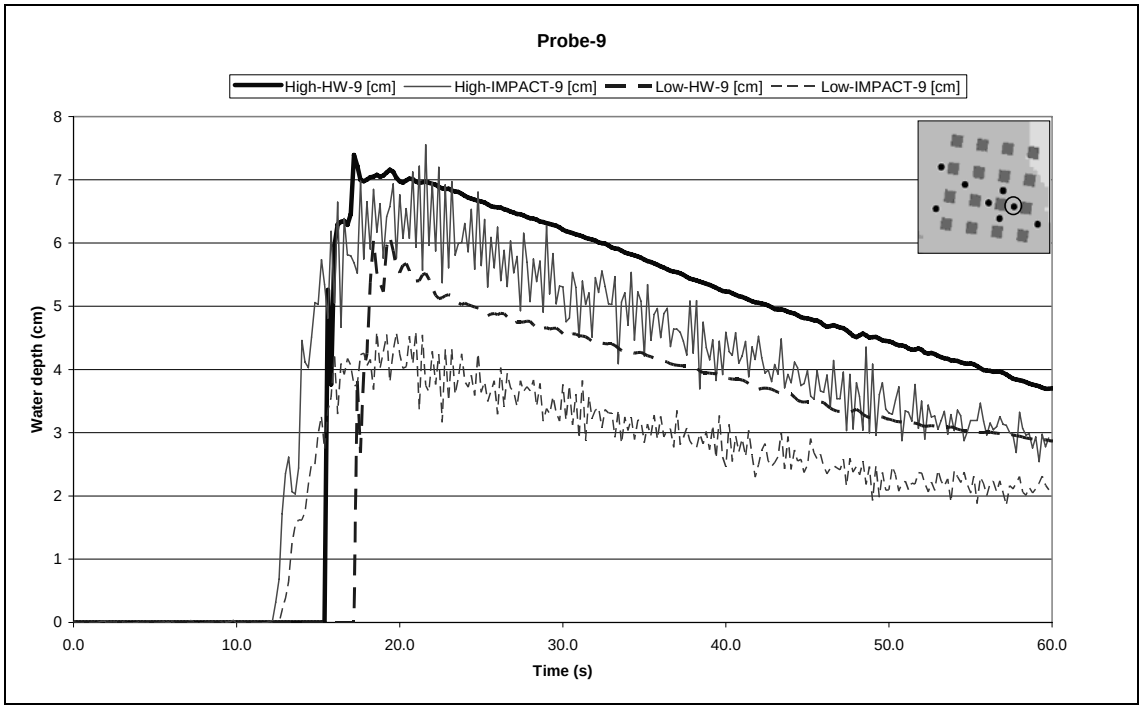

Figure 4.26: Simulated and observed water depths at Probe 9 (Aligned urban district)

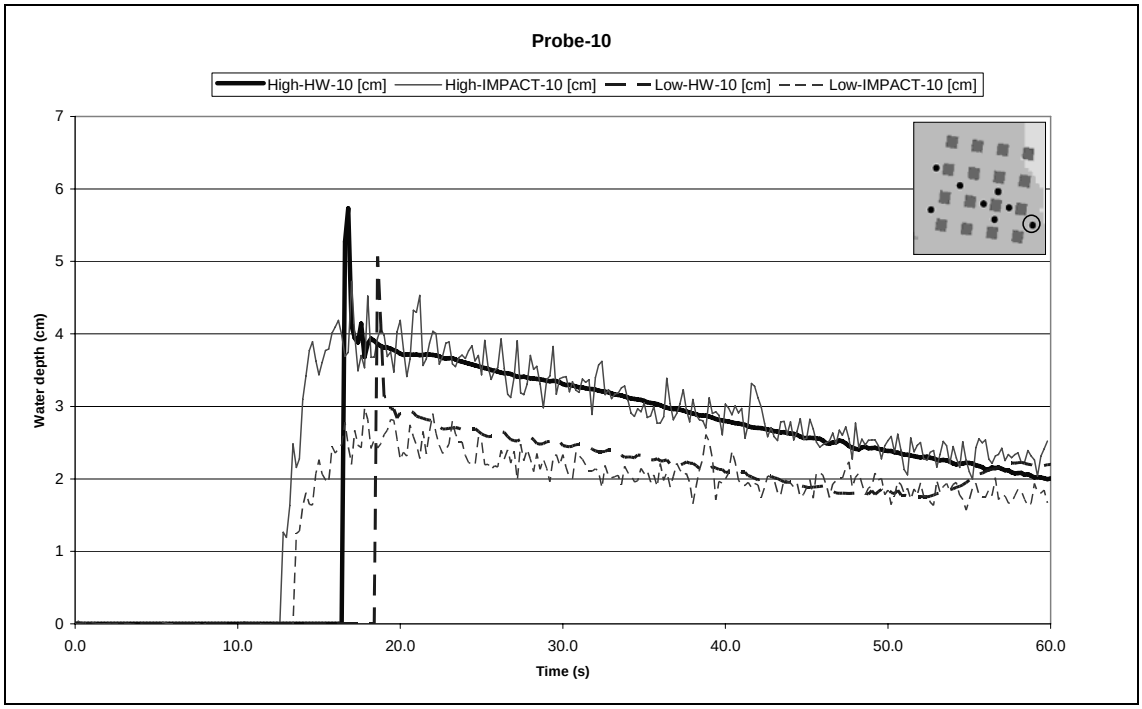

Figure 4.27: Simulated and observed water depths at Probe 10 (Aligned urban district)

The simulated and observed water depths at Probe 2 are not in good agreement and show a consistent bias as is evident from Figure 4.28.

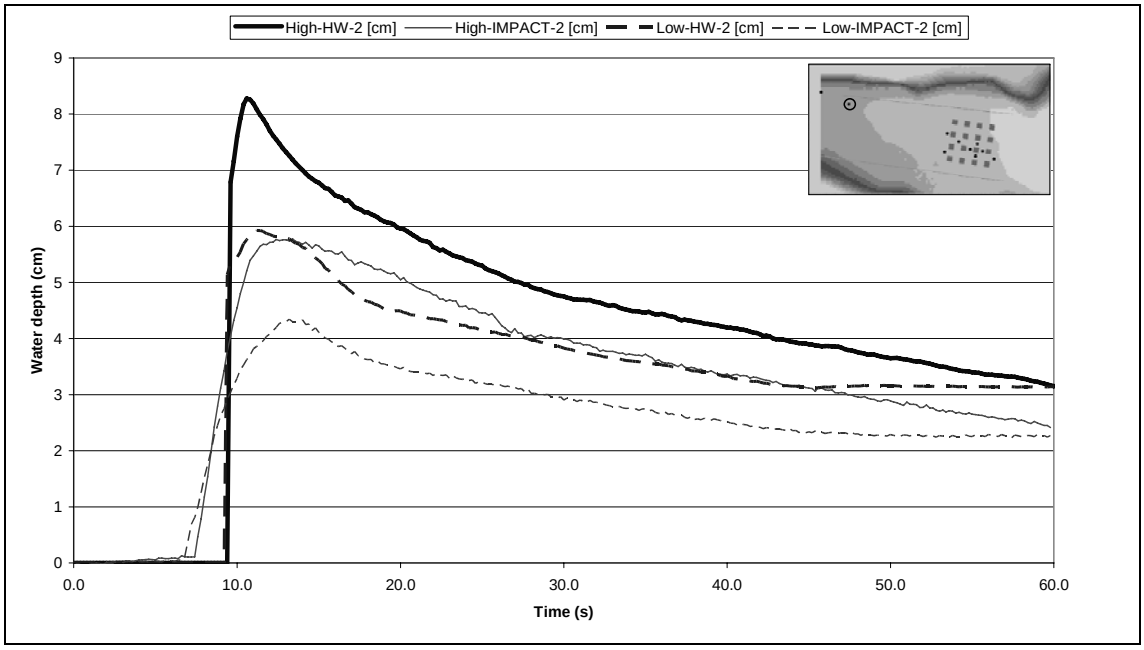

Figure 4.28: Simulated and observed water depths at Probe 2 (Aligned urban district)

4.7.2 Staggered – High and Staggered – Low setups

Figure 4.29 to Figure 4.37 show the comparisons of simulated water depths with those observed during the experimental runs for *Staggered – High* and *Staggered – Low* setups at the probe locations. As like the earlier graphs, the items containing label HW denote the simulated water depths whereas the items containing label IMPACT denote the observed water depths. Continuous lines represent *Staggered – High* setup and dotted lines represent *Staggered – Low* setup. Further, simulated water depths are represented by thick lines and the observed ones with thin lines.

As can be seen in Figure 4.18, Probes 3, 7 and 8 are located around buildings. Probe 4 is located just in front of building number 4 whereas Probes 5 and 6 are located in front of building numbers 8 and 13 respectively. Probes 9 and 10 are located in the wake of building numbers 13 and 17 respectively.

The simulated and observed water depths at probe 1 should be the same as can be seen in Figure 4.29.

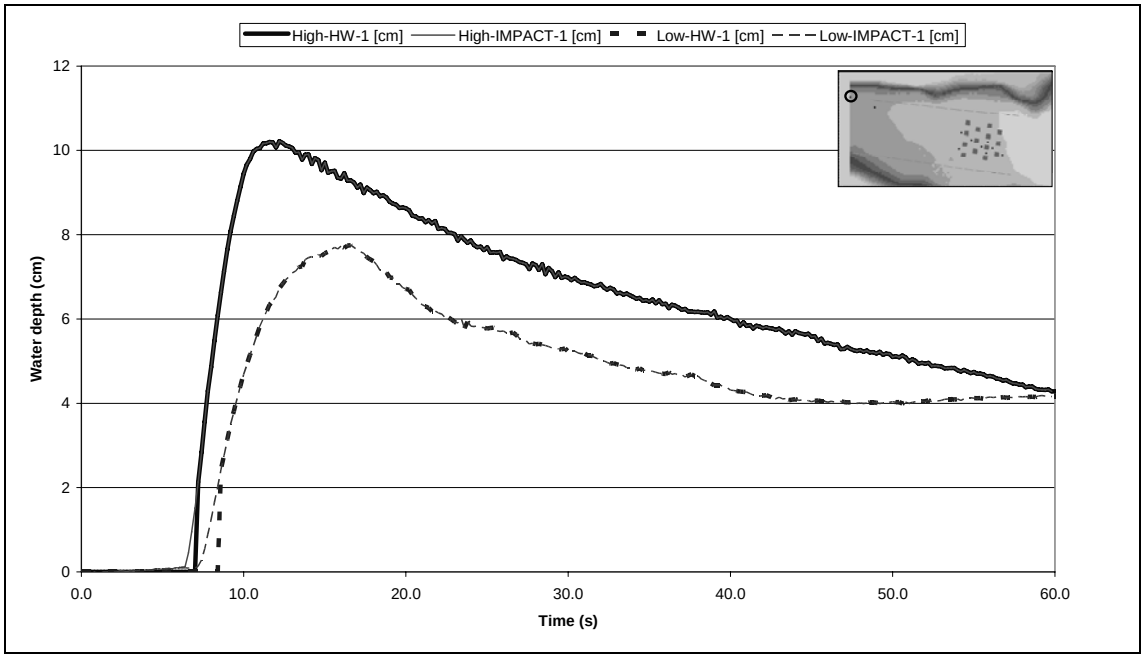

Figure 4.29: Simulated and observed water depths at Probe 1 (Staggered urban district)

From the plots of simulated water depths versus the observed water depths at Probes 3 – 10 below, it can be seen that, in this case too, at almost all the probes the predicted water depths are well or slightly over predicted except at Probes 3, 6, and 8 where there is slight under prediction for high flow, mainly during the early stages. For Probes 7 and 9, the water depths are over predicted by up to 1 cm consistently.

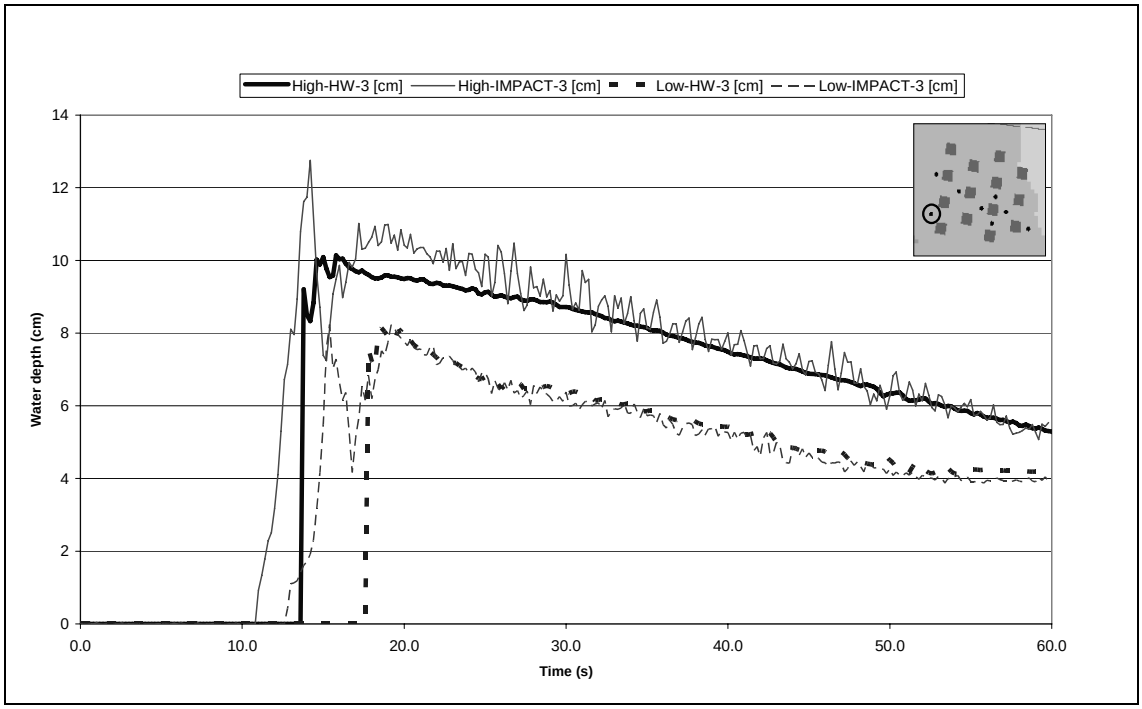

Figure 4.30: Simulated and observed water depths at Probe 3 (Staggered urban district)

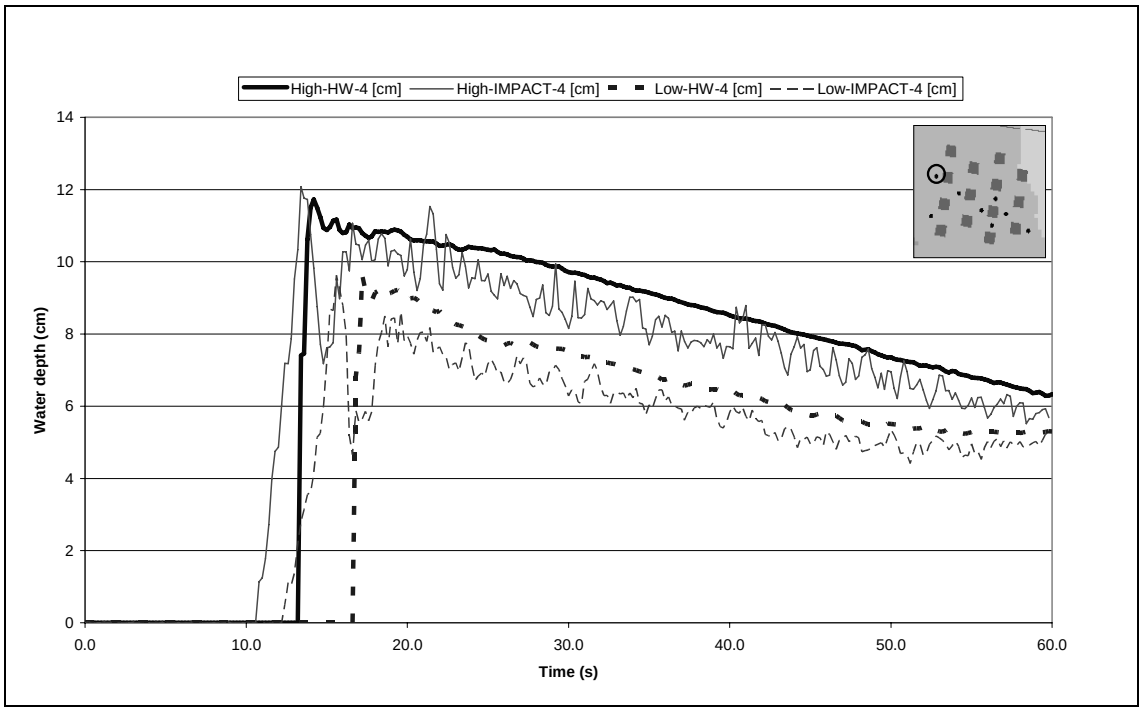

Figure 4.31: Simulated and observed water depths at Probe 4 (Staggered urban district)

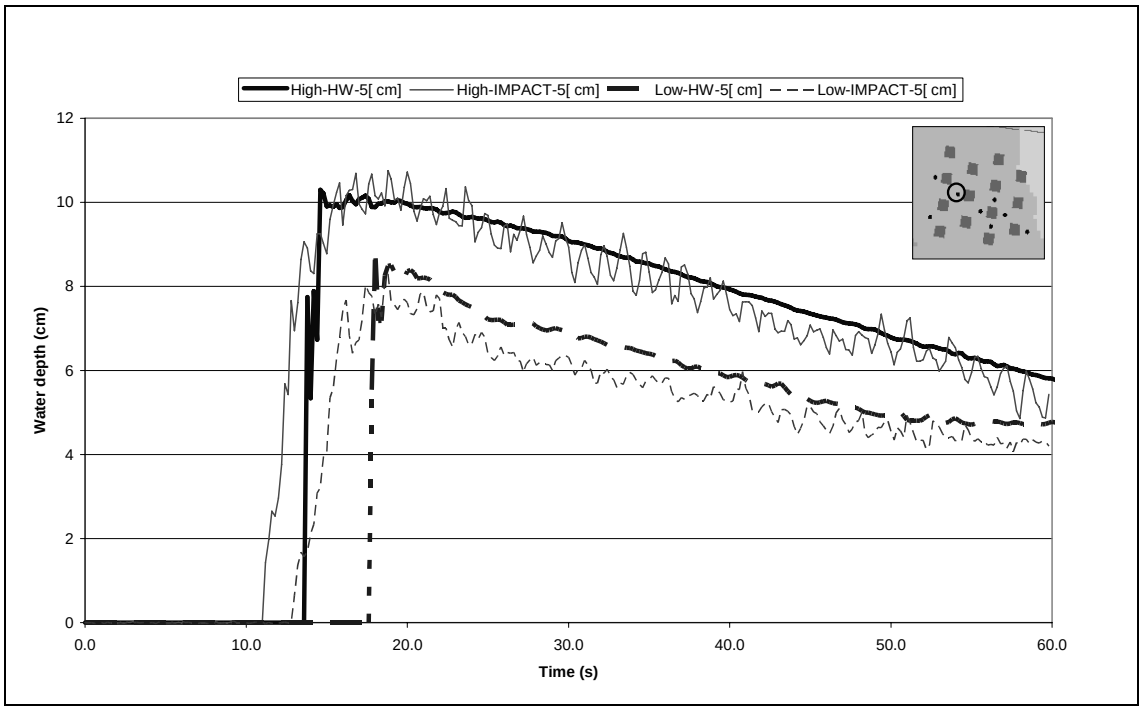

Figure 4.32: Simulated and observed water depths at Probe 5 (Staggered urban district)

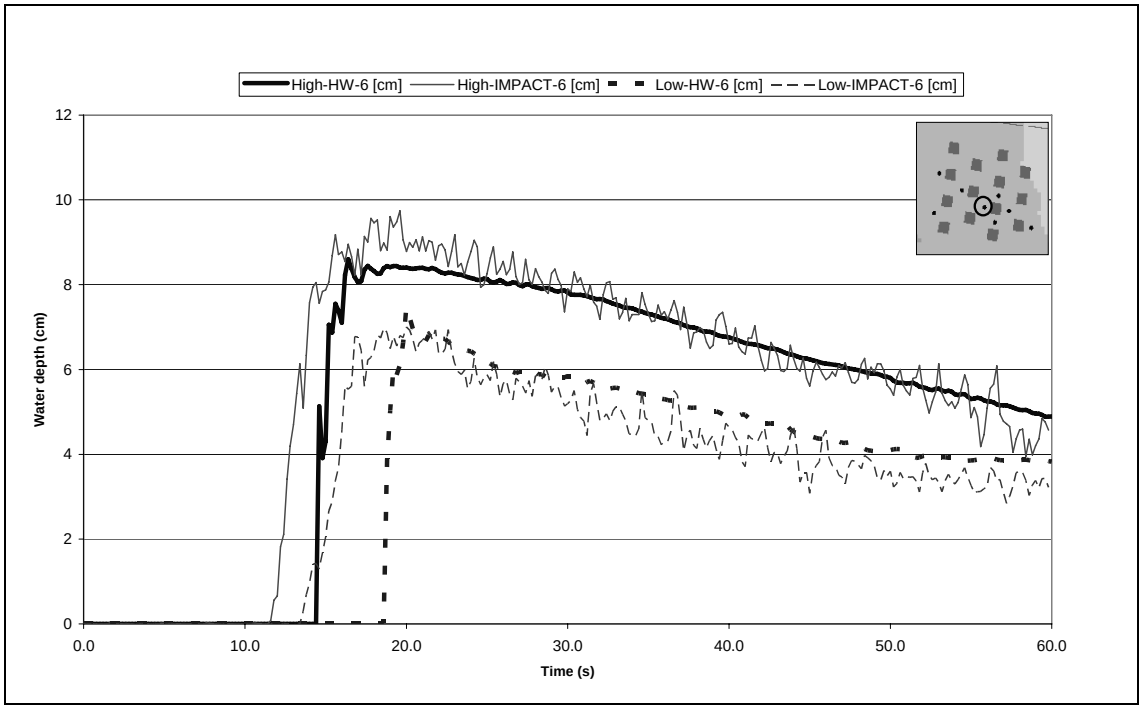

Figure 4.33: Simulated and observed water depths at Probe 6 (Staggered urban district)

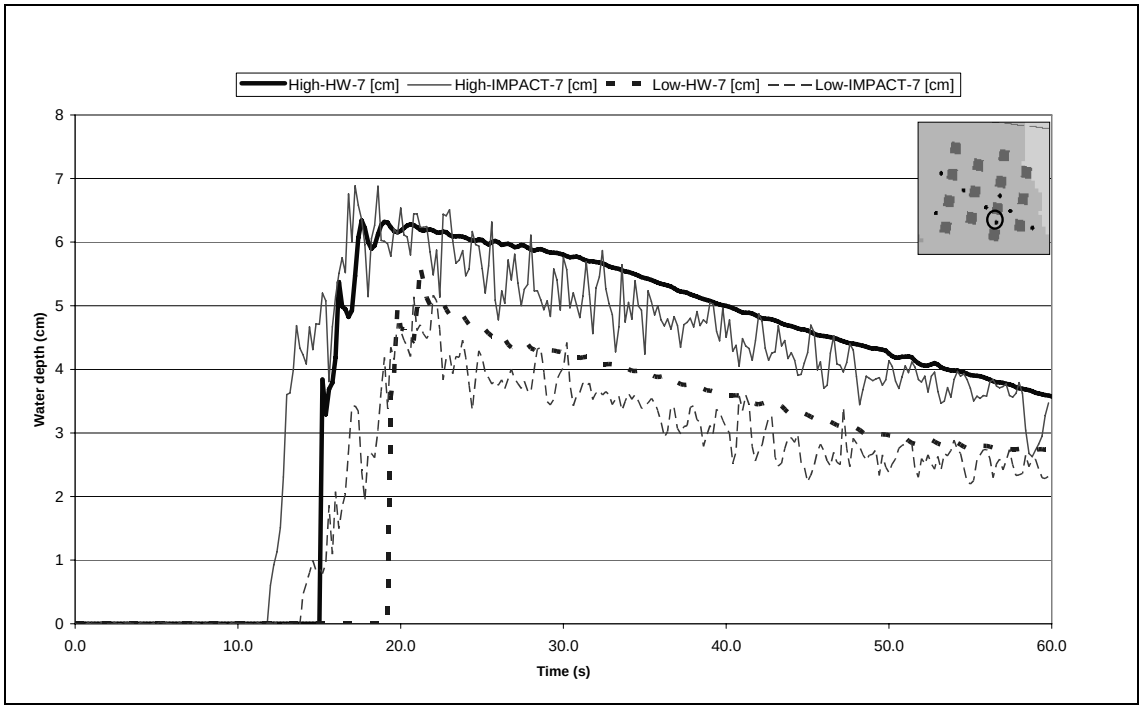

Figure 4.34: Simulated and observed water depths at Probe 7 (Staggered urban district)

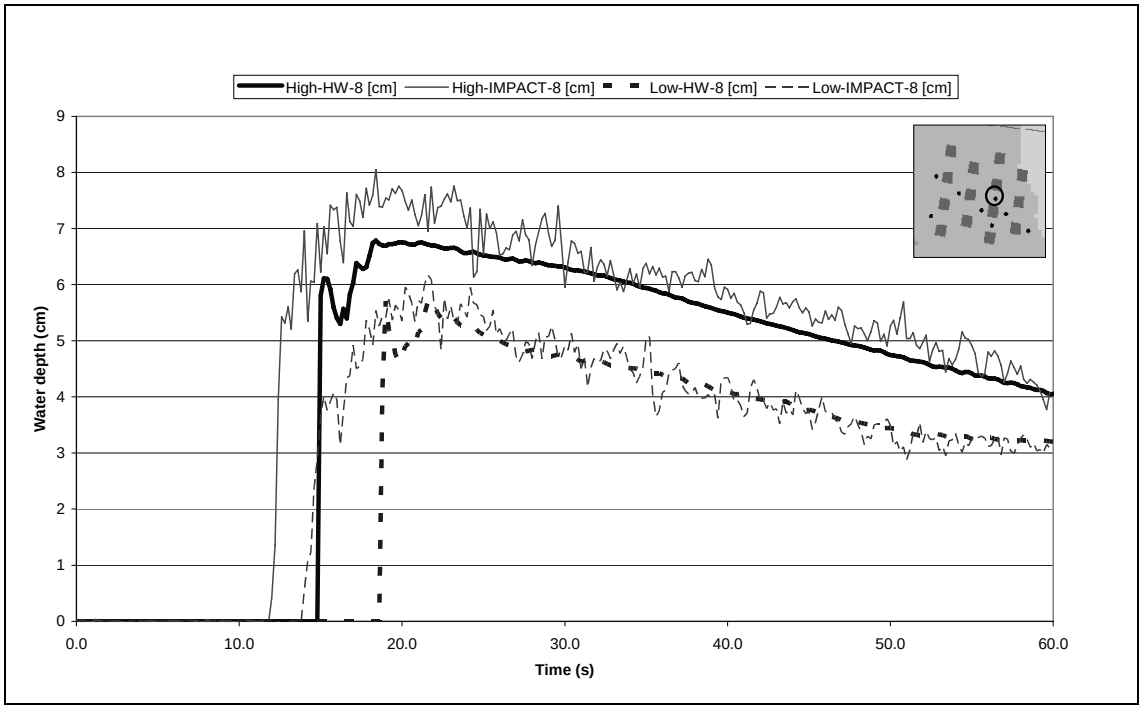

Figure 4.35: Simulated and observed water depths at Probe 8 (Staggered urban district)

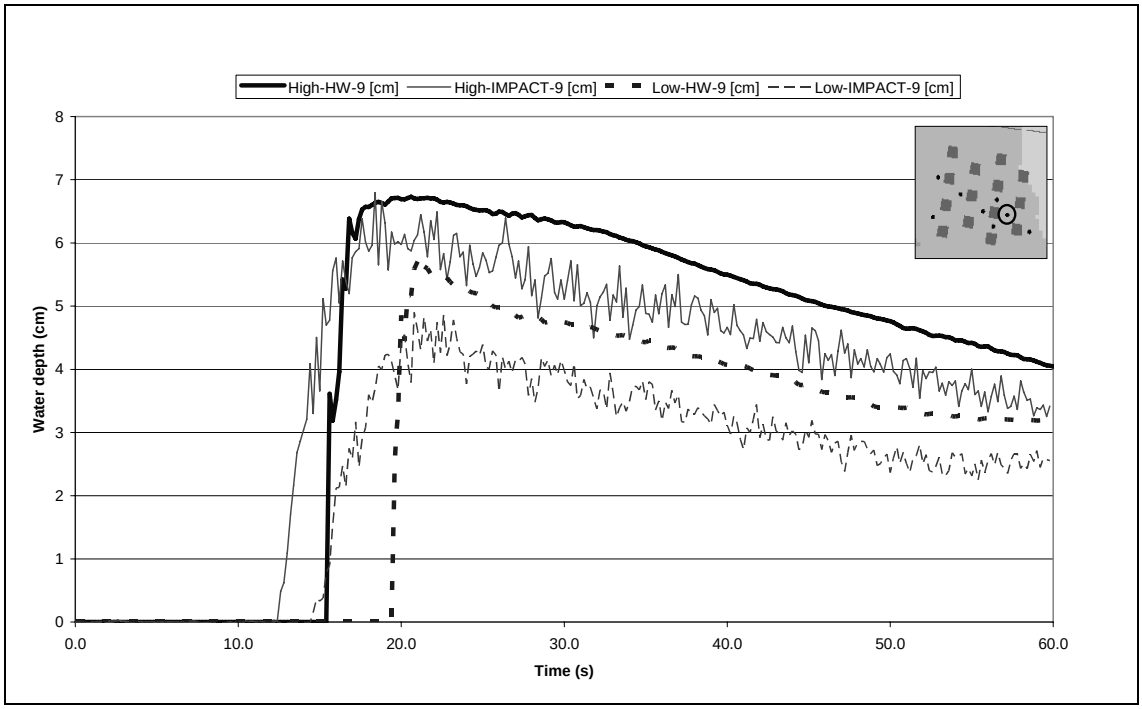

Figure 4.36: Simulated and observed water depths at Probe 9 (Staggered urban district)

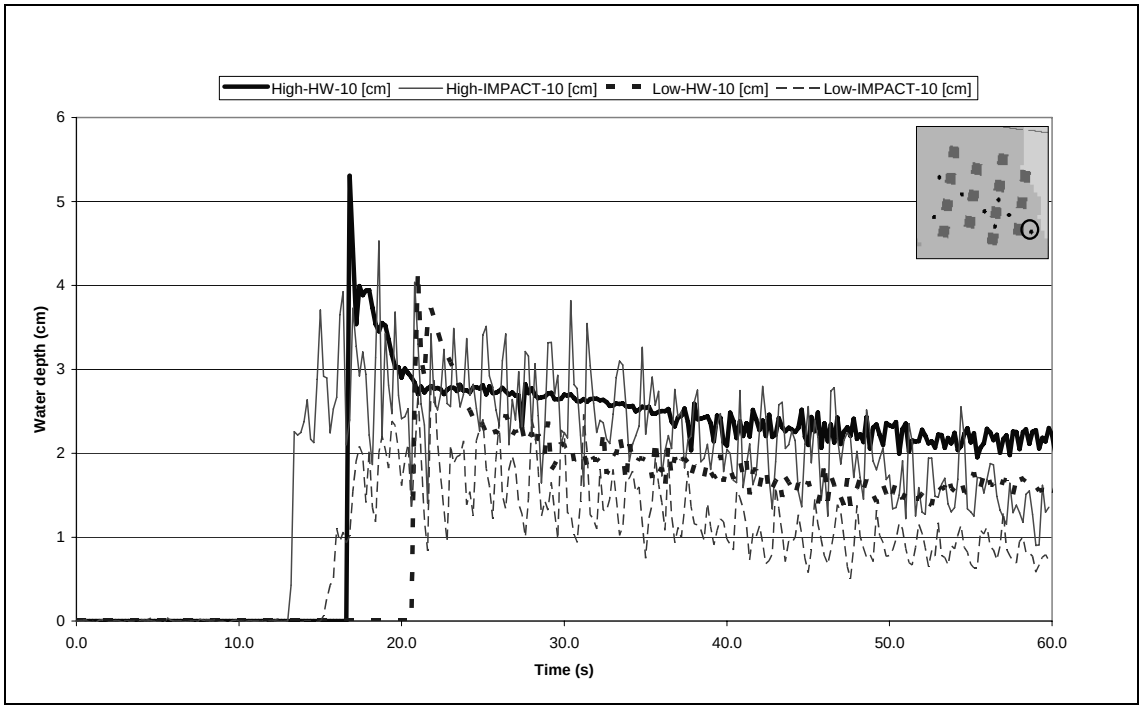

Figure 4.37: Simulated and observed water depths at Probe 10 (Staggered urban district)

The simulated and observed water depths for Probe 2 are not in good agreement and show a consistent bias as is evident from Figure 4.38 below.

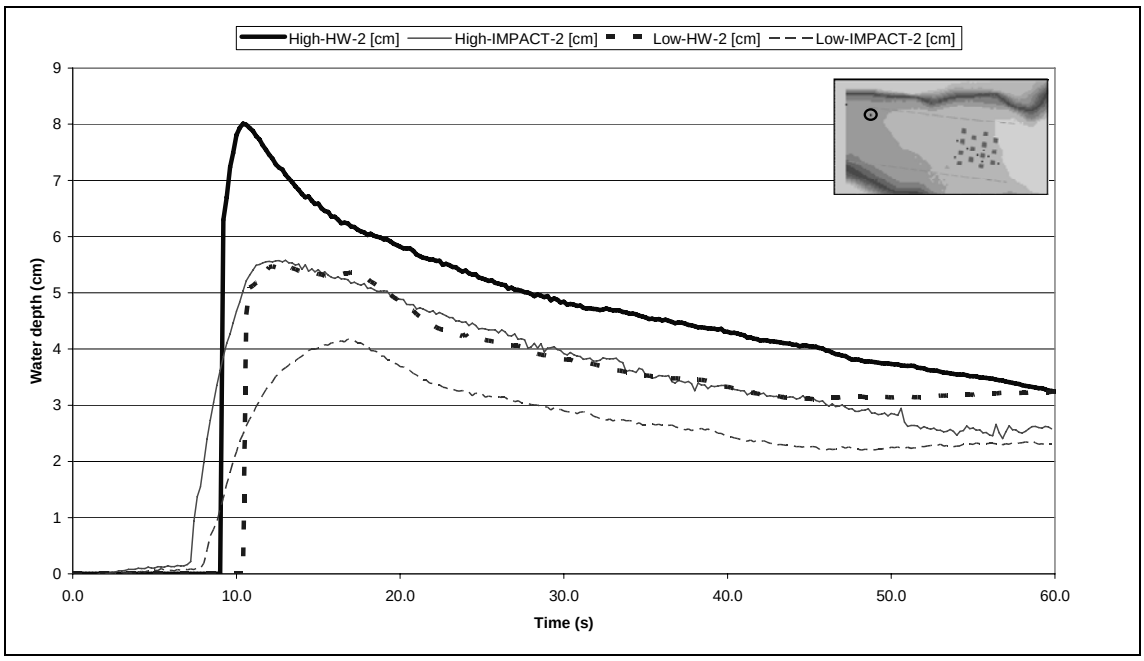

Figure 4.38: Simulated and observed water depths at Probe 2 (Staggered urban district)

4.8 Discussion and conclusions

One way of gaining an insight into the quality of accuracy of water depths predicted at the various probe locations is to carry out a correlation analysis using the observed and the predicted water depths at the various probe locations. Table 4.5 below details the coefficient of correlation (r) and the root mean squared error (RMSE) values between the experimental and simulated water depth values, calculated for each of the probes in the four setups used.

Table 4.5: Statistical analysis for model verification

	Aligned High		**Aligned Low**		**Staggered High**		**Staggered Low**	
	r	**RMSE**	**r**	**RMSE**	**r**	**RMSE**	**r**	**RMSE**
Probe 2	0.96	1.05	0.96	1.04	0.95	1.15	0.95	1.07
Probe 3	0.94	0.85	0.97	0.36	0.92	0.74	0.99	0.27
Probe 4	0.89	1.09	0.91	0.81	0.86	1.05	0.92	0.90
Probe 5	0.88	2.63	0.85	2.08	0.95	0.53	0.96	0.65
Probe 6	0.93	1.08	0.94	1.22	0.92	0.62	0.80	0.81
Probe 7	0.90	0.51	0.93	0.50	0.87	0.55	0.91	0.54
Probe 8	0.96	0.48	0.93	0.72	0.93	0.58	0.95	0.30
Probe 9	0.93	0.97	0.90	1.10	0.87	0.85	0.93	0.88
Probe 10	0.93	0.28	0.76	0.28	0.54	0.63	0.66	0.78

From the calculated values of the coefficient of correlation, it can be seen that the predictions are in very good agreement and that the root mean squared error is small for most of the simulations.

It, however, is noted that the coefficient of correlation is not so good for Probe 10 in three setups so are the root mean squared error values for Probe 5 and Probe 2 in two setups each.

However, a quality assessment based purely on statistical method alone, like the one above, may be misleading since the statistical values are based on an aggregated analysis of the predictions over time. Therefore, for analysis of the quality of the predictions a visual inspection is justified. Such a method of visual inspection to

identify strong and weak points of simulation results has been recently used for a similar analysis (Frazão et al. 2008).

Shown below, see Figure 4.39, is the visual inspection analysis for the *Aligned – High* and *Aligned – Low* simulations at the various probe locations. The quality of prediction is colour coded for ease of understanding. The green colour indicates acceptable prediction quality and the red colour indicates unacceptable prediction quality. Probe 2 is away from the urban district and therefore the figure shows its conceptual position.

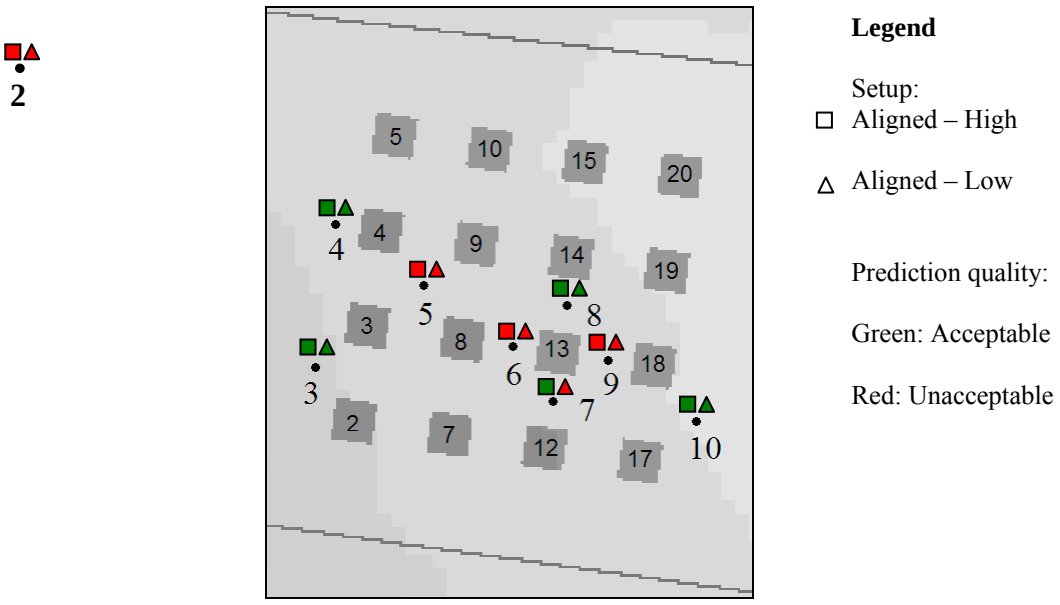

Figure 4.39: Visual inspection of quality of simulation predictions for *Aligned* setups

It can be seen that Probes 6 and 9 are in sheltered locations whereas Probe 5 is in the direct path of the flow; still the prediction quality is bad. As such, there is no correlation between the location and the prediction quality.

Further, the coefficients of correlation for Probes 2 and 9 are very good. However, the visual inspection of the prediction reveals bad prediction quality. Therefore, any statistical justification of the predictions cannot be trustworthy in this case.

Similarly, the visual inspection analysis for the *Staggered – High* and *Staggered – Low* simulations at the various probe locations is shown in Figure 4.40. As earlier, the green

colour indicates acceptable prediction quality and the red colour indicates unacceptable prediction quality.

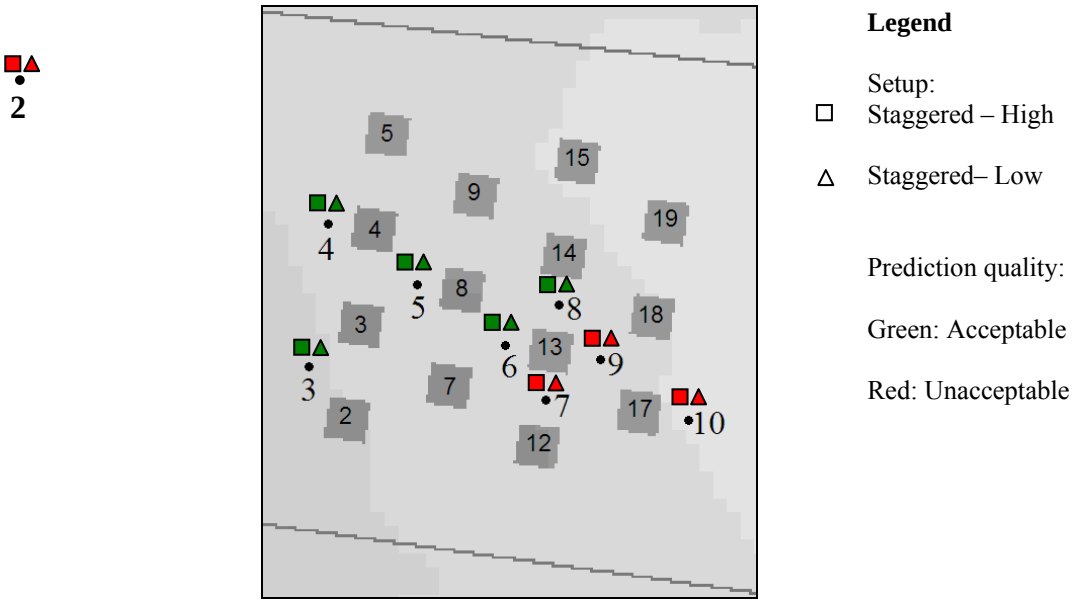

Figure 4.40: Visual inspection of quality of simulation predictions for *Staggered* setups

In the case of *staggered* setups, in addition to Probe 2, the predictions at Probes 7, 9 and 10 are of an unacceptable quality in both the high flow and the low flow cases. However, these findings are neither in agreement with the statistical analysis, see Table 4.5, nor are there any patterns about the location of the probes – sheltered or unsheltered.

Thus, the statistical analysis and visual inspection of the predicted water levels at various probe locations with the corresponding observed water levels do not show a good agreement or a definable pattern of quality of predictions. There can be various reasons for these discrepancies, as explained below.

4.8.1 Uncertain boundary conditions

As stated in section 4.5.2, the water level at Probe 1 is used as the upstream boundary across the inlet of the model. Thus, the water level across the inlet is horizontal during the simulation. However, in reality, the water may not be level and the velocity of

water may vary across the inlet section due to the presence of the river valley in only a part of the width of the inlet. The measurements of only water level and at only one point across the inlet might have been sufficient, had the test section been a uniform channel. However, for a model of a complex river system, this boundary is likely to introduce errors into the computer simulation.

Further simulations by considering the water level at Probe 2 as the input boundary were carried out and it was found that the predictions do not have any agreement with the observed values or the predictions reported above. This further justifies the need to measure the water levels at more number of locations across the input boundary.

4.8.2 Model's computational capability

As can be observed from the model topographies, the flow conditions in and around the urban district can be very complex. The local 3D effects can be of much significance (Morris 1999) affecting the flow pattern around buildings, which the depth averaged equations in the 2D model are not able to cater for. Further, as per the observation by the experimental team, due to the complex flow and wave pattern caused by the buildings, the intensity of flooding inside the urban district depends strongly on the location where water depth is measured (see section 4.4).

One of the earlier validation exercises reported in section 4.2 (Guinot & Soares-Frazao 2006; Frazão et al. 2008) benefitted from calibration of wall and bottom shear stress as well as incorporation of additional head loss due to flow regime variations and the multiple wave reflections against buildings. Similarly, the validation exercise by Sanders et. al. (Sanders et al. 2008) uses a drag formulation akin to vegetative resistance modelling and also accounts for bed shear. It was observed that building drag, dependent on the free surface height, was far more important than bottom shear in the vicinity of the buildings. The model used in this study does not benefit from above formulations or from calibration.

Further, it was observed that strongly curved flow paths may cause the hydrostatic pressure assumption not to be entirely valid in the close neighbourhood of the buildings (Guinot & Soares-Frazao 2006; Frazão et al. 2008).

Many hydraulic models are not able to carry out reliable hydraulic computations at a reduced or small scale. To overcome this, it is common for simulations to be carried out at the prototype scale and the predictions scaled down to the experimental scale for further analysis. The computer model used for this exercise was applied at the physical model scale and the simulations are carried out at this reduced scale. Therefore, the poor performance of the model at some locations and the good performance at other locations may be due to scale effects.

From the above discussion, it can be stated that carrying out simulations and analysis using the published data for model validation was only partially useful for validating the 2D model being used for this research, MIKE 21. It is essential that further publication of observation data of laboratory experiments describes the inlet boundary condition in more detail like incorporating more number of measurement points across the inlet boundary and also observing the velocities, where possible.

In addition, it is worth referring to the

4.9 Summary

The purpose of the study described in this chapter was to carry out a validation exercise for the 2D flood modelling software tool, MIKE 21, to be used for this research.

This chapter describes the experimental setup and the data available for the research. The experimental setup was modelled using the MIKE 21 software for selected test cases.

Simulation runs were carried out on the test cases at the reduced physical model scale and an analysis of the prediction quality carried out.

The study concludes that the available observation data is sufficient only up to an extent in carrying out a validation exercise and therefore, the validation exercise has only been partially useful in validating the 2D model, MIKE 21, being used for this research.

Chapter 5
Hypothetical Urban Topography Study

5.1 Introduction

The study described in Chapter 4 used the 2D modelling software, MIKE 21 to simulate experimental observations representing the propagation of a rapid transient flood wave (flash flood flow) through a simplified urban district for the purpose of validating the software. The following study extends this concept of model studies by using constant and gradually varying flow hydrographs for flooding of an urban floodplain over an extended time ranging from 20 minutes to 6 hours.

As mentioned in section 2.3.1, the LiDAR data that is available for flood modelling is of two types, Digital Elevation Model (DEM) and Digital Terrain Model (DTM). As discussed in section 3.2.2, these topography data types may have an effect on the flood predictions. To study the effects, simulations are carried out using model topographies with and without buildings. The topography with buildings is akin to a DEM whereas the one without any buildings is akin to a DTM.

Further, in line with the research objective explained in section 3.2.2, the effect of considering the buildings in the urban floodplain as storage areas inducing mass storage and momentum losses is studied by replacing buildings by areas of high resistance within the numerical grid.

As discussed earlier in section 2.2.6, dynamically linked nested grid models offer reduced simulation runtimes without any loss of accuracy for the area of interest. In line with the research aims and methodology, see section 3.2.2, this claim and any issues related to (e.g. time, ease of use, correct transfer at boundary) using nested grid models are studied by comparing the results with those obtained from regular grid models (models without nesting).

The earlier study used only two layouts of buildings in urban districts. To obtain a further understanding of flood wave propagation through complex urban districts, this study uses more layouts where the flow direction is parallel, perpendicular or at an angle to the building alignment.

The physical model in the earlier study was a reduced scale (1:100) representation of the Toce River valley with high resolution topographical details. The comparisons between the computer model results and physical model observations were obtained by applying the computer model at the physical model scale. In the following exercises, the computer model simulations are carried out by using the prototype scale of a hypothetical urban floodplain.

Detailed below are the model configurations, the simulation runs, the results and the conclusion for these studies:

5.2 Layout details of hypothetical urban topographies

To achieve the objectives discussed above, the most common type of building layouts in urbanised areas were represented by five different topographies constructed at prototype scale as given below:

1. *Regular building layout* – regularly distributed buildings,
   see Figure 5.3 and Figure 5.4

2. *Parallel building layout* – buildings parallel to the flow direction,
   see Figure 5.5 and Figure 5.6

3. *Perpendicular building layout* – buildings perpendicular to the flow direction,
   see Figure 5.7 and Figure 5.8

4. *Skew45 building layout* – building skewed to the flow direction at an angle of 45°, see Figure 5.9 and Figure 5.10

5. *Skew30 building layout* – building skewed to the flow direction at an angle of 30°, see Figure 5.11 and Figure 5.12

The buildings were placed in a sloping basin. The basin is 174 m wide and 360 m long with a longitudinal slope of 2 in 1000. The sides of the basin are raised to contain the flow. To avoid stability problems at the boundary and ensure smooth entry and exit of water, the upstream 12 m and downstream 10 m of the basin are given a steeper slope of 1 in 10. The topographies are constructed with a grid spacing of 1 m. Figure 5.1 shows the plan view of the basin, whereas Figure 5.2 shows the section through the centre of the basin.

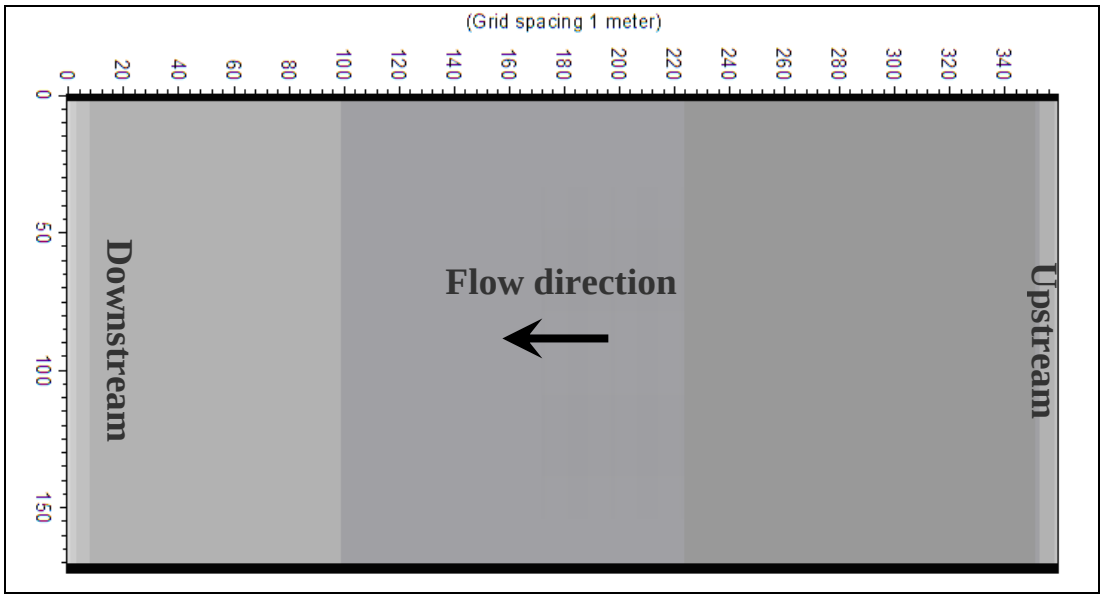

Figure 5.1: Plan view of the basin

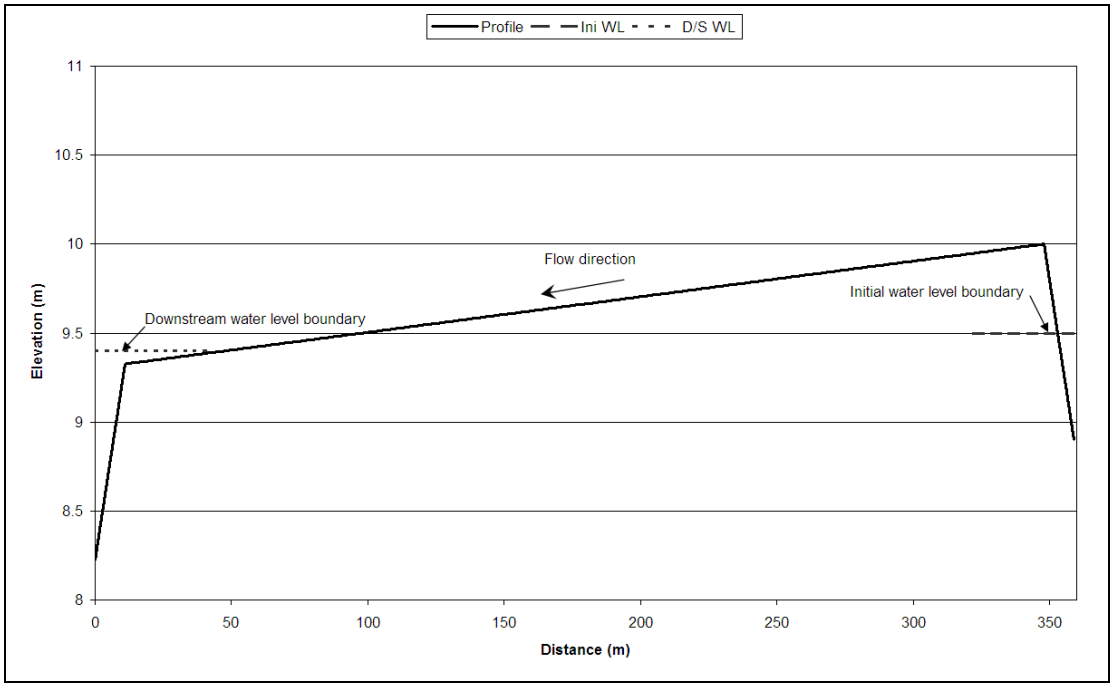

Figure 5.2: Section of the basin

5.2.1 Regular building layout

To achieve a regularly distributed urban building layout, buildings of size 12 m ×12 m are located at a distance of 96 m from the upstream edge and at 45 m distance from left and right side walls. The buildings are placed 6 m apart which is representative of typical street widths. Figure 5.3 shows the plan view whereas Figure 5.4 shows the section through the centre of the basin with the buildings in place.

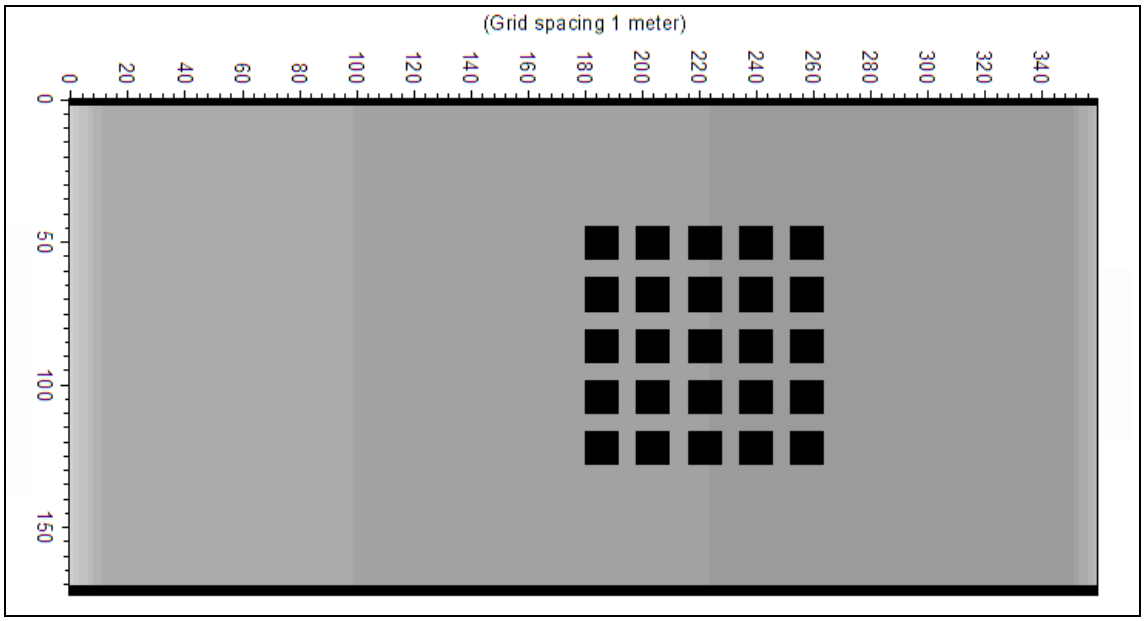

Figure 5.3: Plan view – regular building layout

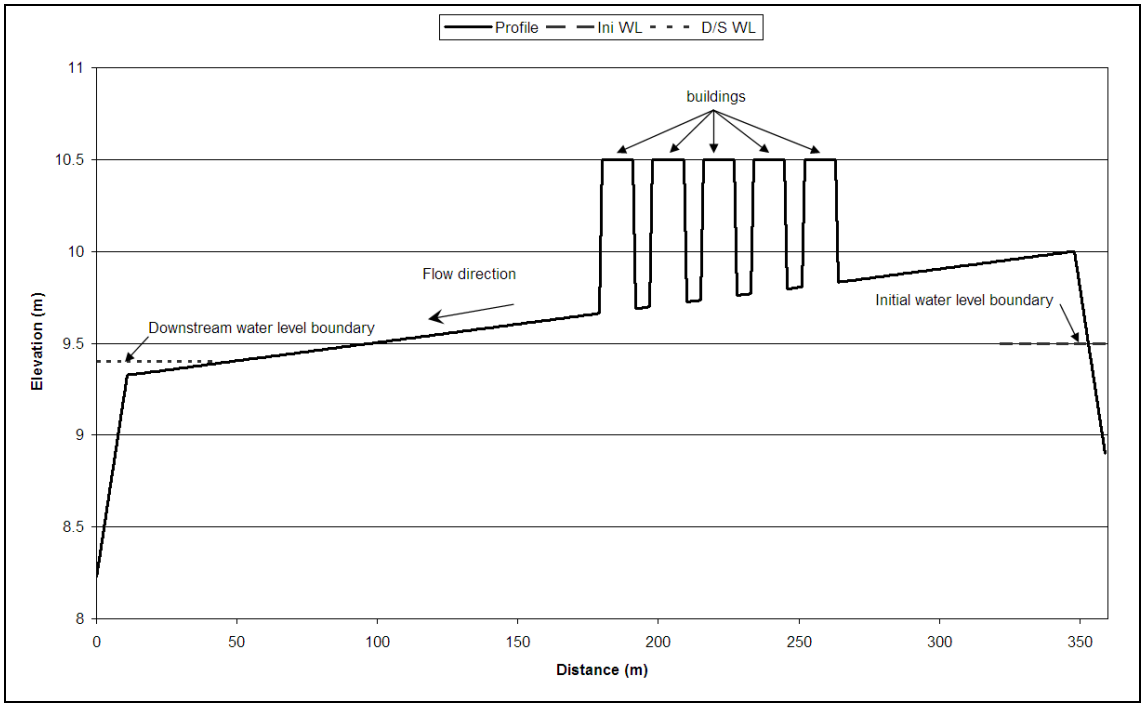

Figure 5.4: Section – regular building layout

5.2.2 Parallel building layout

Taking the *regular building layout* as reference, topography for *parallel building layout* is created by extending the buildings so as to close off the streets perpendicular to the flow direction. Figure 5.5 shows the plan view whereas Figure 5.6 shows a section through the centre of the basin with the buildings in place.

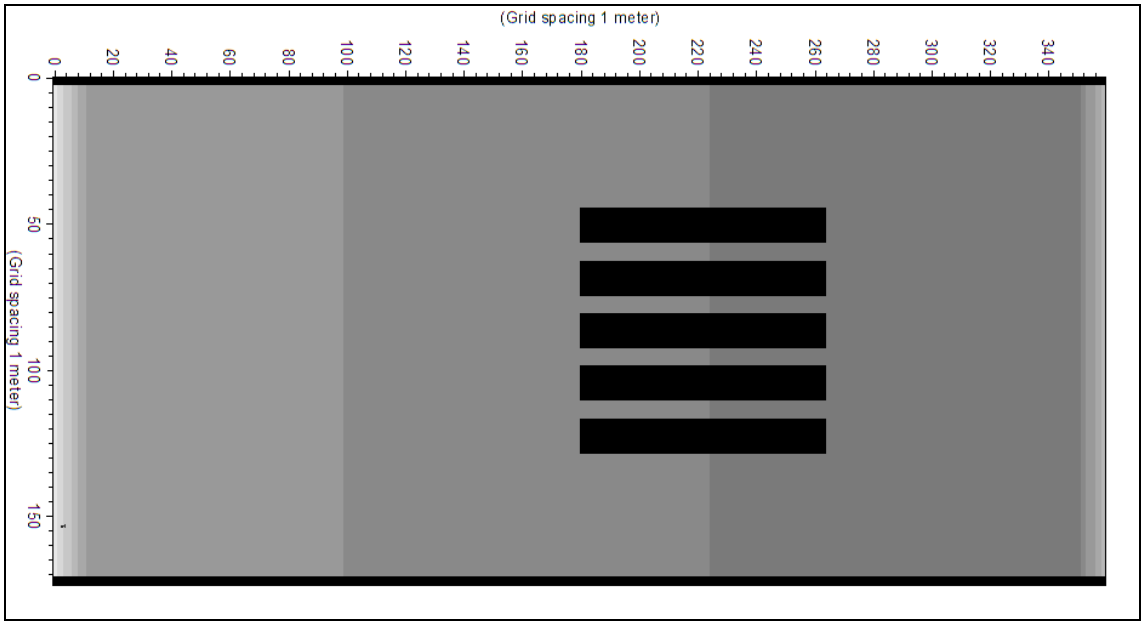

Figure 5.5: Plan view – parallel building layout

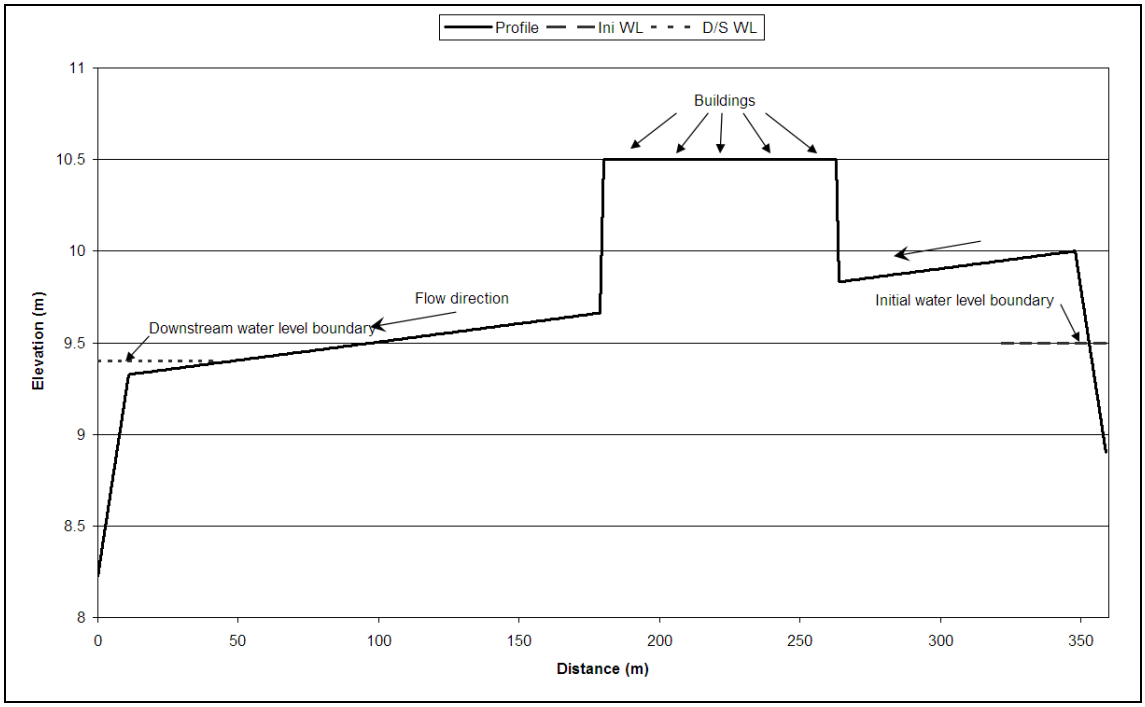

Figure 5.6: Section – parallel building layout

5.2.3 Perpendicular buildings layout

Again, taking the *regular building layout* as reference, topography for *perpendicular building layout* is created by extending the buildings so as to close off the streets parallel to the flow direction. Figure 5.7 shows the plan view whereas Figure 5.8 shows a section through the buildings.

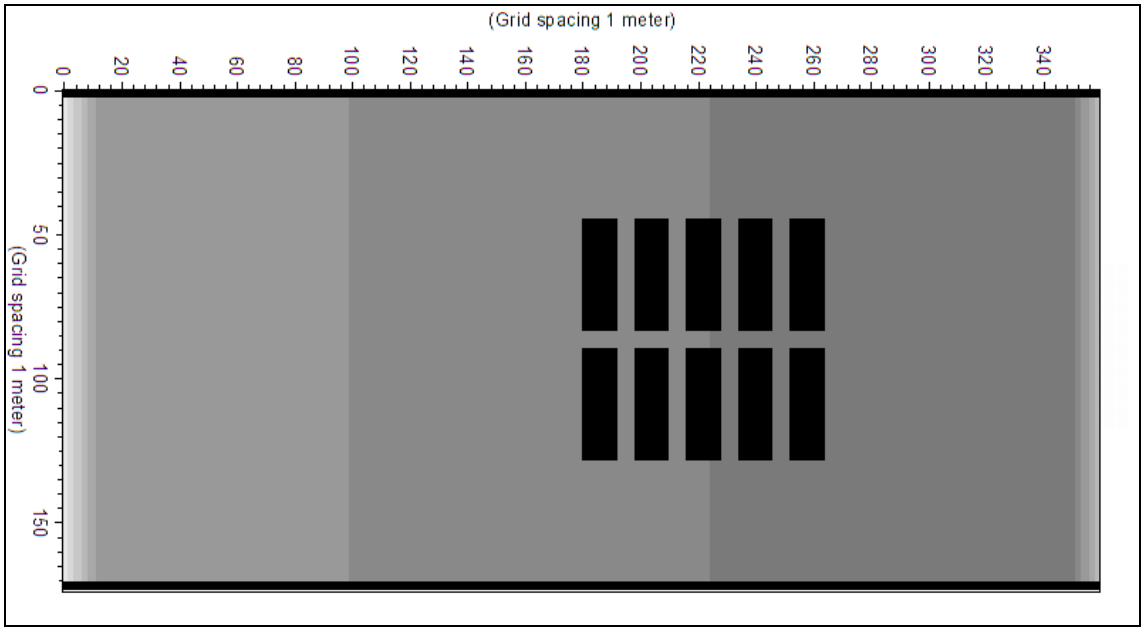

Figure 5.7: Plan view – perpendicular building layout

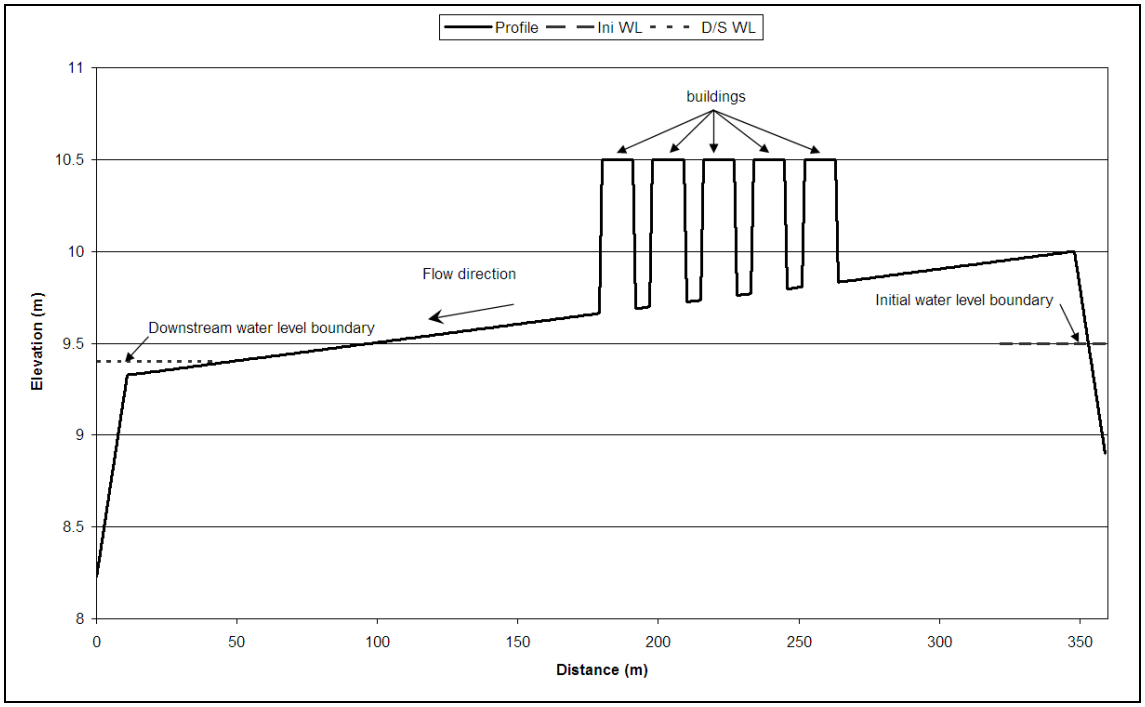

Figure 5.8: Section – perpendicular building layout

5.2.4 Skew45 building layout

Taking the *regular building layout* as reference, topography for *Skew45 building layout* is created by rotating the buildings by an angle of 45°. Figure 5.9 shows the plan view whereas Figure 5.10 shows the section through the centre of the basin with the buildings in place.

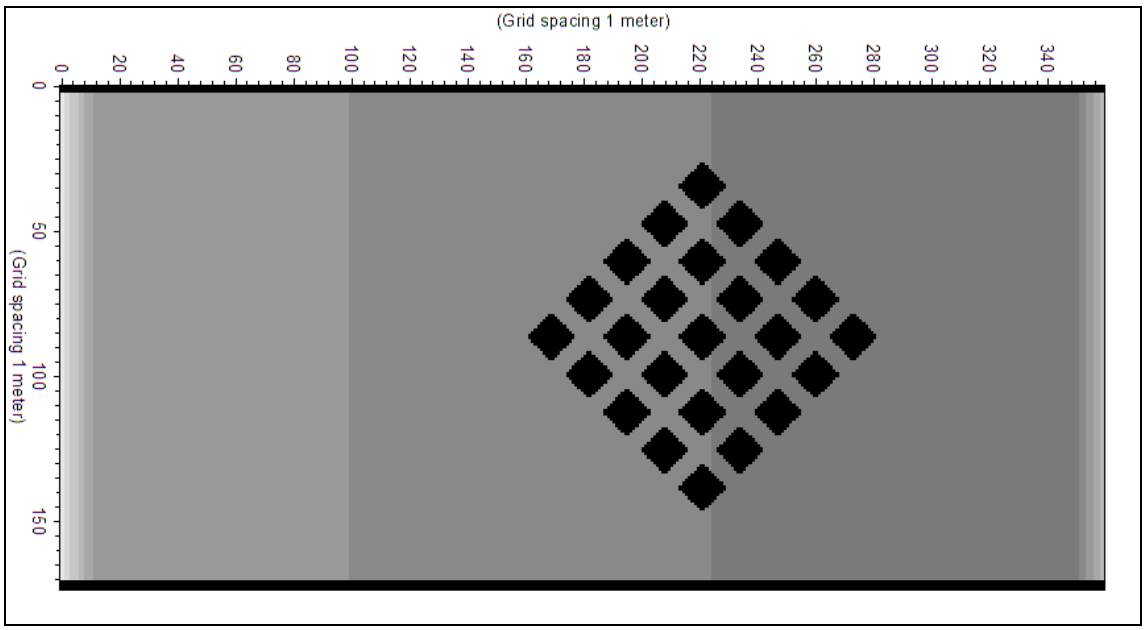

Figure 5.9: Plan view – Skew45 building layout

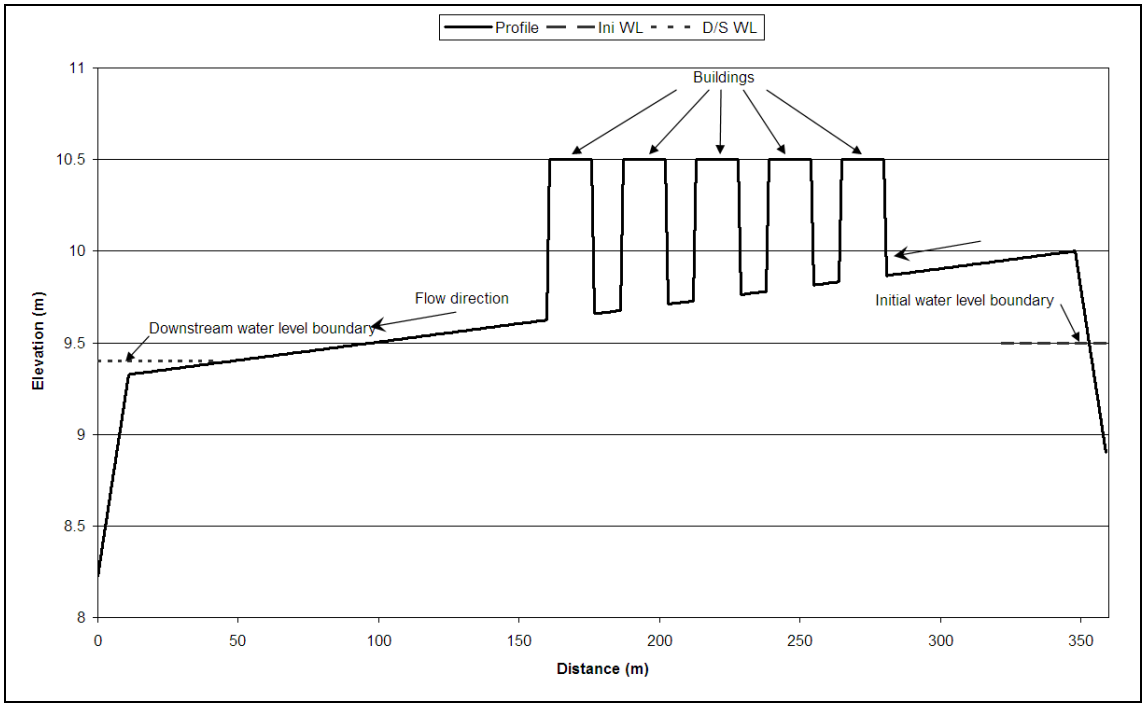

Figure 5.10: Section – Skew45 building layout

5.2.5 Skew30 building layout

In a similar way as above, taking the *regular building layout* as reference, topography for *Skew30 building layout* is created by rotating the buildings by an angle of 30°. Thus, the walls of the buildings are at an angle of 30° or 60° to the flow direction. Figure 5.11 shows the plan view whereas Figure 5.12 shows the section through the centre of the basin with the buildings in place.

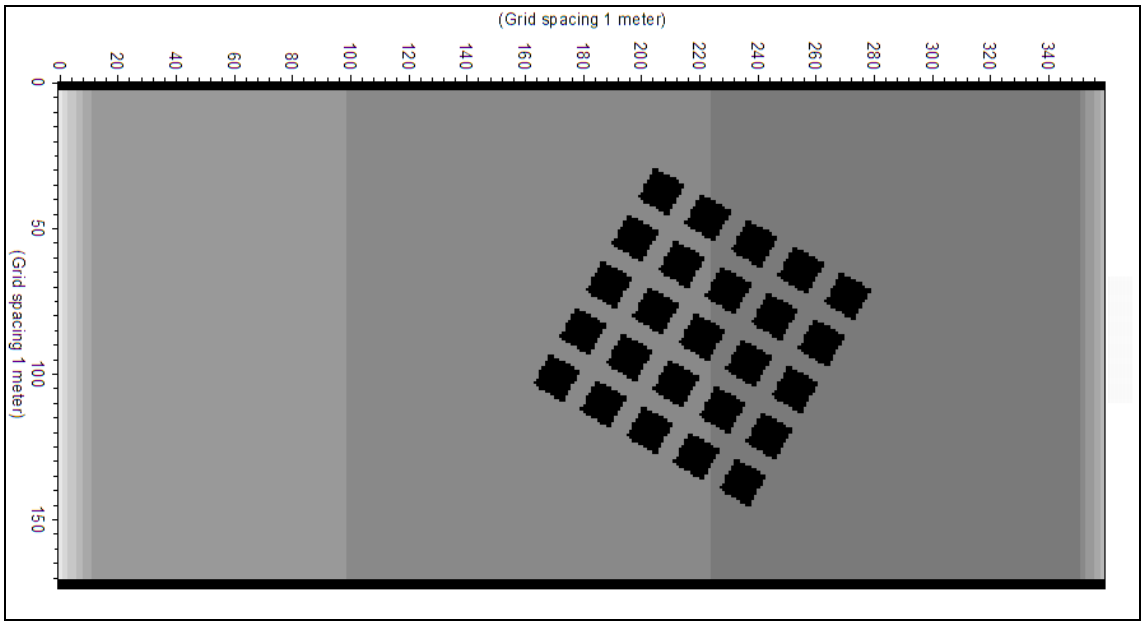

Figure 5.11: Plan view – Skew30 building layout

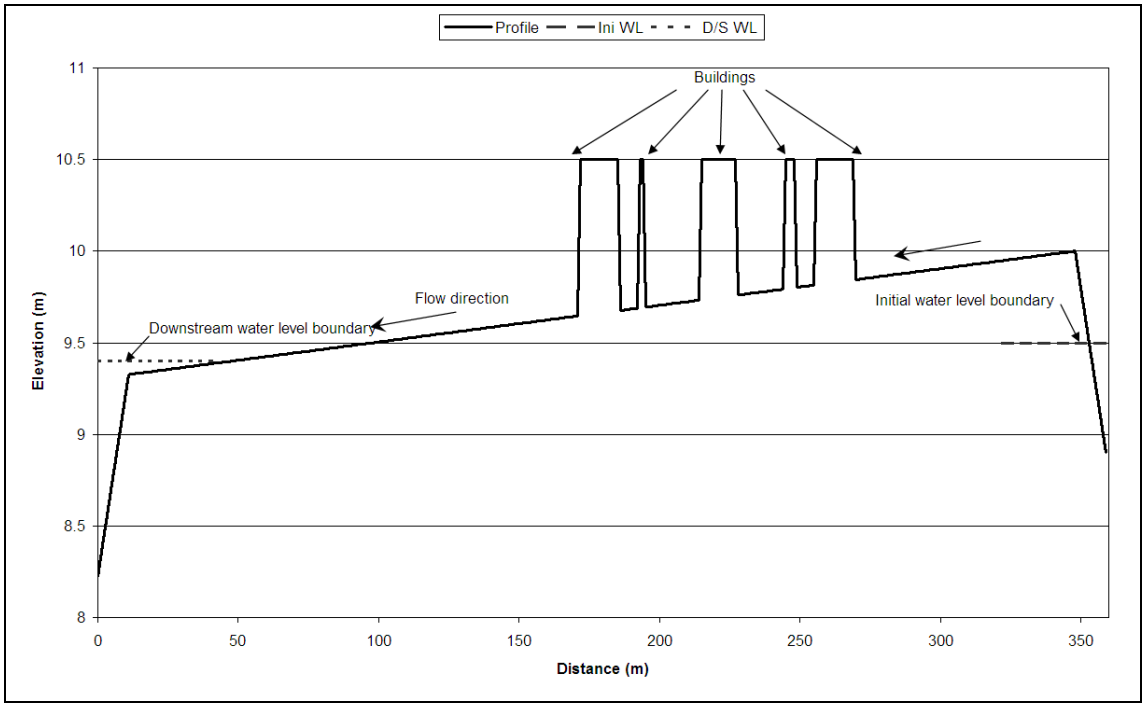

Figure 5.12: Section – Skew30 building layout

5.3 Details of simulation runs – topography data type

The details of boundary conditions and hydraulic and run-time parameters applied for the simulations are given below:

5.3.1 Upstream boundary condition

The simulations were carried out using two different inflow hydrographs; first with a peak of 50 cumec (Q_{50}) representing low flow scenario and the second with a peak of 100 cumec (Q_{100}) representing high flow scenario. The inflow hydrographs are shown in Figure 5.13. In addition, simulations were carried out with a constant discharge of 100 cumec for 20 minutes.

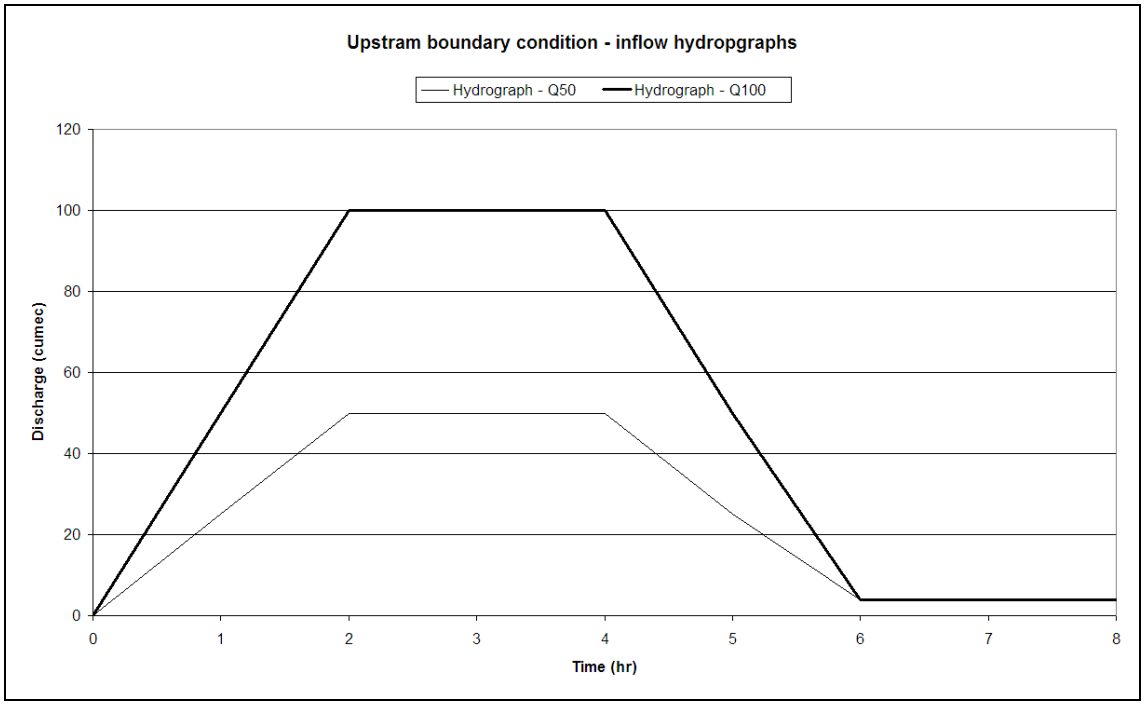

Figure 5.13: Upstream boundary condition - inflow hydrographs

5.3.2 Downstream boundary condition

A constant water level of 9.4 m is applied as downstream boundary for all the simulations. With this water level, part of the basin on the downstream side remains wet at all times and helps in avoiding potential instability problems. Further, with this water level, the extent of submergence is far away from the urban test section and thus does not interfere with the flow characteristics in and around this area.

5.3.3 Initial water level

The initial water level applied for all the simulations is 9.5 m (see Figure 5.4, Figure 5.6, Figure 5.8, Figure 5.10 and Figure 5.12). With this water level, the upstream and downstream boundaries remain initially wet. The water level then quickly recedes to the level of the downstream boundary water level.

5.3.4 Bed resistance

A typical value of Manning's *n* for winding and irregular natural earth channel ranges from 0.035 to 0.05 (Cruise et al. 2007). Therefore, a constant value equal to 0.04 is applied for the Manning's *n* parameter in all the simulations.

5.3.5 Wetting and drying depth

The cell wetting and drying depth applied for the simulations are 0.02 m and 0.01 m respectively. This means that a computational point is taken into calculations once the depth at that point reaches the wetting depth of 0.02 m and is taken out of the calculations when it falls below 0.01 m.

5.3.6 Simulation time step

The simulations are carried out with a time step of 0.5 s. This time step was chosen from model stability considerations based on guidelines for selection of run time steps described in the MIKE 21 documentation and ability to run all the setups at the same time step for logical runtime requirement comparison.

5.4 Results, analysis and conclusions – effect of topography data type

Simulations were carried out for all the five building layout configurations with the boundary conditions and hydraulic and run-time parameters given earlier. In addition, simulations without any buildings were also carried out. The effect of the buildings on the flow characteristics is then assessed by comparing the simulation results with buildings in the basin with those without any buildings. In MIKE 21, the value of V-velocity component and discharge is negative for a flow direction from the top to the bottom of the test reach.

Detailed below are the results and observations from the simulations using an inflow hydrograph with a constant discharge of 100 cumec for the *regular building layout*. Matrices of the maximum values of water depth and the minimum of V-velocity component for the entire flow duration are prepared for both the with and without building cases. To assess the effect of buildings on the flow characteristics, the matrices for the results without buildings in the basin are deducted from the results with buildings in the basin (see Figure 5.14 and Figure 5.15).

As seen in Figure 5.14, the water depth tends to increase in and around the urban test section, the maximum value of increase being 0.267 m in front of the central building in the front row. The water depth tends to decrease downstream of the urban test section,

the maximum decrease being 0.08 m in the wake of central building in the most downstream row.

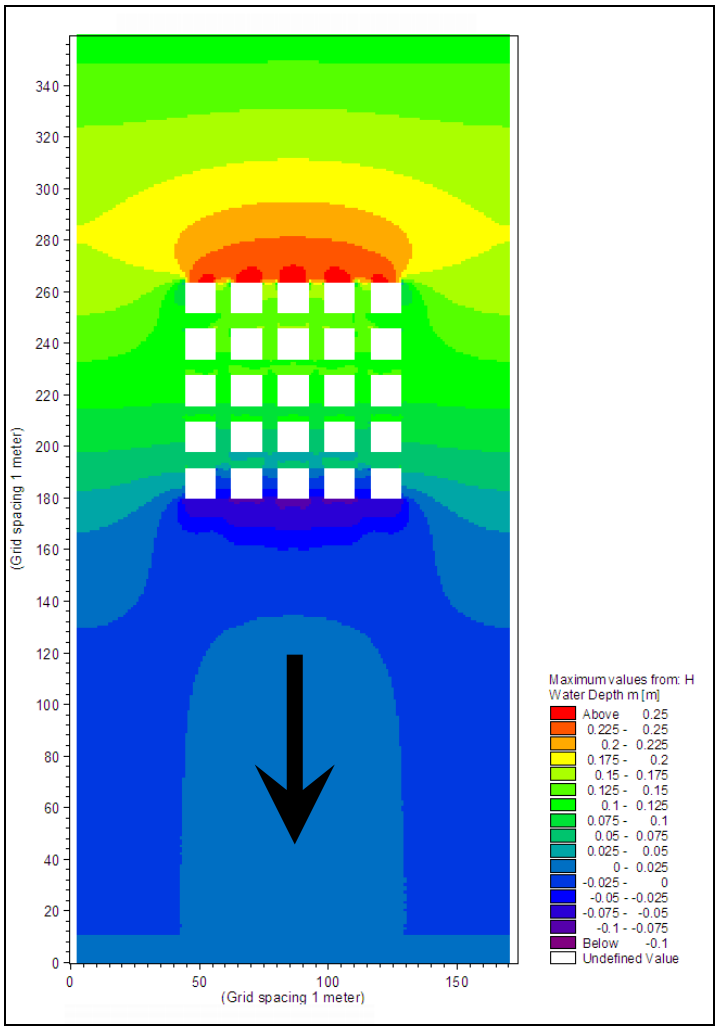

Figure 5.14: Effect of buildings on the flow depth (m)

Similarly, as seen in Figure 5.15, the V-velocity tends to increase in and around the urban test section, the maximum value of increase being 1.337 m/s. The V-velocity tends to decrease downstream of the urban test section, the maximum decrease being 1.457 m.

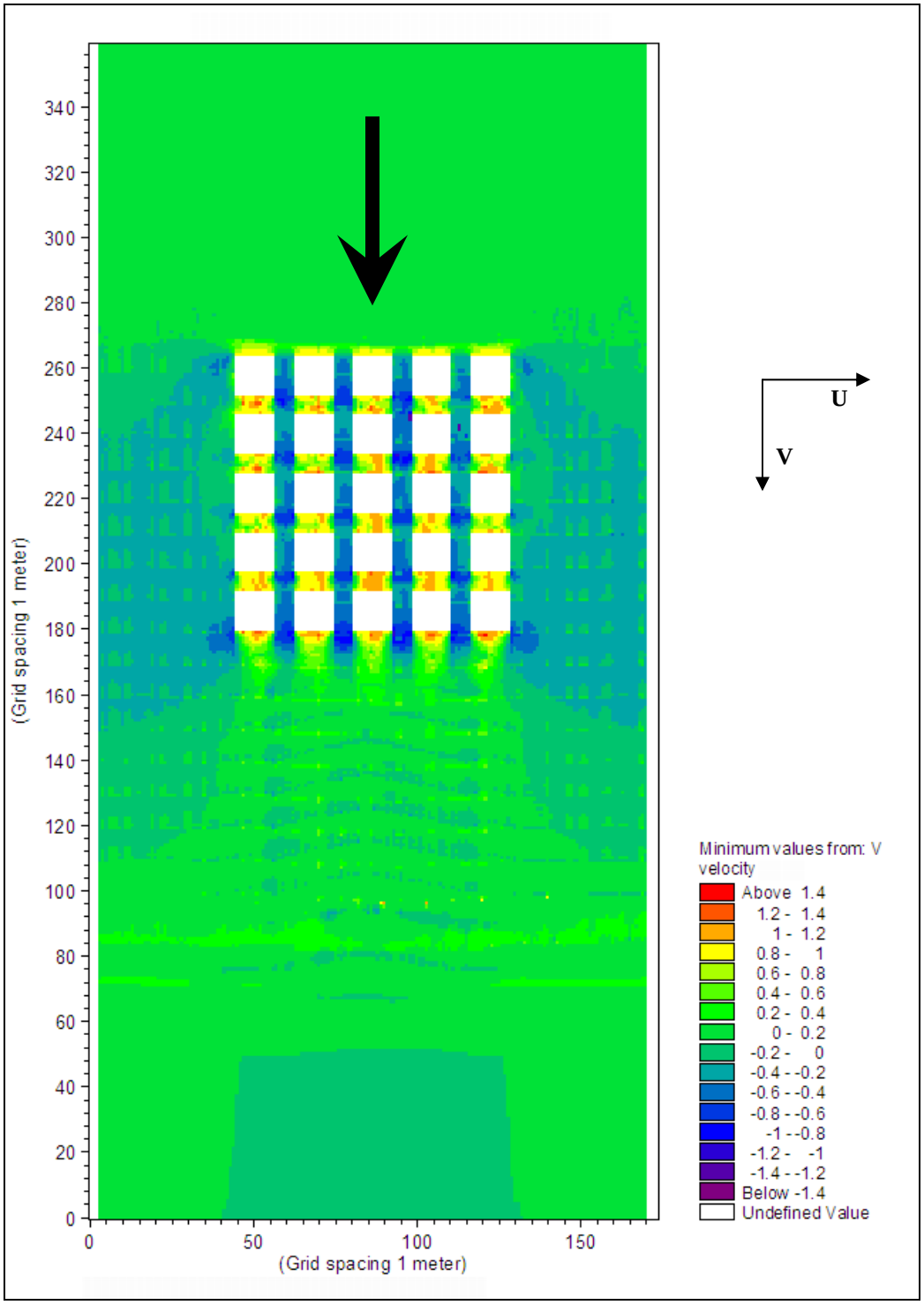

Figure 5.15: Effect of buildings on the flow velocity – V-velocity component (m/s) at t = 20 min

The changes in the V-velocity are not at the corresponding water depth points. This may be due an observed small variation in the U-velocity component. Ideally the value of U-velocity component should be 0.0 m/s for the case with no buildings or obstructions in the basin, but this was observed not to be the case. Figure 5.16 shows the U-velocity component map at t = 20 min.

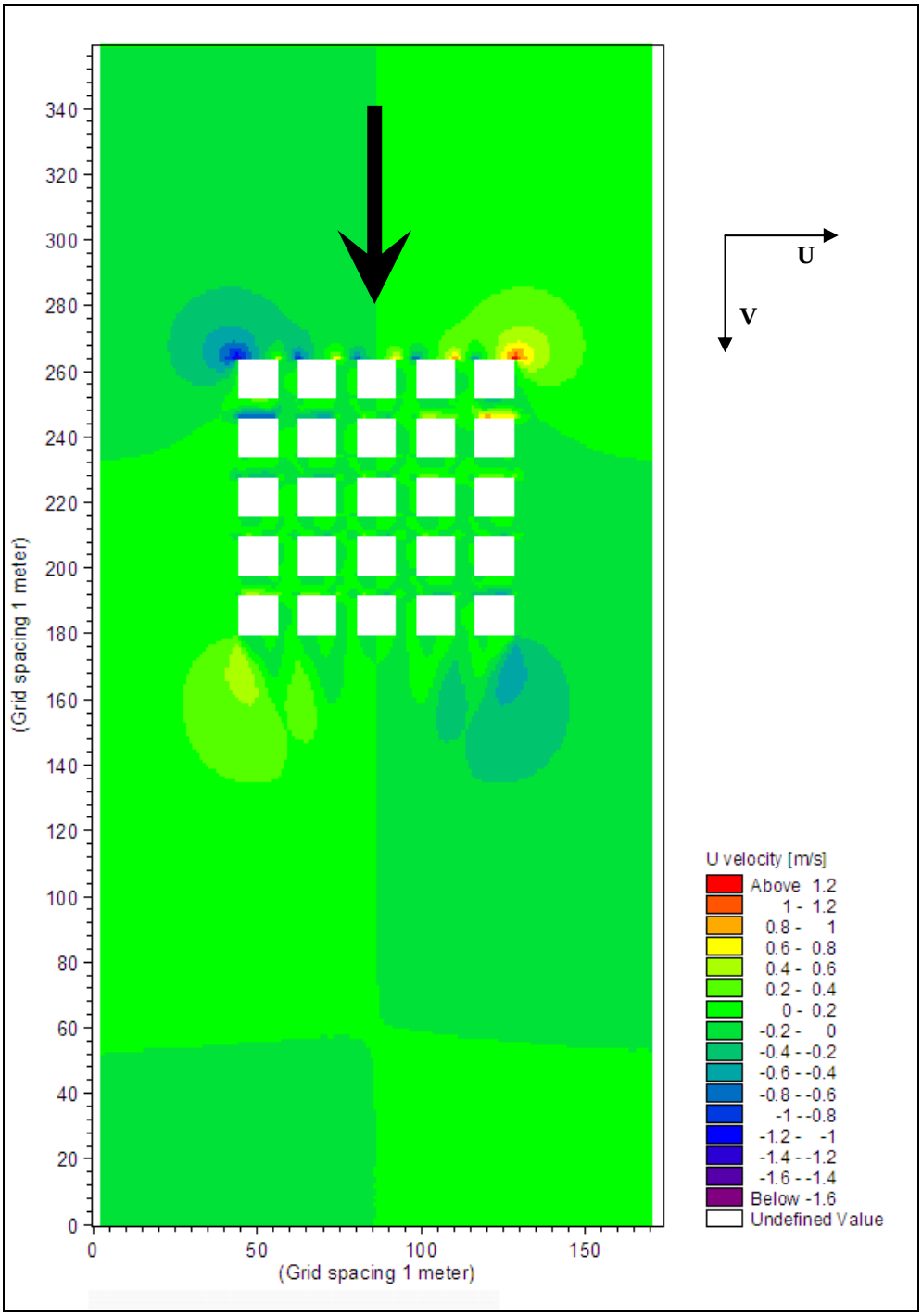

Figure 5.16: U-velocity component (m/s) at t = 20 min

Figure 5.17 shows the effect of buildings on the flow depth at time t = 20 min when the flow is stabilised and has become steady.

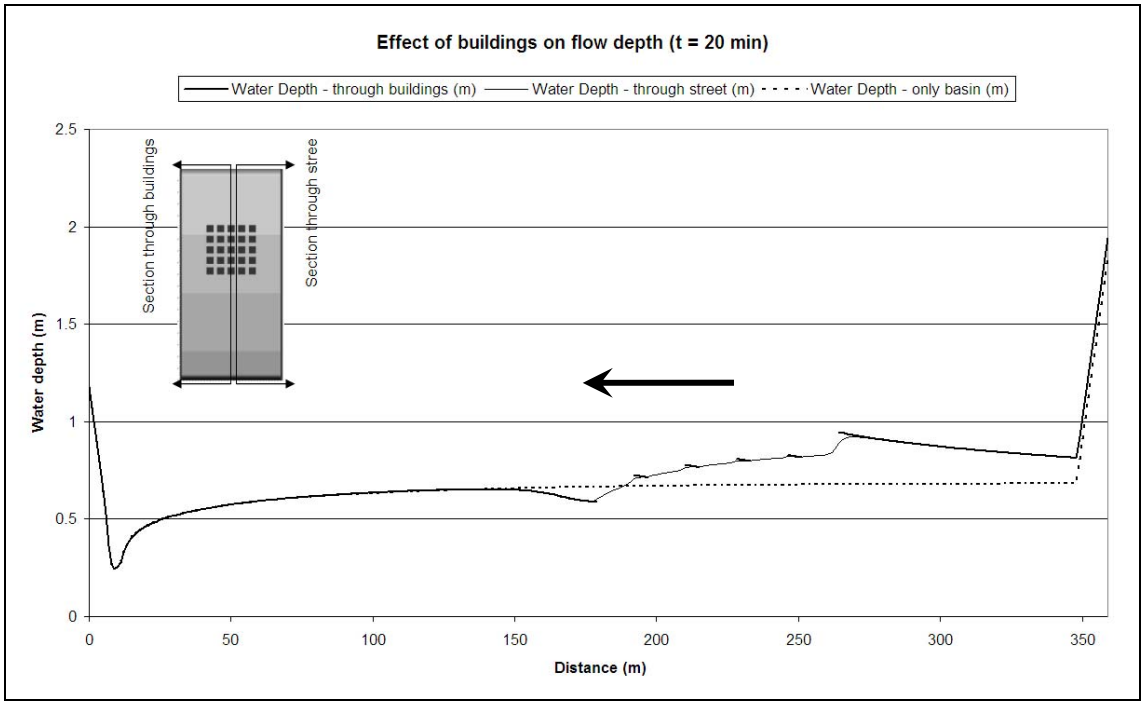

Figure 5.17: Effect of buildings on flow depth

Figure 5.18 shows the effect of buildings on the flow depth for the urban test section in detail. Formation of the shockwave in front of the buildings and wake formation at the downstream of the buildings can be clearly seen.

As mentioned earlier, see section 2.2.5, MIKE 21 employs selective up-winding of the convective momentum terms based on the Froude number to simulate local supercritical flows, flows over levees (considered as broad crested weir flow) and hydraulic jumps. It damps out high frequency numerical instabilities while having little effect on the overall computation and since it is selective, it does not affect accuracy of solutions in other areas (DHI Water, Environment & Health 2005b). In lieu of model validation as detailed and discussed in the previous chapter, the above representation of the shockwave is considered to be a fair representation of the flow phenomenon.

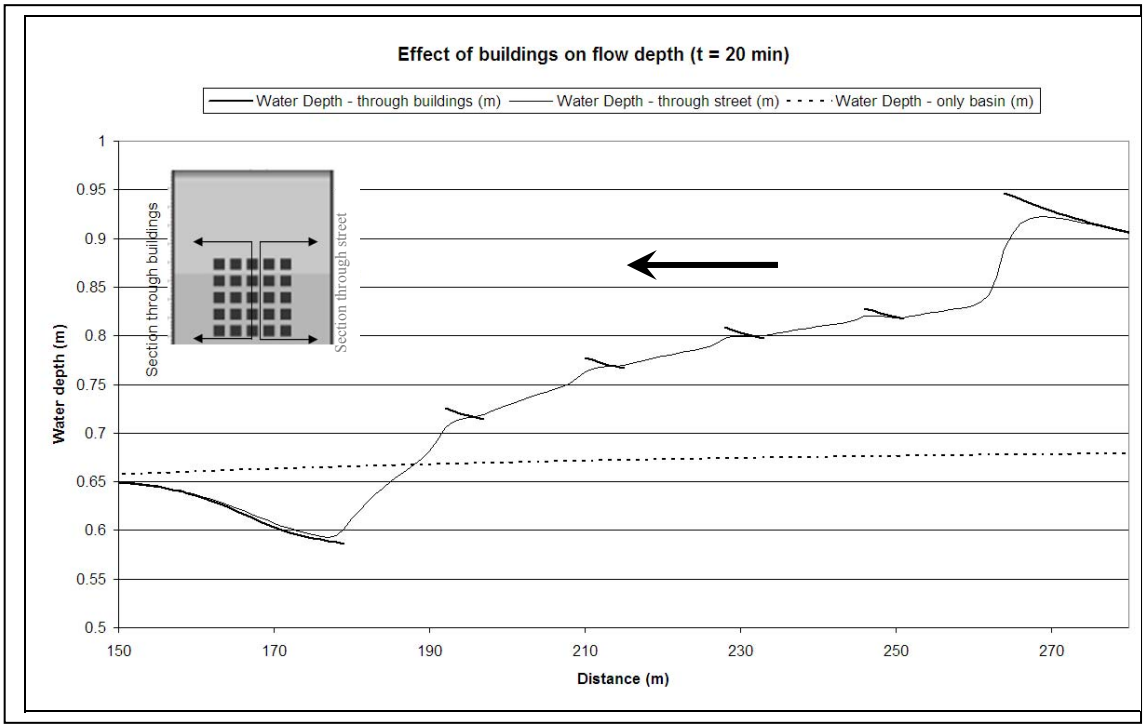

Figure 5.18: Effect of buildings on flow depth - detailed view

Figure 5.19 shows the effect of buildings on the V-velocity component of the flow. It is observed that the flow velocities increase in the streets and decrease in the front and wake of the buildings as compared to the computed velocities when there are no buildings, i.e. only basin.

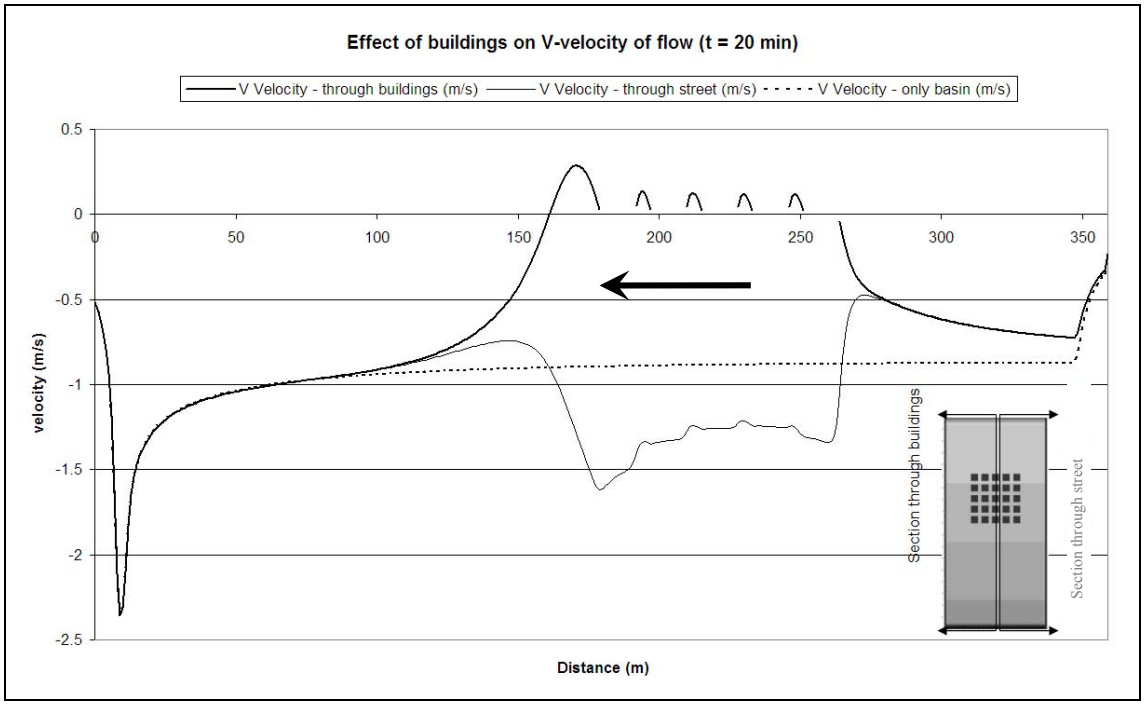

Figure 5.19: Effect of buildings on V-velocity component of flow

Before the water surface profile settles, development of a shockwave was observed in front of the buildings. The shockwave is formed when the water hits the front row of the buildings. The shockwave then progresses upstream before the water surface profile settles. Figure 5.20 shows the development and progression with time of the shockwave in front of the central building of the front row.

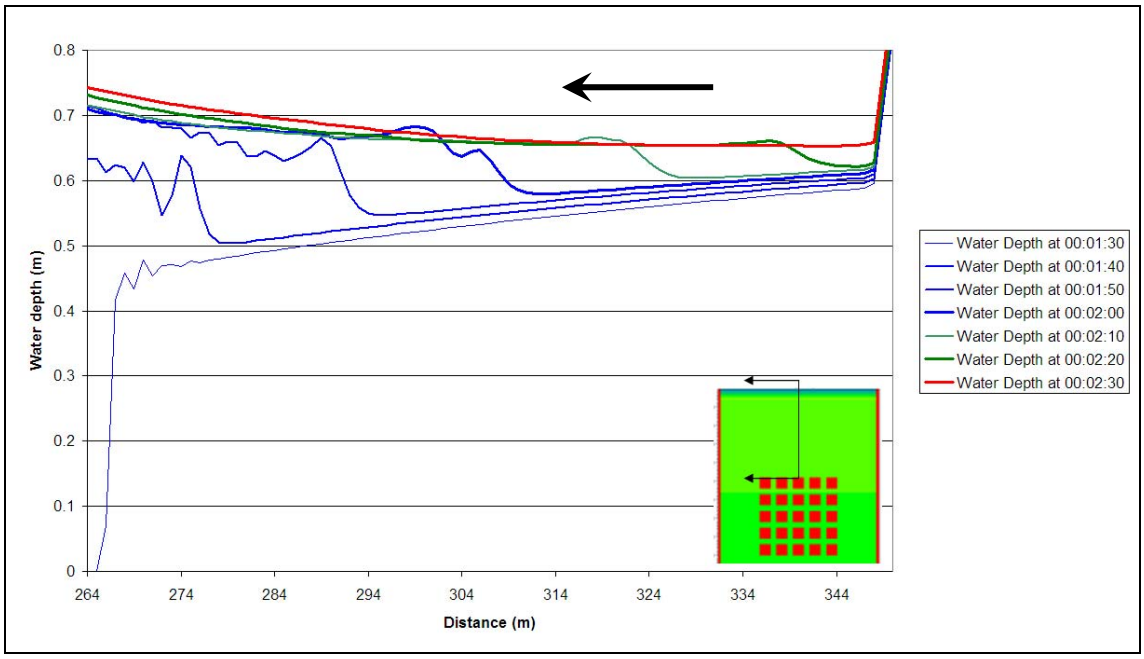

Figure 5.20: Shockwave in front of the buildings – Water depth profile

Although there is no blockage of flow before it enters the streets, a similar phenomenon was observed in front of the streets too. Figure 5.21 shows the development and progression of shockwave in front of the street on the right side of the central building of the front row.

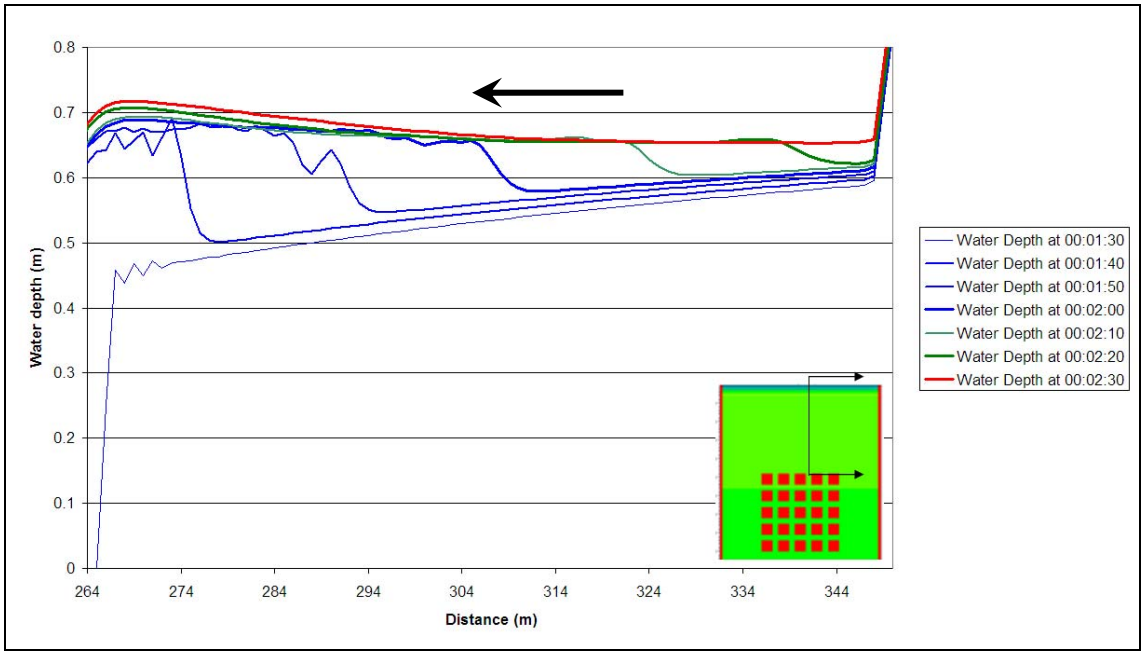

Figure 5.21: Shockwave in front of the street – Water depth profile

The corresponding changes in the V-velocity component are as shown in Figure 5.22 and Figure 5.23.

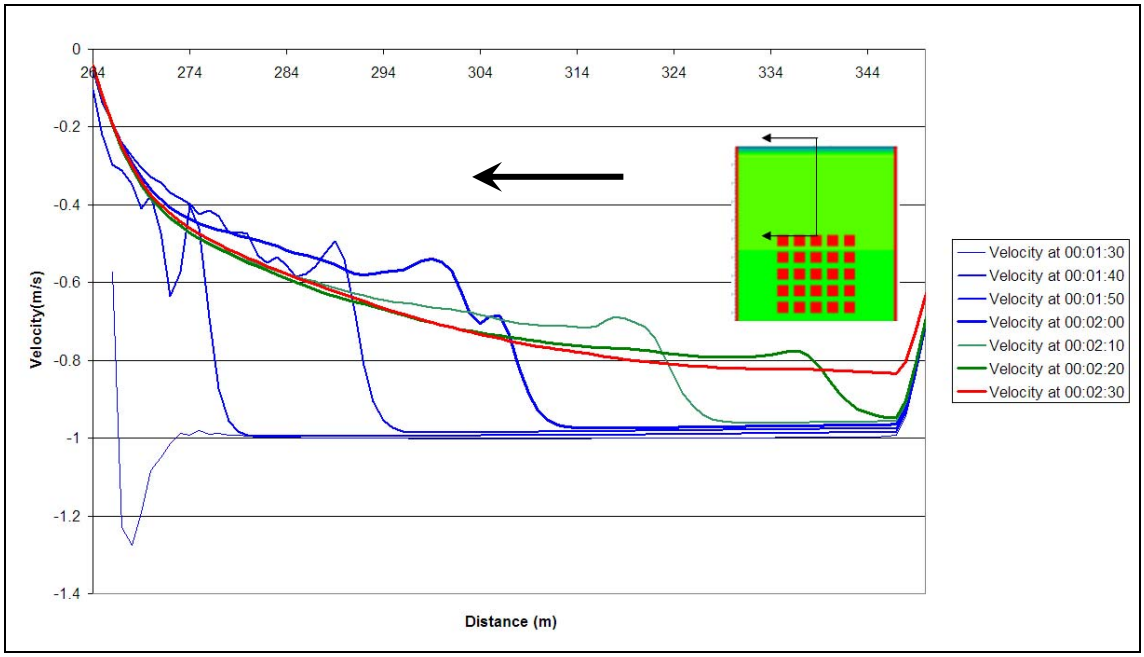

Figure 5.22: Shockwave jump in front of the buildings – V-velocity profile

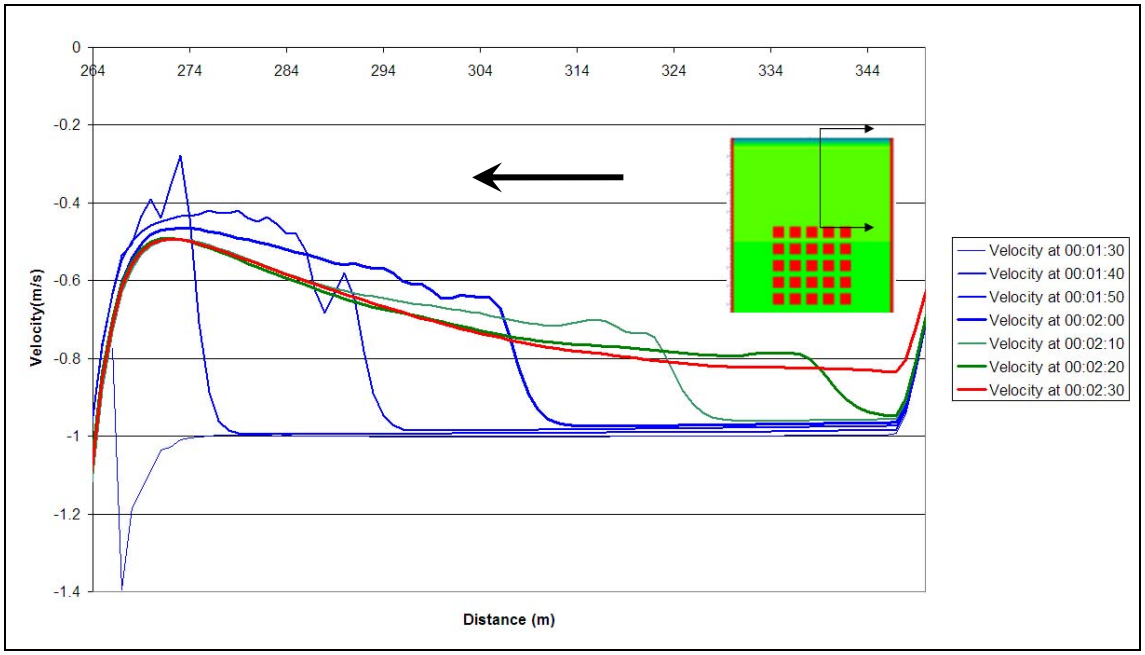

Figure 5.23: Shockwave in front of the street – V-velocity profile.

As the water negotiates the buildings and the streets, formation of eddies and development of complex flow pattern is observed. Figure 5.24 to Figure 5.26 show the development of complex flow pattern in and around the urban test section.

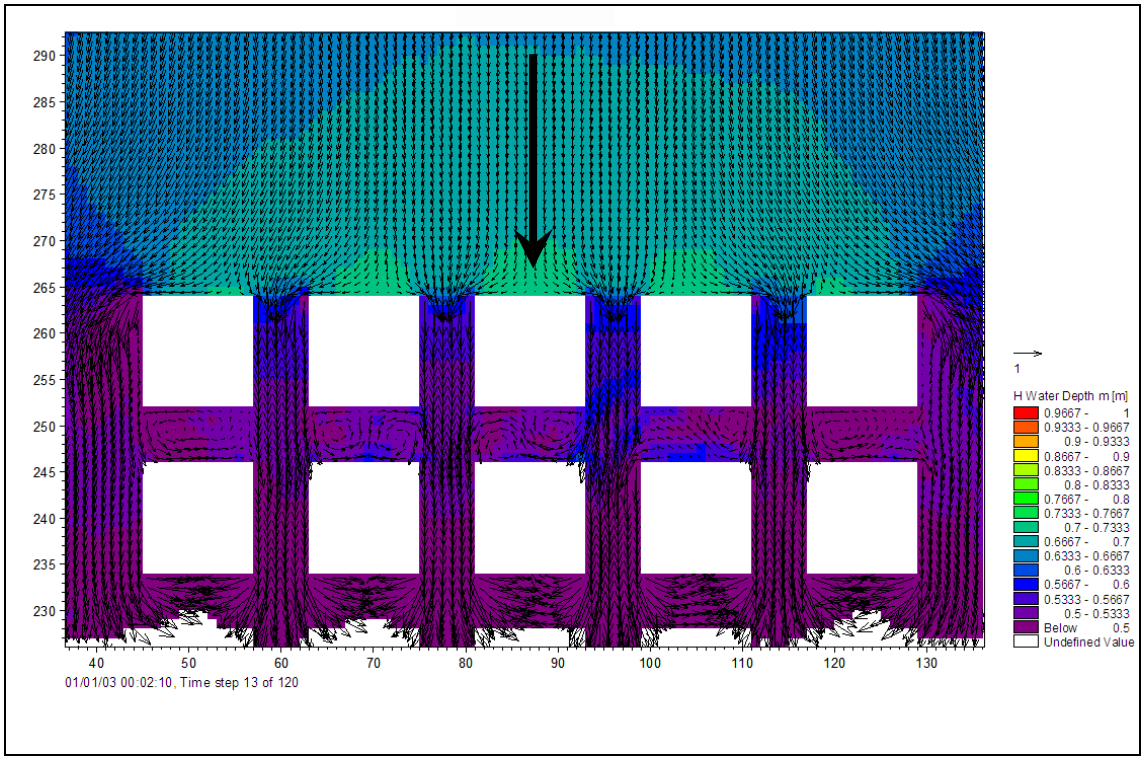

Figure 5.24: Flow mixing and eddy formation in the wake of buildings

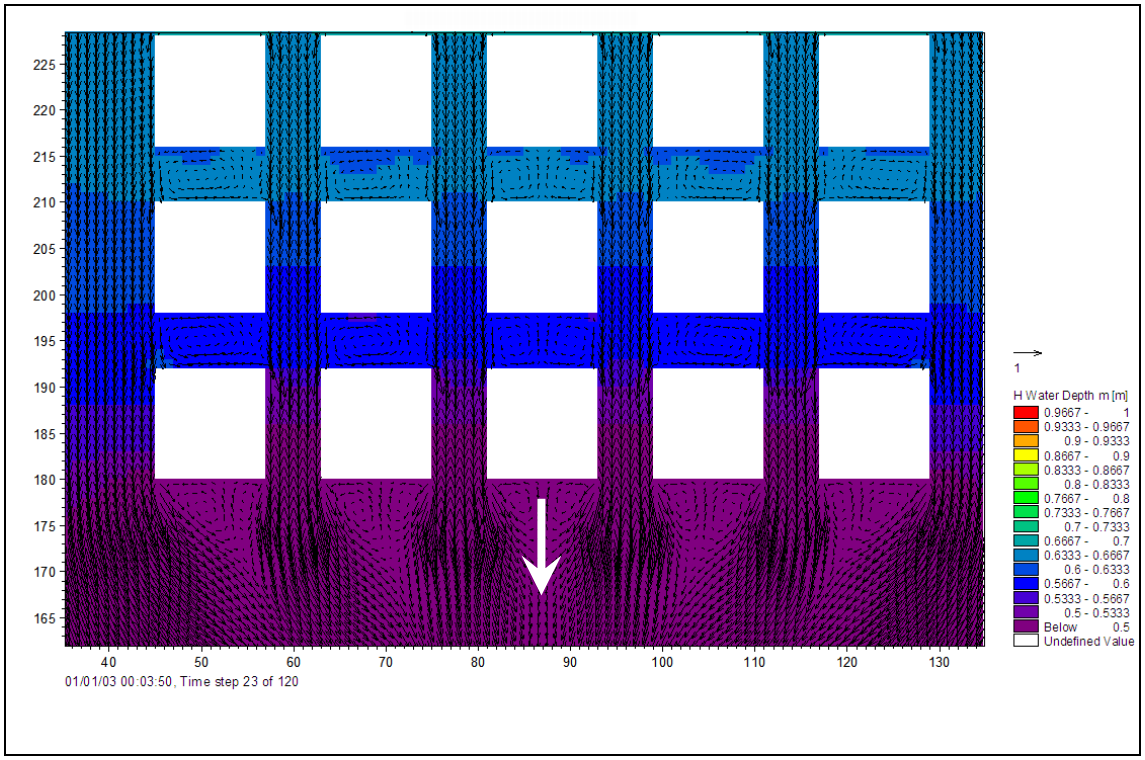

Figure 5.25: Flow pattern downstream of the urban test section

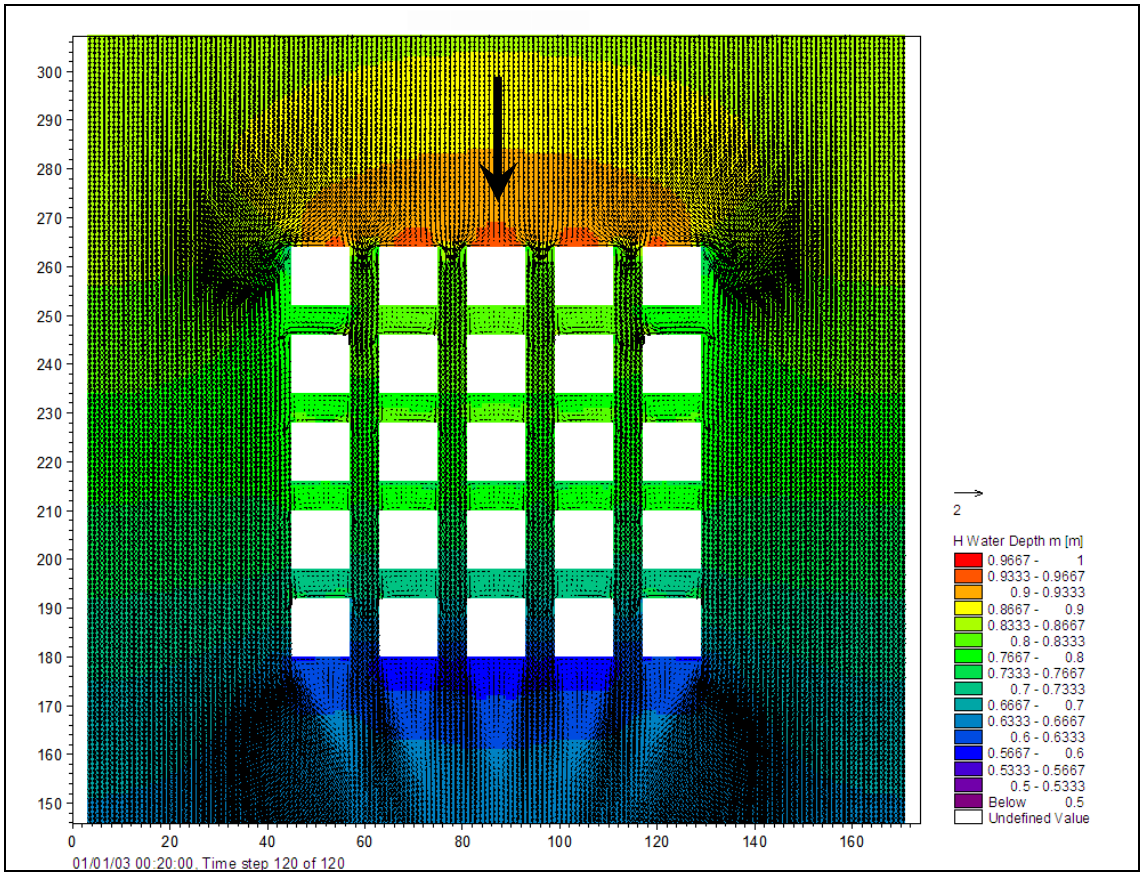

Figure 5.26: Flow pattern around the urban test section

Similar effects on the flood wave flow like development of eddies and complex flow patterns were observed for simulations with other input hydrographs as shown in Figure 5.13 which reach peak discharges of 50 cumec and 100 cumec.

From the water depth and velocity profiles, it is observed that the effect of the buildings on the flow characteristics in and around the *regular building layout* urban test section is substantial. Similar substantial effects on the depths and velocities of the floodwaters in and around the other building layouts in the urban test sections were observed. The effect of buildings on the flood depth and velocity for all the layouts is summarised in Table 5.1 below.

Table 5.1: Effect of buildings on flood depth and velocity

Building layout	Regular	Parallel	Perpendicular	Skew45	Skew30
Maximum increase in depth (m)	0.267	0.263	0.384	0.328	0.343
Maximum decrease in depth (m)	0.080	0.091	0.105	0.095	0.124
Maximum increase in V-velocity (m/s)	1.337	1.367	1.179	0.971	1.243
Maximum decrease in V-velocity (m/s)	1.457	1.023	1.396	1.272	1.396

Among the layouts considered, it was observed that the *perpendicular building layout* offers the highest amount of resistance to floodwater due to the highest blockage effect on the flow path.

From the results discussed above, it can be seen that the buildings in an urban floodplain have significant effect on the depths and velocities of floodwaters. Formation of shockwaves in front of the buildings and eddies in the wake of buildings is observed. These effects on the flood wave are not represented if a DTM is used for the flood modelling instead of a DEM and therefore the predictions from a flood modelling exercise carried out using DEM topography data is more realistic, particularly so when carried out for complex urban areas.

5.5 Buildings as storage areas study

5.5.1 Introduction

The appropriateness and feasibility of representing buildings as storage areas was described and justified earlier, see section 3.2.2. As mentioned therein, the effect of considering buildings as storage area is simulated in this research by applying a very high fictitious resistance value at the building footprints.

5.5.2 Model bathymetries

The model bathymetries are the same as described earlier in section 5.2.

5.5.3 Boundary conditions and hydraulic parameters

To simulate buildings as storage areas, a fictitious very high value of Manning's *n*, equal to 0.8 $m^{1/3}/s$ was applied to the topography cells covered by the footprints of the buildings. In view of the typical values for Manning's *n* for floodplains with heavy brush equal to 0.075, the value selected in this study is considerably high. This consideration therefore is aimed at finding out whether representations of buildings as high resistance blocks is feasible in this way and also to see the effect, if any, more predominantly.

The boundary conditions, initial water level, bed resistance for areas other than building footprints as well as wetting and drying depths applied during the simulations are the same as described in section 5.3 earlier. The time step used during the simulations is either 0.3 s or 0.5 s.

5.6 Results, analysis and conclusions – buildings as storage areas study

As mentioned earlier, the buildings allow the storage of water and the reduction of velocity while it passes through them. Therefore, positive water depths in the footprint of the buildings and lower velocities in the streets are expected when buildings are considered as storage areas as opposed to when considered as being obstacles to flow. Figure 5.27 shows the water depths predicted for these scenarios for two different hydrographs at the same time step using regular building topography. The "Porous

building" notation in the graphs refers to the results for buildings considered as storage areas.

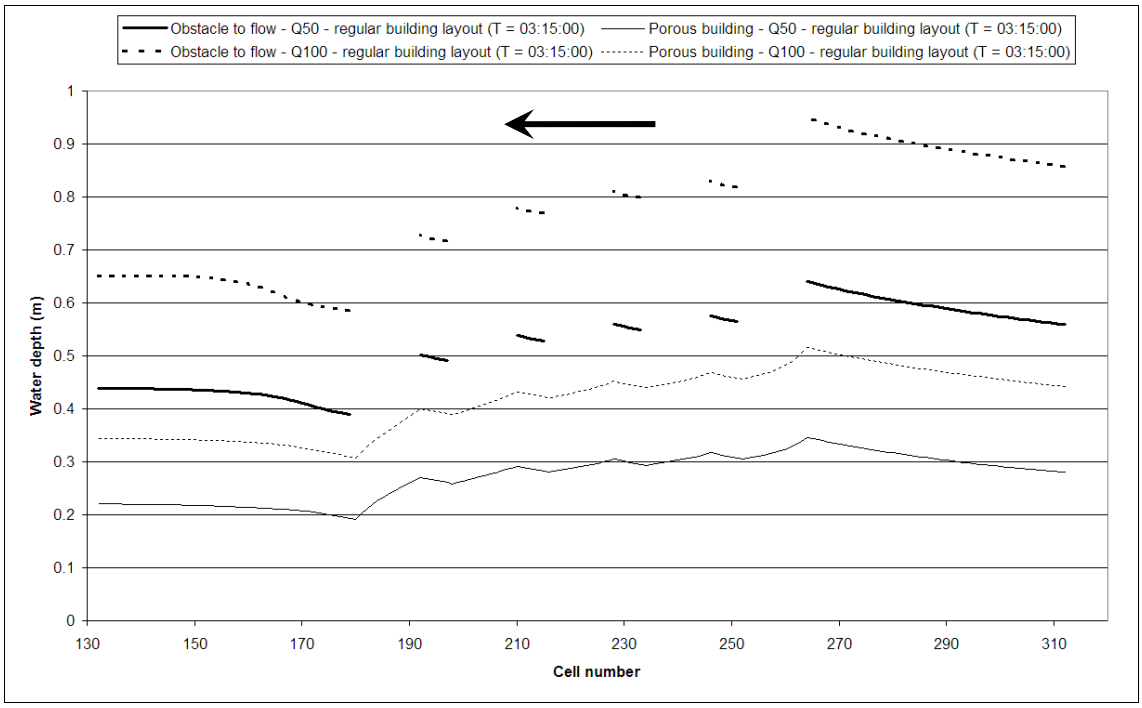

Figure 5.27: Comparison between water depths - buildings as obstacles to flow and when considered as storage areas

It can be observed that the water depths when the buildings are considered as storage areas are on an average 0.25 m lower – the maximum being 0.29 m and the minimum being 0.20 m – than the depths when considered otherwise for the inflow hydrograph with a peak of 50 cumec. The corresponding values when the inflow hydrograph has a peak of 100 cumec are 0.36 m (average), 0.43 m (maximum) and 0.27 m (minimum).

Figure 5.28 shows the V-velocity component values predicted for two different hydrographs at the same time step for the setups under consideration.

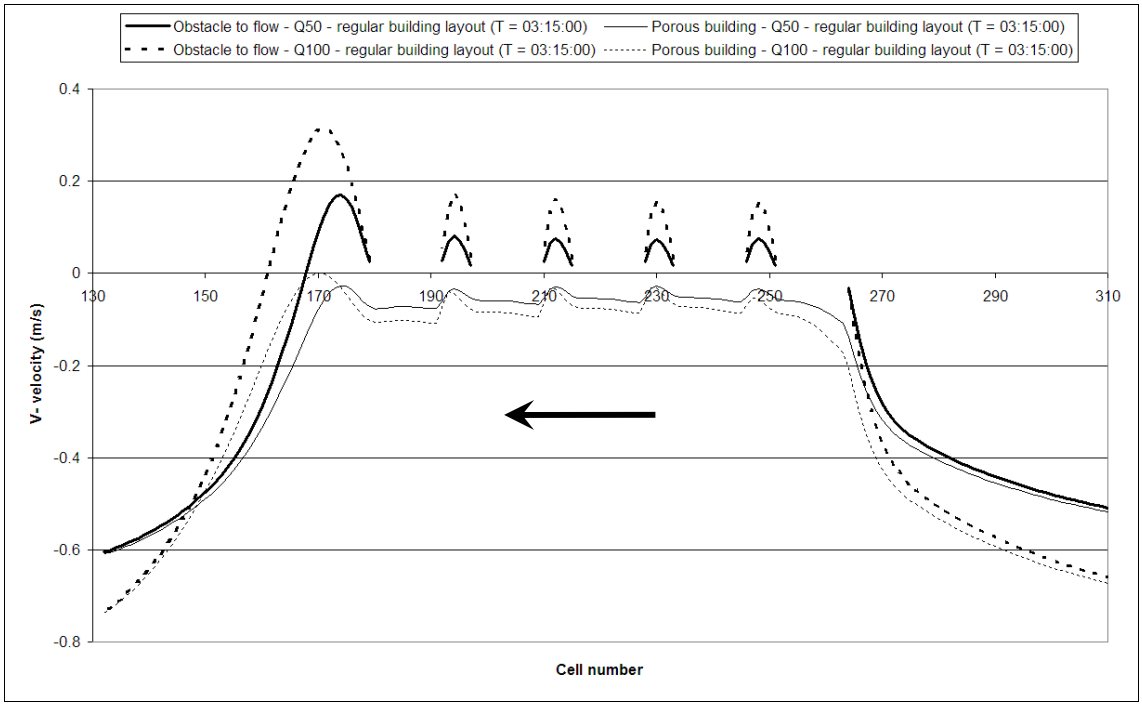

Figure 5.28: Comparison between V-Velocity - buildings as obstacles to flow and when considered as storage areas

It can be observed that the V-velocity component when the buildings are considered as storage areas are on an average 0.05 m / s lower – the maximum being 0.20 m / s – than the velocities when considered otherwise for the inflow hydrograph with a peak of 50 cumec. The corresponding values when the inflow hydrograph has a peak of 100 cumec are 0.11 m / s (average) and 0.45 m / s (maximum).

Similar effects of considering buildings as storage areas on flood water depths and velocities were observed for other building layouts.

From the results and analysis above, it can be concluded that the prediction of water depths and velocities in an urban floodplain is different when the buildings in the floodplain are considered to act as storage areas. It should be noted, however, that the flooding extents may be less with such a consideration and that the flood predictions when buildings are considered as obstacles to flow will tend to be conservative.

5.7 Model grid resolution – Nested grid model study

5.7.1 Introduction

As described in section 2.2.6, nested configurations help in obtaining detailed results for a smaller area of interest in a large model domain, as one may not be interested in the results outside this area. In a nested grid model, the domain outside an area of interest is represented by a coarse grid. The simulation, therefore, requires comparatively less computational effort and as such takes less simulation time. Using nested grid model methodology, simulations which are not feasible to run using normal desktop machines, can then be run using the same machines without losing the accuracy of results in the main area of interest.

In line with the research aims and methodology, see section 3.2.2, the purpose of this study, therefore, is to evaluate the relative merits – in terms of time taken to set up the model, simulation time required and the accuracy achieved. The simulations were run one at a time on the same computer without any other programs running. The nested grid model setups used for the tests and the results and the conclusions drawn are discussed below:

5.7.2 Model bathymetries and nesting

For the nested grid model test simulations, three of the earlier urban test section layouts viz. *Regular building layout*, *Skew45 building layout* and *Skew30 building layout* are used. Other layouts viz. *Parallel building layout* and *Perpendicular building layout* are not used as those are similar to the *Regular building layout*. The bathymetries in these layouts are 174 m wide and 360 m long, are prepared with 1 m spatial resolution, and hence, contain 62,640 computational grid points. In the nested grid model, these bathymetries are re-sampled to 3 m grid size, reducing the number of computational grid points to 6,960; which hereafter, are referred to as coarse grids.

To get better assessment of flooding around the buildings in the urban test sections, an area of 151 m width and 181 m length with the original 1 m spatial resolution is nested within this area; which hereafter is referred to as the fine grid. This constitutes 27,331 computational grid points. MIKE 21 does not carry out computations for the area in the outer coarse grid covered by the fine grid. Therefore, the number of computational

points in the coarse grid is reduced by 3,000 (excluding the 1 m overlap of fine grid with the coarse grid cells on the border of fine grid, which is required by the software). Thus, the setups will have 31,291 computational grid points which is 50 % less than those without nesting. This reduction in the number of computational grid points is expected to give a similar amount of benefit in terms of the reduction in the required CPU time as required CPU time is directly dependent on the number of computational grids. Further, it is also expected that the hydraulic conditions are transferred properly at the boundaries, therefore predicting hydraulic conditions in the nested area similar to those without nesting. The nested grid model geometry for the *regular building layout* is shown in Figure 5.29.

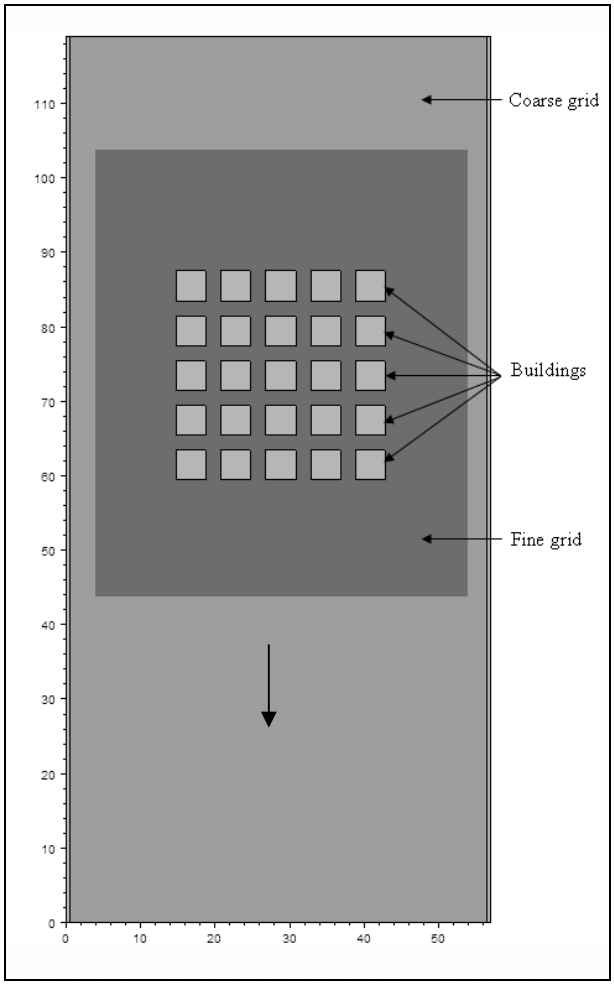

Figure 5.29: Nested grid model - regular building layout

While preparing the nested configuration, certain rules about the grid resolution ratio as well as placement and relative size of the grids need to be followed, requiring lot of

careful planning. If not properly carried out, it can be time consuming and frustrating experience for the modeller. Further, it was ensured that the boundaries of the nested area are sufficiently far away from the area of interest. The time required to prepare the three setups was about two hours.

5.7.3 Boundary conditions and hydraulic parameters

The inflow boundary conditions, initial water level, bed resistance as well as wetting and drying depths applied during the simulations are the same as described in section 5.3 earlier. Thus, simulations were carried out using three inflow hydrographs – first with a peak of 50 cumec, second with a peak of 100 cumec and a third with a constant discharge of 100 cumec. The time step used during the simulations was either of 0.3 s or 0.5 s. In order to have proper comparisons, it was ensured that the time step for simulations with a particular hydrograph was the same for regular as well as nested grid model setups.

5.8 Results, analysis and conclusions – nested grid model study

The time taken by the various model setup simulations is reported in Table 5.2.

Table 5.2: Relative saving in CPU time (in seconds) by nested grid models

Regular building layout			
Hydrograph	Q_{50}	Q_{100}	$Q_{100\ constant}$
Regular grid model	2360 s	2379 s	97 s
Nested grid model	1162 s	1029 s	47 s
CPU time saved	50.76 %	56.75 %	51.55 %
Skew45 building layout			
Hydrograph	Q_{50}	Q_{100}	$Q_{100\ constant}$
Regular grid model	2490 s	2469 s	143 s
Nested grid model	1237 s	1243 s	73 s
CPU time saved	50.32 %	49.66 %	48.95 %
Skew3060 building layout			
Hydrograph	Q_{50}	Q_{100}	$Q_{100\ constant}$
Regular grid model	2400 s	2520 s	147 s
Nested grid model	1175 s	1192 s	74 s
CPU time saved	51.04 %	52.70 %	49.66 %
CPU time saved for all setups		Minimum	49 %
		Maximum	57 %
		Average	51 %

It was observed that, on average, the nested grid models took 51 % less CPU time. The total CPU time required for the entire set of regular grid simulations is 4 hours, 10 minutes and 5 seconds; whereas, that for the nested grid simulations is 2 hours and 32 seconds.

Considering the modeller's 2 hour time, which was required for constructing nested grid model setups, this does not seem to be a feasible option. But the modeller's time required for constructing nested grid models is a one off investment and the same set up can be used multiple times for subsequent studies. Further, for large models of urban floodplains with small area of interest – which otherwise may require days to run – this seems to be a very promising option. This hypothesis will be tested further using a real floodplain data described in Chapter 6.

The water depths predicted by the nested grid models were compared with those predicted by the regular grid model for the same computational time step. Figure 5.30 shows the water depths as predicted by the regular grid model and nested grid model for *Regular building layout* and flood hydrograph with a peak of 50 cumec, for the same time step along the basin centreline. It was observed that the water depths were predicted, to the nearest millimetre, in the area covered by the buildings. However, the water depths predicted downstream of the nested area were slightly lower (see encircled part of the graph in Figure 5.30) by an average of 1 mm, the maximum being 4 mm. For practical purposes these can be considered as the same, pertaining to the fact that the topographies represent prototype scale of a hypothetical urban floodplain and that a few millimetres will not make a difference to the end uses of flood modelling in urban floodplains. Further, it was observed that the above conclusions are not affected by the choice of hydrograph or building layout.

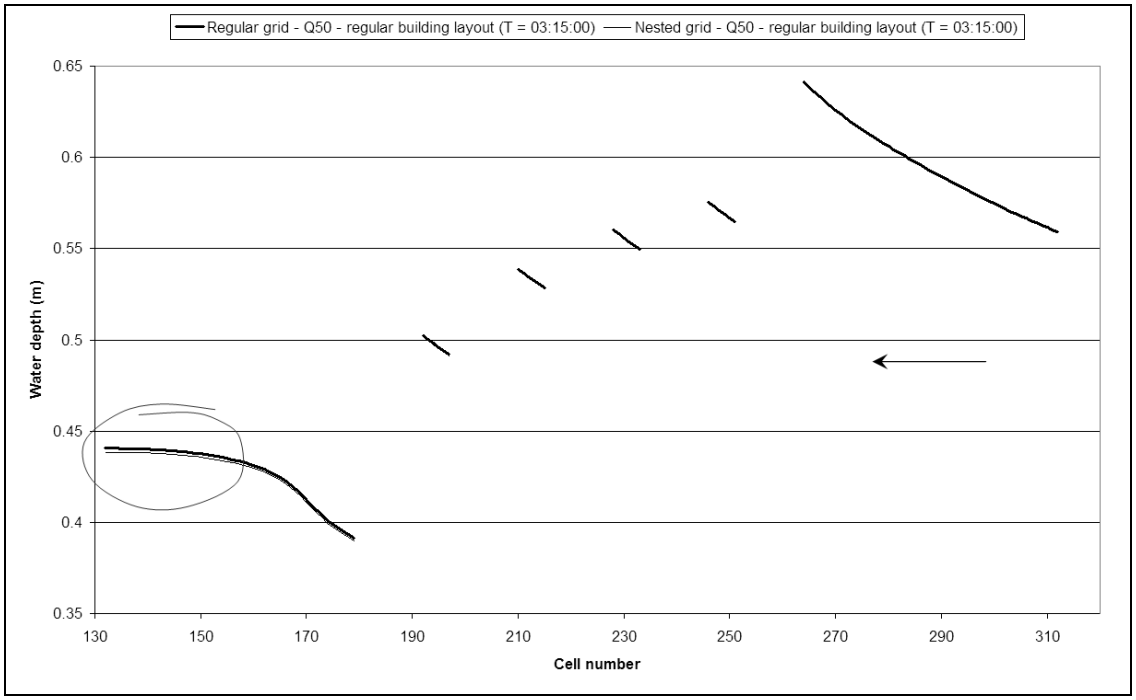

Figure 5.30: Comparison between water depths predicted by regular grid and nested grid models

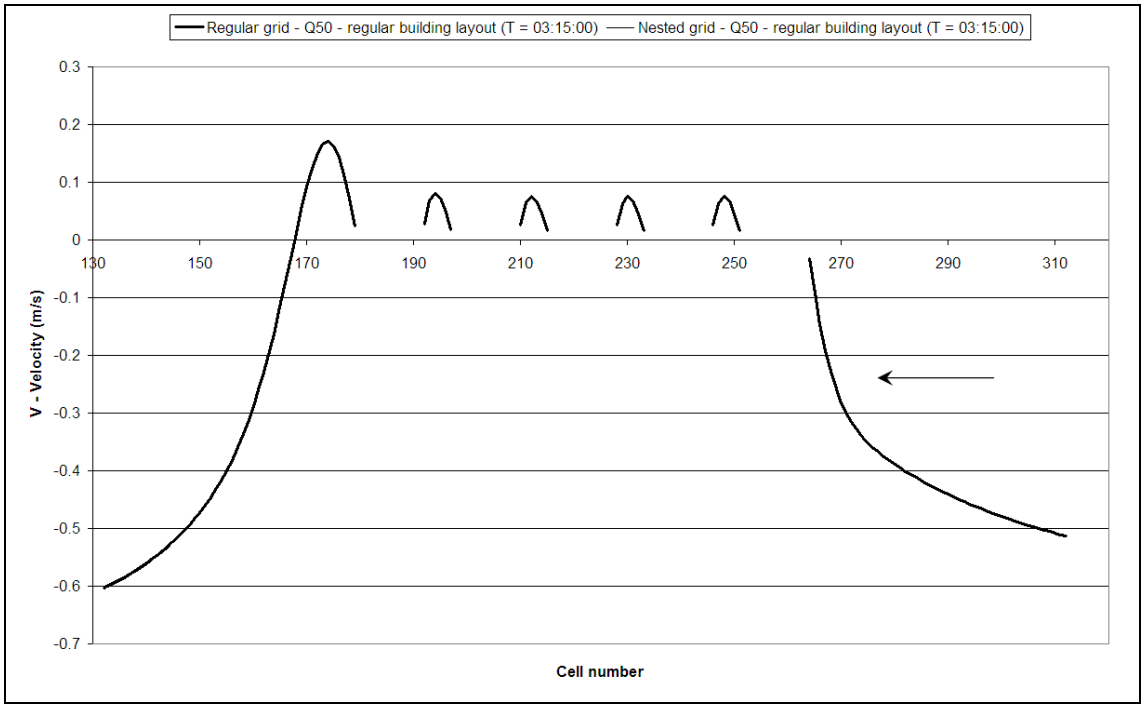

Figure 5.31: Comparison between V-velocity predicted by regular grid and nested grid models

The V-velocity component does not show any noticeable differences in predictions as can be observed from Figure 5.31.

5.9 Summary

One of the objectives of the study was to carry out simulations to analyse the effect of considering DEM and DTM data for flood modelling, i.e. to study the effect of buildings on flood wave propagation in a complex urban area. It concludes that usage of DEM instead of DTM provides a more realistic representation of the flood wave in complex urban areas. The buildings represented by DEM in urban floodplains have considerable effect on the flood wave characteristics affecting the depths and the velocities of the floodwaters significantly and that complex flow patterns are developed in and around the buildings. Since buildings are not represented in a DTM, the effect of buildings on the flood wave will not be represented if modelling studies are carried out using DTM topography data.

Secondly, with an objective of studying the effect of representing buildings as storage areas, thus offering floodwater storage and reducing floodwater velocities was studied by applying a high value of Manning's *n* resistance coefficient at the computational grids covered by the buildings. The study concludes that the consideration of buildings in urban floodplain as storage areas as opposed to obstacles to the flow results in a reduction in the water depths and velocities in the streets. This approach may particularly be useful while assessing the flood inundation depths and velocities due to slow moving floods.

Further, nested grid simulations were carried out to see if the dynamically linked nested grid models offer benefit in terms of the modelling time and computational resources requirement without any losses in terms of the quality of the predictions. This study concludes that nested grid modelling method offers considerable reduction in simulation time without any significant loss in the accuracy of the predictions.

Chapter 6
Glasgow City Case Study

6.1 Introduction

Traditionally, for the purposes of strategic flood risk management (SRFM) and detailed urban flood risk analysis of river systems, 1D modelling studies, see section 2.2.2, as well as more recently 1D modelling with storage cells studies, see section 2.2.3, are being carried out. However, because of availability of high quality LiDAR topographic data, higher computing capacities and the development of the integrated 1D2D modelling approach overcoming the drawbacks of 1D and 2D modelling approaches if undertaken separately, an integrated 1D2D modelling approach is now considered as the preferred option for flood modelling for strategic flood risk management and detailed urban flood risk analysis, see section 2.2.7.

In line with the research aim as described in section 3.2.3, this chapter describes the comparative study of the 1D model with storage cells approach and the integrated 1D2D modelling approach to understand the relative merits and implications of using the 1D2D linked modelling methods for the purposes of strategic flood risk management and detailed urban flood risk analysis.

The hypothetical urban topography study described in Chapter 5 dealt with understanding various characteristics of the flood wave using hypothetical urban topographies at prototype scale. These studies drew important conclusions about the effect of urban floodplain topography, the effect of considering buildings as storage areas and the relative merits of using nested grid models. This chapter describes the application of these findings using data for a section of the River Clyde and its adjoining urban floodplain to understand the implications of the findings on the performance of 1D2D models when applied to a real urban floodplain. The studies are carried out using data for a section of the River Clyde and its adjoining urban floodplain in Glasgow, UK.

An overview of the River Clyde catchment and the data available for this research is presented in the next section.

6.2 Overview of the River Clyde

With a catchment area of about 3900 square kilometres and a length of about 171 kilometres, the River Clyde is the tenth longest river in the UK and the third longest in Scotland. The main tributaries of the River Clyde are Duneaton Water, Medwin Water, Douglas Water, Mouse Water, River Nethan, Avon Water, South Calder Water, Rotten Calder Water, North Calder Water, River Kelvin, White Cart, Black Cart & River Gryfe and River Leven. The River Clyde flows through the centre of Glasgow. An overview of the River Clyde catchment together with the gauging stations in the Lower Clyde catchment is shown in Figure 6.1.

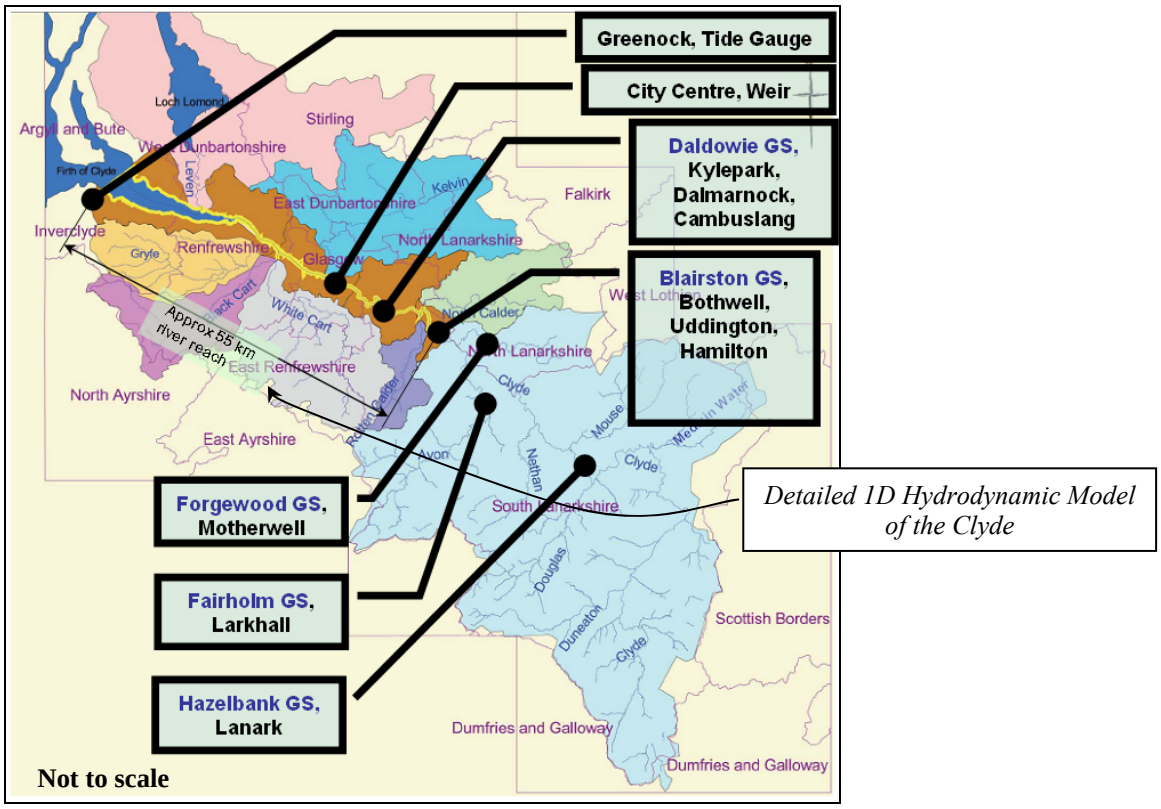

Figure 6.1: Overview of the catchment of the River Clyde

Flooding due to the River Clyde has been studied on many previous occasions. *The River Clyde Dredging Phase I & II study* in 1988/89 was followed by the *South*

Lanarkshire Flood study carried out in 1996. In 2001, hydrodynamic models of the River Clyde were developed and a detailed technical audit of the modelling was carried out in 2005 (Clyde Flood Strategy Team 2005). A further 'The River Clyde Flood Management Strategy Study' *(*RCFMS) was carried out by The Clyde Flood Strategy Team, a Joint Venture of Halcrow Group Ltd and W.A. Fairhurst & Partners by appointment of Glasgow City Council in May 2003. The details of the RCFMS study as described in the RCFMS study report (Clyde Flood Strategy Team 2005) are presented below:

6.3 The RCFMS study

Rating curves for the Daldowie and Blairston gauging stations as well as 15 min flow and level data for the gauging stations shown in Table 6.1 were used during the RCFMS study.

Table 6.1: Flow data availability for gauging stations

Data availability dates
7 Oct 1987
11 – 14 Jan 1989
4 – 6 Jan 1991
10 – 13 Dec 1994
24 – 25 Dec 1999
27 – 29 Oct 2000
2 – 4 and 22 – 25 Mar 2001
27 – 30 Jan 2002
8 – 17 Aug 2004
16 – 25 Sep 2004

Name of River	Gauging station
River Clyde	Blairston and Daldowie
Black Cart Water	Milliken Park
White Cart Water	Hawkhead
North Calder Water	Calder Park
River Gryfe	Craigend
River Kelvin	Killermont
River Leven	Linnbrane
Rotten Calder Water	Redlees

The hourly rainfall data available for the RCFMS study is summarised in Figure 6.2. The encircled rainfall stations in the figure are the only stations for which rainfall data for about 10 years is available.

	Strathclyde Park	Quinloch Farm	Mugdock CP	East Kilbride	Waukmill Glen	Ross Priory
7 Oct 1987	☑	☑	No data			
11-14 Jan 1989	☑	☑				
4-6 Jan 1991 (A)	☑	☑	☑			
10-13 Dec 1994				☑	☑	☑
24-25 Dec 1999				☑	☑	☑
27-29 Oct 2000				☑	☑	☑
2-4 & **22-25 Mar 2001**				☑	☑	☑
27-30 Jan 2002				☑	☑	☑
8-17 Aug 2004				☑	☑	☑
16-25 Sep 2004				☑	☑	☑

Figure 6.2: Hourly rainfall data availability for the River Clyde catchment (compiled from RCFMS report)

Tidal data recorded by Glasgow City Council, SEPA and Clydeport Ltd. at tidal gauging stations as shown in Figure 6.3 were also used for the RCFMS study.

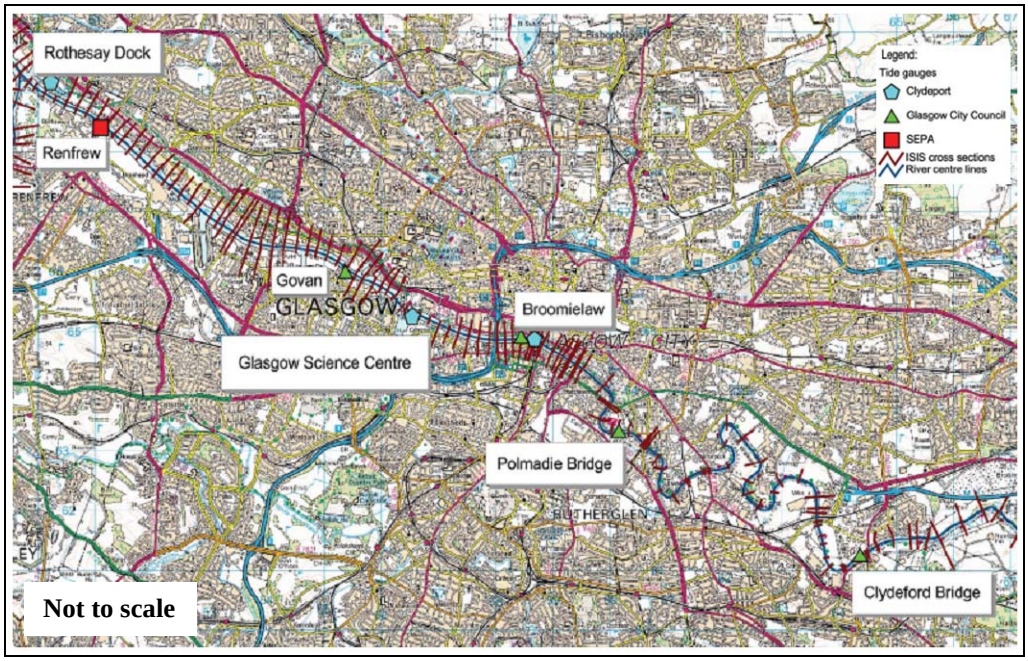

Figure 6.3: Tidal data availability for the River Clyde (Clyde Flood Strategy Team 2005)

The earliest tide data used for RCFMS study is Oct 1987 for the stations maintained by the Clydeport and Dec 1999 for the station maintained by SEPA.

During the RCFMS study, The Clyde Flood Strategy Team upgraded the previously developed hydrodynamic model of the River Clyde to include the latest information associated with extreme flows and tides in the Clyde catchment and up-to-date topographical data acquired from a LiDAR survey of the catchment. The study adopted a catchment-wide approach and developed two models: first, a *Broad Scale Model* of Upper Clyde and second, a *Detailed 1D Hydrodynamic Model* of River Clyde over about 55 km stretch between Bothwell (Blairston gauging station) and Greenock.

In addition to the rainfall, flow gauge and tide level data, the RCFMS study referred to and used the following data:

1. A previous ISIS model developed by Babtie (now Jacobs)

2. Wind data at Abbotsinch (A) & Glasgow Bishopton stations provided by the Meteorological Office

3. Drawings of river cross-sections and bridges, bathymetric data provided by Glasgow City Council and South Lanarkshire Council

4. Combined sewer overflow (CSO) locations provided by Scottish Water

5. GIS data provided by Glasgow City Council

6. The following Digital terrain model (DTM) data:

   - LiDAR data of 1 km × 1 km tiles for River Clyde corridor with spatial resolution of 2 m and vertical accuracy of ± 500 mm

   - NEXTMap data of 10 km ×10 km tiles for River Clyde Catchment. (The values were generally lower than those from the LiDAR survey data)

7. Bathymetric data for the River Clyde as shown in Figure 6.4:

   - Multi-beam data from Dumbarton Milton to Dalbeth for approximately 28 km reach

   - Single beam data from Dalbeth to Daldowie for approximately 7 km reach

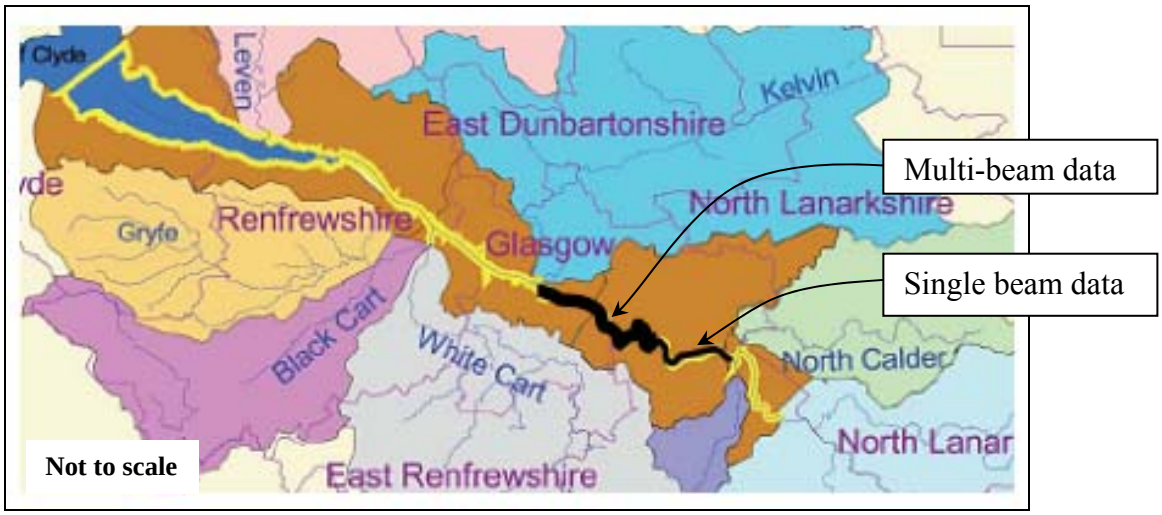

Figure 6.4: Bathymetry data availability for the River Clyde

8. Ordnance Survey maps in digital format

   - 1 in 50,0000 map covering the Clyde Catchment

   - 1 in 10,000 map covering the Clyde corridor

During the RCFMS study, river cross-sections were updated and the floodplain geometry was added to the river cross-sections as flood storage cells based on the LiDAR DTM, bathymetric survey and ground survey information.

In the hydrodynamic models, non-coincident inflow hydrographs for the River Clyde at Blairston, North Calder, Rotten Calder and River Kelvin based on the fluvial flood event of Dec 1994, which lasted for 72 hours, were used. Constant inflow hydrographs

were used for the tributaries White Cart, Black Cart & Gryfe, Leven and for five other urban areas (Lower Clyde, Polmadie, etc.).

Tidal boundary levels used were based on 24 - 25 Dec 1999 event with peak tide values matching the *Joint Probability Study* carried out by HR Wallingford Ltd. for each return period. The *Joint Probability Study* considers the maximum of all the maximum water levels produced for a river reach based on the various 'scenarios' produced by a particular return period flow combined with the tidal boundary (Clyde Flood Strategy Team 2005). The peak tide level at Greenock was set at 43.25 hours.

6.4 Data availability

The above mentioned the *Detailed 1D Hydrodynamic Model* of the River Clyde over about a 55 km reach between Bothwell (Blairston gauging station) and Greenock together with the resulting flood maps for the 10, 25, 50, 100, 200 and 500 years return period flows and for a '200 year return period flow with climate change' (200yr+CC) were available for this research. A plan of the *Detailed 1D Hydrodynamic Model* is shown in Figure 6.5.

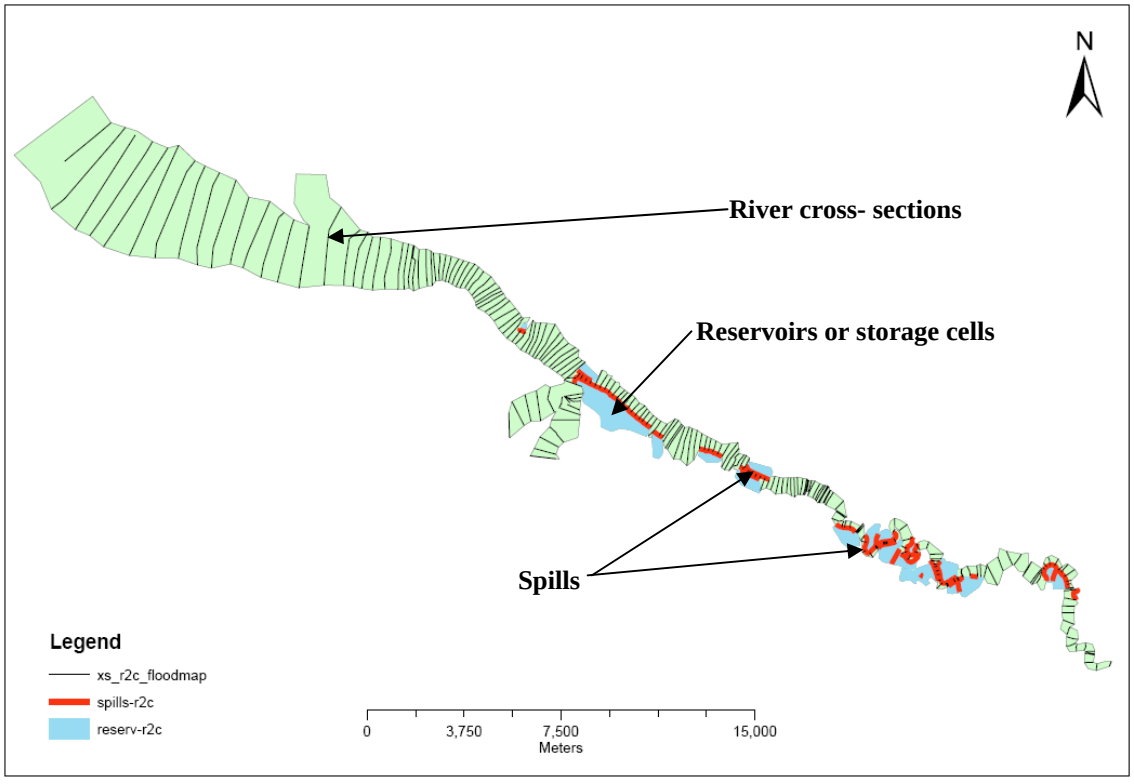

Figure 6.5: Detailed 1D Hydrodynamic Model geometry of the Lower Clyde

Further, two different sets of LiDAR DTM data as shown in Figure 6.6 were also available for this research. The first LiDAR DTM data has a spatial resolution of 2 m and covers only the River Clyde corridor. The second LiDAR DTM data, with a spatial resolution of 1 m, was available for the reach of the River Clyde in between Kenmuir Road and Shawfield Stadium. This second LiDAR DTM covers the adjoining urban floodplain.

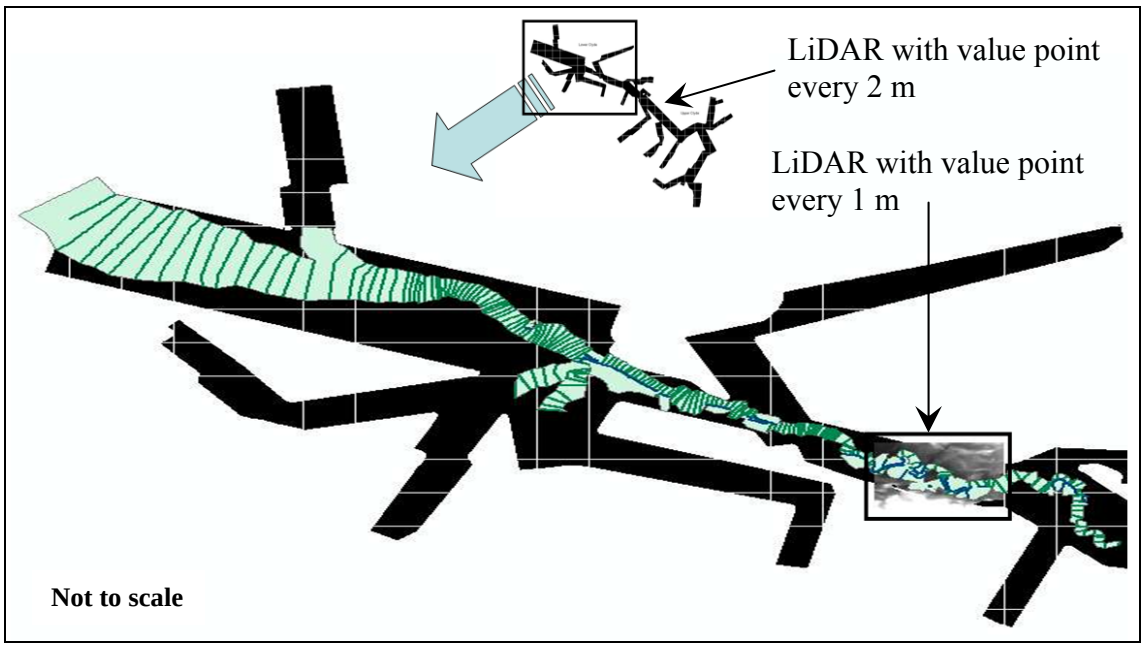

Figure 6.6: LiDAR DTM data availability

6.5 Selection of study reach

The *Detailed 1D Hydrodynamic Model* of River Clyde covers the entire stretch between Bothwell (Blairston gauging station) and Greenock and poses no restriction on selection of study reach. However, the LiDAR DTM data with 2 m spatial resolution covers mainly the river corridor but does not cover the adjoining urban floodplain sufficiently for the 2D modelling planned here. The LiDAR DTM data with 1 m spatial resolution, although available for a smaller area – for the reach of the River Clyde between Kenmuir Road and Shawfield Stadium – does cover the adjoining area in sufficient detail to support 2D urban floodplain modelling. This reach of the River Clyde between Kenmuir Road and Shawfield Stadium has urban settlements located close to the river bank and the river reach includes 52 cross-sections, seven bridges and one weir.

Therefore, this reach is considered to be a good representation of a typical urban floodplain, and as such, was selected as a case study for this research.

Figure 6.7 shows the selected reach of the River Clyde between Kenmuir Road and Shawfield Stadium together with the Ordnance Survey map of the adjoining area. The figure also shows the locations of hydraulic units such as cross-sections, spills and reservoirs as configured in the 1D ISIS model.

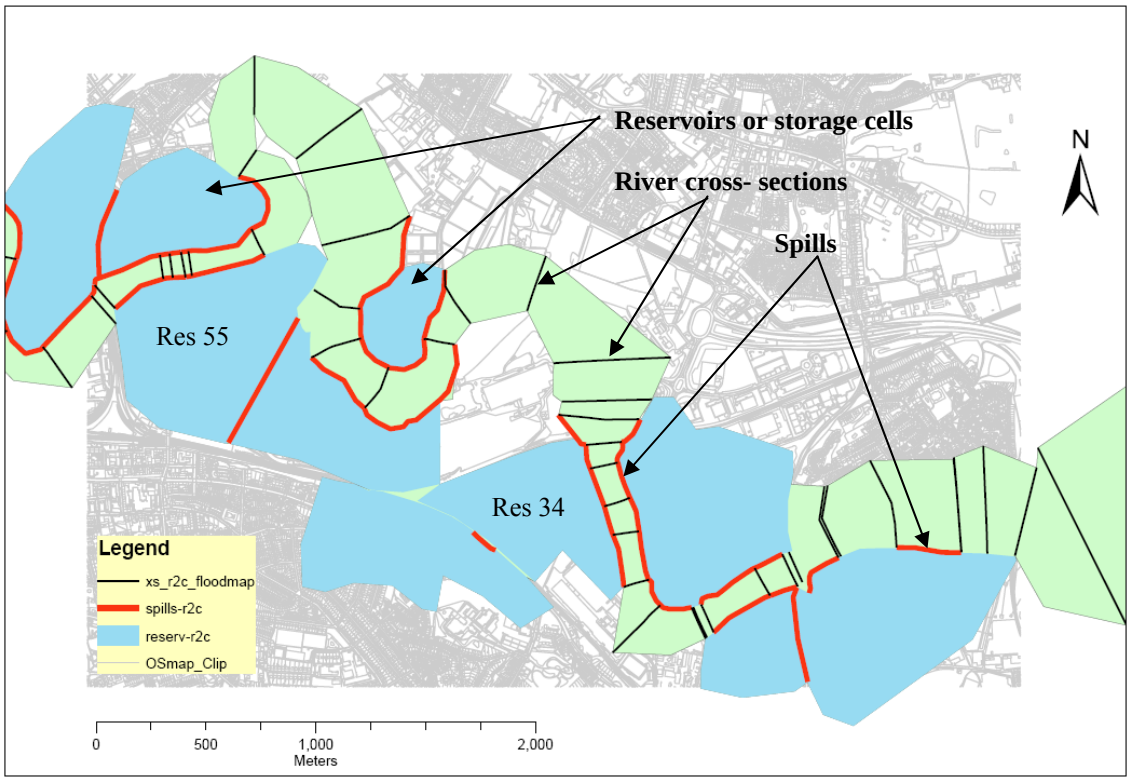

Figure 6.7: Geometry of 1D model with storage cells

From Figure 6.7 it can be observed that the ISIS model simulates flooding using a network of interconnected spills and reservoirs. This is commonly referred to as a 1D model with storage cells (see section 2.2.3).

6.6 Flooding extents obtained by 1D model

The inundation extents predicted for the study reach obtained by 1D model with storage cells during the RCFMS study were inspected. It was observed that the inundation extents obtained by using the hydrograph of 200 year return period with climate change

(200yr+CC) as shown in Figure 6.8 covers the adjoining urban area extensively. This will allow further meaningful 2D studies and therefore this particular hydrograph is selected for this research.

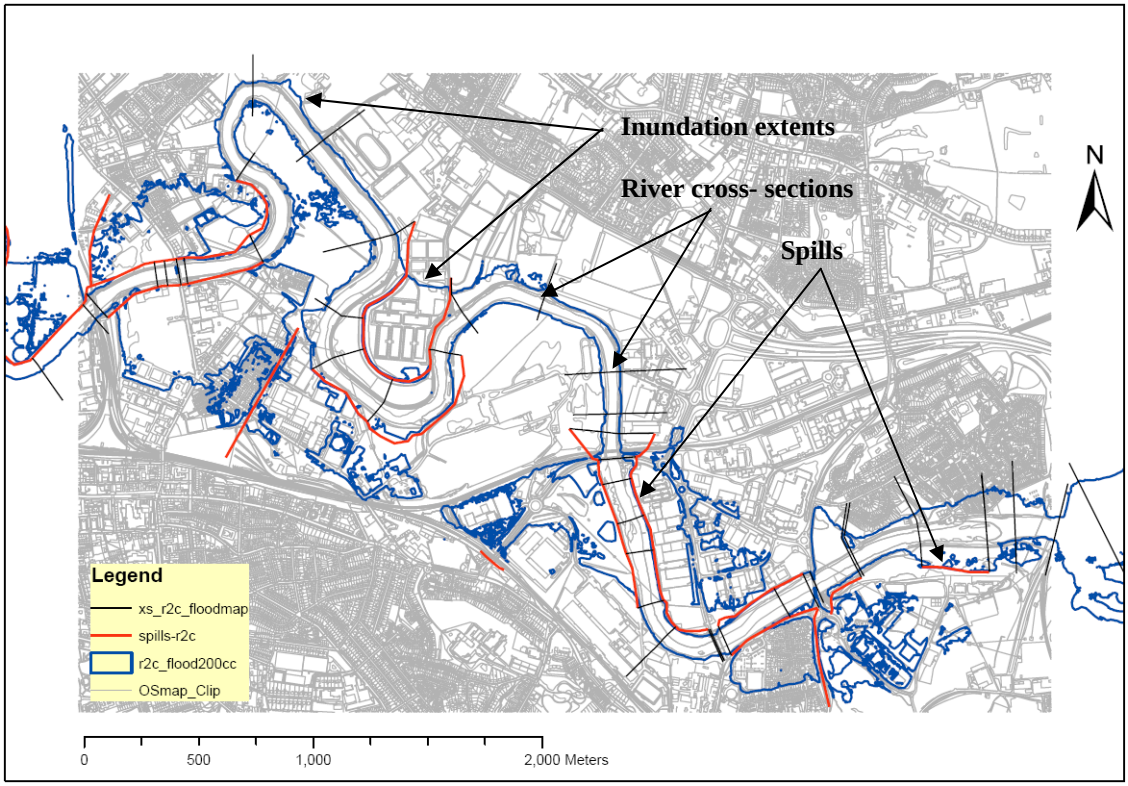

Figure 6.8: Inundation extents obtained by 1D model with storage cells

Further to the discussions in Chapter 3 detailing the research aims and objectives, exercises are carried out using an integrated 1D2D flood modelling method for this research. The research objectives are repeated below for convenience. The research study has the following objectives:

1. To investigate the effect of 2D grid size and topographic data type on flood inundation predictions.

2. To investigate the consequences of representing buildings as areas of high roughness in the computer grid.

3. Compare the benefits of using 1D2D models to predict urban floodplain inundation compared with predictions obtained from $1D^{+}$ models.

4. Investigate the significance on the selection of the location of 1D to 2D model links on flood volume transferred between models and the consequence of this to predicted inundation extents.

5. To investigate if integrated 1D2D model studies for a typical urban floodplain can be carried out using typical desktop computing facilities.

The process of setting up an integrated 1D2D model is described below:

6.7 Setting up an integrated 1D2D model

In the integrated 1D2D modelling method, a 1D model and a 2D model are set up separately and then combined to construct an integrated 1D2D model. For the current research, MIKE 11 software is used for the 1D modelling purposes as it can readily be combined with the selected 2D modelling software program MIKE 21 to be used for this research. The details of the 1D, 2D and the integrated 1D2D model setups are discussed below:

6.7.1 1D model setup

To prepare a MIKE 11 model, the model elements in the ISIS model for the selected reach of the River Clyde are converted from ISIS to MIKE 11. As the reservoir units in the ISIS model will be represented by the 2D model, MIKE 21, there is no need to convert these from ISIS to MIKE 11. Similarly, the spill units also do not need to be converted as spills are configured during the integration process of the 1D MIKE 11 model and 2D MIKE 21 model by using the MIKE FLOOD software interface. The MIKE 11 model, therefore, contains only the cross-sections, the bridges and the weir.

Figure 6.9 shows the geometry of the 1D model for the case study between Kenmuir Road and Shawfield Stadium in MIKE 11 against the backdrop of flood extents from the RCFMS study.

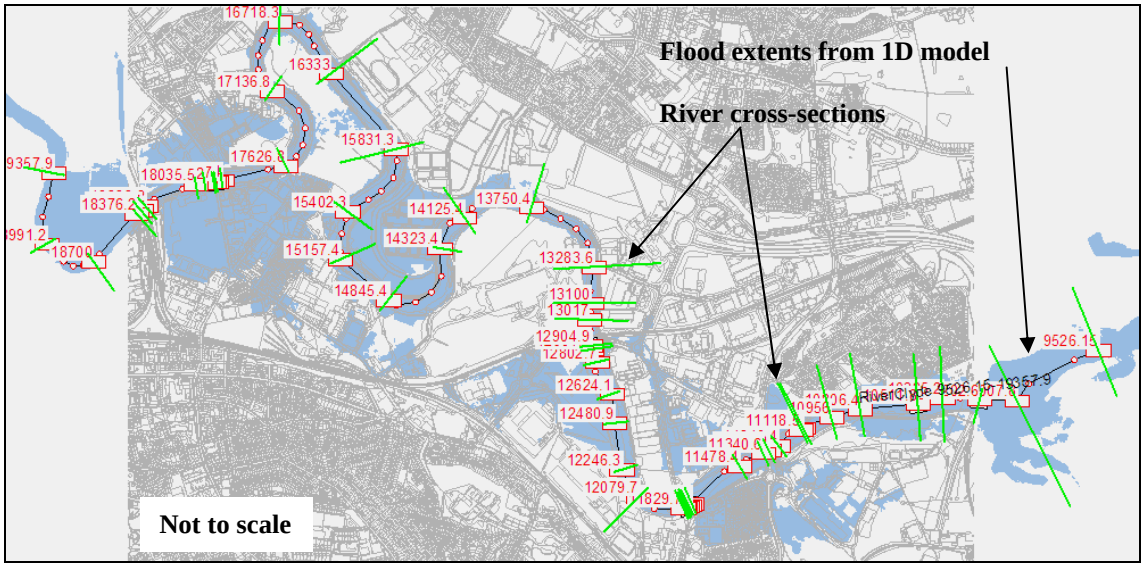

Figure 6.9: 1D model of selected reach of the River Clyde in MIKE 11

6.7.2 2D model setup

As mentioned earlier in section 6.4, two sets of topographical data were available. The second LiDAR DTM dataset with 1 m spatial resolution for the reach of the River Clyde between Kenmuir Road and Shawfield stadium is used for the 2D model for this research. The LiDAR DTM data is converted from GIS format to the MIKE 21's proprietary bathymetry data format.

While carrying out simulations, it was observed that with a spatial resolution of 1 m time required for the simulation was prohibitively long. Therefore, to achieve shorter simulation run times, the topography data were re-sampled to a coarser spatial resolution of 18 m for the current research. The 2D model setup for the selected reach in the MIKE 21 software can be seen in Figure 6.11.

6.7.3 Integration of 1D and 2D models

To construct an integrated 1D2D model, the 1D model is overlaid on the 2D model and the left and right banks in the 1D model are linked to the corresponding cells in the 2D model by using the MIKE FLOOD software interface.

Further, to avoid duplication of flow in the river represented by a 1D MIKE 11 model and to avoid flow passing from a floodplain to a floodplain across the other bank of the river without first passing through the 1D model, the elevations of the 2D model cells falling fully within the cross-section extents of the 1D model, are raised to a land value so as to avoid this situation, see section 2.2.8 and Figure 2.16. Figure 6.10 shows a perspective view of the resultant 2D model geometry in the integrated 1D2D model.

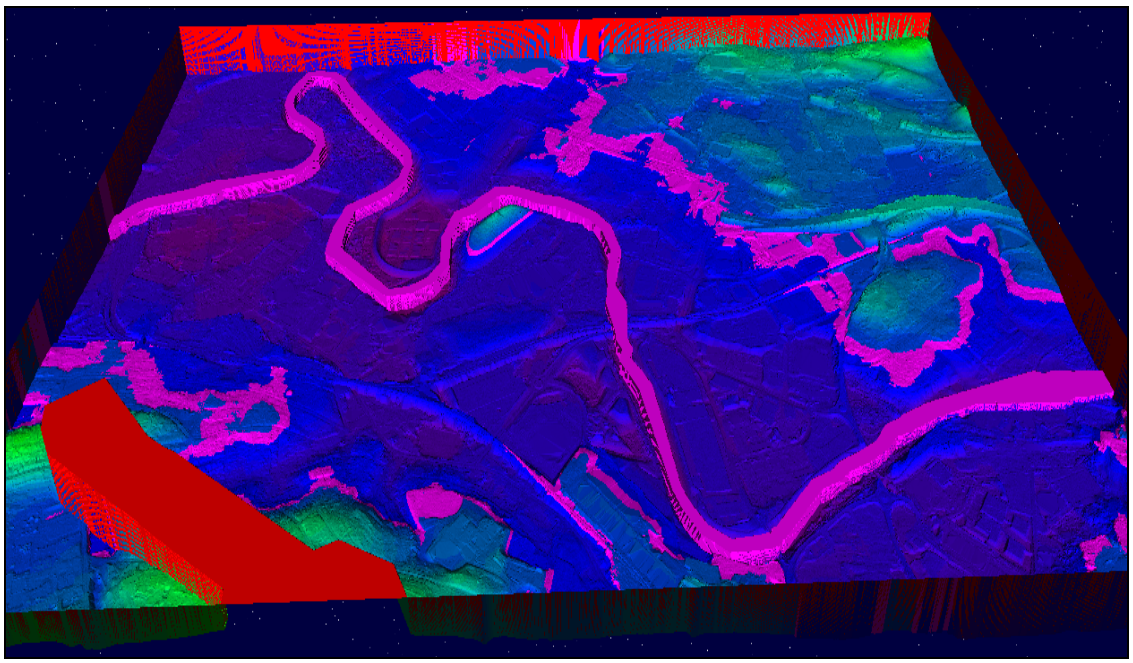

Figure 6.10: 2D model geometry

The integrated 1D2D model layout for the selected case study reach prepared using the MIKE FLOOD software interface is shown in Figure 6.11. It shows the integrated 1D2D model layout together with other interface details like input fields, coordinate information for the bank connection with 2D model, etc.

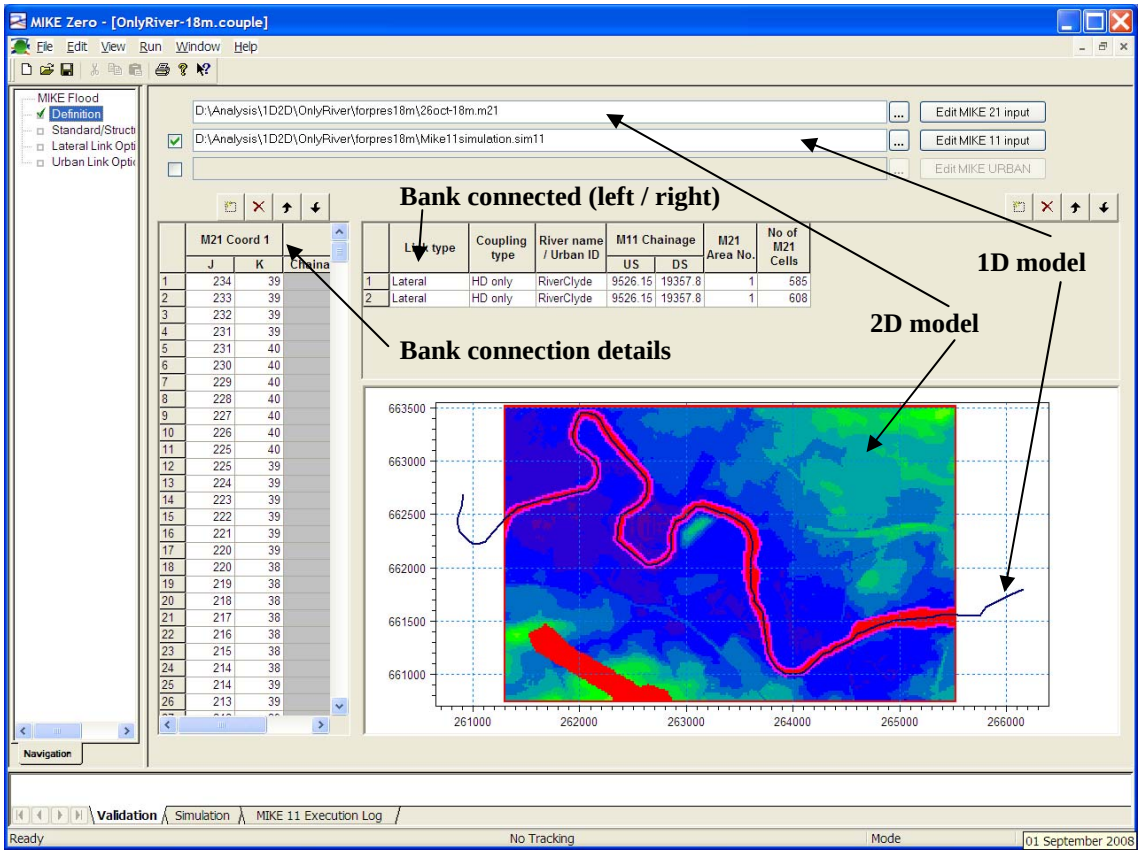

Figure 6.11: Integrating 1D and 2D models for constructing an integrated 1D2D model

During simulation, the 1D and the 2D models exchange flows. The hydrodynamics of the exchange of the flows between the two models is through a lateral link as detailed earlier, see section 2.2.9.

6.7.4 Upstream boundary condition

The upstream boundary condition used for the integrated 1D2D setup is the corresponding 72 hour hydrograph at Kenmuir Road as used by the *Detailed 1D Hydrodynamic Model* for the computation of inundation extents of 200 year return period with climate change (200yr+CC) as shown in Figure 6.8. This hydrograph is shown in Figure 6.12.

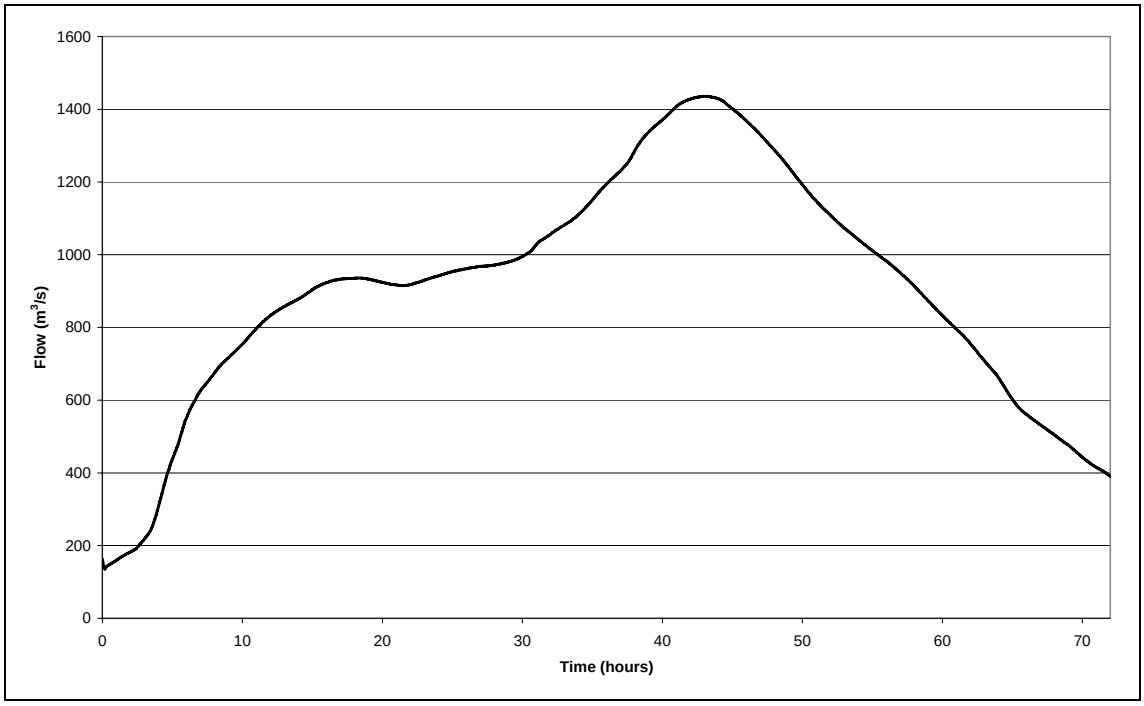

Figure 6.12: Inflow hydrograph at Kenmuir Road cross-section

6.7.5 Downstream boundary condition

A rating curve boundary is applied at the downstream cross-section, Shawfield in the MIKE 11 1D model. The rating curve is obtained by plotting the water level and the discharges computed by the ISIS model at Shawfield cross-section for mean high water spring tide (MHWS) and 200 year return period inflow with climate change (200yr+CC) and fitting a second order polynomial line to the data. The rating curve is shown in Figure 6.13.

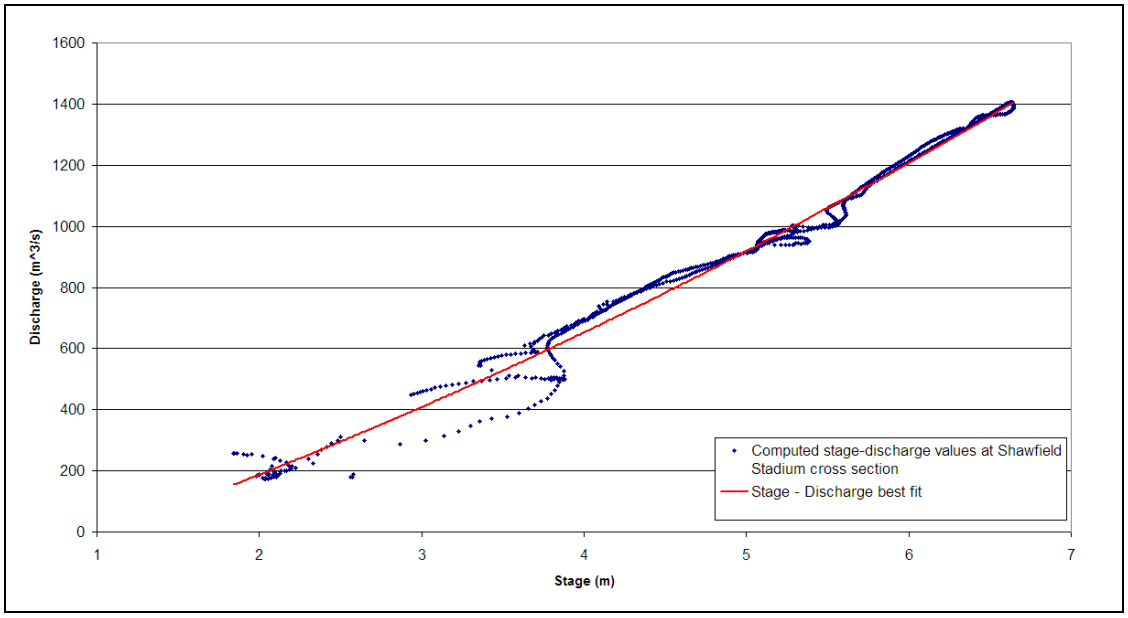

Figure 6.13: Rating curve at downstream boundary in the MIKE 11 1D model

6.7.6 Urban inflow

In addition to the hydrographs for all the tributaries of the River Clyde, the *Detailed 1D Hydrodynamic Model* for the Lower Clyde also considers the spatial lateral discharges from adjoining urban areas. The constant urban inflow of 37 m^3/s as in the *Detailed 1D Hydrodynamic Model* is distributed over a length of 3943.62 m, out of which a linearly proportionate 24.83 m^3/s needs to be applied to the model extents selected for the current research. This urban inflow is applied as constant lateral inflow, in a similar way as the ISIS model, over each reach in proportion to its length.

6.7.7 Bed resistance

The same values of Manning's roughness coefficient, *n* as used in the *Detailed 1D Hydrodynamic Model* were used for the MIKE 11 1D model prepared for the current study. From a review of the Manning's *n* values for the floodplain in the 1D model, for all of the 2D model area a constant value of Manning's roughness coefficient equal to 0.065 is used.

6.7.8 Wetting and drying depth

For the 2D model, wetting depth of 0.15 m and drying depth of 0.1 m is used. This means that a computational point is taken into calculations once the computed depth reaches the wetting depth of 0.15 m and is taken out of the calculations when it falls below 0.1 m.

6.7.9 Initial conditions

The water levels from the steady state simulation with a constant inflow of 25 m^3/s and the urban inflow as described above are used as the initial conditions for the MIKE11 1D model. Figure 6.14 shows the initial conditions for the 1D model used in the current study.

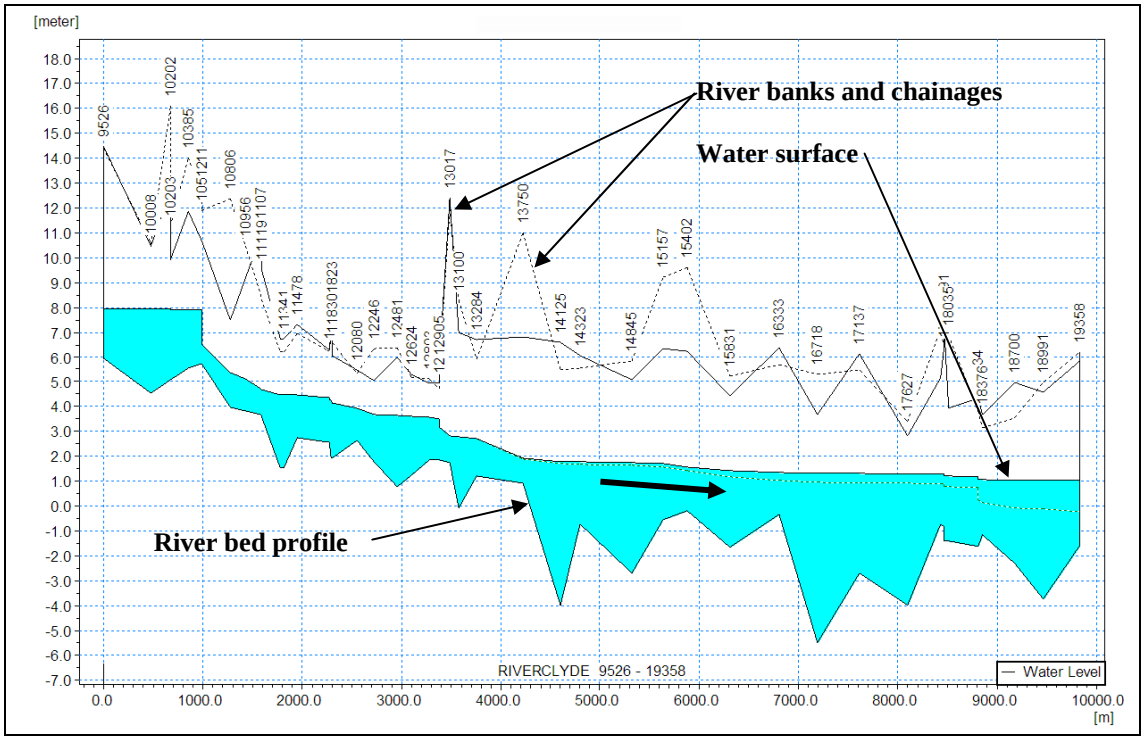

Figure 6.14: Initial conditions - 1D model

6.8 Comparison of 1D and integrated 1D2D model predictions

A 1D model with storage cells and an integrated 1D2D model are configured differently, and process the data differently. The model predictions reflect these characteristics during the simulation process and in the model predictions.

As detailed earlier, while integrating a 1D model with a 2D model a modeller has several options available for linking a 1D model with a 2D model, see Table 2.2 in section 2.2.8. These options are evaluated in this research by analysing the maximum inundation extents obtained by using those options. The details of the various model configurations and the results are presented below:

6.8.1 Construction of models and model runs

While constructing an integrated 1D2D model according to options 1 – 3, the full width of the surveyed cross-section is used. The riverbanks, thus, are located at the start and the end points of the cross-sections. Figure 6.15 shows the geometry of the integrated 1D2D model setup for options 1 – 3.

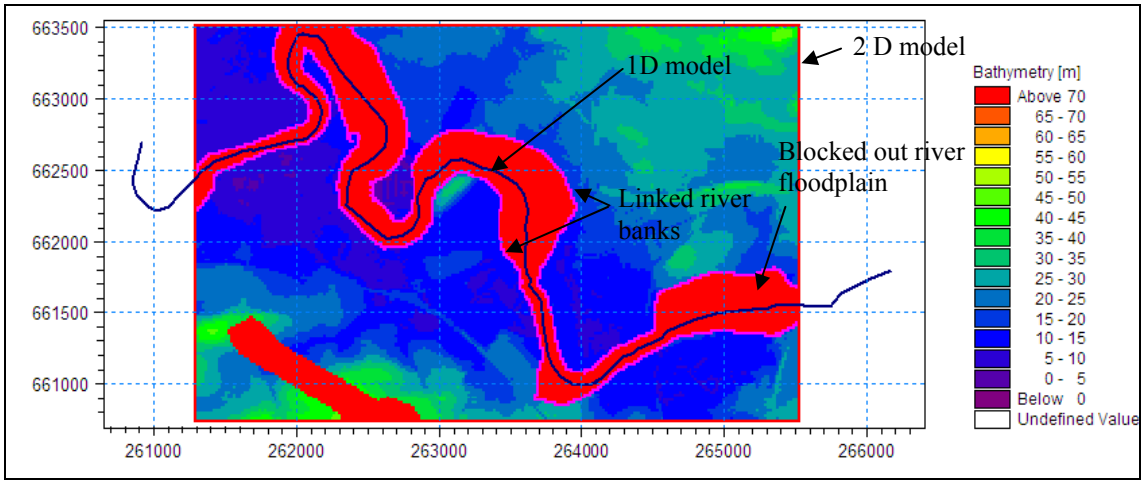

Figure 6.15: Geometry of integrated 1D2D model setup - Options 1- 3

While constructing an integrated 1D2D model according to options 4 – 6, only the width of the main river channel from the cross-section data is used. The riverbanks, thus, are located at the points defining the main river channel in the cross-section data. Figure 6.16 shows the geometry of the integrated 1D2D model setup for options 4 – 6.

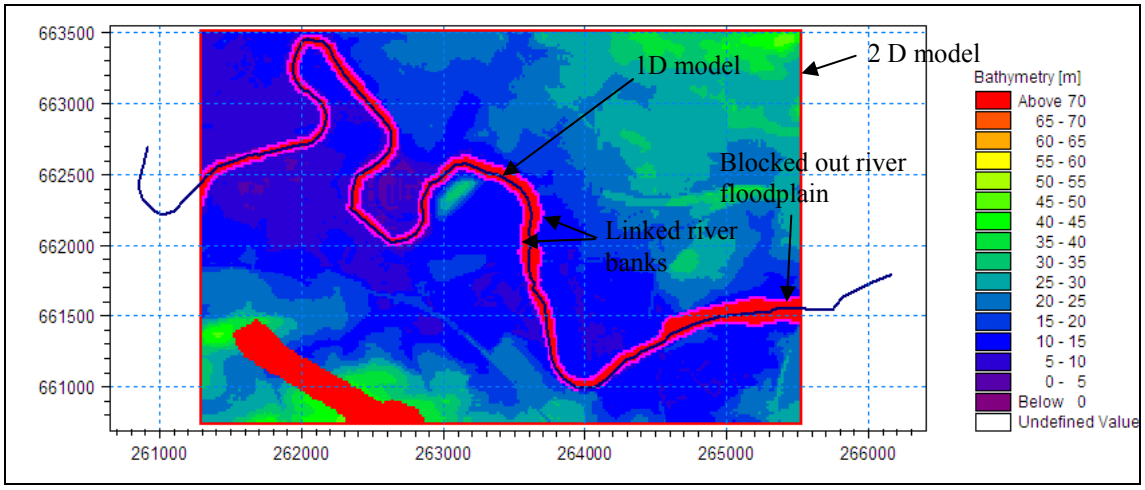

Figure 6.16: Geometry of integrated 1D2D model setup - Options 4 – 6

It can be observed from Figure 6.16 that the width of the river channel in the 1D model is considerably smaller than the earlier geometry.

As mentioned earlier, see section 2.2.8, sometimes the existing cross-sections are updated by extending them onto the adjoining floodplain by using data from any subsequent surveys. Such an exercise was carried out for the cross-section data being used for this study. The cross-sections were updated based on LiDAR survey data during the RCFMS study, see section 6.3.

The ground elevations obtained from the LiDAR survey are not reliable near riverbanks due to the presence of thick vegetation which may conceal some flow paths. The LiDAR elevation data tends to become unreliable also for areas with steep slopes - which is the case close to a river bank (see section 2.3.1). An inspection of the available cross-section and LiDAR topography data revealed elevation discrepancies. These, however, are not considered in the integrated 1D2D model setups using earlier options, options 1-6.

To limit the impact of these elevation discrepancies, visual inspection of each cross-section was undertaken. Starting from a bank marker point, portions of a cross-section beyond a point that is thought not to be on steep sloping ground, and also is far enough from the main channel were deleted. Further, even if a point is on steep ground, but if its elevation is close to the elevation in the topography data, that point was taken as the

cut-off point for the cross-section. Not all the cross-sections are modified; and even if a cross-section is modified, not both the left and right sides are modified. Further, the cross-sections outside the 2D model domain are not modified. Some of the cross-sections where this exercise is carried out are shown in Figure 6.17.

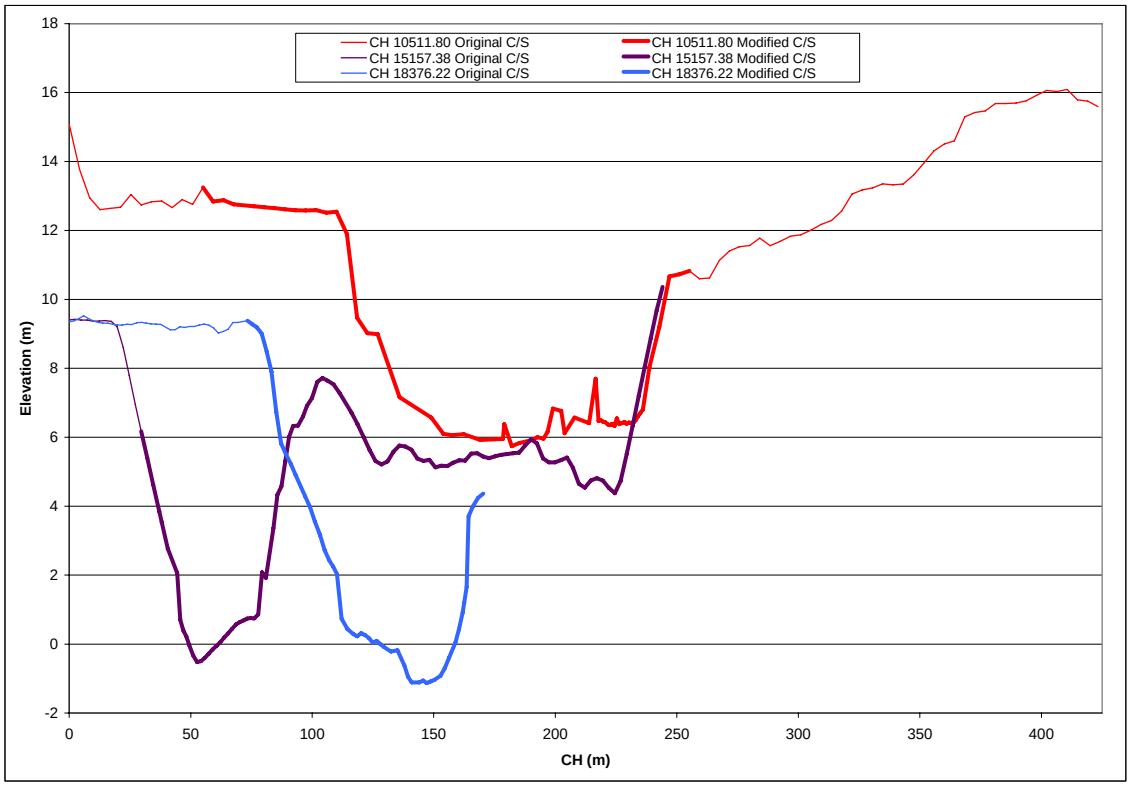

Figure 6.17: Typical original and modified cross-sections

It should be noted that, in addition to elevation discrepancies, there may be other factors such as steep bank, which may require such type of alteration of cross-section extents. Further, as the exercise is carried out using no set rules, the cross-section extents may be different from modeller to modeller depending on the individual's judgement. Figure 6.18 shows the geometry of the integrated 1D2D model setup for options 7 – 9.

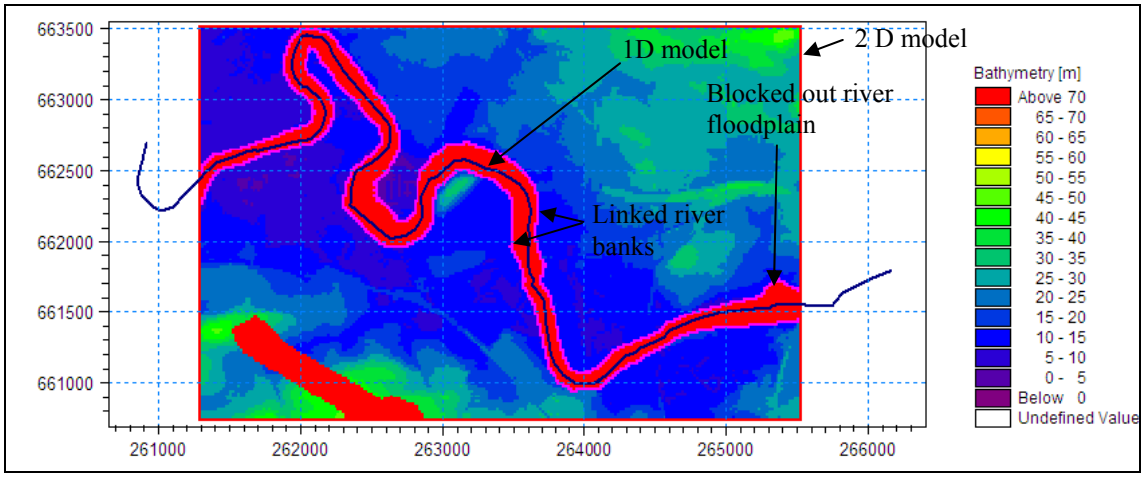

Figure 6.18: Geometry of integrated 1D2D model setup - Options 7- 9

It can be observed from Figure 6.18 that the width of the river channel in the 1D model ranges between the widths as observed in Figure 6.15 and Figure 6.16.

For option 1, 4 and 7, the elevations for the lateral links defining the left and the right banks are taken from the interpolated bank elevations obtained by connecting the endpoints of cross-sections by straight line whereas, for option 2, 5 and 8, the bank levels are taken from the 2D topography data alone. For option 3, 6 and 9, the bank elevations are taken as the maximum of the interpolated bank elevations obtained by connecting the endpoints of cross-sections by straight line and the corresponding elevations from the 2D topography data.

6.8.2 Results, analysis and discussion

Simulation runs for the integrated 1D2D model setups of the River Clyde for the selected stretch from Kenmuir Road to Shawfield Stadium pertaining to options 1 – 9 were carried out for the 72 hour duration of the inflow hydrograph and with the other boundary conditions described earlier.

The maximum flood extents corresponding to options 1 to 9 against the backdrop of the flood extents obtained from the 1D model with storage cells are shown in Figure 6.19 to Figure 6.27 respectively.

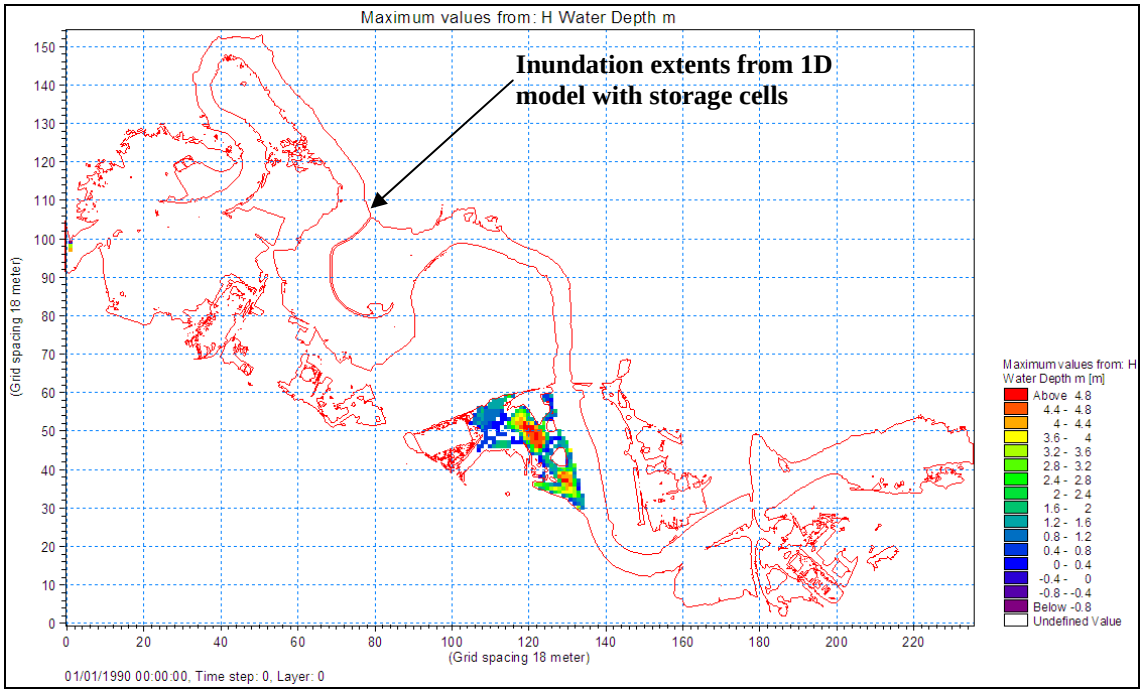

Figure 6.19: Maximum flood extents for Option 1 setup

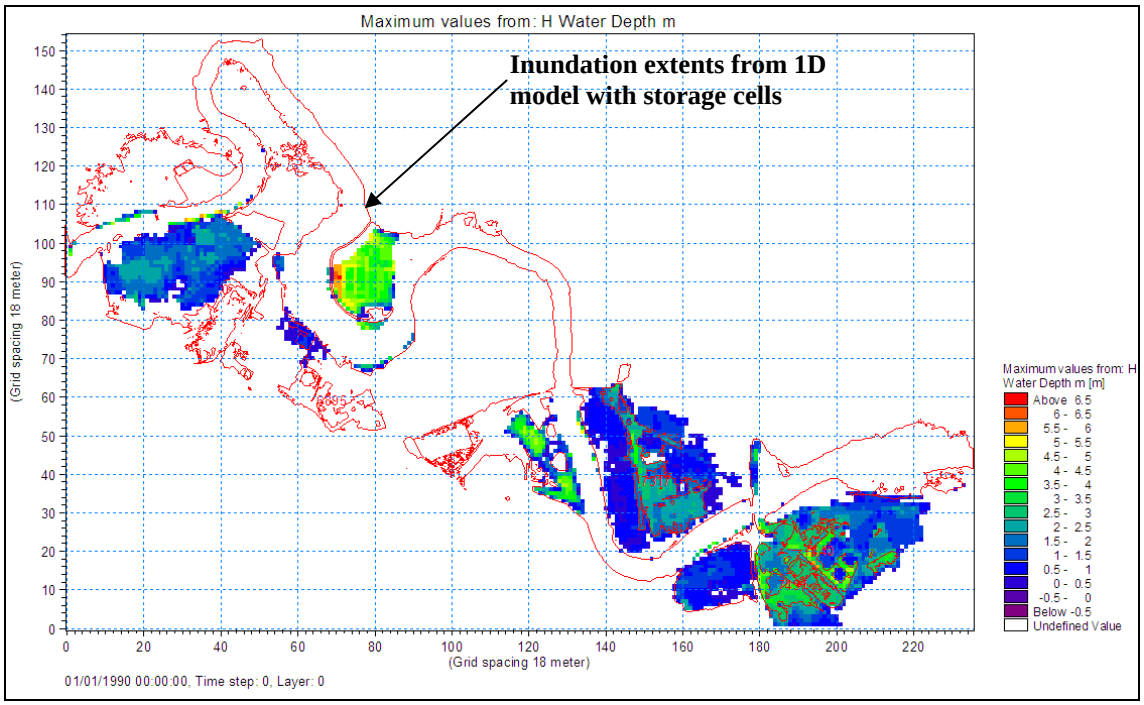

Figure 6.20: Maximum flood extents for Option 2 setup

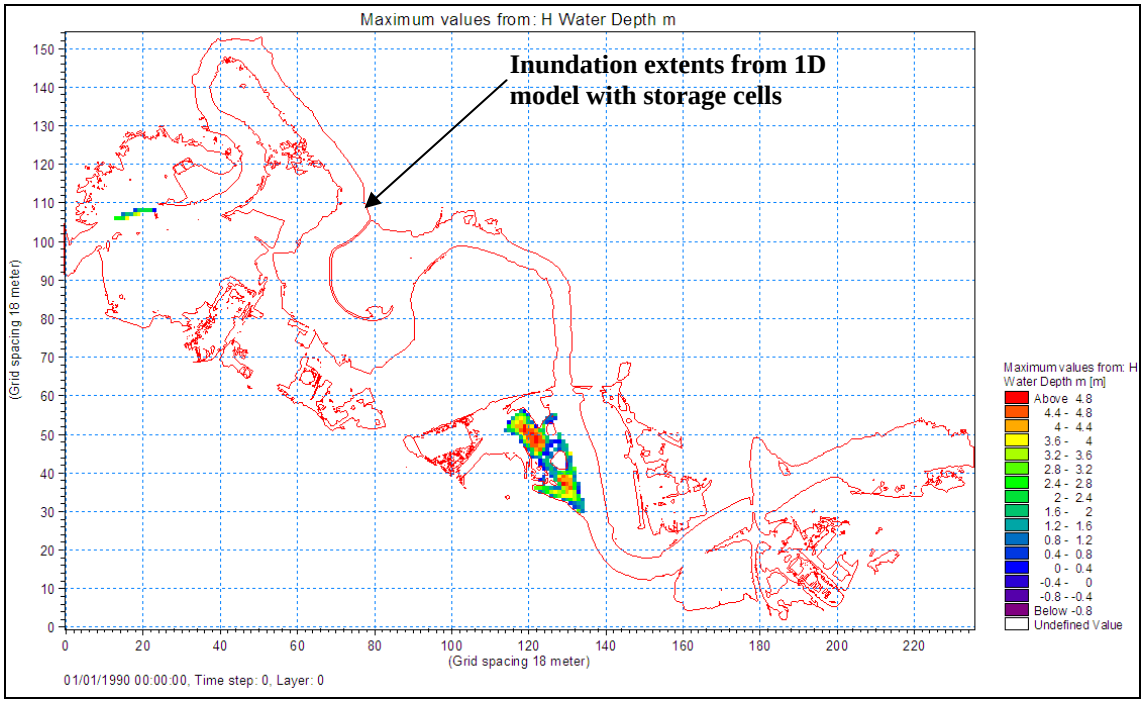

Figure 6.21: Maximum flood extents for Option 3 setup

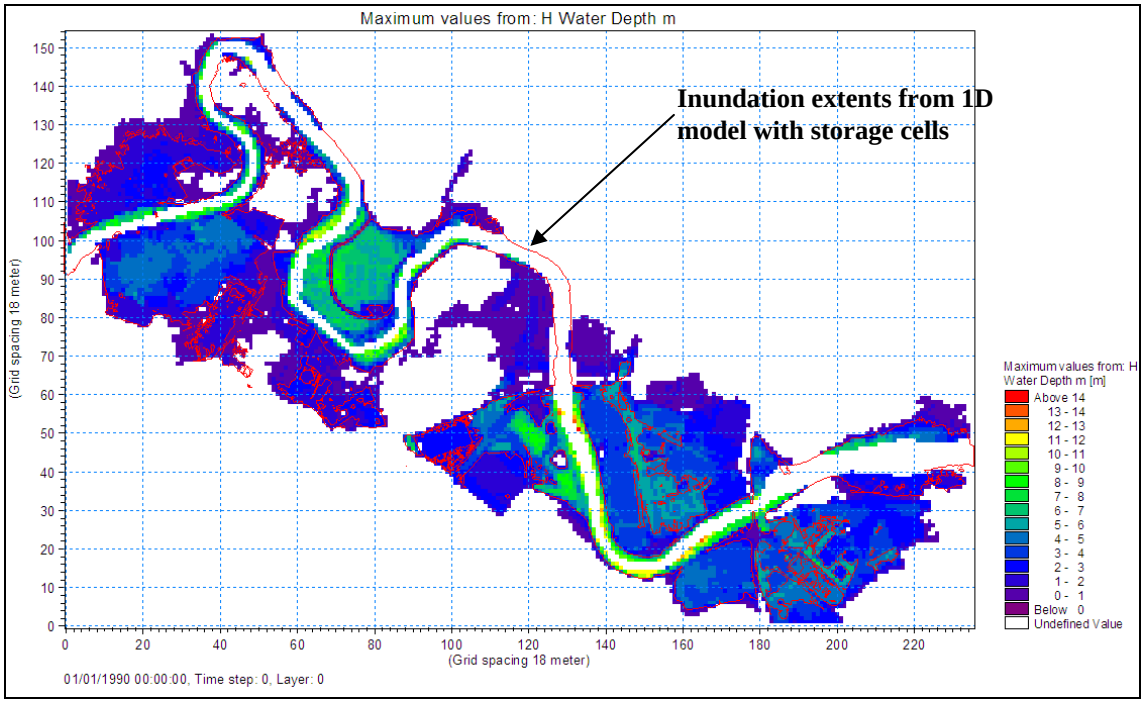

Figure 6.22: Maximum flood extents for Option 4 setup

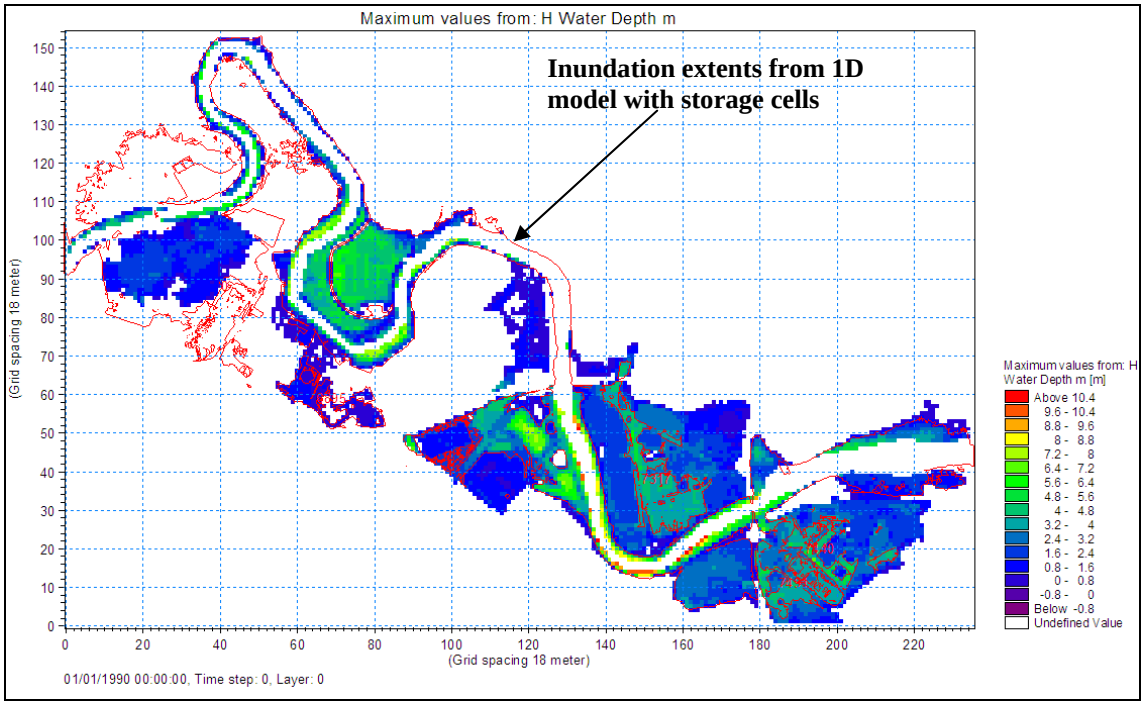

Figure 6.23: Maximum flood extents for Option 5 setup

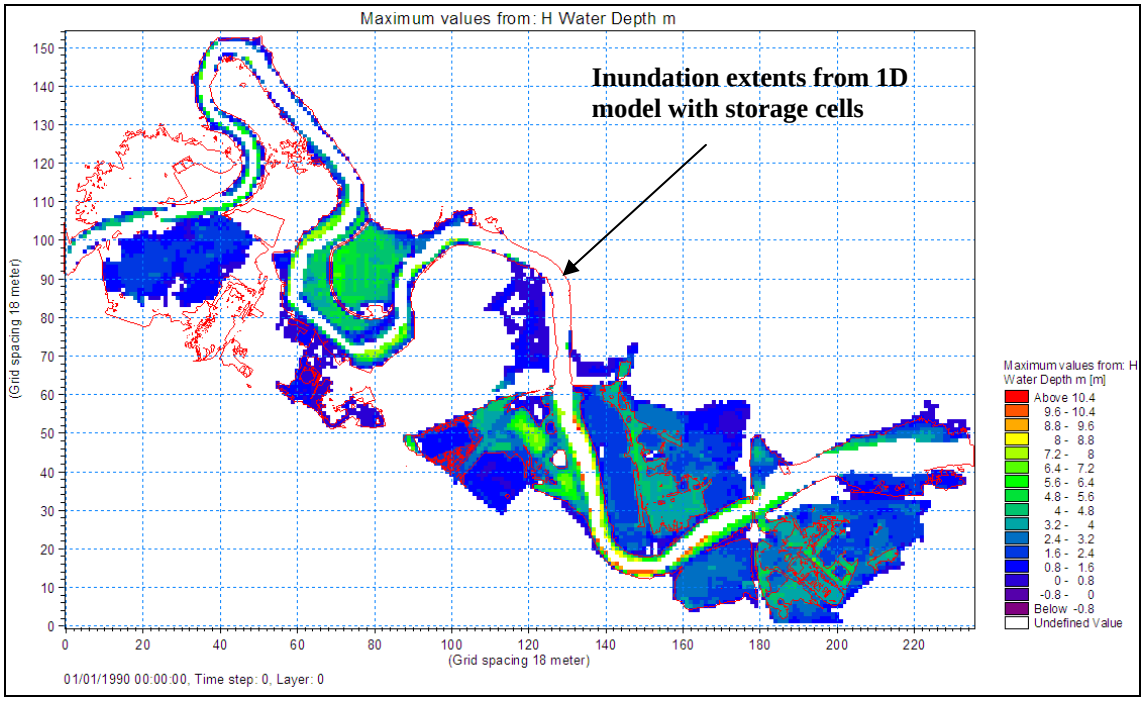

Figure 6.24: Maximum flood extents for Option 6 setup

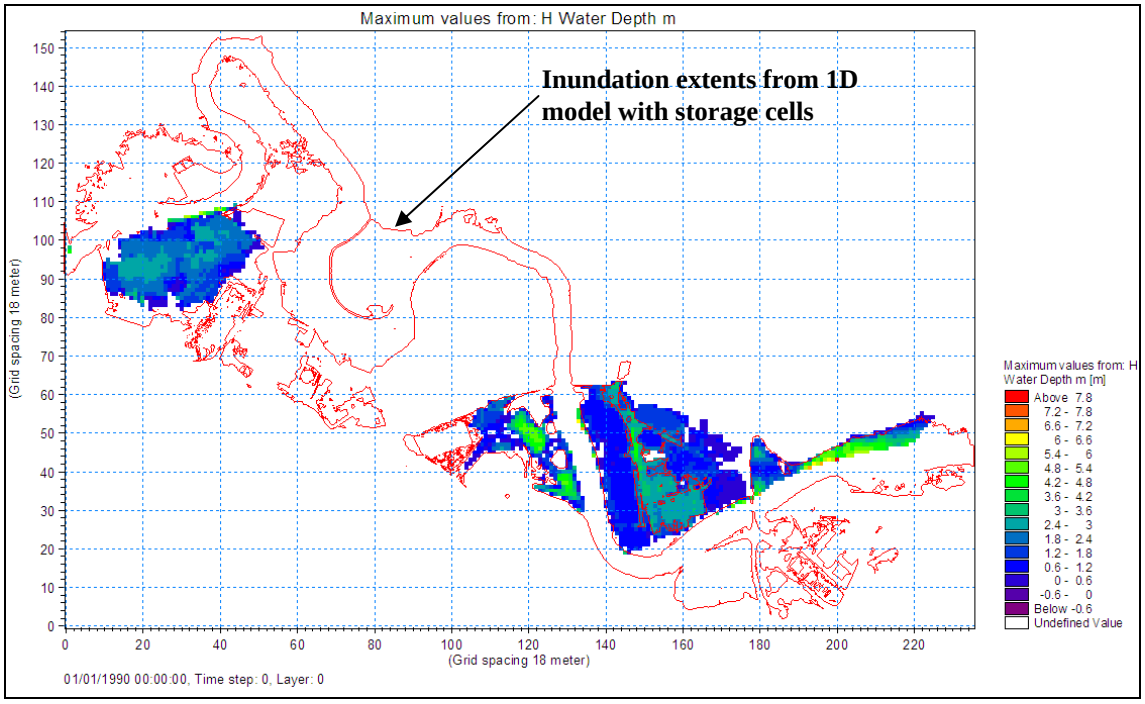

Figure 6.25: Maximum flood extents for Option 7 setup

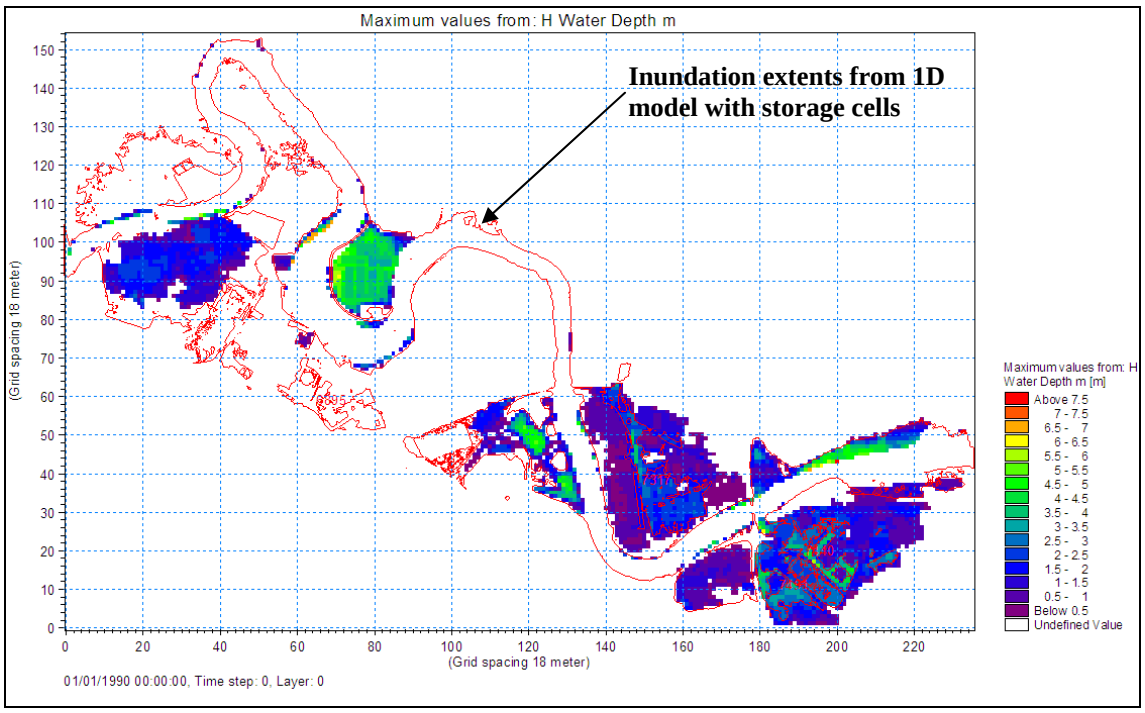

Figure 6.26: Maximum flood extents for Option 8 setup

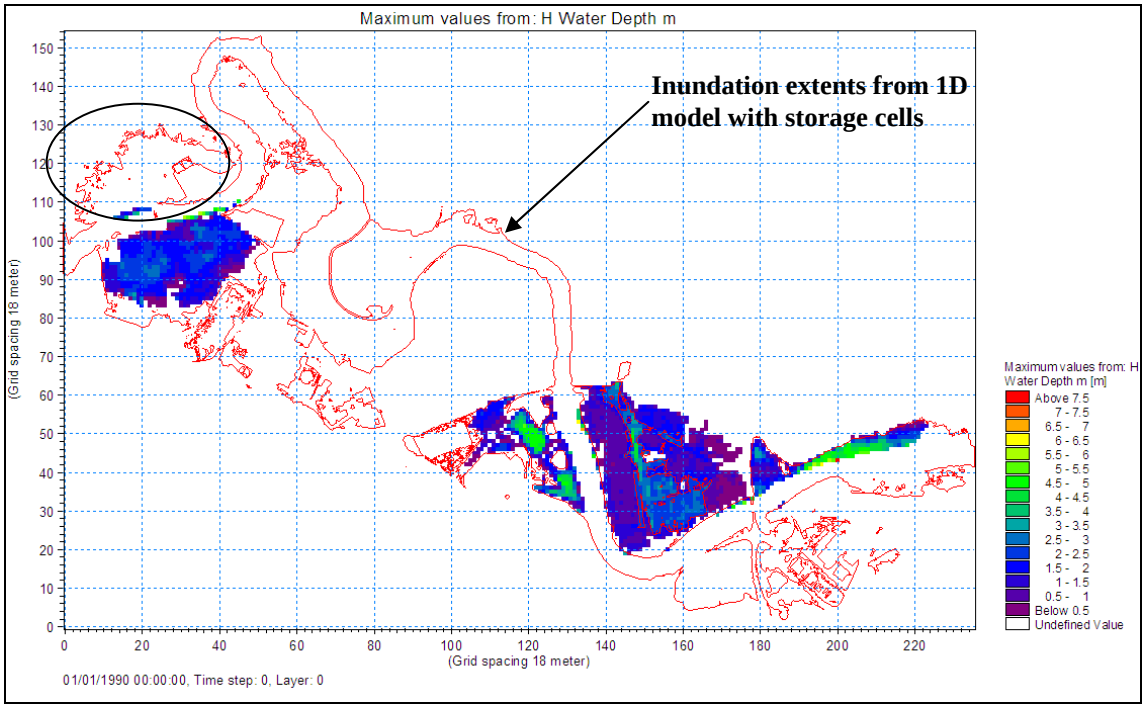

Figure 6.27: Maximum flood extents for Option 9 setup

There are considerable differences in the maximum flood extents as can be observed from Figure 6.19 to Figure 6.27 for options 1 to 9 respectively. The maximum flood extents vary from case to case. It can be observed, however, that the maximum flood extents for options 1 and 3 are similar, so are for options 2 and 8, options 5 and 6, and options 7 and 9. There is no obvious reason for the similarities other than the fact that similar volumes of floodwater have been transferred leading to similar flood extents. The flood extents from Option 4 are the maximum of all the options considered.

Further, the flood extents from all of the options above differ from the maximum flood extents obtained in earlier studies using 1D model with storage cells.

These differences in the maximum flood extents among the integrated 1D2D model setups and the maximum flood extents obtained from the 1D model with storage cells differ because of the different representation of the left and the right banks in each setup. Consequently, different volume of floodwaters is transferred from the 1D model to the floodplain.

As an illustration, the left and the right bank elevations as configured in the integrated 1D2D model setup for Option 6 are shown in Figure 6.28 and Figure 6.29 respectively and those for Option 9 are shown in Figure 6.30 and Figure 6.31 respectively.

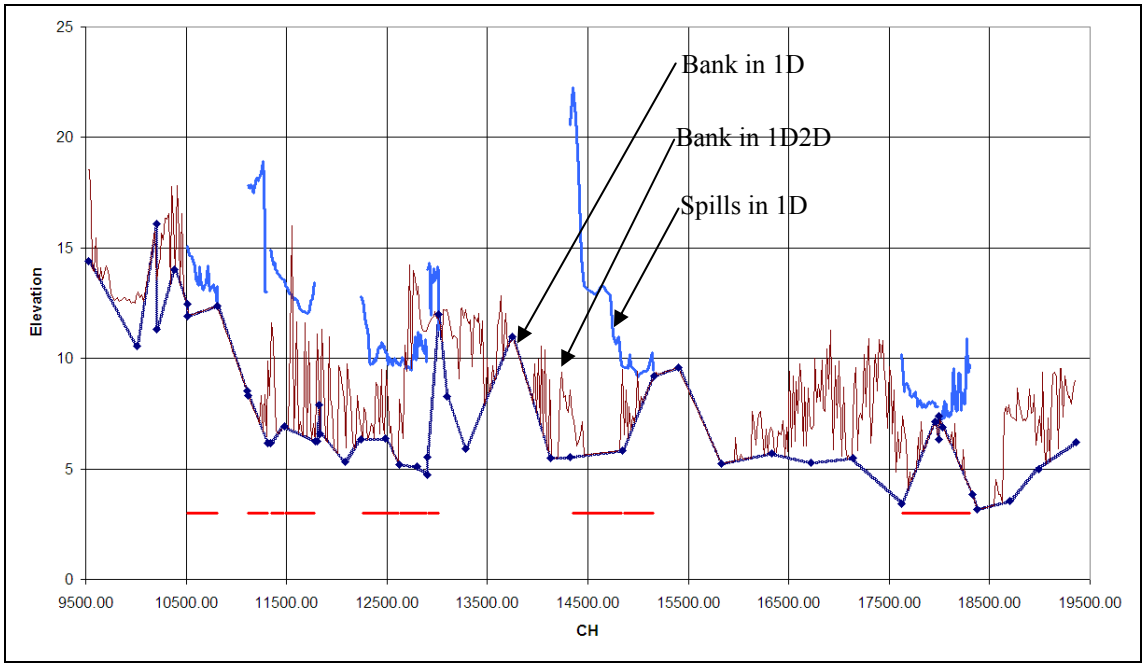

Figure 6.28: Left bank geometry – Option 6

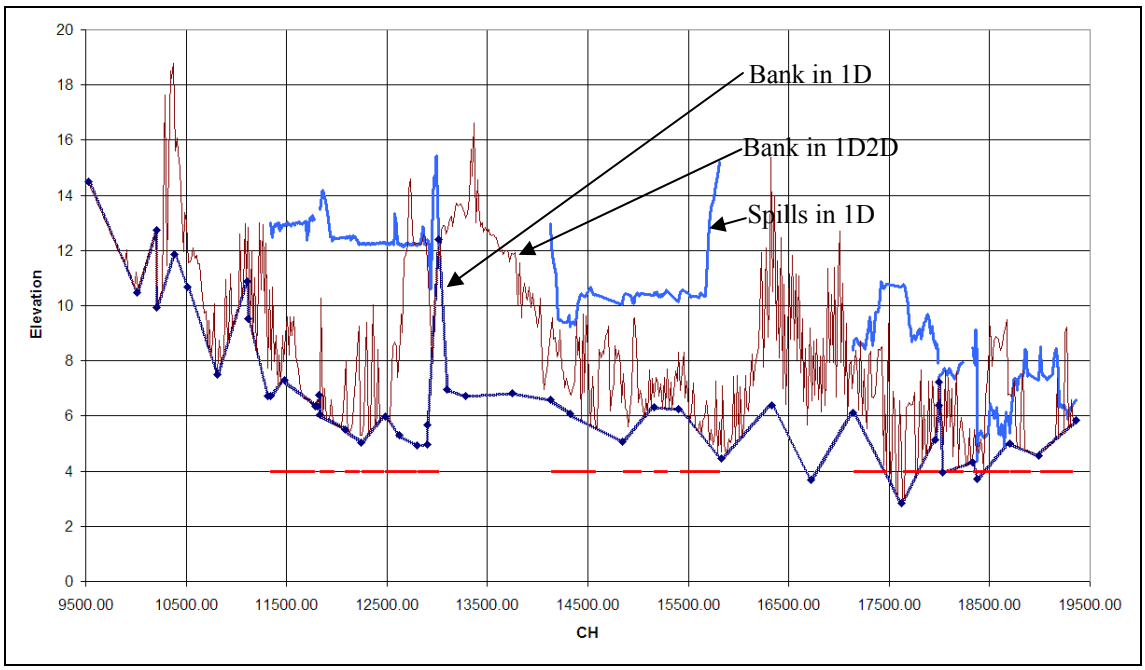

Figure 6.29: Right bank geometry – Option 6

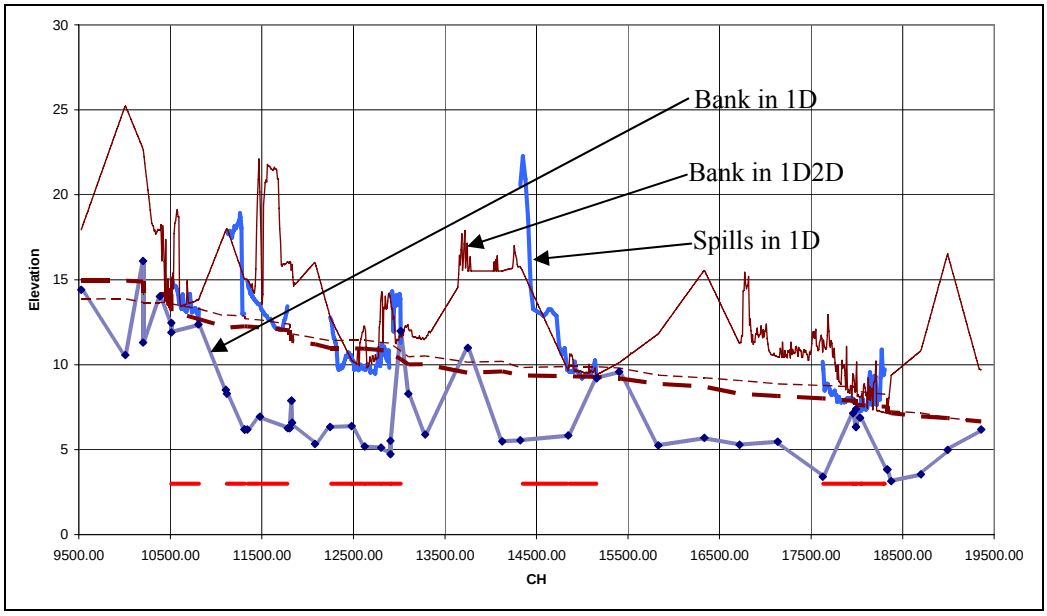

Figure 6.30: Left bank geometry – Option 9

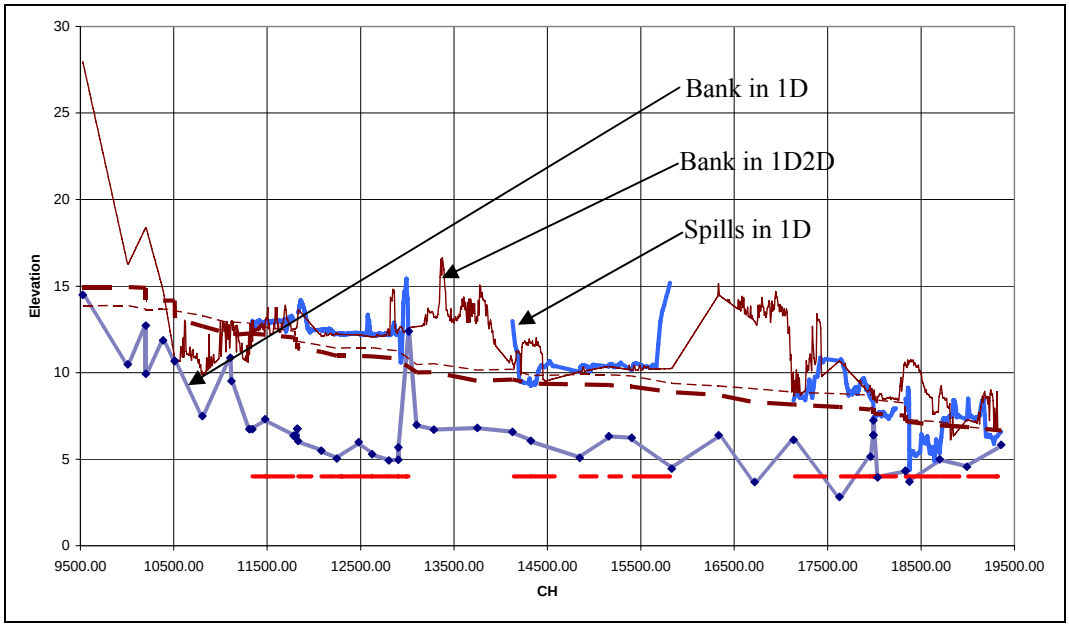

Figure 6.31: Right bank geometry – Option 9

Thus, the difference in the flood extents must be caused by the volume of floodwater transferred from the main channel to the floodplain. To confirm this, the volume of water transferred into storage cells from the 1D model with storage cells and the volume of water on to the floodplain from the integrated 1D2D model for the integrated 1D2D model setup according to Option 9 were compared. The outcome of this comparison for

two reservoirs (see Figure 6.7) in the 1D model with storage cells, Res55 and Res34 is shown in Figure 6.32.

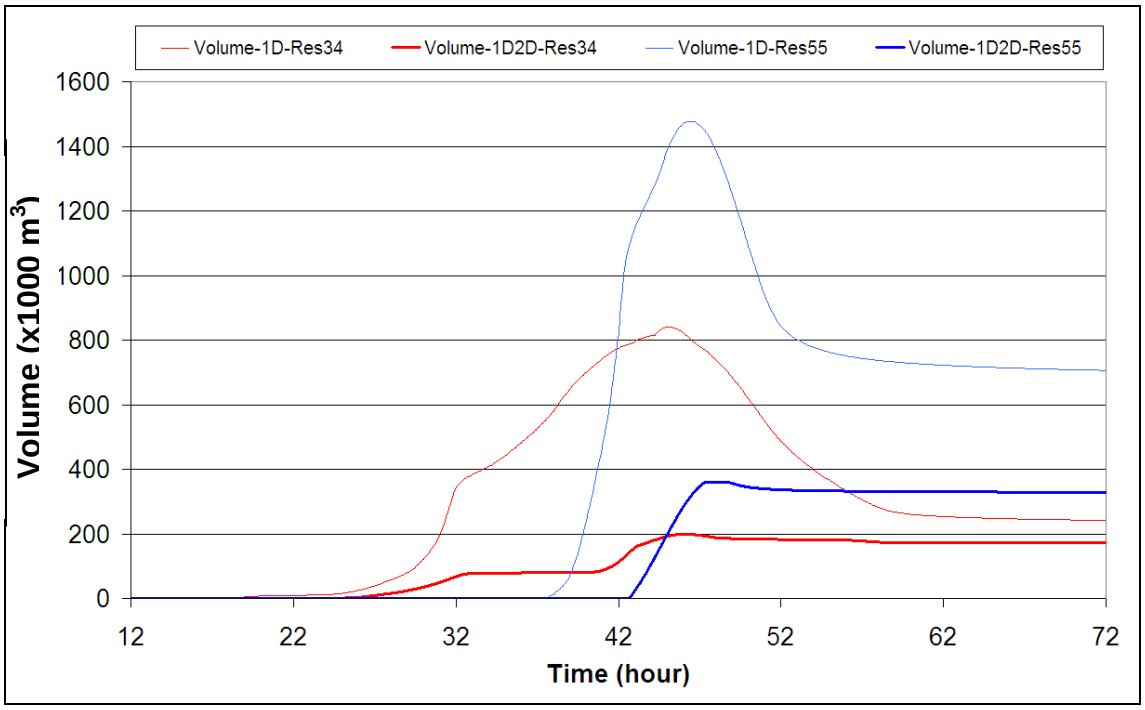

Figure 6.32: Comparison of floodwater volume in reservoirs in 1D and integrated 1D2D models

It can be observed that the flows onto the floodplain at the location of reservoirs Res34 and Res55 from the integrated 1D2D model results are consistently less than those from the 1D model with storage cells. Therefore, as expected and shown in Figure 6.27, the flood extents for areas covered by both of these reservoirs are lesser in the integrated 1D2D model than those in the 1D model with storage cells.

Further, an analysis was carried out to see if the integrated 1D2D model produces similar in-channel water level predictions as those obtained from the 1D model with storage cells. For this analysis, stage and discharge hydrographs along the river reach were examined. Figure 6.33 and Figure 6.34 show two such hydrographs.

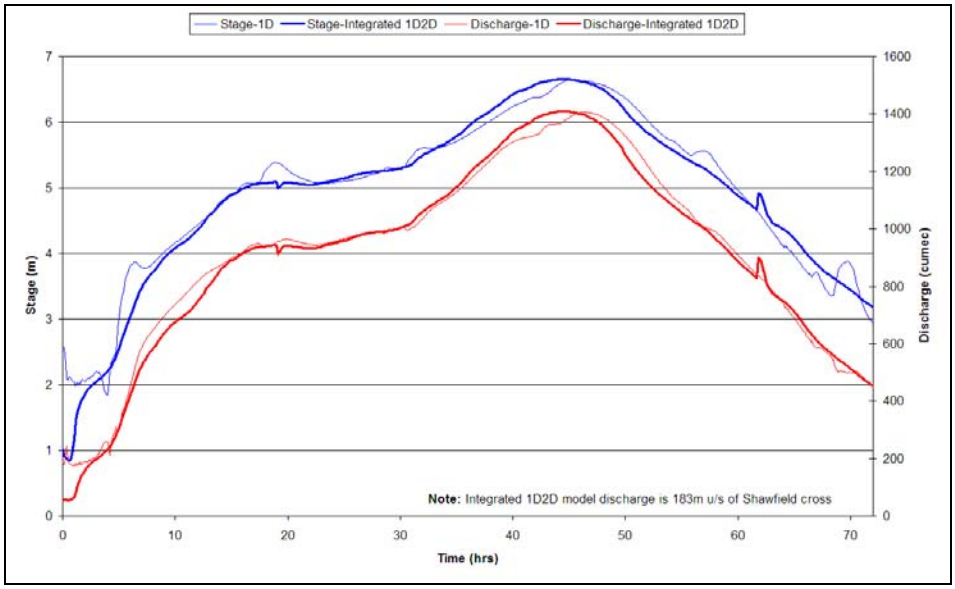

Figure 6.33: Stage and discharge hydrographs at the downstream boundary (Shawfield Stadium cross-section)

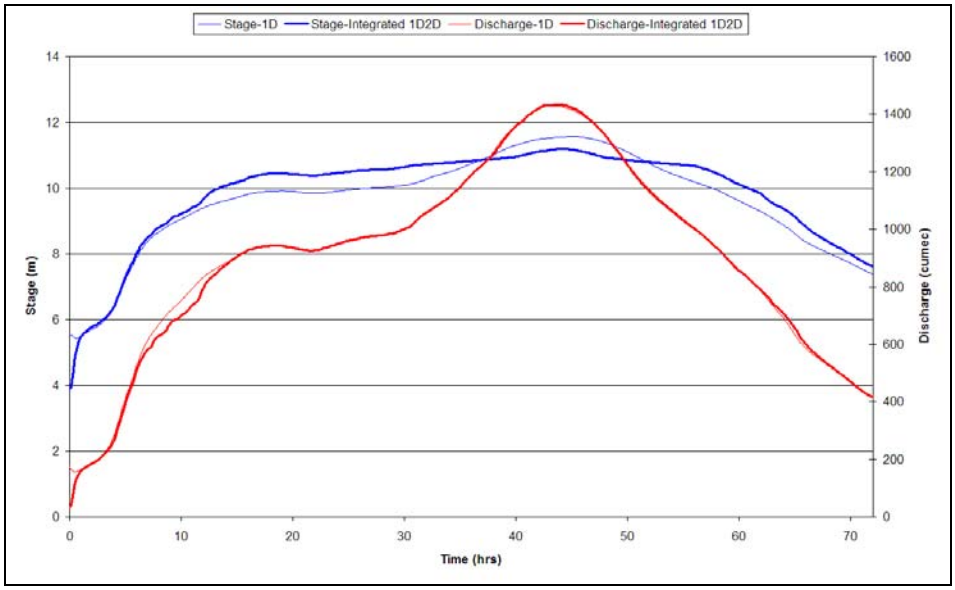

Figure 6.34: Stage and discharge hydrographs at an intermediate (U_EL_MW) cross-section

The stage and discharge hydrographs along the river reach did not show any significant differences or unusual behaviour of the integrated 1D2D model.

In addition to the above, following observations were made from the simulation results:

Identification of flow paths

The identification of potential flow paths in the 1D model with storage cells requires an assessment by the modeller, and is therefore subject to differences across modellers. Whereas, during the configuration process of an integrated 1D2D model, potential flow paths do not need to be defined beforehand since they are automatically determined by the model geometry and topography.

An incorrect assessment of flow paths during modelling using 1D model with storage cells can lead to a 'false' or 'forced' flooding of an area. The area circled in the figures Figure 6.27 is an example of such a case.

Similarly, an area which would be flooded, may not be shown as flooded by a 1D model with storage cells if a modeller does not correctly identify the potential flow paths, i.e. a spill is not identified and connected to a reservoir unit.

Flooding of isolated areas

Details about how the floodwaters are spread in the floodplain during a flooding event cannot be analysed in a 1D model with storage cells. The flood extents are plotted by marking all the areas in a reservoir below the calculated flood level as flooded. This leads to isolated areas, which are not connected with the river being marked as flooded. Figure 6.35 shows some locations where isolated areas are shown as flooded in the results from the 1D model with storage cells approach.

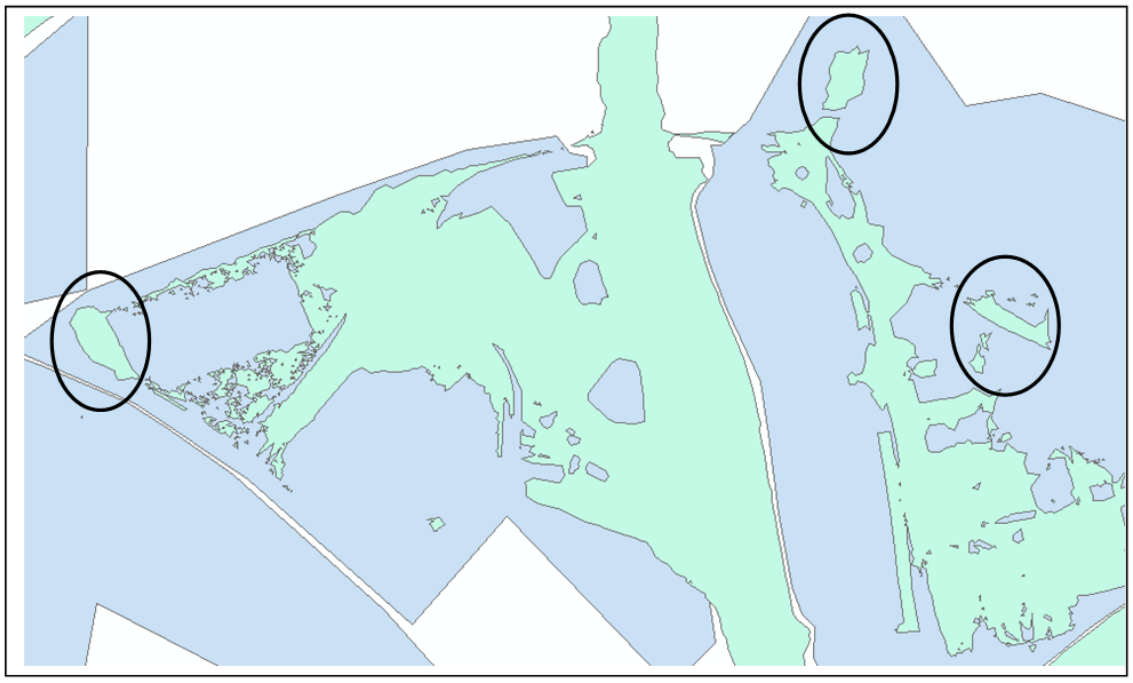

Figure 6.35: Isolated areas flooded in the 1D model with storage cells

Proper or correct assessment of possible flow paths over a floodplain is an important element of integrated 1D2D model. The flooding extents are calculated as the floodwaters spread over the floodplain. Therefore, an integrated 1D2D model approach does not show any isolated areas as flooded.

Flood wave characteristics

The integrated 1D2D model simulation results predict the depth and velocity of floodwaters through time for each of the computational grid cells. This information can be important for some end uses of the flood modelling study, particularly for planning and emergency operations.

From the integrated 1D2D model simulation results, the locations prone to water logging after floods have receded, thus having inadequate natural drainage, can be identified. This information can be of importance for various planning and management purposes.

Results visualisation

The model elements in the 1D model with storage cells are a conceptual representation of the river system being modelled. Whereas, the topographic data in the integrated 1D2D model gives a model view of the river system. The model results like flow depth and velocity can be overlaid on the topographic data. Animations of the simulations for different flood scenarios can be prepared for wider audience to improve understanding and interpretation. Such types of outputs are difficult, and in many cases not possible, from the results of 1D model with storage cells.

6.8.3 Conclusions

Using three different sets of cross-section extents in 1D model viz. floodplain extents, main river channel extents and modeller defined extents together with bank levels taken from only 1D data, only 2D topography data and the maximum values from the 1D and 2D topography data were used to compare the differences in the maximum flood extents predicted by integrated 1D2D model with those predicted by 1D model with storage cells. LiDAR DTM topography data acquired for the floodplain under consideration was used for the 2D model. These integrated 1D2D model setup configurations are summarised in Table 2.2 in section 2.2.8.

The integrated 1D2D model simulations using the above setups show that the model results are highly sensitive to the cross-section extents in the 1D model as well as the source of the bank levels. This is because of the different representation of the left and the right banks in the setups under consideration. Consequently, different volumes of floodwaters are transferred from the 1D model to the floodplain leading to significantly different flood inundation extents.

The maximum flood extent predictions from the integrated 1D2D model can be made comparable to those from the 1D model with storage cells provided that the volume of floodwater transferred to the 2D model or reservoirs are similar.

Therefore, if both the modelling approaches are predicting similar results, 1D models with storage cells are comparatively much faster to run making them preferable for strategic flood risk management studies (SFRM). This modelling approach, however,

suffers from few drawbacks like possibility of an inaccurate identification of flow paths, flooding of isolated areas, inability to describe the flow paths followed by floodwaters in the floodplain and the details of flood wave characteristics with time e.g. depth and velocity.

Integrated 1D2D models for smaller areas – such as the area in this case study – can be run using normally available desktop computers. The time required for configuring, pre-processing of input data as well as post-processing of model results in the case of an integrated 1D2D modelling approach is comparatively less than that in the case of 1D model with storage cells approach and can be an advantage for undertaking detailed flood risk assessment studies of small urban areas in a river system.

6.9 Topography data types and grid resolution studies

6.9.1 Introduction

The 2D elevation data used in the simulations so far is Digital Terrain Model (DTM) data. The data is produced after using algorithms to filter out the presence of vegetation and man made structures like buildings from the acquired raw topography data and aims at providing the profile of terrain or ground elevations beneath buildings and vegetation, see section 2.3.1.

However, in urban areas, the flow paths of floodwaters may get significantly altered due to the presence of buildings, roads, bridges and other man made structures. Therefore, while modelling an urban floodplain, it is essential to consider the presence of these changes in the topography to get more realistic assessment of flooding phenomenon. These features are mainly not filtered out of Digital Elevation Model (DEM) data, see section 2.3.1. However, DEM data was not available for this research. Instead, DEM is constructed by identifying the locations of buildings from the relevant layers in the MasterMap® data available from Ordnance Survey (see Figure 6.36) and then raising the elevations of the cells covered by the buildings in the DTM data (see Figure 6.37 and Figure 6.38).

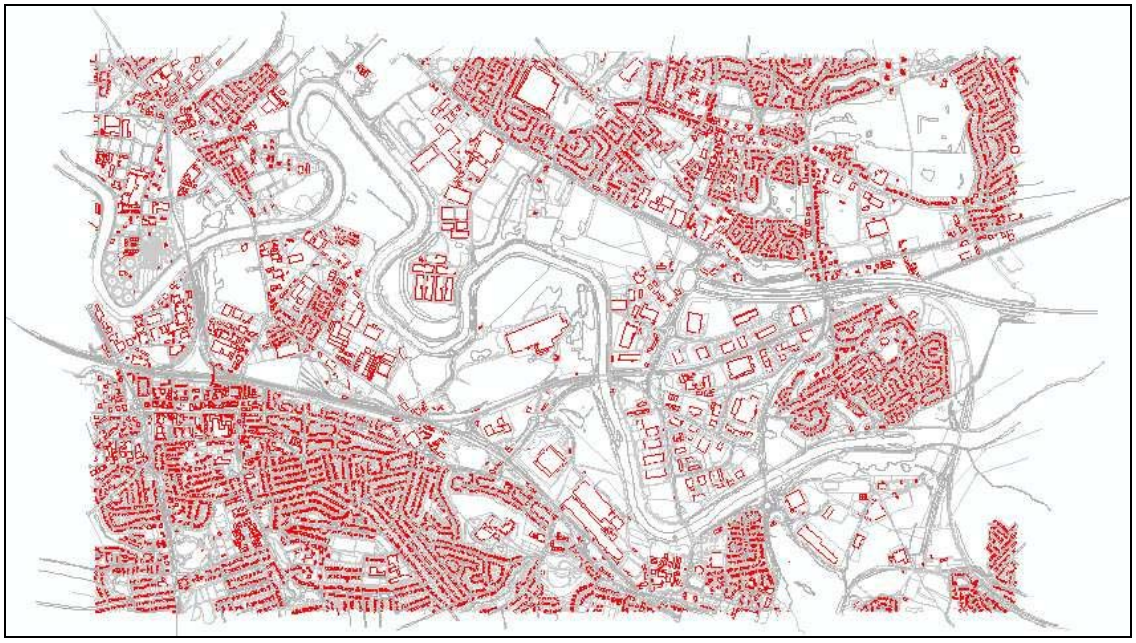

Figure 6.36: Identification of buildings in MasterMap® data

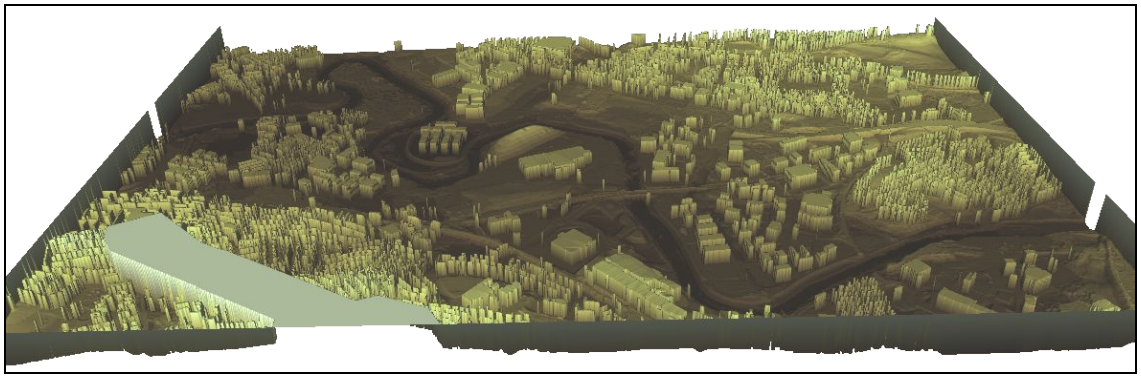

Figure 6.37: Creation of DEM data from DTM and MasterMap® data

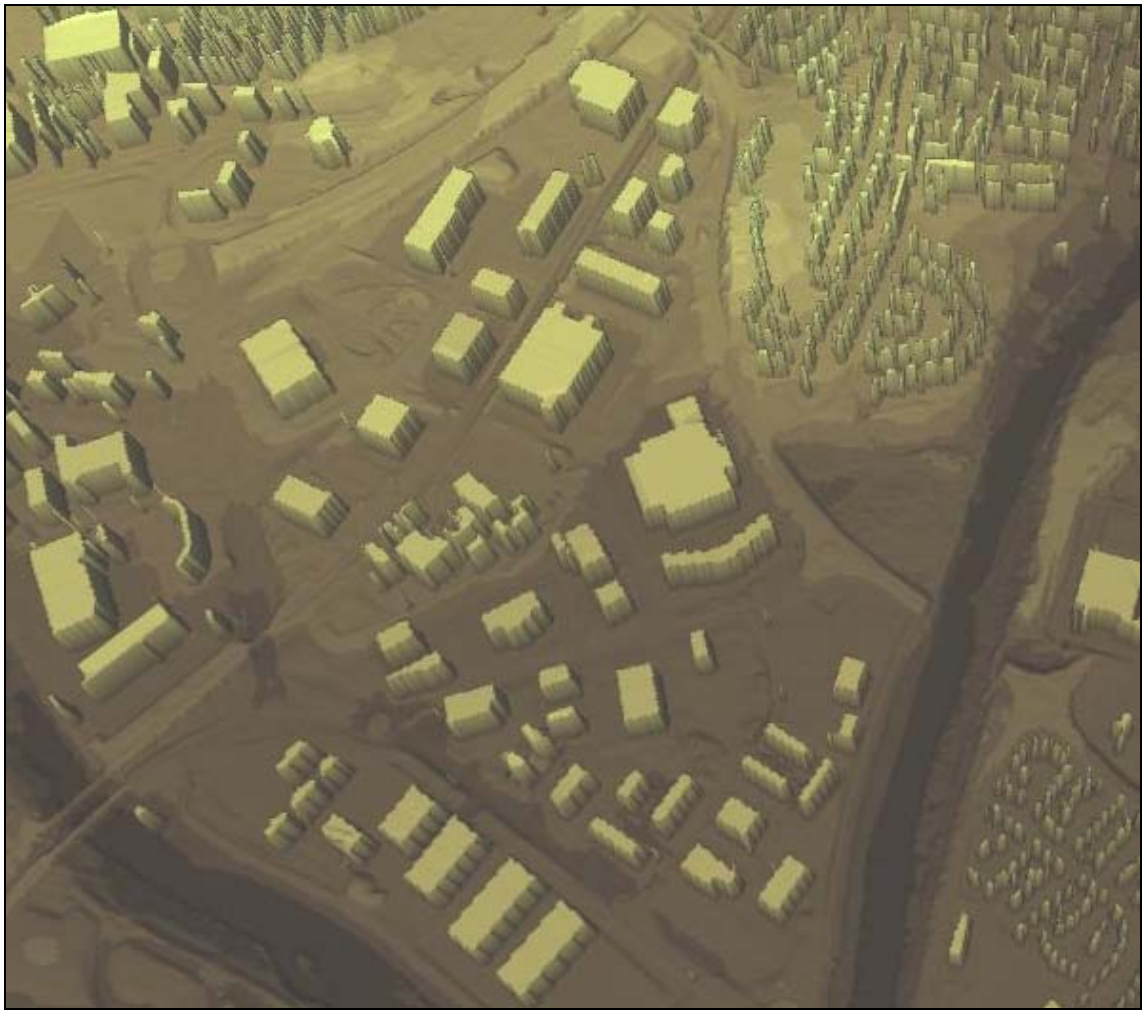

Figure 6.38: Closure view of DEM data created from DTM and MasterMap® data (grid resolution = 3 m)

As described and justified, see section 3.2.2, and demonstrated, see section 5.5.1, buildings can be considered as storage areas as opposed to obstacles to flow. To simulate this effect, a new topographical data, called hereafter as DTMporous, was prepared by using the DTM data as base and applying a fictitious high value of Manning's *n* equal to 0.8 $m^{1/3}/s$ at the grids covered by the buildings.

Thus, to study the effect of different topographical data types and the different grid sizes on the flood wave characteristics, simulations are carried out using the integrated 1D2D model setup pertaining to Option 9 (see Table 2.2 in section 2.2.8) and using DEM, DTM and DTMporous topography data types of 18 m, 9 m and 3 m computational grid

sizes. The results are discussed in sections 6.9.2 and 6.9.3 below and the conclusions from the study are presented in section 6.9.4.

6.9.2 Effect of different topography data types

Maximum flood extents using DTM, DEM and DTMporous topography data types for an area near Dalmarnock Road, Rutherglen, as obtained from integrated 1D2D model simulations with 18 m, 9 m and 3 m computational grid sizes are shown in Figure 6.39, Figure 6.40 and Figure 6.41 respectively.

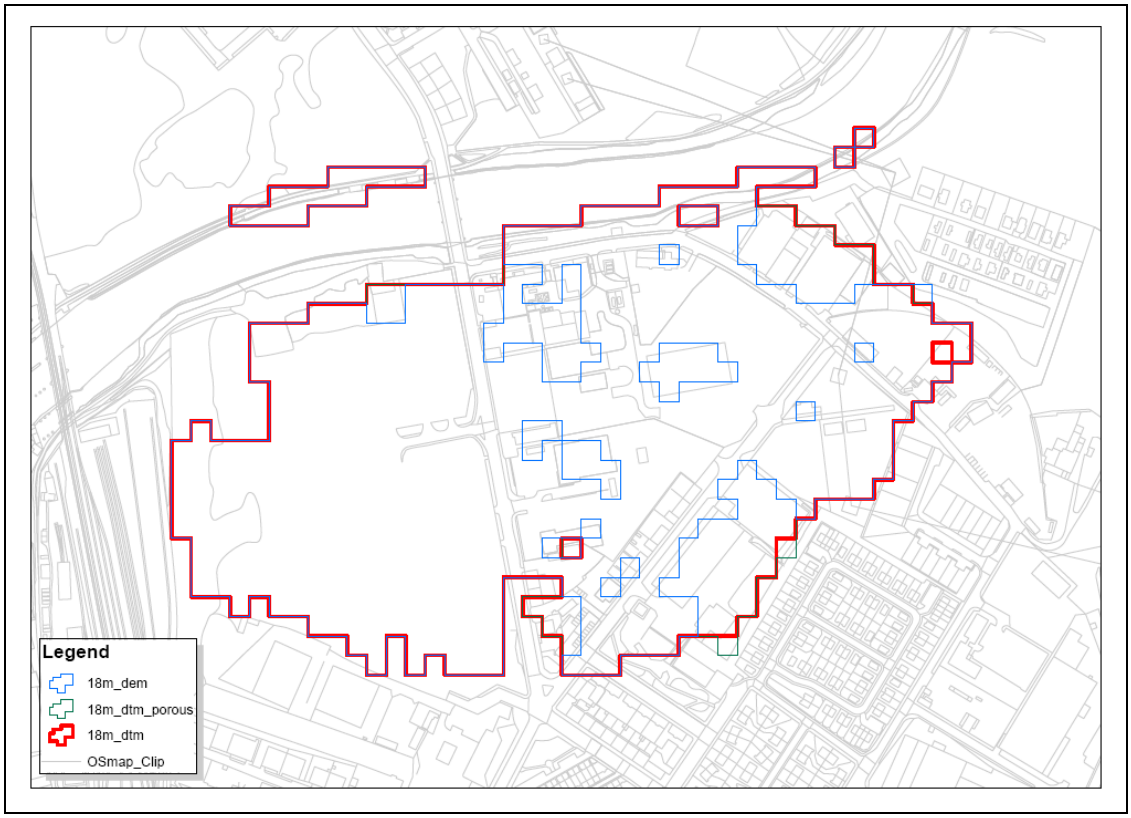

Figure 6.39: Maximum flood extents with different data types (18 m grid)

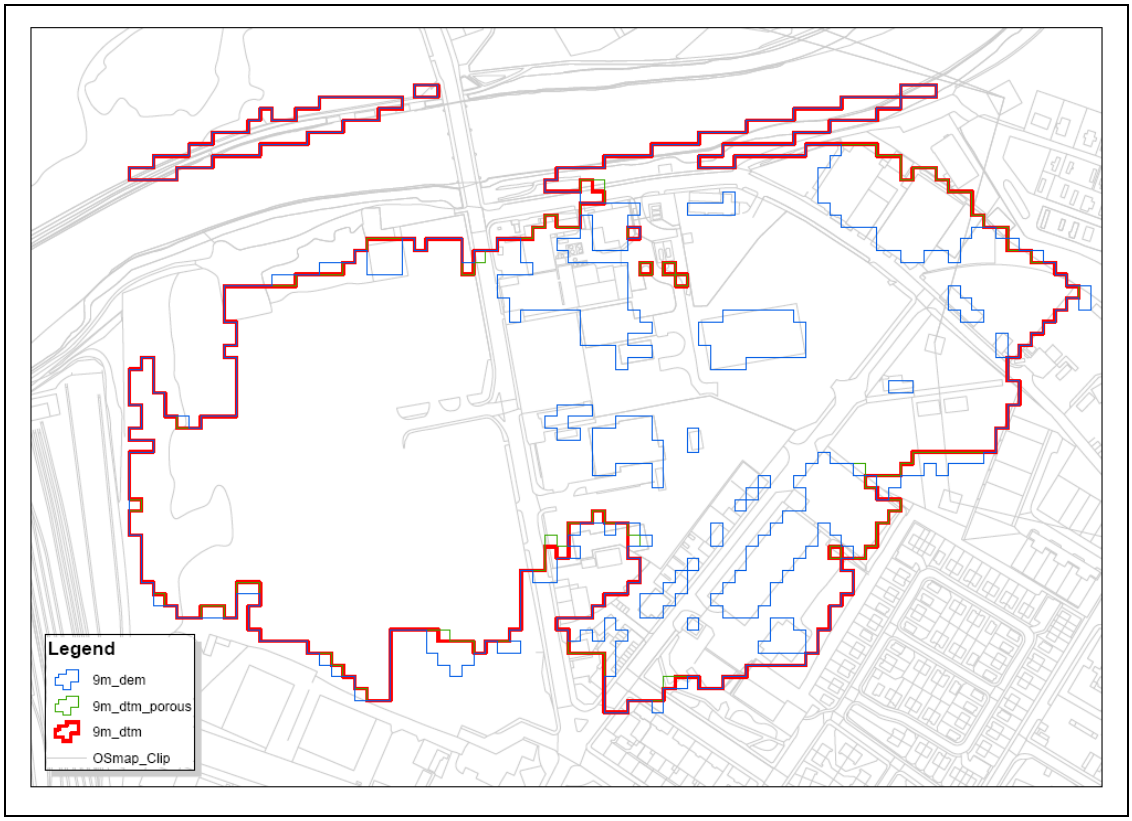

Figure 6.40: Maximum flood extents with different data types (9 m grid)

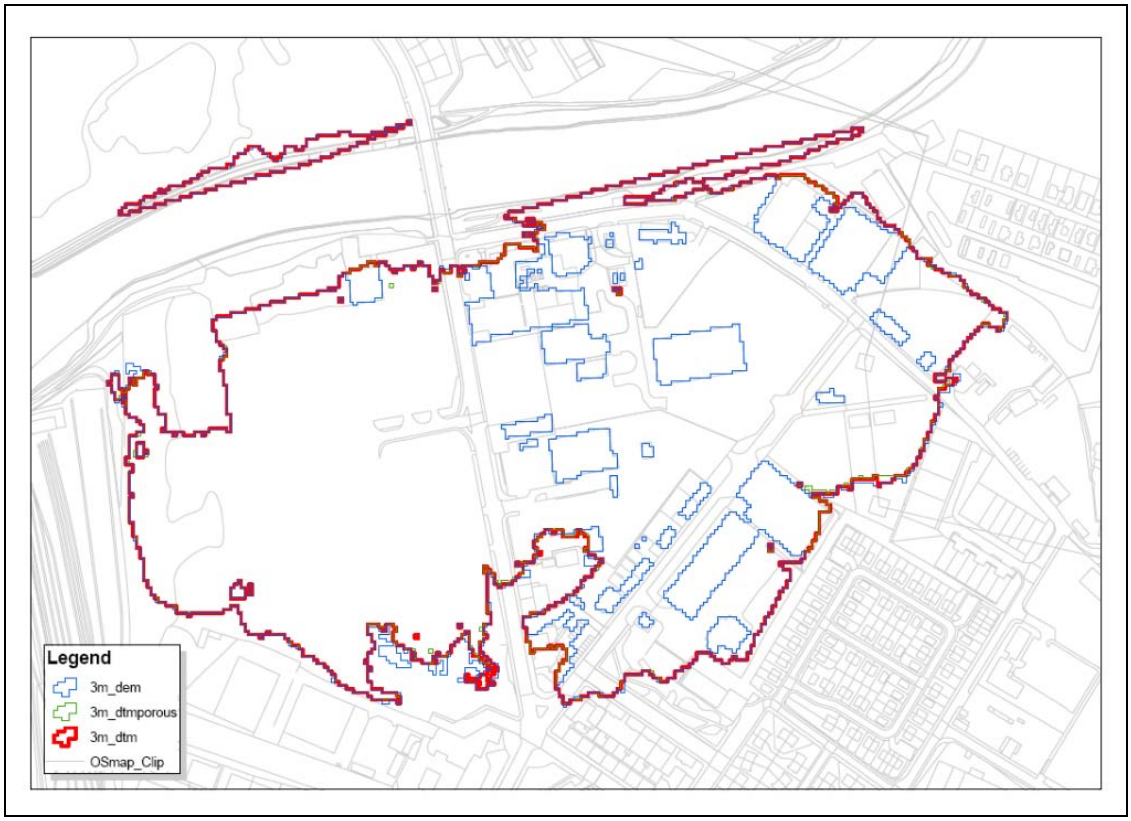

Figure 6.41: Maximum flood extents with different data types (3m grid)

It was observed that the maximum flood extents using different topographical data types, when compared at individual grid sizes, are almost the same. The flood extents, however, are refined with a lower grid size.

Further, it was observed that the difference between the maximum flood depths predicted by the integrated 1D2D models using DTM, DEM and DTMporous are higher or lower, but with no pattern, by approximately 0.1 m in the urban areas.

Thus, it can be concluded that for an urban area with medium density, such as the areas in this study, usage of any particular data type is not significant for detailed flood risk assessment studies.

6.9.3 Effect of different topographical grid resolutions

The maximum flood extents using 18 m, 9 m and 3 m topographical grid sizes for an area near Dalmarnock Road, Rutherglen, as obtained from integrated 1D2D model simulations using DTM, DEM and DTMporous topography data types are shown in Figure 6.42, Figure 6.43 and Figure 6.44 respectively.

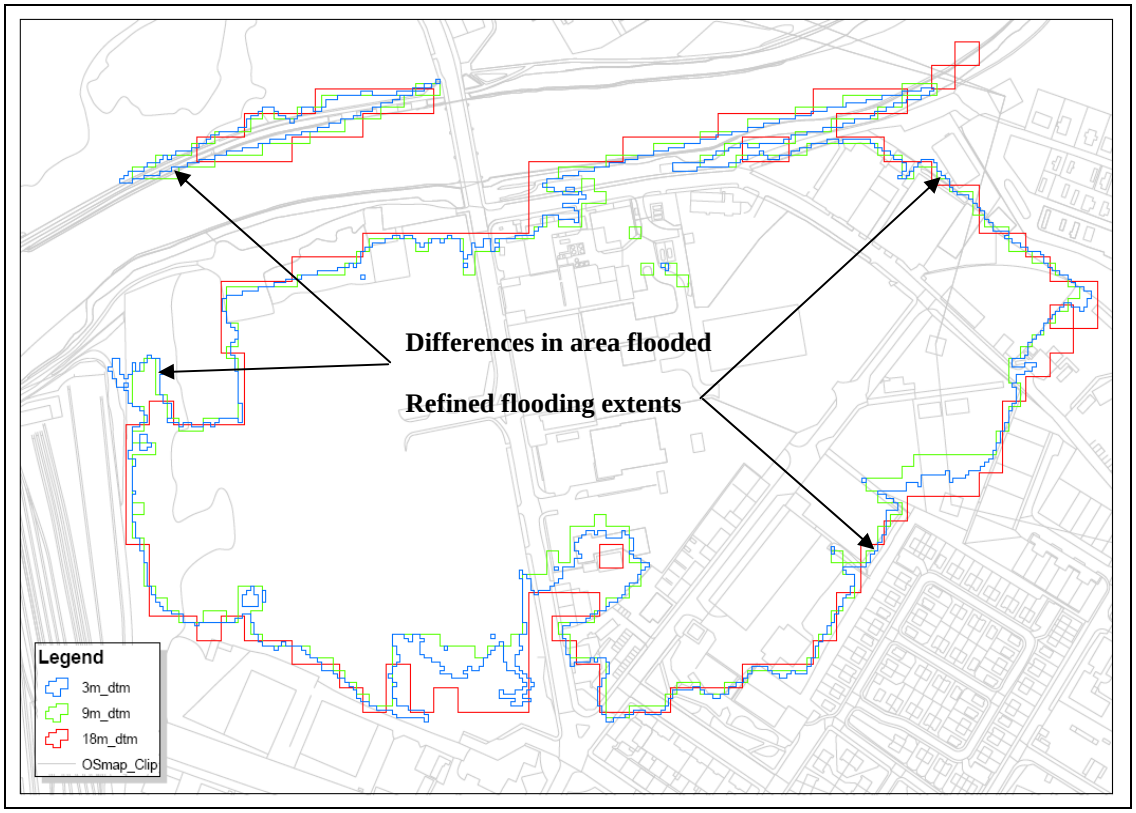

Figure 6.42: Maximum flood extents with different grid sizes using DTM data

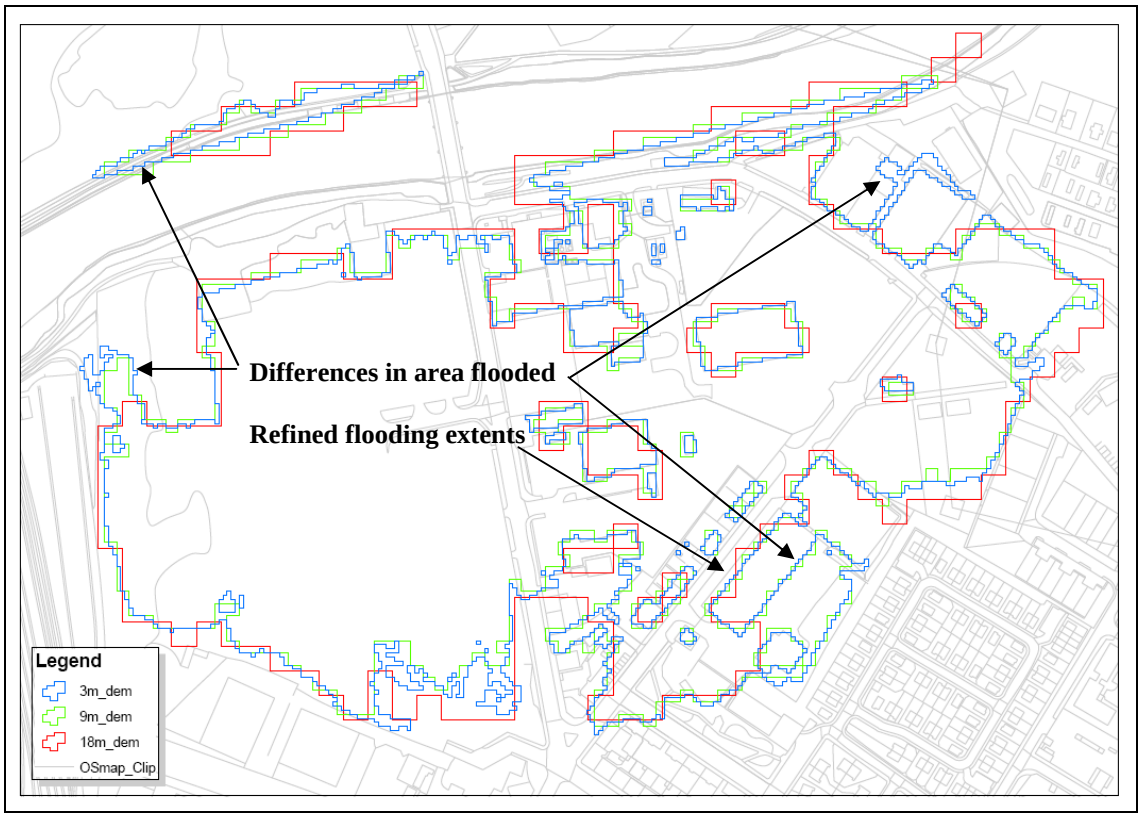

Figure 6.43: Maximum flood extents with different grid sizes using DEM data

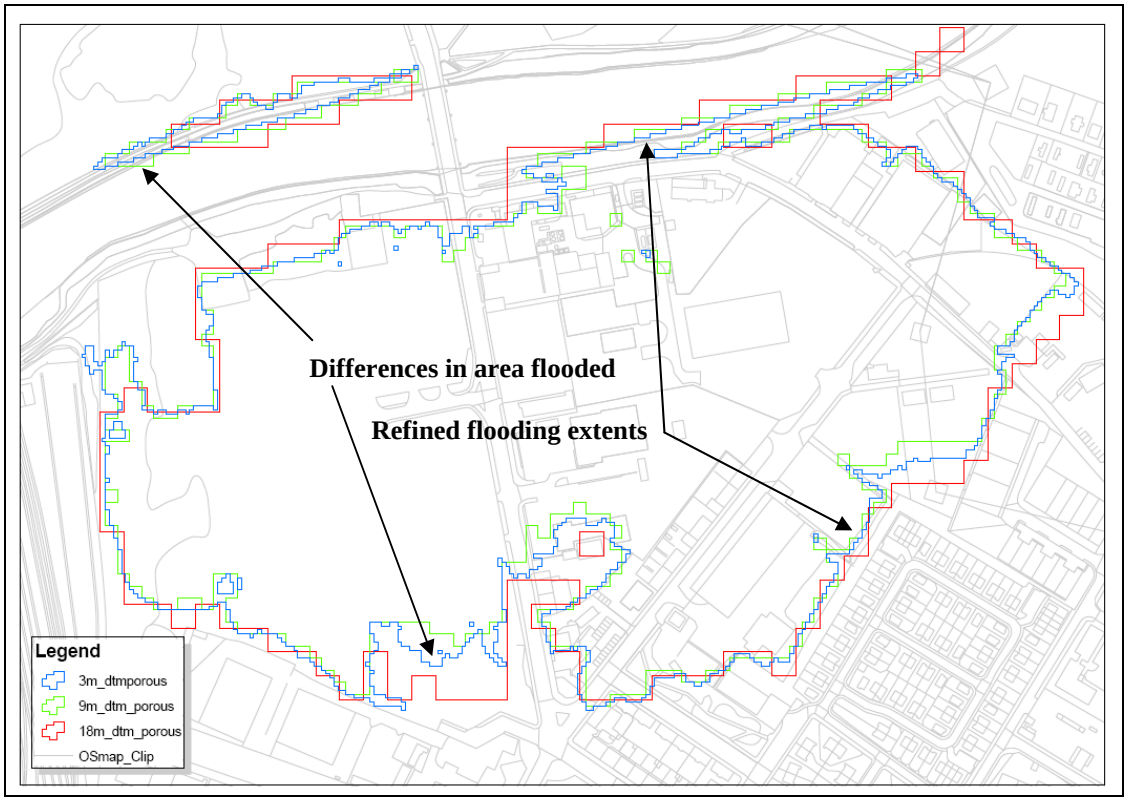

Figure 6.44: Maximum flood extents with different grid sizes using DTMporous data

It was observed that the maximum flood extents using different topographical data types, when compared at individual data type, are slightly different. The flood envelope is more defined with finer grid sizes. On the periphery of the flood map, differences in flooded areas are identified in results with finer grid sizes, thus, further supporting the assumption that detailed flood risk analysis is better with lower grid sizes.

Further, it was observed that the difference between the maximum flood depths predicted by the integrated 1D2D models using different grid sizes are higher or lower, but with no pattern, by approximately 0.8 m in the urban areas. Thus, it can be concluded that for flood risk assessment studies of an urban area, finer grid resolutions are preferable.

6.9.4 Conclusions

From the observations of the results using different topography data types, see section 6.9.2, it can be concluded that for an urban area with medium density, such as the areas in this study, usage of any particular data type is not significant for detailed flood risk assessment studies.

Further, from the observations of the results using different topography grid sizes, see section 6.9.3, it can be concluded that for flood risk assessment studies of an urban area, finer grid resolutions are preferable.

6.10 Model grid resolution – Nested grid model study

6.10.1 Introduction

As concluded in section 6.8.3 above, integrated 1D2D models give additional information about the flood wave characteristics such as velocity, depth, duration and timing of flooding and, thus, are very suitable for detailed flood risk analysis of an urban floodplain.

Although, integrated 1D2D models for limited areas – such as the area in this case study – can be run using desktop computers, the runtime can further be reduced by use of a

nested grid approach. This approach allows the adoption of finer grid size in areas where detailed results are required.

The advantage of using nested grid models was also emphasized by the nested grid model studies using hypothetical urban topographies described in section 5.7. It was concluded that the use of dynamically linked nested grid model results in considerable reduction in the simulation run time requirements without compromising the accuracy of the results in the area of interest.

The aim of this study, therefore, is to analyse the feasibility of using nested grid models for flood risk analysis of an urban floodplain. This is achieved here by analysing the maximum flood extents and the velocity of the flood water as it flows over the floodplain and comparing the model runtimes with and without nesting.

6.10.2 Model setup and runs

The integrated 1D2D model setup constructed according to Option 9 as listed in Table 2.2 is used for the analysis. To assess the flow velocity around buildings, the setup used DEM topography data constructed by identifying the locations of buildings from the Topography layer in the MasterMap® data available from Ordnance Survey and then raising the elevations of the cells covered by the buildings in the DTM data. From the maximum flood extents for this setup, see Figure 6.27, it can be observed that the area to be used for this exercise is not flooded. Therefore, a breach is introduced on the left bank of the River Clyde from CH 11478.39 to CH 11782.72 by lowering the left bank level at CH 11478.39 from 7.338 m to 5.626 m and that at CH 11782.72 from 8.081 m to 5.114 m. This breach then leads to flooding of the area between Bridge Street and Main Street near Cambuslang Railway Station, see the callout for the nested area in Figure 6.45.

The simulations were repeated for integrated 1D2D model setups with 3 m, 9 m, 18 m and 27 m computational grid sizes. Nested model approach is used for 3 m grid size model simulations. The nested area as shown in Figure 6.45 is chosen for the exercise as it has a comparatively higher urban density than other areas which can be flooded by the River Clyde.

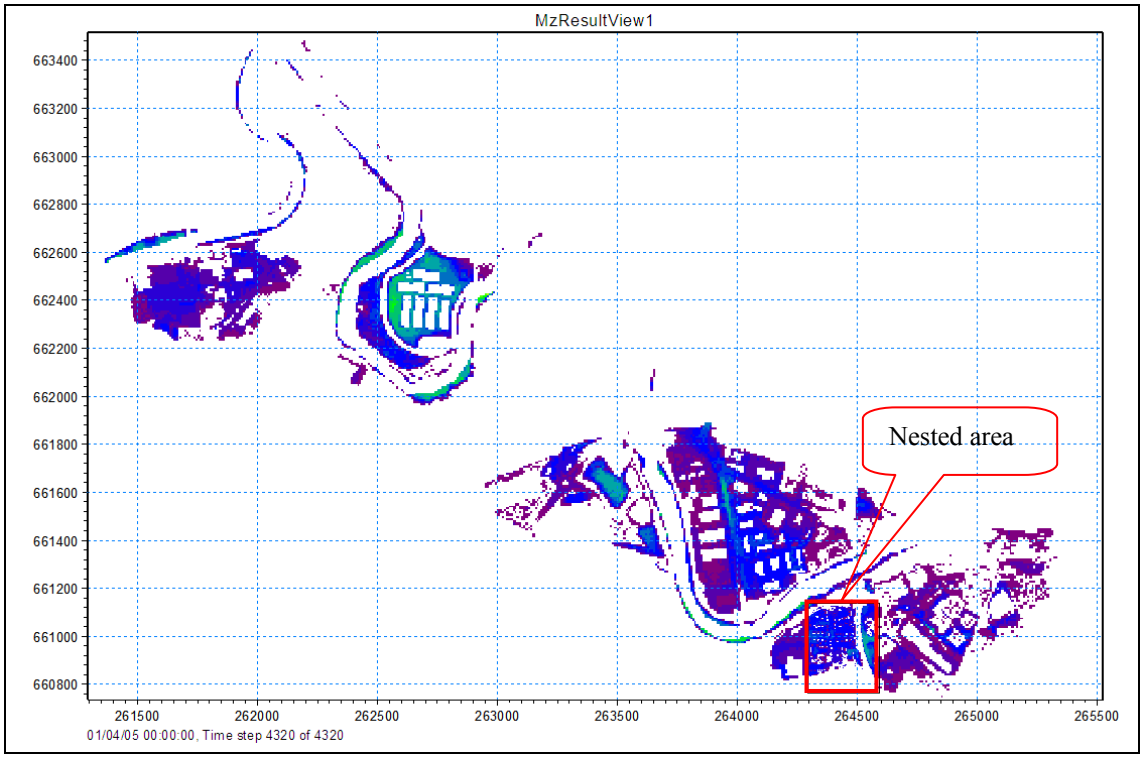

Figure 6.45: Nested grid model configuration

6.10.3 Results and discussion

The inundation extents for 3 m, 9 m, 18 m and 27 m grid sizes are shown in Figure 6.46, Figure 6.47, Figure 6.48 and Figure 6.49 respectively. The points at which water velocity comparisons are made are shown in Figure 6.46.

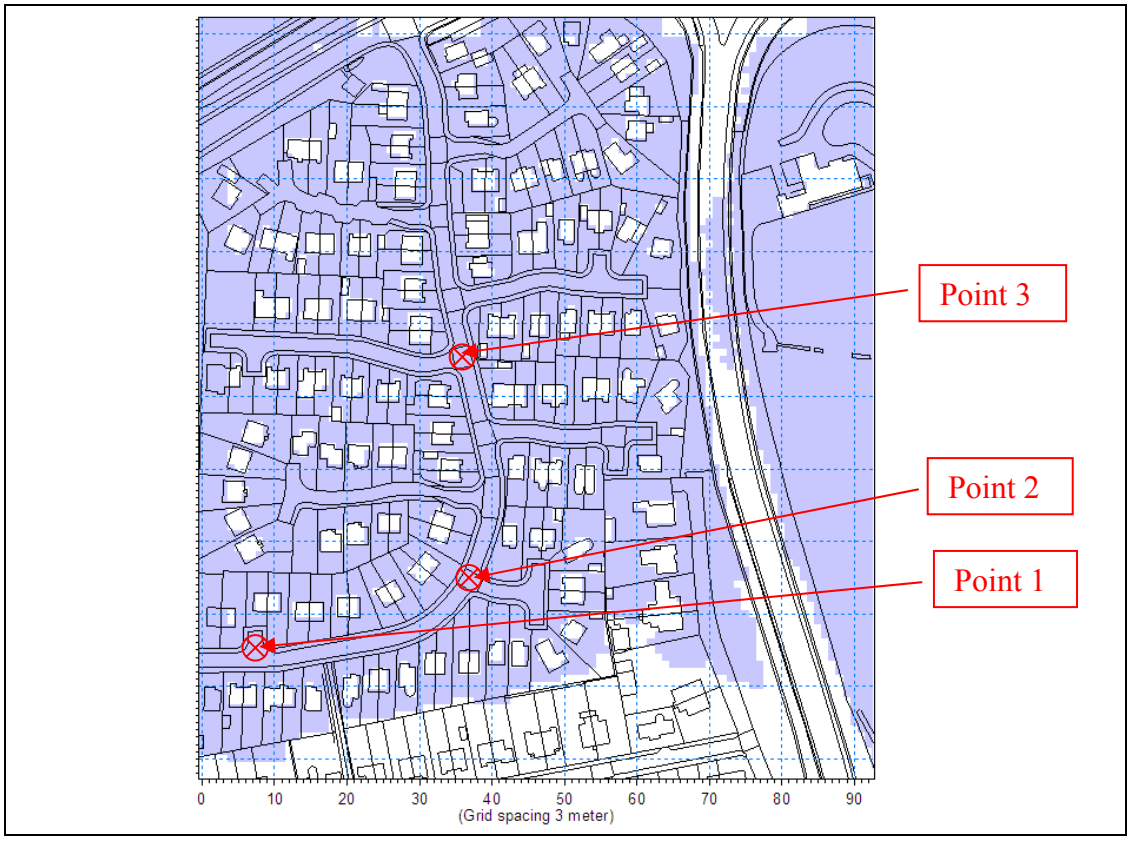

Figure 6.46: Maximum flood extents using 3 m grid and water velocity measurement points

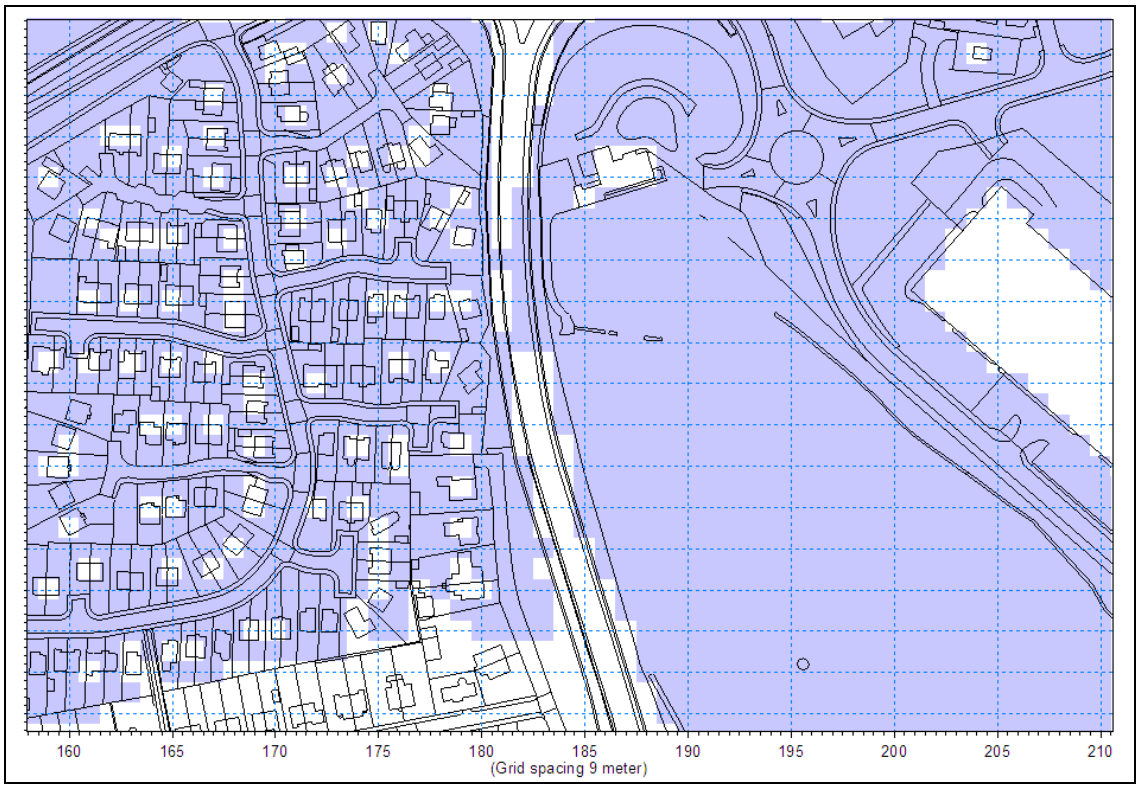

Figure 6.47: Maximum flood extents using 9 m grid

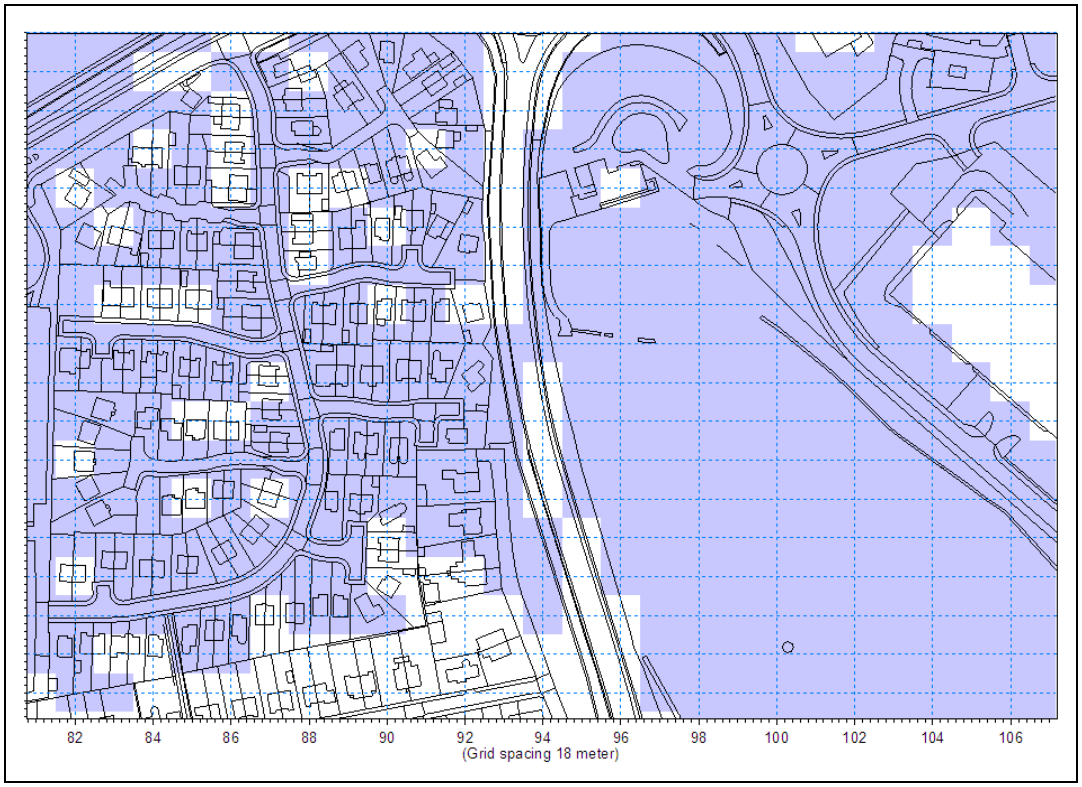

Figure 6.48: Maximum flood extents using 18 m grid

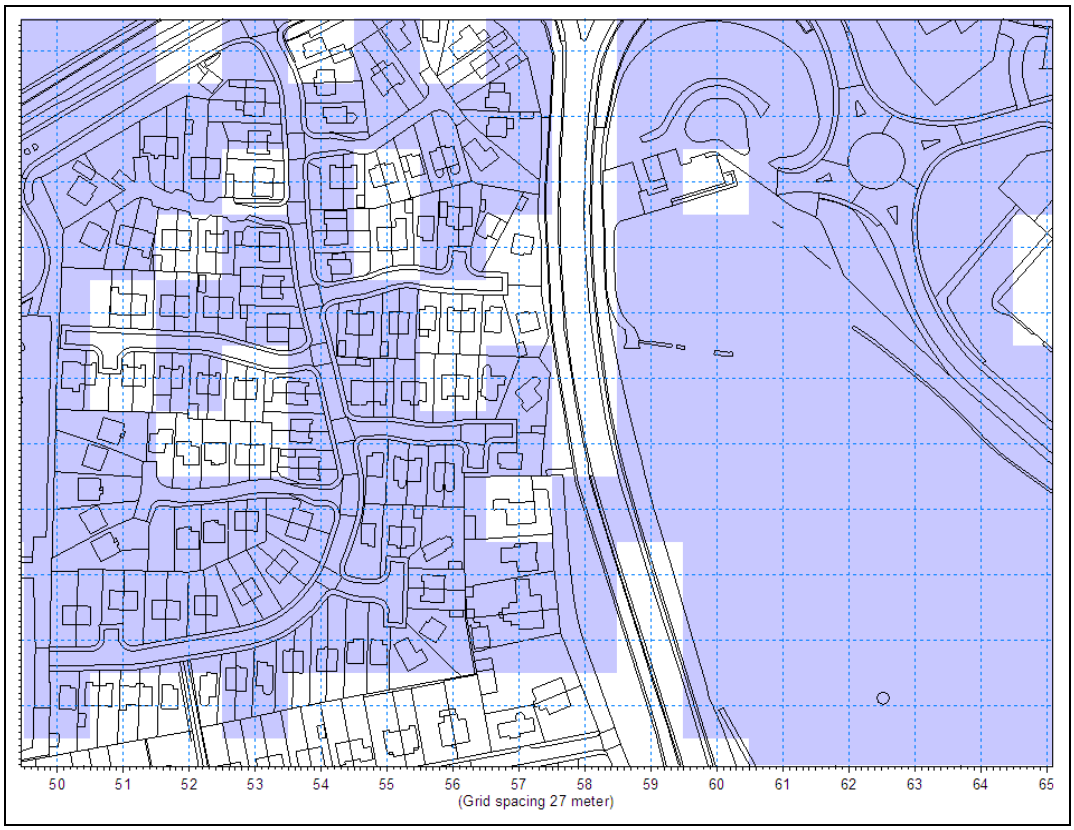

Figure 6.49: Maximum flood extents using 27 m grid

From the maximum flood extents from Figure 6.46 to Figure 6.49, it can be observed that the flood envelope becomes detailed and more defined with lower grid sizes in the dense urban area. Further, the flow paths, as observed along the major road running vertically in the approximate centre of the map, are different at different grid sizes. With an assumption that the finer grids represent the area topography better, detailed flood risk analysis is the most reliable with the least grid size. This was found to be true earlier, see section 6.9.4.

The CPU runtime required for the simulation with 3 m grid without the introduction of breach is 895,851 seconds. This run time will be more if the breach is introduced as additional area is flooded and the computer model will need additional CPU time to compute flood at the additional locations. Nested grid simulation using a 3 m fine grid nested within a 9 m coarse grid required 84,619 seconds. This is less than 10 % of the runtime that was needed without nesting.

Figure 6.50 shows the graph of the floodwater velocities for the nested integrated 1D2D model using 3 m fine grid and 9 m coarse grid.

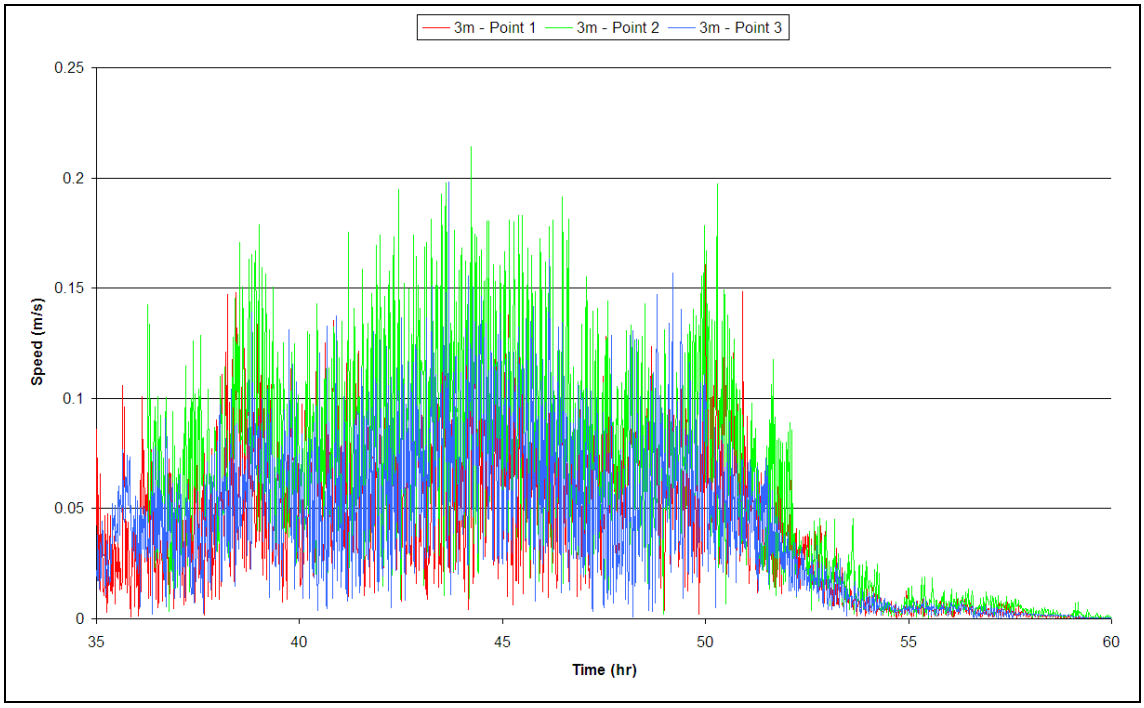

Figure 6.50: Velocity of floodwater at the selected observation points – 3 m grid

From the above graph, it can be observed that the velocities are having large fluctuations. Similar fluctuations in velocity values were observed for 9 m grid size results too. These large fluctuations in the velocity, most likely, can be attributed to model instabilities at such a small grid size. Simulations using larger grid sizes, 18 m and 27 m, do not show such fluctuations in the predicted values of the velocity of the floodwater.

Following figures show the predicted velocities at the three observation points. For legibility purpose, the graphs corresponding to 3 m and 9 m grid sizes use moving average plots of the predicted values.

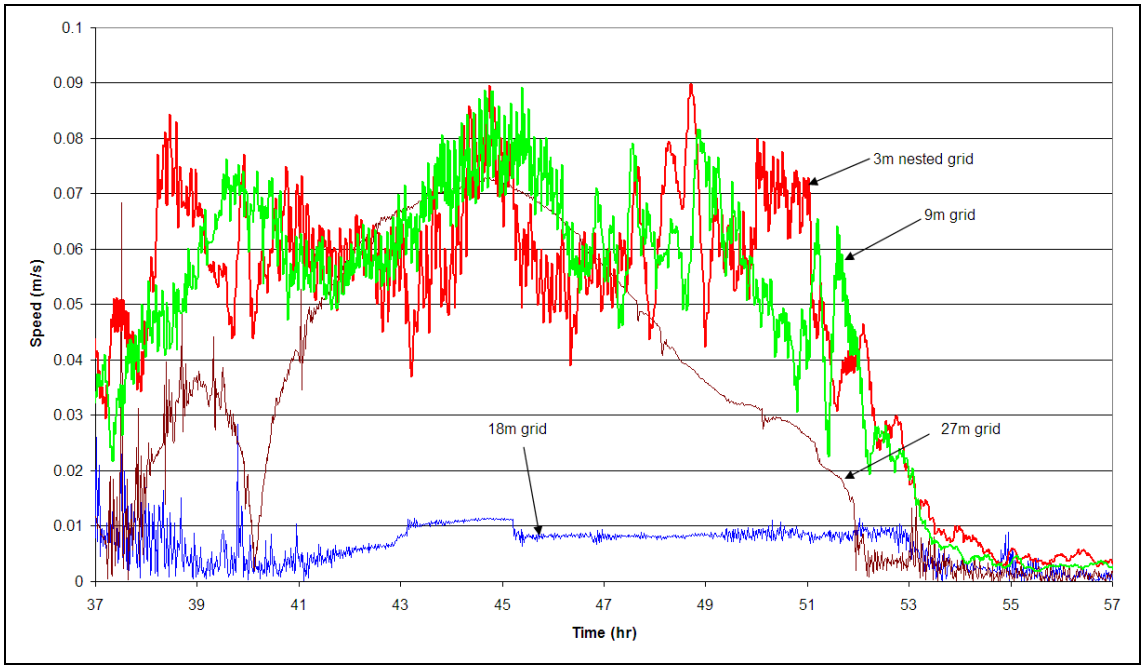

Figure 6.51: Predicted water velocities at Point 1

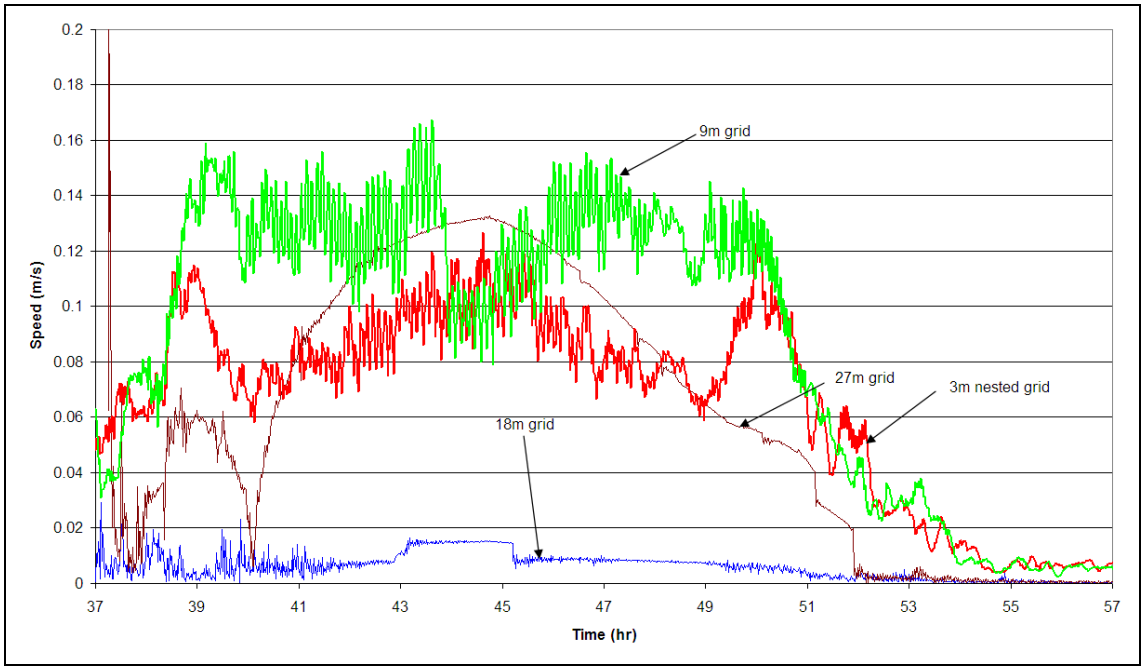

Figure 6.52: Predicted water velocities at Point 2

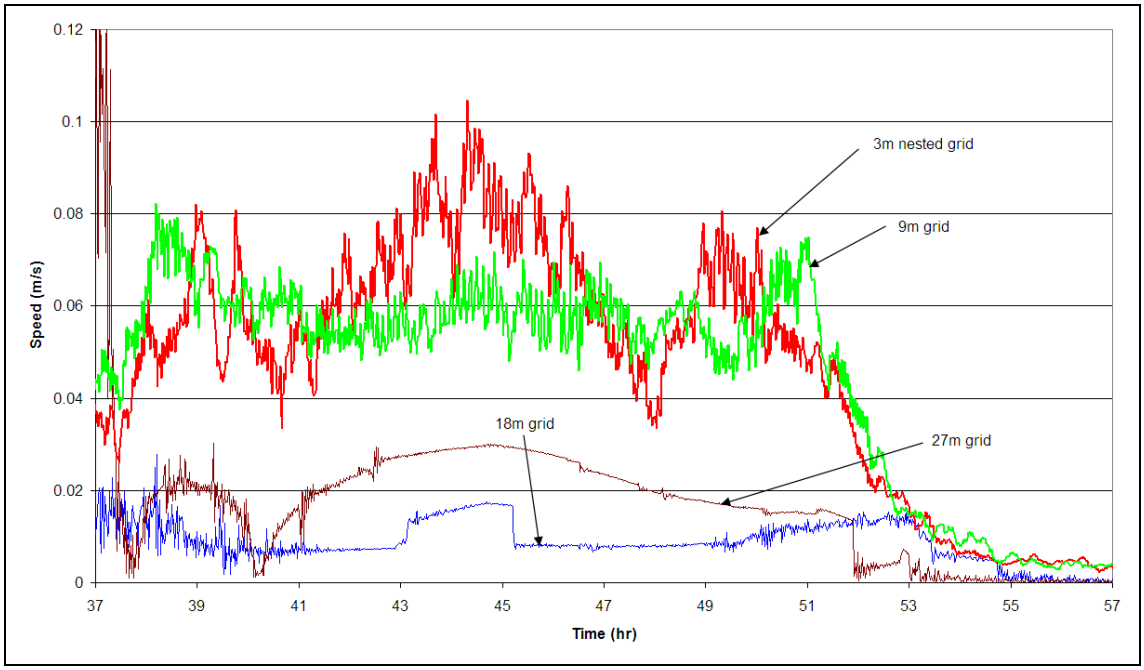

Figure 6.53: Predicted water velocities at Point 3

The above graphs indicate considerable differences in the predicted water velocities. The maximum velocities at Point 1, Point 2 and Point 3 are 0.339 m/s (1.220 kmph), 0.336 m/s (1.209 kmph) and 0.244 m/s (0.878 kmph) respectively.

It can be observed that the differences in the velocities of the floodwaters obtained by using different grid sizes are significant. Therefore, it can be of particular benefit to use lower grid sizes if the purpose of the study is where knowledge of flow velocities is vital, such as emergency planning.

6.10.4 Conclusions

Integrated 1D2D models with finer computational grid resolution can be used for detailed flood risk analysis. The computer time requirement for a model using a fine grid such as 3 m can be significant, but this time requirement can be substantially reduced by using nested grid models. For the nested 1D2D model setup employed here, the runtime requirement was found to be less than 10% of the runtime that was required without nesting. The finer grids show detailed and more defined flood envelopes. The flood map with a 3 m grid size shows precise flooding around houses and can be considered as the preferred grid size for detailed flood risk analysis of urban floodplains.

The floodwater velocity representation with models using finer grid sizes is unreliable as the simulations carried out in this research are unstable. But it can be concluded that velocities predicted with lower grid sizes, such as 3 m, shall be used for purposes like emergency planning.

6.11 Summary

This chapter describes the comparative study of the flood risk predictions using a 1D model with storage cells and the integrated 1D2D modelling method using a previously constructed 1D model and newly acquired LiDAR topography data for a section of the River Clyde and adjoining urban floodplain in Glasgow, a major city in Scotland, UK.

The details of the River Clyde catchment and the data available for this study are presented at the outset of the chapter, see sections 6.2 to 6.4. The integrated 1D2D model setting up procedure and the details of the model are described in section 6.7 whereas the details of the modelling results, discussion and the conclusions are presented in section 6.8.

It was concluded that the flood predictions from an integrated 1D2D model are significantly different from a 1D model with storage cells and that the model results are highly sensitive to the cross-section extents and the source of the bank levels in the integrated 1D2D model. This discrepancy was identified to be due to the different representation of the left and the right banks in the various setups.

Further, it was concluded that integrated 1D2D models are less prone to modelling errors like misidentification of flow paths, flooding of isolated areas and are capable of better describing the flood wave characteristics like the propagation of flood wave, depths and velocities of floodwaters, duration of flooding as well as the flooding scenario after the floods have receded and thus facilitate an enhanced presentation of model results.

The studies described earlier in Chapter 5 (see section 5.5) concluded that consideration of buildings as storage areas as opposed to obstacles to flow has significant effect on the flood wave characteristics, the study described in section 6.9.2 using different topography data types for a real floodplain, however, suggests no such benefit – at least from the maximum flood extents consideration.

Section 6.9.3 describes the study carried out to analyse the effect of topography grid sizes. The study used different topographic data types and compared the results using the same data type but different spatial resolution. From the results analysis, it was concluded that finer spatial resolutions yield more detailed flood maps as the flood envelopes are defined and blockages to flow or new flow paths are identified.

Although integrated 1D2D models for a large river system are not computationally feasible, a nested grid modelling approach described in section 6.10 concluded that a nested grid approach significantly reduces the time requirement and are thus found to be feasible for detailed flood risk analysis of urban areas of interest. This study used a minimum grid size of 3 m and the model results show that a 3 m grid can be a feasible option, from the detail and time requirement point of view, for a detailed flood risk assessment of an urban floodplain. Secondly, it was concluded that the velocity predictions with lower grid sizes are preferable for studies like emergency planning.

Chapter 7
Conclusions and Recommendations

7.1 Summary and conclusions from the research

Flooding is a major risk facing mankind today. It is projected to increase in view of the future predictions of climate change.

Traditionally, flood risk assessment studies of urban floodplains have been carried out using 1D and 1D models with storage cells. Flood risk assessment using 2D computer models has gained a momentum recently due to the availability of high resolution LiDAR topography data together with a substantial improvement in computing power and advances in numerical computational methods. The comparative assessments of benefits of using 1D and 2D models suggests a logical adoption of integrated 1D2D models for the flood risk assessment on urban floodplains.

The findings reported in this thesis evaluate this modelling method by comparison with results from the traditionally used 1D model with storage cells.

Computer models using 1D method have undergone numerous applications worldwide and therefore any validation exercise of the 1D modelling software was not carried out. Validation exercise for the 2D modelling software is carried out using observed experimental data from a physical model study of an urban settlement in a river system.

Validation is carried out by comparing the computer model prediction of temporal variations in water level with those from published physical model experiments. The study found that the published data was only partially useful in validating the computational ability of the software.

Further modelling studies using different urban settlement layouts are carried out at a prototype scale on a hypothetical urban test section.

It concluded that the presence of buildings on the floodplain affects the predicted floodwater depths and velocities significantly and leads to the development of a shockwave and complex flow patterns in and around the buildings. In addition, as during flooding, floodwaters may enter and leave buildings through any openings, a study to assess the effect of considering this phenomenon was carried out. It concludes that such a consideration has significant effect on the flood water depths and velocities.

This hypothetical urban floodplain study was also used to evaluate the use of a nested grid model. The results demonstrated a considerable saving in computing time without compromising the quality of predictions.

Thus, with the software validated and findings about the flood wave characteristics in an urban test section, further studies were undertaken using a real river and urban floodplain system for a section of the River Clyde in Glasgow.

From this analysis, it was concluded that the predictions from the integrated 1D2D models are highly sensitive to the cross-section extents in the 1D model component of an integrated 1D2D model and the source of the linked bank level data. Therefore, carrying out a field survey, before any integrated 1D2D model studies are carried out, to indentify the accurate extents of the river channel and the bank levels is recommended. This will lead to a more realistic representation of the river and the floodplain dynamics in a 1D2D model.

The study also found that the predicted flood extents from the integrated 1D2D model are significantly different among different integrated 1D2D model configurations. None of the above predictions were in close agreement with the predictions from the 1D model with storage cells.

However, analysis of the results from integrated 1D2D model suggest some advantages over a 1D model with storage cells, e. g. identification of flow paths, no flooding of areas isolated from flood waters, detailed description of the flood wave and enhanced results prediction.

The above study, therefore, concludes that while integrated 1D2D models are of much benefit for a detailed flood risk analysis, specific attention needs to be paid towards the lateral extents of 1D model and the bank levels when integrating it with a 2D model, particularly so when such a study is carried out for urban floodplains.

As mentioned earlier, the hypothetical urban floodplain study suggested considerable effect of buildings in a floodplain on the predicted flood wave. To confirm these findings, exercises were carried out using Digital Elevation Model (DEM), Digital Terrain Model (DTM) topography data and using high value of hydraulic resistance coefficient at building footprints to simulate the storage effect of buildings.

The study found no significant differences in the maximum flood extents for the integrated 1D2D model setup for the case study, probably due to the low density of buildings in the floodplain. However, the flood extents predictions are better defined with high resolution topography data and showed additional or less areas flooded compared to coarser resolution data implying that finer resolution data might have predicted new flow paths or blockages to flow.

Further study to validate the benefit of using a nested grid approach was carried out. The study concluded that the nested grid approach results in considerable saving in computing time required and allows use of smaller grid sizes, thus, making integrated 1D2D modelling method suitable for detailed flood risk analysis of urban floodplains.

7.2 Recommendations for further research

7.2.1 Identification of an appropriate 1D2D model setup

The study used nine possible integrated 1D2D model setups to predict flood inundation extents on an urban floodplain and concluded that the model predictions are sensitive to the source of the bank elevation data and the 1D model extents. This study, however, could not recommend an appropriate 1D2D model setup.

Further research in this regard can, therefore, be undertaken to identify the most appropriate source of the bank elevations and the 1D model extents in an integrated

1D2D model setup. This research shall also consider the feasibility and usefulness of a reconnaissance survey for identifying the river banks and including the surveyed bank elevations along the identified left and right bank alignments.

7.2.2 Integrated 1D-2D-1D flood modelling

In a 1D model for subsurface sewerage and drainage systems modelling, the volume of water spilled over a surcharged manhole is held in a fictitious storage reservoir and returned to the system when it ceases to be surcharged.

However, in reality, the spilled-over volume of water may find alternative routes – and in some cases may leave the catchment and never or partially return to the source manhole. Secondly, the catchment of the subsurface drainage system and the surface catchment(s) are not necessarily the same. In many cases, the subsurface drainage systems encompass many surface catchments. Thirdly, in many low lying areas, particularly so where the tide levels are higher than the neighbouring floodplains, pumping stations are operated to alleviate the flooding which in turn changes the flood scenario. These may have effect on the flooding dynamics in an area at flood risk and consequently affect the flood risk related assessments.

Integrated 1D2D model studies, similar to the research detailed in this thesis, where the 1D model is not the river but is the subsurface sewerage drainage system, are already being carried out (Han et al. 2007; Coulet et al. 2008). These types of studies are helpful in gaining an insight into the performance of the subsurface sewerage drainage system and an assessment of pluvial flooding scenarios; but may not be of much help for fluvial flooding.

Thus, the integrated model, as proposed here, will have a 1D model representing the river, a 2D model representing the area and a 1D subsurface sewerage and drainage model with surface-rainfall component, forming an integrated 1D-2D-1D model. The model reach can be extended further to communicate with a groundwater model, although, to an extent, this component can also be considered in the subsurface sewerage and drainage model.

It should be mentioned that, some studies employing similar approach have already been carried out (Syme et al. 2004) and proposed (Saul 2007) but do not fully consider the issues raised above.

7.2.3 Use of resistance obtained from LiDAR data

For the simulations carried out during this research, a single uniform roughness value was used for the urban floodplain that is represented by the 2D model. However, in reality, the floodplain surface has many features like buildings, roads, gardens, vegetated and paved surfaces, etc. Therefore, a uniform resistance value represents the floodplain friction very approximately. Further, in some particular cases the friction parameter becomes a more dominant factor than the topographic error (Hunter et al. 2008) and can have significant effect on the hydrodynamics.

The currently available LiDAR data can be processed to generate spatially distributed friction map of an area (Mason et al. 2007; Schumann et al. 2007). However, informed judgment about these values needs to be made while modelling using these values off–the–shelf; as it is identified that LiDAR based DEMs have an artificial roughness that significantly slows down the flow in the floodplains, resulting in an inaccurate representation of the flow dynamics (Néelz & Pender 2006; Sanders & Mrse 2007).

The estimated resistance values from LiDAR data can be supported by landcover and feature height data analysis from other sources such as aerial orthophotography and digital cartographic data, e.g. MasterMap® (Schubert et al. 2008).

The roughness values in 1D and 2D models represent different phenomenon. The 1D representation uses the friction factor to represent the shear stress exerted by the entire bed and the banks bounding the flow whereas a 2D model is using the factor to represent the shear stress exerted at the base of a vertical column of water (Morvan et al. 2008). An explicit inclusion of turbulence terms is sometimes implemented in 2D models. In the integrated 1D2D model, the turbulent momentum interaction between main channel and overbank flow is not explicitly taken into account by typical modelling codes resulting in a possible overestimate of the discharge capacity of the main channel. Applying these codes to flood extent modelling, therefore, requires

calibration of roughness values to account for this additional momentum transfer. The calibrated resistance values, thus, should no longer represent the physical friction values only, but also the combined friction and momentum correction factors (Werner & Lambert 2007).

Thus, with a proper understanding of roughness in 2D models, integrated 1D2D models can be configured to represent the real flow dynamics of an urban floodplain in an enhanced way.

References

1. Alcrudo, F., P. Garcia, P. Brufau, J. Murillo, D. Garcia, J. Mulet, G. Testa, and D. Zuccalà. 2003. *The model city flooding experiment*. EC Contract EVG1. available at http://www.samui.co.uk/impact-project /AnnexII_DetailedTechnicalReports /AnnexII_PartB_WP3 /Model_City_Flooding_Experiment.pdf.

2. Andres, J. G., J. Lhomme, A. Weisgerber, A. Cooper, B. Gouldby, and J. Mulet-Marti. 2008. Testing and application of a practical new 2D hydrodynamic model. *Flood Risk Management: Research and Practice – Samuels et al. (eds)*: 31-40.

3. Apel, H., G. T. Aronica, H. Kreibich, and A. H. Thieken. 2007. Evaluation of different modelling strategies for flood risk assessment in urban areas. *Proceedings of the 32nd congress - International Association for Hydraulic Research* 32, no. 1: 121.

4. Asselman, N., J. ter Matt, A. de Wit, G. Verhoeven, S. S. Frazão, M. Velickovic, L. Goutiere, Y. Zech, T. Fewtrell, and P. Bates. 2008. Flood inundation modelling: Model choice and application. *Flood Risk Management: Research and Practice – Samuels et al. (eds)*: 195.

5. Association of British Insurers. 2003. Flood resilient homes.

6. Bates, P. D., and M. G. Anderson. 1993. A two-dimensional finite-element model for river flow inundation. *Proceedings: Mathematical and Physical Sciences* 440, no. 1909: 481-491.

7. Bates, P. D., and A. P. J. De Roo. 2000. A simple raster-based model for flood inundation simulation. *Journal of Hydrology* 236, no. 1-2: 54-77.

8. Black, A. R. and J. C. Burns. 2002. Re-assessing the flood risk in Scotland. *The Science of the Total Environment* 294, no. 1-3: 169-184.

9. Bleninger, T., J. D. Fenton and R. Zentgraf. 2006. One-dimensional flow modelling and a case study of the river Rhine. *River flow: proceedings of the International Conference on Fluvial Hydraulics*.

10. Borthwick, A. G. L., S. C. Leon, and J. Jozsa. 2001. The shallow flow equations solved on adaptive quadtree grids. *International Journal for Numerical Methods in Fluids* 37, no. 6: 691-719.

11. Chanson, H. 2004. *The Hydraulics of Open Channel Flow: An Introduction*. Second Ed. Elsevier Publications.

12. CIRIA. 2003. Flood resilience: Improving the flood resistance of your home or business.

13. Clyde Flood Strategy Team. 2005. River Clyde Flood Management Strategy Study - Hydrodynamic Modelling report. Glasgow City Council.

14. Coulet, C., L. Evaux, and A. Rebai. 2008. Floods study through coupled numerical modelling of 2D surface and sewage network flows. *Flood Risk Management: Research and Practice – Samuels et al. (eds)*: 41-47.

15. Cruise, J. F., V. P. Singh, and M. M. Sherif. 2007. *Elementary Hydraulics*.

16. Dale, M. 2005. Impact of climate change on UK flooding and future predictions. *Water Management* 158, no. 4: 135-140.

17. Dankers, R., L. Feyen, A. De Roo, and O. B. Christensen. 2007. Climate change impact on extreme precipitation and flood hazard in Europe. *Geophysical Research Abstracts* 9: 08464.

18. Delft Hydraulic Software, 2009. SOBEK 1D2D online help. Available at: http://delftsoftware.wldelft.nl/index.php?option=com_docman&task=cat_view&gid=45&Itemid=82 [Accessed July 29, 2009].

19. Department for Environment, Food and Rural Affairs. 2008a. Property-level flood protection and resilience. available at http://www.defra.gov.uk/environ/fcd/adaptationandresilience/propertyresilience.htm.

20. Department for Environment, Food and Rural Affairs. 2008b. Adapting to climate change in England - A framework for action.

21. DHI Water, Environment & Health. 2005a. MIKE 11 Reference manual.

22. DHI Water, Environment & Health. 2005b. MIKE 21 Scientific documentation.

23. DHI Water, Environment & Health. 2005c. MIKE 21 user guide.

24. DHI Water, Environment & Health. 2005d. MIKE FLOOD user manual.

25. Dhondia, J.F. and G. S. Stelling. 2002. Application of one dimensional–two dimensional integrated hydraulic model for flood simulation and damage assessment. *Proceedings of the Fifth International Conference on Hydroinformatics, Cardiff*. pp. 265–276.

26. Dhondia, J.F. and G. S. Stelling. 2004. SOBEK One dimensional–Two dimensional integrated hydraulic model for flood simulation–its capabilities and features explained. *Proceedings of the 6th International Conference on Hydroinformatics: Singapore, 21-24 June 2004*. p. 1867.

27. Douglas, I., M. Kobold, N. Lawson, E. Pasche, and I. White. 2007. Characterisation of Urban Streams and Urban Flooding. *Advances in Urban Flood Management*, 29.

28. Environment Agency, UK. 2006. Flood risks to people: Phase 1 and 2.

29. Fleming, G. 2002. How can we learn to live with rivers? The findings of the institution of Civil Engineer's Presidential Commission on flood-risk management. *Philosophical transactions- Royal Society. Mathematical, physical and engineering sciences* 360, no. 1796: 1527-1530.

30. Fortune, D. 2008. Dispelling the myths of urban flood inundation modelling. *Flood Risk Management: Research and Practice – Samuels et al. (eds)*: 195.

31. Frazão, S. S., J. Lhomme, V. Guinot, and Y. Zech. 2008. Two-dimensional shallow-water model with porosity for urban flood modelling. *Journal of Hydraulic Research* 46, no. 1: 45-64.

32. Frazão, S. S., and Y. Zech. 1999. Computation of extreme flood flow through the Toce Valley. *Proceedings of the 3 rdCADAM workshop*.

33. Gems, B., J. Nemmert, and P. Rutschmann. 2007. Three-dimensional modelling of an extreme flood event for the city of Innsbruck. *Proceedings of the 32nd congress - International Association for Hydraulic Research* 32, no. 1: 29.

34. Gouldby, B., and P. Samuels. 2005. Language of Risk: Project Definitions. FLOODsite. available at http://www.floodsite.net/html/partner_area /project_docs/ FLOODsite_Language_of_Risk_v4_0_P1.pdf.

35. Gouldby, B., P. Sayers, J. Mulet-Marti, M. Hassan, and D. Benwell. 2008. A methodology for regional-scale flood risk assessment. *Water Management* 161, no. 3: 169-182.

36. Graf, W. H., and Z. Qu. 2004. Flood hydrographs in open channels. *Water Management* 157, no. 1: 45-52.

37. Guinot, V. and S. Soares-Frazao. 2006. Flux and source term discretization in two-dimensional shallow water models with porosity on unstructured grids. *International Journal for Numerical Methods in Fluids*, 50(3).

38. Hall, J. W., R. J. Dawson, P. B. Sayers, C. Rosu, J. B. Chatterton, and R. Deakin. 2003. A methodology for national-scale flood risk assessment. *Water & Maritime Engineering* 156, no. 3: 235-247.

39. Hall, J. W., P. B. Sayers, and R. J. Dawson. 2005. National-scale assessment of current and future flood risk in England and Wales. *Natural Hazards* 36, no. 1: 147-164.

40. Han, K. Y., J. W. Noh, C. H. Lee, and P. B. Kim. 2007. Development of DEM based flood inundation analysis model in urban areas. *32nd IAHR Congress, Venice, Italy, 1-6 July*.

41. Hartnack, J. M., H. G. Enggrob, and M. Rungø. 2008. 2D overland flow modelling using fine scale DEM with manageable runtimes. *Flood Risk Management: Research and Practice – Samuels et al. (eds)*: 119-124.

42. Haynes, H., R. Haynes, and G. Pender. 2007. Integrating socio-economic analysis into decision-support methodology for flood risk management at the development scale (Scotland). *Water and Environment Journal* 22, no. 2.

43. Helmiö, T. 2005. Unsteady 1D flow model of a river with partly vegetated floodplains - application to the Rhine River. *Environmental Modelling and Software* 20, no. 3: 361-375.

44. Hulme, M., G. J. Jenkins, X. Lu, J. R. Turnpenny, T. D. Mitchell, R. G. Jones, J. Lowe, et al. 2002. Climate Change Scenarios for the United Kingdom: The UKCIP02 Scientific Report. Tyndall Centre for Climate Change Research, School of Environmental Sciences, University of East Anglia, Norwich, UK. available at http://www.ukcip.org.uk/images/stories/Pub_pdfs/UKCIP02_tech.pdf.

45. Hunt, J. C. R. 2002. Floods in a changing climate: a review. *Philosophical Transactions Mathematical Physical and Engineering Sciences* 360, no. 1796: 1531-1543.

46. Hunter, N. M. 2005. Theoretical and practical limits to the use of storage cell codes for flood inundation modelling. *Geophysical Research Abstracts* 7: 02921.

47. Hunter, N. M., P. D. Bates, M. S. Horritt, and M. D. Wilson. 2006. Improved simulation of flood flows using storage cell models. *Water Management* 159, no. 1: 9-18.

48. Hunter, N. M., P. D. Bates, S. Néelz, G. Pender, I. Villanueva, N. G. Wright, D. Liang, et al. 2008. Benchmarking 2D hydraulic models for urban flooding. *Proceedings of the Institution of Civil Engineers, Journal of Water Management* 161, no. WMI: 13-30.

49. Hunter, N. M., M. S. Horritt, P. D. Bates, M. D. Wilson, and M. G. F. Werner. 2005. An adaptive time step solution for raster-based storage cell modelling of floodplain inundation. *Advances in Water Resources* 28, no. 9: 975-991.

50. Intergovernmental Panel on Climate Change. 2007. Climate Change 2007: Synthesis Report. available at http://www.ipcc.ch/pdf/assessment-report/ar4/syr/ar4_syr.pdf.

51. Jonkman, S N. 2005. Global perspectives on loss of human life caused by floods. *Natural Hazards* 34: 151-175.

52. Krámer, T., and J. Józsa. 2007. Solution-adaptivity in modelling complex shallow flows. *Computers and Fluids* 36, no. 3: 562-577.

53. Krukpa, M., G. Pender, S. Wallis, P. B. Sayers, and J. Mulet-Marti. 2007. A rapid flood inundation model. *32nd IAHR Congress, Venice, Italy, 1-6 July*.

54. Lehner, B., P. Döll, J. Alcamo, T. Henrichs, and F. Kaspar. 2006. Estimating the Impact of Global Change on Flood and Drought Risks in Europe: A Continental, Integrated Analysis. *Climatic Change* 75, no. 3: 273-299.

55. Lhomme, J., P. Sayers, B. Gouldby, P. Samuels, M. Wills, and J. Mulet-Marti. 2008. Recent development and application of a rapid flood spreading method. *Flood Risk Management: Research and Practice – Samuels et al. (eds)*: 15-24.

56. Li, B., M. Phillips, and C. A. Fleming. 2006. Application of 3D hydrodynamic model to flood risk assessment. *Water Management* 159, no. 1: 63-75.

57. Liang, D., B. Lin, and R. A. Falconer. 2007. Simulation of rapidly varying flow using an efficient TVD-MacCormack scheme. *International Journal for Numerical Methods in Fluids*, 53(5).

58. Liang, Q., A. G. L. Borthwick, and G. Stelling. 2004. Simulation of dam- and dyke-break hydrodynamics on dynamically adaptive quadtree grids. *International Journal for Numerical Methods in Fluids* 46, no. 2: 127-162.

59. Liang, Q., J. Zang, A. G. L. Borthwick, and P. H. Taylor. 2007. Shallow flow simulation on dynamically adaptive cut cell quadtree grids. *International Journal for Numerical Methods in Fluids* 53, no. 12: 1777.

60. Liggett, J A, and J A Cunge. 1975. Numerical methods of solution of the unsteady flow equations. In *Unsteady flow in open channels*, 1: Water Resources Publications Fort Collins, Colorado.

61. Macchione, F., and G. Viggiani. 2004. Simple modelling of dam failure in a natural river. *Water Management* 157, no. 1: 53-60.

62. Mark, O., S. Weesakul, C. Apirumanekul, S. B. Aroonnet, and S. Djordjevic. 2004. Potential and limitations of 1D modelling of urban flooding. *Journal of Hydrology* 299, no. 3-4: 284-299.

63. Marks, K., and P. Bates. 2000. Integration of high-resolution topographic data with floodplain flow models. *Hydrological Processes* 14, no. 11-12: 2109-2122.

64. Martin-Vide, J P, P J M Moreta, and S Lopez-Querol. 2008. Improved 1-D modelling in compound meandering channels with vegetated floodplains. *Journal of Hydraulic Research* 46, no. 2: 265-276.

65. Mason, D. C., M. S. Horritt, N. M. Hunter, and P. D. Bates. 2007. Use of fused airborne scanning laser altimetry and digital map data for urban flood modelling. *Hydrological Processes. Vol. 21*, no. 11: 1436-1447.

66. Mignot, E., A. Paquier, and S. Haider. 2006. Modeling floods in a dense urban area using 2D shallow water equations. *Journal of Hydrology* 327, no. 1-2: 186-199.

67. Morris, M. W. 1999. CADAM Project - Issues and conclusions from the Milan meeting.

68. Morvan, H., D. Knight, N. G. Wright, X. Tang, and A. Crossley. 2008. The concept of roughness in fluvial hydraulics and its formulation in 1D, 2D and 3D numerical simulation models. *Journal of Hydraulic Research* 46, no. 2: 191-208.

69. Nardi, F., J. S. O'Brian, R. Garcia, G. Cuomo, and S. Grimaldi. 2008. Updating flood maps using 2D models in Italy: A case study. *Flood Risk Management: Research and Practice – Samuels et al. (eds)*: 177-183.

70. Néelz, S., J. Hall, and G. Pender. 2008. Improving the performance of fast flood inundation models by incorporating results from very high resolution simulations. available at http://www.ima.org.uk/Conferences/Flood%20Risk%202007/Hall.pdf.

71. Néelz, S., and G. Pender. 2006. The influence of errors in digital terrain models on flood flow routes. *River flow: proceedings of the International Conference on Fluvial Hydraulics*.

72. Néelz, S., and G. Pender. 2008. Grid resolution dependency in inundation modelling: A case study. *Flood Risk Management: Research and Practice – Samuels et al. (eds)*: 109-117.

73. Néelz, S., G. Pender, I. Villanueva, M. Wilson, N. G. Wright, P. Bates, D. Mason, and C. Whitlow. 2006. Using remotely sensed data to support flood modelling. *Water Management* 159, no. 1: 35-43.

74. Paquier, A., C. Peyre, N. Taillefer, and M. Chenaf. 2008. Flood risk in urban areas caused by levee breaching. *Flood Risk Management: Research and Practice – Samuels et al. (eds)*: 197-204.

75. Pender, G. 2006. Introducing the Flood Risk Management Research Consortium. *Water management* 159, no. 1: 3-8.

76. Pender, G., and S. Néelz. 2007. Use of computer models of flood inundation to facilitate communication in flood risk management. *Environmental Hazards* 7, no. 2: 106-114.

77. Pitt, M. 2008a. The Pitt Review: Learning lessons from the 2007 floods. available at http://www.cabinetoffice.gov.uk/thepittreview/final_report.aspx.

78. Pitt, M. 2008b. The Pitt Review: Evaluation of modelling approaches for urban flood risk assessment. available at http://www.cabinetoffice.gov.uk/~/media/assets/www.cabinetoffice.gov.uk/flooding_review/evidence/evaluation_modelling_urban_flood_risk%20assess%20pdf.ashx.

79. Rehman, H., R. Thomson, and R. Thilliyar. 2008. Flood risk assessment using broad scale two-dimensional hydraulic modelling – a case study from Penrith, Australia. *Flood Risk Management: Research and Practice – Samuels et al. (eds)*: 143-150.

80. Samuels, P. G., M. E. Bramley, and E. P. Evans. 2002. Reducing uncertainty in conveyance estimation. *River Flow*: 293-302.

81. Sanders, B. F. 2007. Evaluation of on-line DEMs for flood inundation modeling. *Advances in Water Resources* 30: 1831-1843.

82. Sanders, B. F., and J. W. Mrse. 2007. Resistance to flooding by mega-roughness. *32nd IAHR Congress, Venice, Italy, 1-6 July*.

83. Sanders, B.F., J. E. Schubert and H. A. Gallegos. 2008. Integral formulation of shallow-water equations with anisotropic porosity for urban flood modeling. *Journal of Hydrology*, 362(1-2), 19-38.

84. Saul, A., 2007. Integrated surface and sub-surface interactive flooding and inundation model. FRMRC Research Report UR4 . available at www.floodrisk.org.uk.

85. Sayers, P. B., Hall J. W., and Meadowcroft I. C., 2002. Towards risk-based flood hazard management in the UK. *Civil Engineering* 150, no. 5: 36-42.

86. Schubert, J.E., B. F. Sanders, M. J. Smith, and N. G. Wright, 2008. Unstructured mesh generation and landcover-based resistance for hydrodynamic modeling of urban flooding. *Advances in Water Resources*, 31(12), 1603-1621.

87. Schumann, G., P. Matgen, L. Hoffmann, R. Hostache, F. Pappenberger, and L. Pfister. 2007. Deriving distributed roughness values from satellite radar data for flood inundation modelling. *Journal of Hydrology* 344, no. 1-2: 96-111.

88. Scottish Executive. 2004. Planning Advice Note 69: Planning and building standards advice on flooding.

89. Singh, V. P. 2004. *Flow routing in open channels: some recent advances*.

90. Smith, M, E. P. Edwards, G. Priestnall, and P. Bates. 2006. Exploitation of new data types to create digital surface models for flood inundation modelling. FRMRC Research Report UR3. FRMRC Research Report UR3. available at www.floodrisk.org.uk.

91. Smith, S. L., D. A. Holland, and P. A. Longley. 2004. The importance of understanding error in LiDAR digital elevation models. *International Archives of the Photogrammetry, Remote Sensing and Spatial Information Sciences* 35: 996-1001.

92. Sole, A., and G. Zuccaro. 2005. New urban area flood model: a comparison with MIKE 11-quasi 2D. *Advances in Geosciences* 2: 279-284.

93. Sturm, T. W. 2002. *Open Channel Hydraulics*. MacGrawHill.

94. Syme, W. J., M. G. Pinnell, and J. M. Wicks. 2004. Modelling flood inundation of urban areas in the UK using 2D / 1D hydraulic models. *8th National Conference on Hydraulics in Water Engineering, Institution of Engineers, Australia*. available at http://www.tuflow.com/Downloads/Modelling%20Flood%20Inundation%20of%20Urban%20Areas%20in%20the%20UK,%20Syme,%202004.pdf.

95. Tarrant, O., M. Todd, D. Ramsbottom, and J. Wicks. 2005. 2 D floodplain modelling in the tidal Thames: Addressing the residual risk. *Water and Environmental Management Journal* 19, no. 2: 125-134.

96. Tayefi, V., S. N. Lane, R. J. Hardy, and D. Yu. 2007. A comparison of one-and two-dimensional approaches to modelling flood inundation over complex upland floodplains.

97. Tchamen, G. W., T. T. Quach, and R. Kahawita. 2006. A robust implementation of Riemann solvers for one-dimensional free surface flow simulation in natural rivers. *River flow: proceedings of the International Conference on Fluvial Hydraulics*.

98. Testa, G., D. Zuccala, F. Alcrudo, J. Mulet, and S. S. Frazão. 2007. Flash flood flow experiment in a simplified urban district. *Journal of Hydraulic Research* 45: 37-44.

99. United Nations. 2004. Guidelines for reducing flood losses. *International Strategy for Disaster Reduction*. Geneva.

100. UNU-EHS. 2004. Two billion people vulnerable to floods by 2050: Number expected to double or more in two generations due to climate change, deforestation, rising seas, population growth. *News release*. available at www.unu.edu/news/ehs/floods.doc.

101. Verwey, A. 2007. Numerical modelling support to flood studies. *Presentation at the 32nd IAHR Conference*.

102. Villanueva, I., and N. G. Wright. 2006. Linking Riemann and storage cell models for flood prediction. *Water management* 159, no. 1: 27-33.

103. Villanueva, I., and N. G. Wright. 2006. Performance of several hybrid numerical schemes to determine flooding extent. *River flow: proceedings of the International Conference on Fluvial Hydraulics*.

104. Wallingford Software Ltd and Halcrow Group Ltd. 2005. ISIS user guide / manual - help file. Wallingford Software Ltd and Halcrow Group Ltd.

105. Werner, M. G. F., and M. F. Lambert. 2007. Comparison of modelling approaches used in practical flood extent modelling. *Journal of Hydraulic Research* 45, no. 2: 202-215.

106. Wicks, J., B. Syme, M. Hassan, B. Lin, and O. Tarrant. 2004. 2D modelling of floodplains - is it worth the effort. *Proceedings of the River and Coastal Flooding Conference, Defra, UK*: 1–10.

107. Williams, R. D., M. R. Lawless, and J. Walker. 2008. Coastal flood risk modelling in a data rich world. *Flood Risk Management: Research and Practice – Samuels et al. (eds)*: 161-169.

108. Wood, W. L. 1993. *Introduction to numerical methods for water resources*. Oxford University Press, USA.

109. World Health Organization. 2002. Floods: Climate Change and adaptation strategies for human health - Report on a WHO meeting. available at www.safecoast.nl/editor/databank/File/WHO%20floods%202002.pdf .

110. Yasuda, H. 2006. 1-Dimensional numerical analysis of tsunami in river. *River flow: proceedings of the International Conference on Fluvial Hydraulics*.

111. Ying, X., and S. S. Y. Wang. 2008. Improved implementation of the HLL approximate Riemann solver for one-dimensional open channel flows. *Journal of Hydraulic Research* 46, no. 1: 21-34.